UNIVERSITY OF CALIFORNIA SAN DIEGO

Thermal Improvement of the Pullout Capacity of Offshore Piles in Soft Clays

A dissertation submitted in partial satisfaction of the
requirements for the degree of Doctor of Philosophy

in

Structural Engineering

by

Ismaail Ghaaowd

Committee in charge:

Professor John S McCartney, Chair
Professor Kevin Michael Brown
Professor Ahmed Elgamal
Professor Gilberto Mosqueda
Professor Ingrid Tomac

2018

The Dissertation of Ismaail Ghaaowd is approved, and it is acceptable in quality and form for publication on microfilm and electronically:

Chair

University of California San Diego

2018

Dedication

To my parents, Ibrahim Ghaaowd and Kiria Eshmila,

my wife, Israa Najeeb,

my daughter, Joury Ghaaowd

my son, Yousif Ghaaowd

and

my parents-in-law, Hanaa Al Gburi and Abdulkarim Abdulkarim.

Epigraph

"Unfortunately, soils are made by nature and not by man, and the products of nature are always complex… As soon as we pass from steel and concrete to earth, the omnipotence of theory ceases to exist. Natural soil is never uniform. Its properties change from point to point while our knowledge of its properties is limited to those few spots at which the samples have been collected. In soil mechanics the accuracy of computed results never exceeds that of a crude estimate, and the principal function of theory consists in teaching us what and how to observe in the field."

Karl Terzaghi

Table of Contents

List of Symbols

α_w	Cubical coefficient of thermal expansion of the pore water
α_s	Cubical coefficient of thermal expansion of the mineral solids
V_w	Initial volume of pore water before heating is the volume of solids
V_s	Volume of solids
V_m	Total volume of the soil mass equal to the sum of V_w and V_s
ΔT	Change in temperature of the soil
ΔV_{st}	Volume change of the soil due to the reorientation and relative movement of the soil particles during heating
m_v	Compressibility of the soil skeleton
m_w	Compressibility of the water
n	Porosity of a saturated soil
α_{st}	Physico-chemical coefficient of structural volume change
$(m_v)_r$	Compressibility of the soil skeleton determined from the recompression curves
e_0	Initial void ratio
p'	Mean effective stress
e_0	Initial void ratio
σ'	Effective stress
w	Water content
LL	Liquid limit
PL	Plastic limit
LI	Liquidity index
PI	Plasticity index
κ	Slope of the recompression line

λ	Slope of the compression line
ε	Axial strain
$\sigma_1-\sigma_3$	Principal stress difference
q	Principal stress difference
p'	Mean effective stress
c_u	Undrained shear strength
$(\Delta V_{DR})_{\Delta T}$	Volume of water drained from a specimen due to a temperature change
$(\Delta V_m)_{\Delta T}$	Change in volume of the soil specimen
LVDT	Linearly variable differential transformer
PPT	Pore pressure transducer
$D_{T\text{-}bar}$	T-bar diameter
F_v	T-bar pushing force
N_b	T-bar bearing factor
H	Height of soil above the T-bar rod
Q	Pile total bearing capacity
Q_s	Pile skin friction bearing capacity
Q_p	Pile end bearing capacity
A_s	Pile surface area
A_p	Pile end bearing area
$H_{penetration}$	Pile penetration depth below the clay surface
$c_{u,penetration}$	Undrained shear strength measured during T-bar penetration
$c_{u,extraction}$	Undrained shear strength measured during T-bar extraction
S_T	Soil sensitivity
T_{pile}	Pile temperature at the pile wall

$T_{soil}(r)$	Temperature change in the soil at radius r
$r_{container}$	Container radius
$c_{u,XX}$	Undrained shear strength of the clay at the interface of a pile heated to a temperature of XX °C
$c_{u,23}$	Undrained shear strength of the clay at the interface of an unheated pile at an ambient temperature of 23 °C
$\Delta c_u/c_{u,23}$	Percent change in undrained shear strength with respect to the undrained shear strength at an ambient temperature of 23 °C
$\Delta Q/Q_{23}$	Percent improvement in pile pullout capacity with respect to the capacity at an ambient temperature of 23 °C
Q_{XX}	Maximum pullout pile capacity for pile heated to a temperature of XX °C
Q_{23}	Maximum pullout capacity for an unheated pile at an ambient temperature of 23 °C

List of Figures

List of Tables

Acknowledgments

I would like to thank Professor John McCartney, who has taught me so much, his support and advice has helped me to grow both as a researcher and as a person.

My deepest gratitude also to my fellow graduate students: Nahed Alsherif, Tugce Baser, Yewei Zheng, Radhavi Samarakoon, Leticia Nocko, Wenyong Rong, Muhammed Zayed, Ahmed Ebido, Abdullah Elmutairi, Kyungtae Kim, Rodrigo Carreno, and Woongju Mun, to name a few. I will always be grateful for their guidance and friendship throughout the years.

Thanks to the Powell lab staff: Dr. Chris Latham, Darren McKay, Danny Innamorato, Michael Sanders, Edward Stovin, Noah Aldrich, Andrew Sander and Abdullah Hamid for their invaluable help and advice during the experimental part of this work.

Also, I would like to thank the Department of Structural Engineering at UCSD staff, especially Yvonne Wollmann, Julie Storing, Amber Samaniego and Lindsay Walton for their support.

I would also like to express my gratitude to the Libyan High Education Ministry for the graduate scholarship that supported the first three years of my doctoral program. I also thank the Department of Structural Engineering at UCSD for the financial support provided in the last years of my program.

Finally, I want to thank the members of my committee for the time they dedicated and their valuable contribution to define the objectives for this dissertation.

Funding from University of California at San Diego that supported this project is greatly appreciated.

This thesis contains a mix of published conference/journal papers and new content. A summary of the published work in this thesis is given below.

Chapter 2, in full, has been published as it appears in the following journal publication (The dissertation author was the primary investigator and author of this paper):

Ghaaowd, I., Takai, A., Katsumi, T. and McCartney, J.S. (2016). "Pore water pressure prediction for undrained heating of soils." Environmental Geotechnics. 1-9. 10.1680/jenge.15.00041.

Chapter 3, in full, has been published as it appears in the following conference publication (The dissertation author was the primary investigator and author of this paper):

Takai, A., Ghaaowd, I., Katsumi, T., and McCartney, J.S. (2016). "Impact of drainage conditions on the thermal volume change of soft clay." GeoChicago 2016: Sustainability, Energy and the Geoenvironment. Chicago. Aug. 14-18. pp. 32-41.

Chapter 4, in full, has been published as it appears in the following conference publication (The dissertation author was the primary investigator and author of this paper):

Samarakoon, R. Ghaaowd, I. and McCartney, J.S. (2018). "Impact of drained heating and cooling on undrained shear strength of normally consolidated clay." International Symposium on Energy Geotechnics 2018. September 26-28. 8 pg.

Chapter 5 and Chapter 6, in full, are currently being prepared for submission for publication of the material as it may appear appears in the following journal publication (The dissertation author was the primary investigator and author of this paper):

Ghaaowd, I. and McCartney, J.S. (In preparation). "Test setup for centrifuge modeling of energy piles in saturated soft clay." To be submitted to ASTM Geotechnical Testing Journal.

Chapter 7 and Chapter 8, in full, are currently being prepared for submission for publication of the material as it may appear appears in the following journal publication (The dissertation author was the primary investigator and author of this paper):

Ghaaowd, I. and McCartney (In preparation). "Centrifuge modeling of temperature effects on the pullout capacity of energy piles in saturated soft clay." To be submitted to Journal of Geotechnical and Geoenvironmental Engineering.

Chapter 9, in full, has been published as it appears in the following conference publication (The dissertation author was the primary investigator and author of this paper):

Ghaaowd, I. and McCartney (In preparation). "Centrifuge modeling of temperature effects on the pullout capacity of Torpedo piles in saturated soft clay." To be submitted to the 2019 Deep Foundation Institute Conference.

Vita

2004	Bachelor of Engineering in Civil Engineering
	Tripoli University, Libya.
2004 –2006	Project Engineer
	Alsadeer Engineering Consultancy Company, Libya.
2005 –2008	Teaching Assistant, Civil Engineering Department
	Tripoli University, Libya**.**
2006-2008	Site Manager
	Cemonex Consulting Bureau**,** Tripoli, Libya.
2008-2012	Executive Manager
	Enmaa Alaqari Engineering Consultancy Co, Libya.
05/2008	Master of Science in Civil Engineering
	Tripoli, Libya.
2008- 2012	Lecturer, Civil Engingeering Department
	Tripoli University, Libya.
2013-2014	Research Assistant, Civil Engineering Department
	University of Colorado Boulder.
2015-2018	Graduate Student Researcher
	University of California, San Diego.
2018	Doctor of Philosophy in Structural Engineering
	University of California, San Diego.

Publications

Ghaaowd, I. and McCartney, J.S. (in preparation). "Test setup for centrifuge modeling of energy piles in saturated soft clay." To be submitted to ASTM Geotechnical Testing Journal.

Ghaaowd, I. and McCartney, J.S. (in preparation). "Centrifuge modeling of temperature effects on the pullout capacity of energy piles in saturated soft clay." To be submitted to Journal of Geotechnical and Geoenvironmental Engineering.

Ghaaowd, I. and McCartney, J.S. (in -preparation). "Centrifuge modeling of temperature effects on the pullout capacity of Torpedo piles in saturated soft clay." To be submitted to DFI 2019.

Ghaaowd, I., Fox, P.J., and McCartney, J.S. (In preparation). "Shearing behavior of tire derived aggregate with large particle sizes. III: Soil interface direct shear behavior." To be submitted to Journal of Geotechnical and Geoenvironmental Engineering.

Ghaaowd, I. and McCartney, J.S. (In preparation). "Evaluation of pullout strength of geosynthetics in tire derived aggregate with large particle size." To be submitted to Journal of Geotechnical and Geoenvironmental Engineering.

Ghaaowd, I. and McCartney, J.S. (In preparation). "Large-scale pullout testing device for geosynthetics embedded in tire derived aggregate." To be submitted to Geosynthetics International.

McCartney, J.S., **Ghaaowd, I.,** and Fox, P.J. (2018). Evaluation of Geosynthetic Pullout Strength and Soil Interface Shear Strength for Tire Derived Aggregate with Large Particle Size – Phase III. Final Report to California Department of Resources Recycling and Recovery

Samarakoon, R. **Ghaaowd, I.** and McCartney, J.S. (2018). "Impact of drained heating and cooling on undrained shear strength of normally consolidated clay." International symposium on Energy Geotechnics 2018. September 26-28. 8 pg.

Ghaaowd, I. and McCartney, J.S. (2018). "Centrifuge modeling of temperature effects on the pullout capacity of energy piles in clay." 3rd Annual Conference on Deep Foundations 2018. Anaheim, CA, USA. October. 24-27. 10 pg.

Ghaaowd, I. and McCartney, J.S. (2018). "Issues with centrifuge modeling of energy piles in soft clays." International Conference Physical Modeling in Geotechnical 2018. London, UK. July. 17-20. 6 pg. In review

Ghaaowd, I. and McCartney, J.S. (2017). "Large-scale pullout testing device for geosynthetics embedded in tire derived aggregate." GeoAfrica 2017. Marrakesh, Morroco. Oct. 8-11. 10 pg.

Ghaaowd, I., McCartney, J.S., Thielmann, S., Sanders, M. and Fox, P.J. (2017). "Shearing behavior of tire derived aggregate with large particle sizes. I: Internal and concrete

interface direct shear behavior." Journal of Geotechnical and Geoenvironmental Engineering.

McCartney, J.S., **Ghaaowd, I.,** Fox, P.J., Sanders, M., Thielmann, S., and Sander, A. (2017). "Shearing behavior of tire derived aggregate with large particle sizes. II: Cyclic simple shear behavior." Journal of Geotechnical and Geoenvironmental Engineering.

Fox, P.J., Sanders, M., Latham, C., **Ghaaowd, I.,** and McCartney, J.S. (2017). "Large-scale direct-simple shear test for large-particle tire-derived aggregates." ASTM Geotechnical Testing Journal.

Ghaaowd, I., Takai, A., Katsumi, T. and McCartney, J.S. (2016). "Pore water pressure prediction for undrained heating of soils." Environmental Geotechnics. 1-9. 10.1680/jenge.15.00041.

Takai, A., **Ghaaowd, I**., Katsumi, T., and McCartney, J.S. (2016). "Impact of drainage conditions on the thermal volume change of soft clay." GeoChicago 2016: Sustainability, Energy and the Geoenvironment. Chicago. Aug. 14-18. pp. 32-41.

McCartney, J.S., **Ghaaowd, I**., Sanders, M., Sander, A., Thielmann, S., and Fox, P.J. (2016). Large Scale Measurement of Internal and Interface Shear Strength of Tire Derived Aggregate – Phase II. Final Report to California Department of Resources Recycling and Recovery.

Ghaaowd, I. and McCartney, J.S. (2015). "Prediction of excess pore water pressure during undrained heating of clays." 15th Pan-American Conf. on Soil Mechanics and Geotechnical Engineering (XV PCSMGE). Buenos Aires. Nov. 16-18. pp. 1-8.

Zhang, M., **Ghaaowd, I.,** McCartney, J.S. (2013). Centrifuge Modeling of Cyclic Loading of Foundations Systems in Soft Clay. Report to Ocean Renewable Power Corporation. 85 p.

Abstract of the Dissertation

Thermal Improvement of the Pullout Capacity of Offshore Piles in Soft Clays

by

Ismaail IB Ghaaowd

Doctor of Philosophy in Structural Engineering

University of California San Diego, 2018

Professor John McCartney, Chair

Because of their relatively low shear strength, high compressibility, and complex dynamic response, soft clay deposits routinely pose challenges to geotechnical engineers interested in improving the load-carrying capacity of deep foundations. Beyond increasing the dimensions or

mass of the foundation, the primary techniques that have been used to enhance the behavior of soft clays include preconsolidation with surcharge loading, electro-osmosis, or installation of vertical drains. While these soil improvement techniques have been shown to work well for clay deposits on land, they may be difficult to apply in offshore clay deposits. To address this issue, this study investigates a comprehensive approach to improve the properties of soft clays through in-situ heating to enhance the pullout capacity of an offshore foundation. In particular, this study focuses on two types of offshore foundation that could incorporate internal heating devices – a cylindrical pile jacked into place and a torpedo pile installed under self-weight.

Soil improvement using in-situ heating in saturated, normally consolidated clays is a complex coupled thermo-hydro-mechanical process. Increases in pile temperature will leads to the generation of thermally-induced excess pore water pressure due to the differential thermal expansion of the clay particles and water. The generation of these pore water pressures will lead to a flow of water away from the heat source, leading to time-dependent, elasto-plastic volumetric contraction (consolidation). A further decrease in void ratio is expected during pile cooling due to elastic contraction. The decrease in void ratio of the clay due to a change in temperature leads to an increase in undrained shear strength of the clay, and a corresponding increase in the pullout capacity of the pile.

To study this coupled problem, an empirical model was developed and applied to predict the distribution of thermally-induced excess pore water pressure during undrained heating of a saturated clay layer. This model was combined with a conduction analysis to estimate the changes in pore water pressure as a function of radius and depth in the clay layer surrounding a heated pile. Next, a poro-mechanics model was developed to estimate the amount of volumetric contraction of the clay as a function of the magnitude of pore water pressure. An experimental correlation

between the undrained shear strength and the void ratio based on results from triaxial tests was then used to estimate the pullout capacity of the pile. Finally, a series of geotechnical centrifuge physical modeling experiments were performed to evaluate the different heat transfer, water flow, and volume change processes in a clay layer surrounding a heated pile, followed by measurement of the changes in pullout capacity of the pile. The pullout capacity estimated using the empirical models and undrained shear strength correlations were found to match well with the pullout capacities measured in the geotechnical centrifuge physical modeling experiments.

Chapter 1. Introduction

1.1. Motivation

Because of their relatively low shear strength, high compressibility, and complex dynamic response, soft clay deposits routinely pose challenges to geotechnical engineers interested in improving the load-carrying capabilities of offshore foundations. Different from coarse-grained soils, there are not a wide range of effective soil improvement techniques available to enhance the behavior of soft clays besides preconsolidation with surcharge loading, electro-osmosis, or installation of vertical drains. While these improvement techniques have been shown to work well for clay deposits on land, they are difficult to apply for offshore clay deposits. Although one approach to gain additional capacity is to increase the size of offshore foundations (i.e., their diameter and length), in some cases the sizes of the foundations are at the limit. For example, the size of torpedo piles used to support offshore floating structures in deep water areas off the coast of Brazil is limited by the size of the vessels used to transport the torpedo piles to a site. If the size of an offshore foundation cannot be increased, the number of offshore foundations typically must be increased, which comes with significant cost. Accordingly, soil improvement techniques that can be used to improve the pullout capacity of offshore piles may help reduce the total number of piles needed to support an offshore floating structure.

1.2. Concept of Soil Improvement using In-Situ Heating

This study focuses on a novel approach to improve soft clays through in-situ heating of the offshore pile, with the goal of enhancing the vertical pullout capacity of the pile. This soil improvement concept builds upon recent research in the area of energy piles, where closed-loop fluid circulation pipes are embedded into a reinforced concrete pile to convert it to a geothermal heat exchanger (Brandl 2006). However, most studies on energy piles have focused on the

behavior of the pile in relatively stiff soil deposits with axial downward loading (e.g., Brandl 2006; Laloui et al. 2006; Bourne-Webb et al. 2009; Murphy et al. 2015; Murphy and McCartney 2015; McCartney and Murphy 2017). In most of these studies the soil surrounding the energy pile is assumed to be inert and only the thermal expansion and contraction of the pile because of changes in the pile temperature are considered. In this study, the changes of temperature of the pile are used to cause thermal contraction of normally consolidated, soft clay to result in an improvement in the undrained shear strength of the clay and a corresponding increase in pile capacity. Different from stiff, overconsolidated soils, which expand and contract thermo-elastically during heating and cooling, respectively, normally consolidated soils will contract plastically during heating and contract further elastically during cooling (Campanella and Mitchell 1968; Hueckel and Baldi 1989; Vega and McCartney 2012).

The concept of improvement of offshore piles in this study is proposed to increase the temperature of the pile by a certain increment and maintain this increased temperature for a certain time before cooling back to ambient temperature, as shown in Figure 1.1(a). This change in temperature of the pile, which is assumed to be uniform with depth, is expected to result in an initial undrained heating of the soil which will result in thermal pressurization and an increase in pore water pressure. This change in pore water pressure may be different at different depths (Uchaipichat and Khalili 2009). However, as soon as the pore water pressure is generated, it is expected that water flow will occur in the direction of the unheated soil (away from the pile) and the pore water pressure will decrease with time as shown in Figure 1.1(b). The initial undrained heating of the clay will also lead to initial thermal expansion, but as drainage occurs the soil is expected to volumetrically contract as shown in Figure 1.1(c). This permanent contraction,

followed by additional volumetric contraction during cooling, is expected to result in an increase in undrained shear strength of the clay and an increase in the pullout capacity of the offshore pile.

The process described in the previous paragraph is a complex, coupled thermo-hydro-mechanical process, with coupling between heat transfer, water flow, and deformation. Heat transfer may be due to a combination of both conduction and convection in saturated soils, as changes in the pore water density with temperature may lead to buoyancy-driven water flow. However, Saviddou (1988) found that for clays with low hydraulic conductivity, heat transfer due to convection will be slower than that due to conduction. Accordingly, this study only considers conductive heat transfer in the saturated clay layer. As mentioned, changes in temperature will lead to changes in pore water pressure of the soil if drainage is not allowed (Campanella and Mitchell 1968; Uchaipichat and Khalili 2009; Ghaaowd et al. 2015). However, in reality the soil surrounding the pile will not be fully undrained and the increases in pore water pressure will start to dissipate soon after generation. Additional coupling will occur as thermal volumetric contraction will lead to an increase in the thermal conductivity of the clay, affecting the heat transfer process.

Ideally, a fully-coupled thermo-hydro-mechanical model should be used to simulate this problem, such as the ACMEG-T model of Laloui and Francois (2009) or the CODE_BRIGHT model (Olivella et al. 1996a, 1996b). However, these advanced models require a significant testing program to identify a number of parameters governing the soil response. The approach used in this study is to use a set of uncoupled models to consider the different physical processes separately, then compare the outcomes of the uncoupled models with measurements from centrifuge physical modeling experiments involving application of a heating-cooling cycle to a scale-model offshore foundation in a soft clay layer. The uncoupled models will include a radial conduction analysis to predict changes in temperature in the soil surrounding the foundation, a thermal pressurization

model to predict the excess pore water pressure during undrained heating for the estimated changes in temperature, a model to predict the thermal volumetric strains that will occur after drainage of the thermally-induced excess pore water pressures, an empirical correlation to relate the change in volume of the clay with the change in undrained shear strength of the clay, and a bearing capacity analysis to estimate the pullout capacity of the foundation after the heating-cooling cycle This analysis will be performed for two offshore foundations that could benefited from the incorporation of internal heating devices: a cylindrical pile jacked into place and a torpedo pile installed under self-weight. A schematic of offshore foundations during in-situ heating is shown in Figure 1.2, showing the process of heat transfer, drainage of pore water pressures during in-situ heating. This study will focus on the pullout of these piles in the vertical direction, although in the field the direction of pullout may vary.

1.3. Objectives

The overall objective of this study is to understand the process of thermal improvement of soft clays to enhance the pullout capacity of offshore foundations. Specific objectives include:

- Understand the thermally-induced excess pore water pressure of saturated, normally consolidated clay for a given change in temperature during undrained heating.
- Estimate the thermal volumetric strain of saturated, normally consolidated clays due to a heating and cooling cycle.
- Estimate the duration of heating needed to cause thermal volumetric contraction under a sustained elevated temperature.
- Understand the change in the undrained shear strength of the clay due to the thermal volumetric strains occurring after drainage.
- Understand the role of initial effective stress (e.g., depth within the clay layer) on the

increase of the undrained shear strength.

- Verify the assumption that conduction can be used to analyze heat transfer processes in clay layers surrounding an offshore pile during in-situ heating.

1.4. Background

The thermo-hydro-mechanical behavior of clayey soils has been of significant interest to geotechnical engineering in the last several decades in the areas of buried power lines (Abdel-Hadi and Mitchell 1979), storage of radioactive waste in compacted bentonite (Gens et al. 1998; Kanno et al. 1999), disposal of metal canisters of radioactive waste in deep seabeds (Schiffmann 1971; Booker and Savvidou 1985; Houston et al. 1985), energy extraction from geothermal reservoirs (Lee and Ghassemi 2011), soil-structure interaction in energy foundations (Brandl 2006; Laloui et al. 2007; McCartney 2011; Abdelaziz et al. 2011), heat storage in soil layers (Bergenstahl et al. 1994; Moritz 1995), and consolidation of soft clay layers using thermal drains (Abuel-Naga et al. 2006). Of these different applications, the lessons learned from previous research on heat flow and consolidation of clay surrounding metal canisters of radioactive waste is of most interest to this study (Booker and Savvidou 1985; Houston et al. 1985; Maddocks and Savvidou 1985).

In studies of the thermo-mechanical behavior of soils, an underlying assumption is that temperature does not have a major impact on the basic soil properties, including the compression indices (Paaswell 1967; Campanella and Mitchell 1968) and the friction angle (Laloui 2001; Hueckel et al. 2009). Instead, temperature affects the behavior of soil through thermal consolidation and thermal softening (i.e., a change in the yield stress). The root cause of thermal consolidation is the excess pore water pressure generation induced by the differential expansion of the pore water and soil skeleton (Campanella and Mitchell 1968). The range of magnitudes of excess pore water pressures for a given change in temperature can be assessed using undrained

heating tests on soils. Specifically, the coefficient of thermal expansion of pore water is approximately 7-10 times that of most soil particles (McKinstry 1965; Mitchell and Soga 2005).

It must be emphasized that drainage of excess pore water pressures must occur for thermal consolidation to occur: undrained heating without dissipation of pore water pressures will lead to recoverable elastic expansion (Uchaipichat and Khalili 2009). An example of the pore water pressures generated in saturated silt specimens during heating under different initial effective stresses is shown in Figure 1.3(a). The change in pore water pressure with temperature is greater for soils with a larger initial effective stress. The relationship between specific volume and isotropic effective stress during heating is shown in Figure 1.3(b). During undrained heating the specimens expand thermo-elastically along a linear unloading-reloading curve. After cooling in undrained conditions, all the thermal strains are recovered. This indicates that if a soil is heated and cooled before time is permitted for drainage of excess pore water pressures, no permanent contraction will occur. The implication of this finding is that sufficient time must be permitted for thermally-induced excess pore water pressures to dissipate, with a time that depends on the soil characteristics. A second implication is that the elevated temperature must be maintained until drainage occurs or the thermally-induced pore water pressures will return to their original values.

Several studies have tried to predict the magnitude of excess pore water pressure in saturated soils due to a change in temperature using thermo-elastic theories (Campanella and Mitchell 1968; Booker and Savvidou 1985; Ghaaowd et al. 2015). The theories developed in these studies require knowledge of the coefficients of thermal volume change of the water and soil particles, as well as the modulus of the soil skeleton that must be experimentally derived. Ghaaowd et al. (2015) provided improvements upon the previous models by developing correlations to define the parameters and by providing an approach to consider the role of stress history. This

paper is included in this thesis in Chapter 2. Several studies have evaluated the excess pore water pressure in saturated clays during undrained heating experimentally and have used this as an indicator of the potential thermal improvement. The excess pore water pressure normalized by the initial vertical effective stress for several soils reported in the literature is summarized in Figure 1.4(a). The data indicate that the thermally induced excess pore water pressure may be greater than half the vertical effective stress during a temperature change of 35 °C, making it a feasible target for thermal improvement applications. Based on the data set in Figure 1.4(a), the following empirical equation can be used to estimate the mean excess pore water pressure ratio as a function of temperature for changes in temperature less than 35 °C:

$$\frac{\Delta u}{\sigma_v'} = \frac{\Delta T}{28.6+\Delta T} \tag{1.1}$$

where Δu is the change in pore water pressure during undrained heating, σ_v' is the initial vertical effective stress, and ΔT is the change in temperature.

After drainage of the excess pore water pressure occurs, a decrease in volume will occur (Campanella and Mitchell 1968; Takai et al. 2016). This decrease in volume will lead to an increase in undrained shear strength. The percent changes in undrained shear strength after drainage of the thermally induced excess pore water pressure for several soft clays reported in the literature are summarized in Figure 1.4(b). These results show an increase in undrained shear strength of up to 50%. Many of these studies observed a reduction in the shear-induced pore water pressure response. This may be due to the apparent overconsolidation effect induced by the contraction during heating. The data in Figure 1.4(b) reflects the magnitude of soil improvement that can be gained through heating. Specifically, in-situ heating may lead to equal or better improvement compared to the use of a surface surcharge, which can only induce a change in pore water pressure proportional to its depth.

Consideration of the possible negative side-effects of heating should be carefully considered. Generation of excess pore water pressures under temperatures above 100 °C may lead to high hydraulic gradients (Houston et al. 1985), potentially causing hydro-fracturing or thermal failure/instability of clay (Brandon et al. 1989). A schematic of the stress paths during drained and undrained heating for anisotropically- and isotropically-consolidated soil are shown in Figure 1.5. The temperature at the heating element will likely be the highest in the soil layer, so the heat input needs to be carefully controlled so that the change in pore water pressure does not lead to zero effective stress conditions (for isotropic stress states) or thermal failure (for anisotropic stress states). It should be possible to engineer the heat input pattern over time to stay within acceptable operational limits for a given initial effective stress state, like pressure control during grouting.

A wealth of experience on the volume change of saturated soft clays during drained heating from element-scale tests has been established in the literature (Baldi et al. 1988, 1991; Towhata et al. 1993; Hueckel et al. 1998; Burghignoli et al. 2000; Graham et al. 2001; Sultan et al. 2003; Laloui and Cekerevac 2004, 2008; Abuel-Naga et al. 2007a, 2007b). Examples of the results from drained heating tests on clays with different stress histories under isotropic stress conditions are shown in Figures 1.6(a) and 1.6(b). These results indicate that normally consolidated (NC) clays having an overconsolidation ratio ($OCR = \frac{Maximum\ Previous\ Mean\ Effective\ Stress}{Current\ Mean\ Effective\ Stress}$) equal to 1.0 will experience a plastic volumetric contraction strain of up to 1 to 2% during heating to temperatures up to 90 °C, which may be followed by additional elastic contraction during cooling. Regardless of the OCR of the clay, the slope of the elastic contraction curve during cooling will be the same, as observed in Figure 1.6(b). Several studies have indicated that cyclic heating and cooling will lead to an increasing amount of permanent contraction after each cycle, but the majority of the permanent contraction occurs after the first heating-cooling cycle (Campanella and

Mitchell 1969; Burghignoli et al. 2000; Vega and McCartney 2014). It is not expected that all clays will have the same amount of thermal volume change, with the clay mineralogy playing a major role in the amount of permanent contraction during heating of normally consolidated clays. The data in Figure 1.7 indicates that clay with higher activity (Activity = Plasticity Index/Percent Fines) will experience greater plastic, contractile thermal volumetric strains.

Although Campanella and Mitchell (1968) hypothesized that the thermal volume changes observed in Figures 1.6 and 1.7 is due to drainage of thermally induced pore water pressures, other elasto-plastic models have linked the thermal volume change to changes in the preconsolidation stress. Although the preconsolidation stress (the maximum previous effective stress applied to a specimen) is equal to the current stress state for normally consolidated soils, loading of normally consolidated soils after heating have revealed that there may be an increase in the apparent preconsolidation stress during mechanical loading to higher stresses. Constant rate of strain consolidation tests on soft clays under elevated temperatures reveal lower preconsolidation stresses than that expected from the virgin compression curve under ambient temperature [Figure 1.8(a)]. However, mechanical loading of clays after a heating-cooling cycle has been observed to lead to a hardening effect and a greater preconsolidation stress [Figure 1.8 (b)]. The decreases in preconsolidation stress with temperature observed in Figure 1.8 have been incorporated into different thermo-elasto-plastic constitutive models (Hueckel and Borsetto 1990; Cui et al. 2000; Laloui and Cekeravac 2003; Cui et al. 2009; Abuel-Naga et al. 2009). Most of these thermo-elasto-plactic models are based on the work of Hueckel and Borsetto (1990), who adapted the Cam Clay model for non-isothermal conditions. Laloui and Cekeravac (2003) developed a constitutive relationship that can be used for isotropic stress states, which permits straightforward calibration using axisymmetric heating tests. Consideration of anisotropic stress states like those observed in

horizontal soil layers is complex, but Coccia and McCartney (2012) provided empirical relationships on how thermal strains may be different in the directions of anisotropic stresses. Abuel-Naga et al. (2009) developed a constitutive relationship for NC clays based on experiments on Bangkok clay (Abuel-Naga et al. 2007a, 2007b, 2007c).

It is important to emphasize that heating does not lead to a major change in many of the fundamental soil properties. Instead, it leads to permanent volumetric contraction of soft clays, which affects the undrained shear strength and stiffness. Campanella and Mitchell (1968) observed that heating does not lead to an impact on the compression index of clays, indicating that isothermal consolidation tests on clays under various temperatures should have similar slopes for the virgin compression line and the loading-unloading line. Several studies indicate the drained friction angle of saturated soils is not sensitive to temperature (Laloui 2001).

Large-scale heating of soft clay layers has been investigated by Bergenstahl et al. (1994) and Moritz (1995). Bergenstahl et al. (1994) observed a generation of significant excess pore water pressures and surface settlement in a 10 m thick clay layer, as observed in Figure 1.9. An interesting observation is the fact that the soil layer initially expanded before eventually contracting. This reflects the coupled process of heat transfer initially leading to undrained thermal expansion followed by water flow leading to drainage and consolidation. They also observed a change in pore water pressure generation depending on the rate of heating and depth. Maddocks and Savvidou (1985) also performed a centrifuge-scale evaluation of thermal consolidation around a heating probe in a soft layer of soil and found that permanent contraction of the soil due to heating was observed. Ng et al. (2014) evaluated the behavior of energy piles in soft clay but focused primarily on the soil-structure interaction of the pile and not on the thermal improvement of the soil layer. Accordingly, physical modeling of thermal improvement of soft clays using in-situ

heating that has not been fully explored in the literature and could benefit from further experimental evaluations like those in this study.

1.5. Approach

The research approach used in this study involved a combination of element-scale tests to measure soil properties and thermo-mechanical response, analyses of heat flow away from an infinite line source, and N-g physical modeling tests in a geotechnical centrifuge to characterize the full system response and to provide validation data. All the laboratory and centrifuge tests were performed on saturated Kaolinite clay layers that are primarily normally consolidated and are relatively soft (i.e., initial undrained shear strengths ranging from 3 to 18 kPa). The five phases of this research project are: (1) development of a prediction model for excess pore water pressure generation during undrained heating, (2) development of a prediction model for thermal volumetric strains after drainage, (3) development of a prediction model for undrained shear strength changes after drainage, (4) combination of the prediction models with a conductive heat transfer analysis to predict the spatial improvement of a clay layer due to in-situ heating, and (5) centrifuge modeling of thermal effects on the offshore foundation pullout capacity.

As mentioned, it is assumed in this study that the processes of heat transfer and consolidation are uncoupled for simplicity. This is because it is assumed that the process of radial heat transfer away from the cylindrical source will initiate undrained heating of the clay, and that consolidation of the clay will not start until after the undrained pore water pressures have been generated. It is possible that there is coupling, but less coupling is expected for lower permeability soils like clay. The thermal conductivity of the clay was measured in this study using two approaches. For high void ratios ranging from 3.0 to 1.2 a thermal needle was embedded in the centrifuge container to measure the change in thermal conductivity during consolidation of the

clay from slurry. For lower void ratios ranging from 1.2 to 0.8, the triaxial cell method of McCartney et al. (2013) was used. The relationship between thermal conductivity and void ratio was then used in the conductive heat transfer analysis.

During centrifuge testing, the temperature of the pile wall was controlled using an electrical heating element embedded inside the pile, with the temperature monitored using a thermocouple on the pile surface for the jacked-in pile and a thermocouple attached to the heating element in the Torpedo pile. Accordingly, the change in temperature in the saturated clay layer around the circular pile was estimated using an analytical solution to the heat diffusion equation for an infinite line source with a constant temperature developed by Carslaw and Jaeger (1959). The calculated temperature distribution after 10 hours for the same tested model were then matches with the measured temperature results from different tests. As the pullout capacity of the piles depends on the undrained shear strength at the pile interface, the target zone limit at the prototype scale is assumed to be at a radius equal to twice the pile radius ($r = 2\ r_{pile}$).

Increases in pile temperature will lead to the generation of thermally-induced excess pore water pressure due to the differential thermal expansion of the clay particles and water. A thermo-elastic analysis was calibrated using experimental data presented in the literature for normally consolidated soils having different mineralogical compositions. The magnitude of thermally induced excess pore water pressure for these soils was observed to depend on the initial void ratio, the initial effective stress, the thermal coefficient of cubical expansion of the soil particles, the change in temperature, the compressibility of the soil skeleton, and the physico-chemical coefficient of structural volume change. An empirical relationship between the physico-chemical coefficient of structural volume change and the plasticity index was proposed to predict the thermally induced excess pore water pressure for saturated, normally consolidated soils. To

validate the model, an undrained heating test was performed independently on a specimen of normally consolidated Kaolinite clay as well as other soils from the literature having different stress histories.

The generation of thermally-induced excess pore water pressures will lead to a flow of water away from the pile heat source, leading to time-dependent, elasto-plastic volumetric contraction (consolidation) for normally consolidated clays. The change in the void ratio as function of the thermal excess pore water pressure was predicted using model developed and validated in this study using drained heating in triaxial tests on Kaolinite clay. The decrease in void ratio of the clay due leads to an increase in undrained shear strength of the clay. Triaxial tests at different effective stresses following different heating paths were performed to investigate the impact of the cooling heating cycle on the undrained shear strength. In addition, the role of the initial mean effective stress on the undrained shear strength change due to a heating/cooling cycle was investigated using drained heated triaxial tests on specimens consolidated to different mean effective stresses.

Although a large zone of soil surrounding the pile may be improved by in-situ heating, the pullout capacity of the pile is expected to depend primarily on the undrained shear strength at the interface of the pile wall. Once the undrained shear strength of the soil at the interface with is predicted, the improvement at the pullout capacity can be defined. A schematic of the different components of the uncoupled prediction model is shown in Figure 1.10, which includes a conductive heat transfer analysis, a prediction model for thermally induced pore water pressure during undrained heating, a prediction model to relate the change in pore water pressure to the change in void ratio of normally consolidated soils after drainage of the excess pore water pressures, an empirical relationship to relate the decreases in the void ratio with changes in

undrained shear strength, and finally a pile capacity analysis to predict the pullout capacity of the pile in the improved soil layer. The measured improvements in the pullout capacity from the centrifuge tests can then be compared with the predicted pullout capacity from the uncoupled prediction model shown in Figure 1.10.

1.6. Outline

This section presents a brief description of the following nine chapters included in this dissertation:

- *Chapter 2: Excess Pore Water Pressure Prediction for Undrained Heating of Saturated Soils.* This chapter describes the research work done to establish model that can be used to predict the thermally-induced excess pore water pressure. The model was validated by using undrained heating test was performed independently on a specimens of normally consolidated Kaolinite clay, and the measured thermally induced excess pore water pressures were found to match well with the model predictions.
- *Chapter 3: Impact of Drainage Conditions on Thermal Volume Change of Soft Clay*. This chapter focuses on an evaluation of the thermal volume change of normally-consolidated Kaolinite clay under drained and undrained conditions. For both drained and undrained conditions, separate clay specimens were heated in a modified triaxial test setup from ambient temperature (23°C) to approximately 60 °C and subsequently cooled. In both tests, the thermal volume change of the clay specimen was inferred using image analysis.
- *Chapter 4: Impact of Drained Heating and Cooling on Undrained Shear Strength of Normally Consolidated Clay*. This Chapter focuses on the effects of a heating-cooling cycle on the undrained shear strength of normally consolidated clay specimens at different effective mean stresses.

- *Chapter 5: Centrifuge Modeling of Energy Piles in Saturated Soft Clay: Materials*. This chapter focuses on the engineering properties of the Kaolinite clay, and the dimension of the scale-model piles used in this study. In addition, the properties of the Ottawa sand used as the drainage soil layer under the clay layer are presented.
- *Chapter 6: Centrifuge Modeling of Energy Piles in Saturated Soft Clay: Test Setup*. This chapter describes the test procedure to construct the model, testing procedures, and typical results. Also, details about the sensors and equipment are explained.
- *Chapter 7: Centrifuge Modeling of Offshore Piles in Saturated Soft Clay: Results*. This chapter describes detailed results from seven centrifuge tests involving the jacked-in piles. In addition, this chapter reports the results from in-situ tests to measure the shear strength in the soil layer used in each test.
- *Chapter 8: Centrifuge Modeling of Offshore Piles in Saturated Soft Clay: Analysis*. This chapter focuses on the analysis of the tests results. The relationship between the temperature change and pile pullout improvement were defined. Also, pullout capacity improvement prediction model was developed and compared with the measured results.
- *Chapter 9: Centrifuge Modeling of Temperature Effects on the Pullout Capacity Torpedo Piles in Soft Clay*. This chapter describes the test setup, test procedures, results, and analysis of the effect of the temperature increase on the pullout capacity of Torpedo piles.
- *Chapter 10: Conclusions*. This chapter summarizes the main findings of this study.

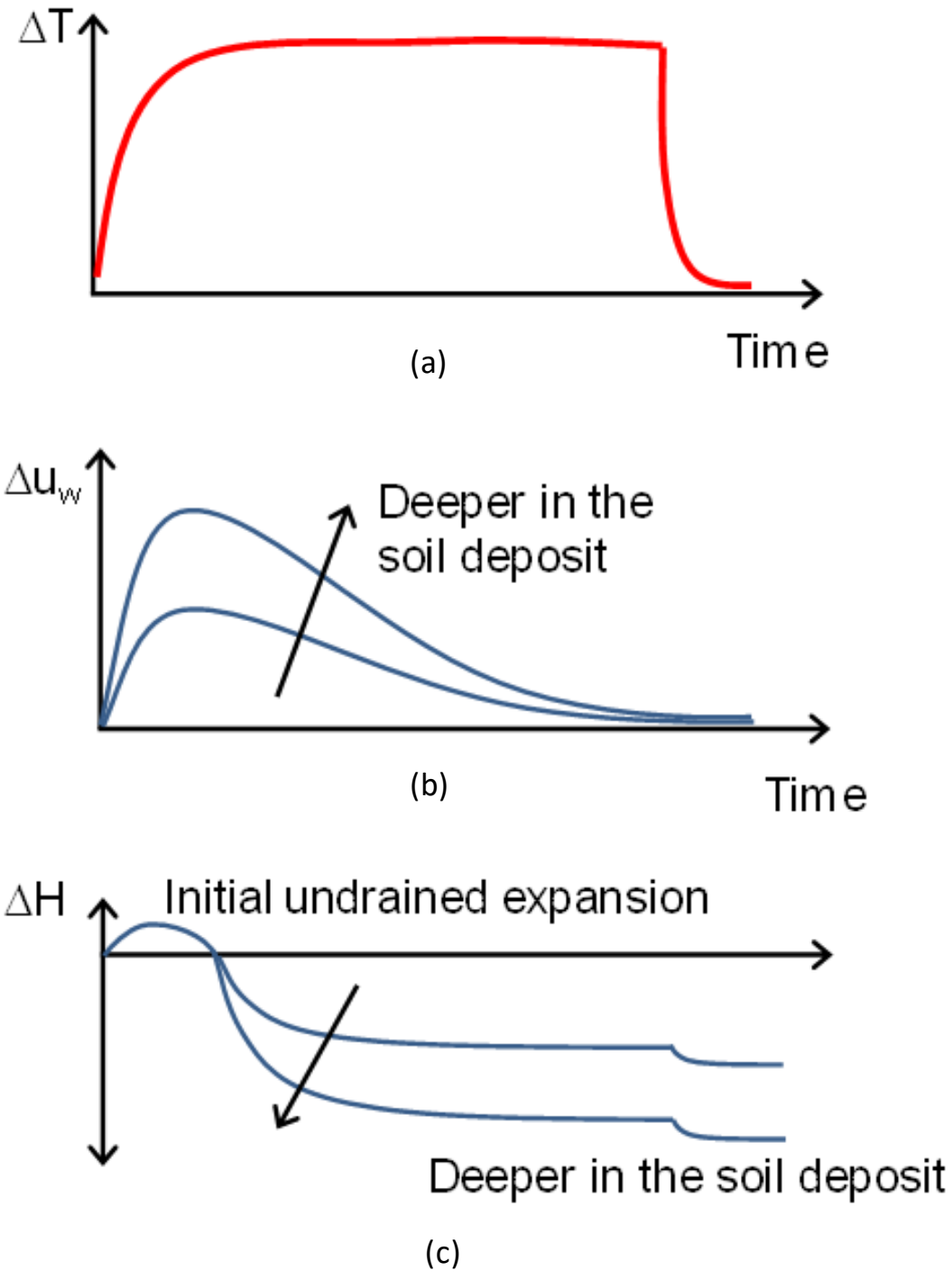

Figure 1.1: Expected time series soil response around the pile during thermal improvement: (a) Temperature versus heating time, (b) Thermal excess pore water pressure versus heating time, (c) Thermal strain versus heating time

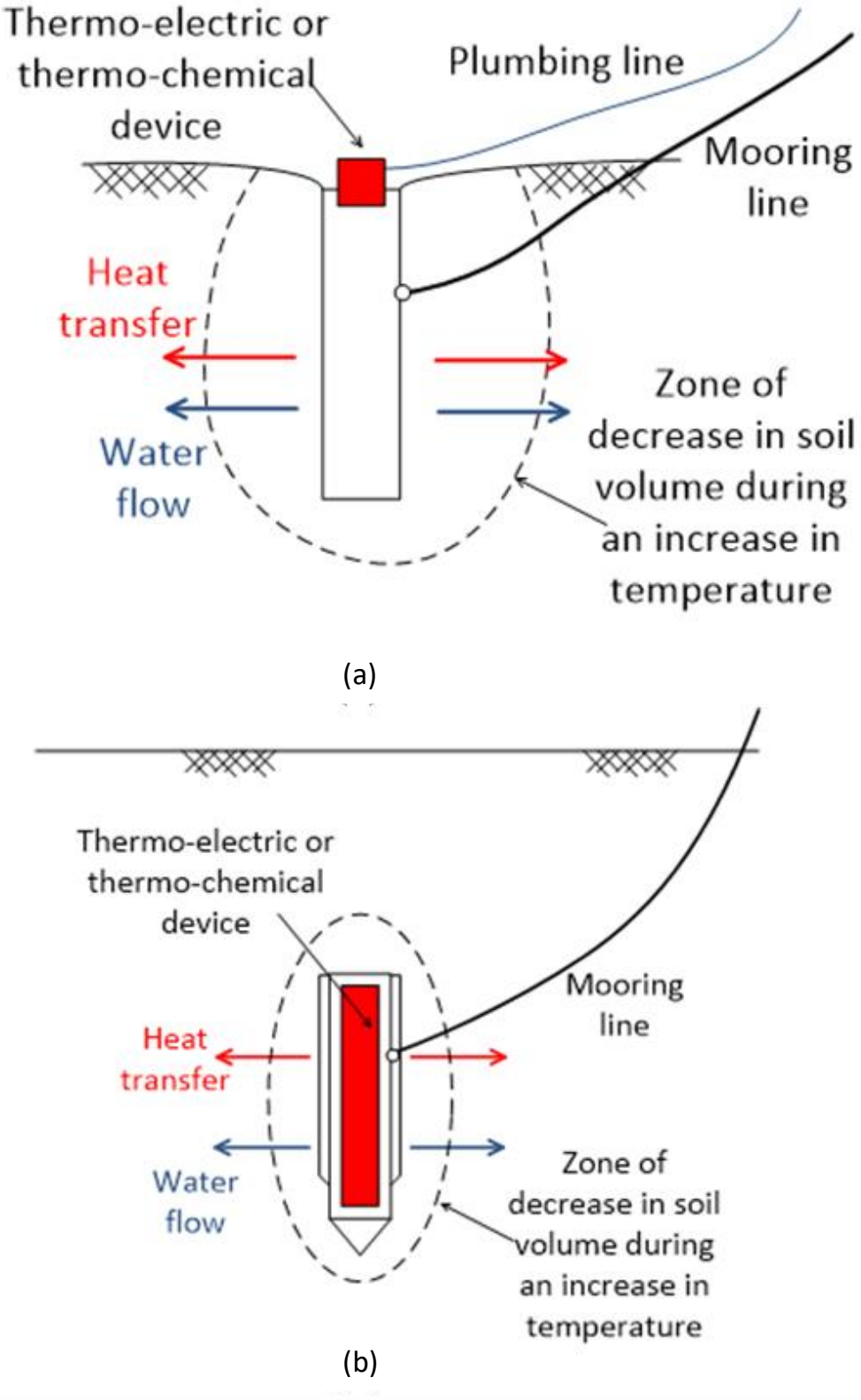

Figure 1.2: Examples of offshore foundations during in-situ thermal improvement of the surrounding soil: (a) Jacked-in pile; (b) Torpedo pile

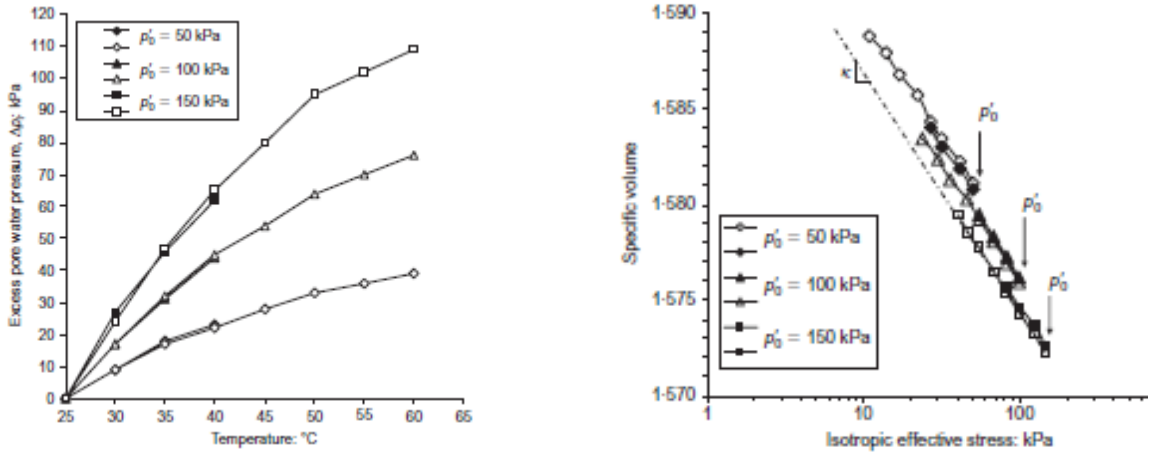

(a) (b)

Figure 1.3: Results from undrained heating of saturated silt (Uchaipichat and Khalili 2009); (a) Excess pore water pressure generation at different initial mean effective stress values; (b) Elastic expansion along the loading-unloading line

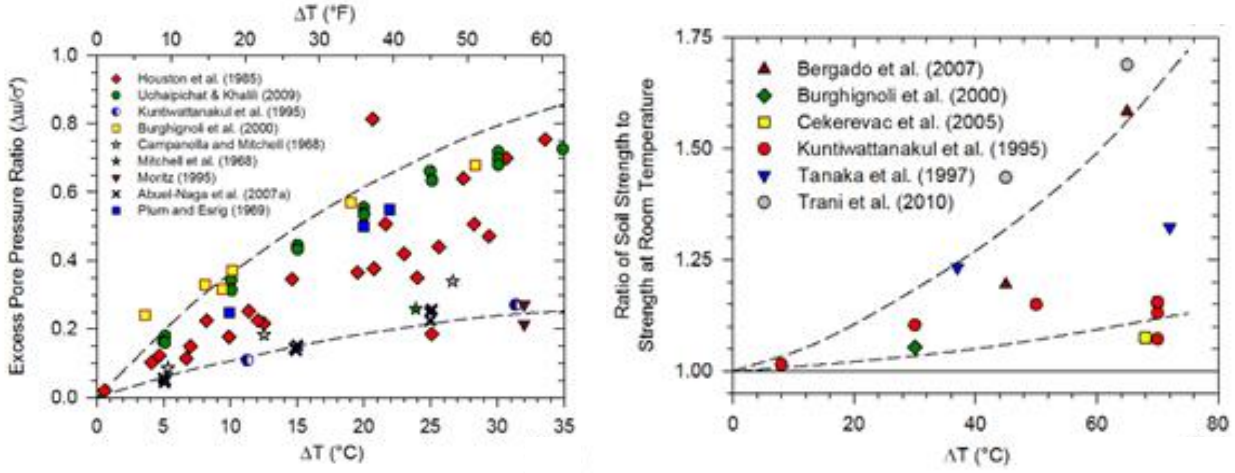

(a) (b)

Figure 1.4: Thermal effects on NC clays from the literature: (a) Thermally-induced excess pore water pressure; (b) Change in undrained shear strength after drainage of thermally induced excess pore water pressures

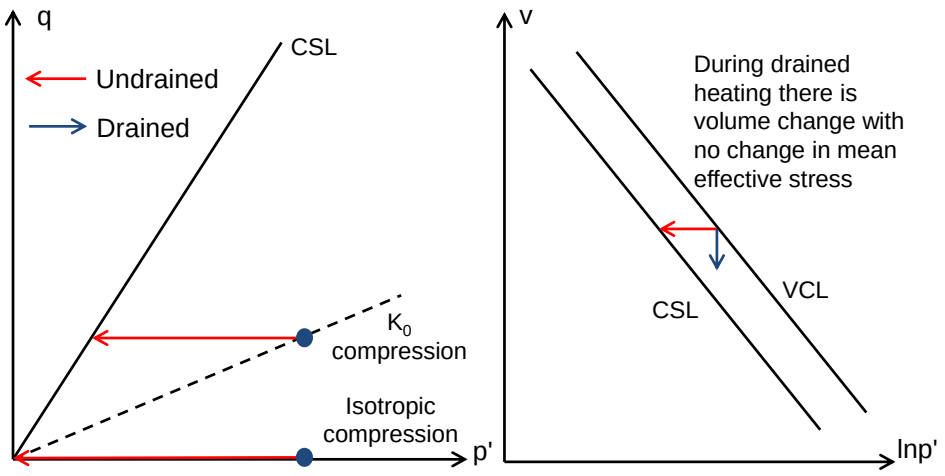

Figure 1.5: Critical state evaluation of thermal instability for different initial stress states during undrained heating

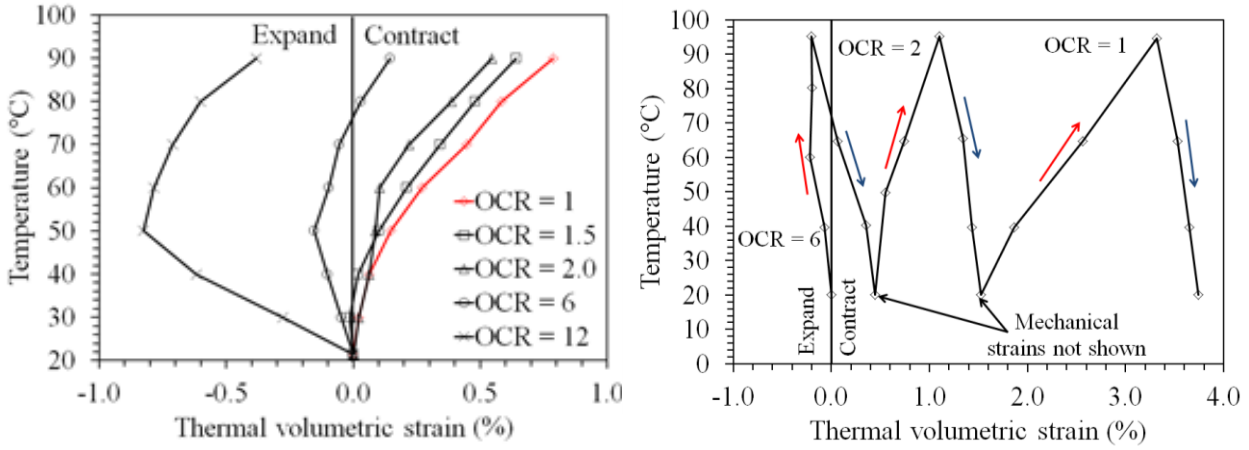

(a) (b)

Figure 1.6: Volumetric strain as a function of temperature: (a) During heating for Kaolinite clay with different overconsolidation ratios (Cekeravac and Laloui 2004); (b) During heating and cooling of Pontida clay for three overconsolidation ratios (Baldi et al. 1998)

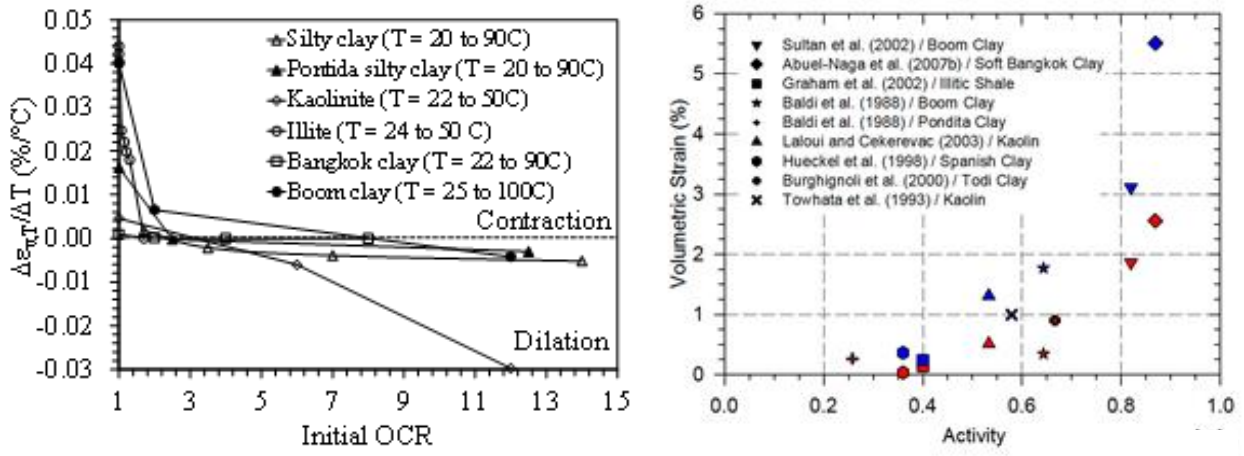

(a) (b)

Figure 1.7: (a) Volumetric strain per change in temperature as a function of OCR for different clays; (b) Volumetric strain as a function of clay activity (ratio of plasticity index to fines content)

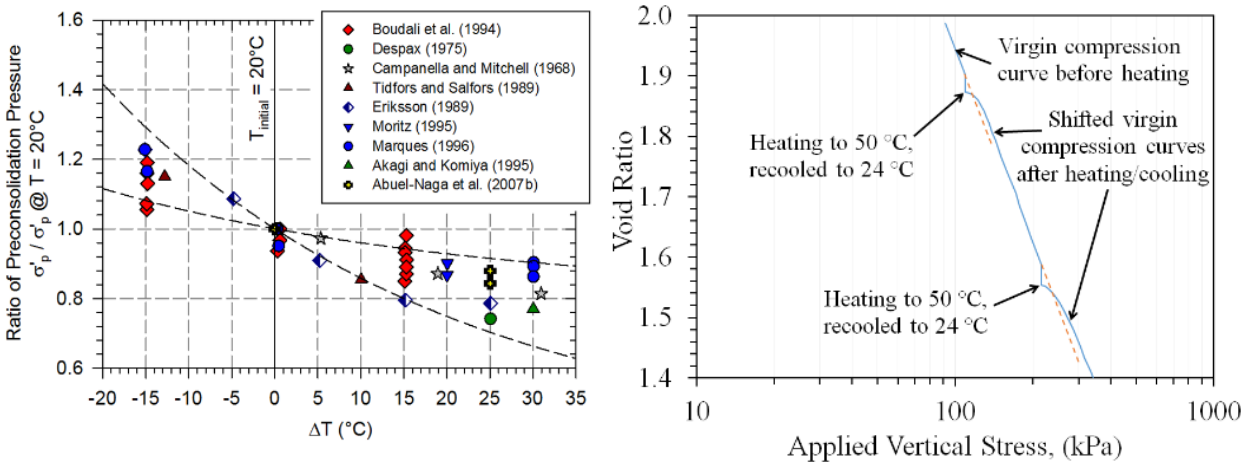

(a) (b)

Figure 1.8: (a) Preconsolidation stress of clays during recompression of initially NC clays that had been heated to different temperatures; (b) Thermal effects on the reloading behavior of initially NC clay after a heating-cooling cycle (Plum and Esrig 1969)

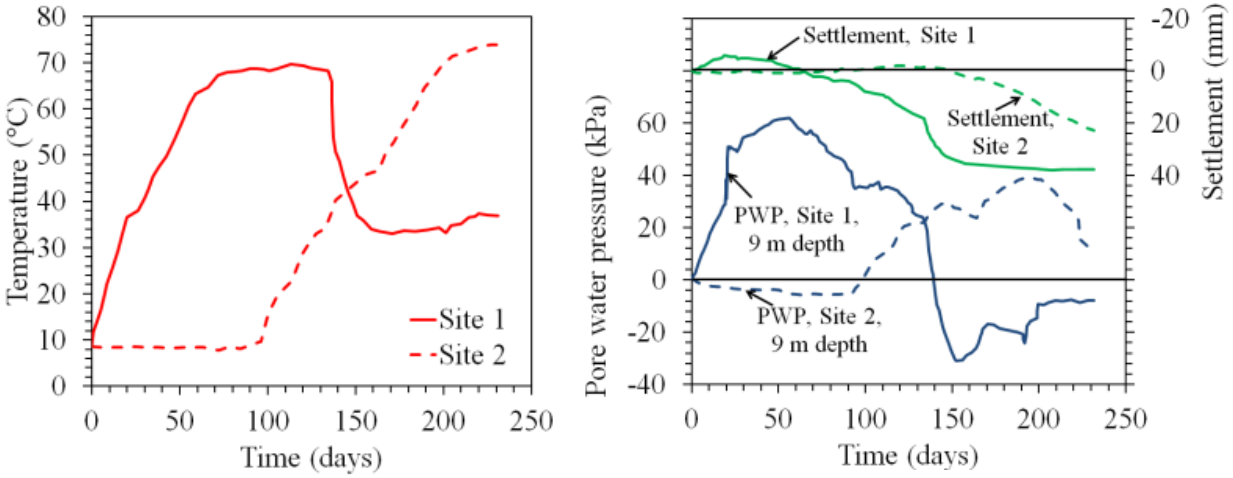

(a) (b)

Figure 1.9: Field evidence of thermal soil improvement (Bergenstahl et al. 1994): (a) Temperature changes; (b) Pore water pressure and surface settlement

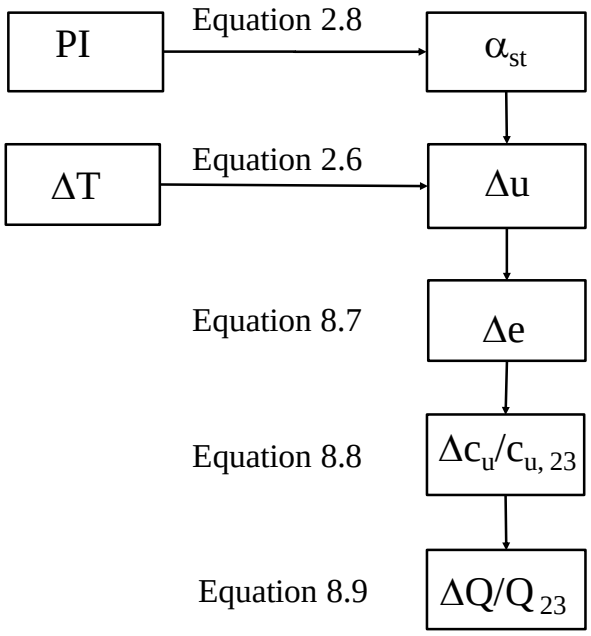

Figure 1.10: Flow chart detailing the combination of uncoupled models to predict the pullout capacity of offhore foundations in soft clays due to thermal improvement

Chapter 2. Prediction of Excess Pore Water Pressure during Undrained Heating of Clays

2.1. Abstract

This chapter focuses on the validation of a prediction model for the thermally induced excess pore water pressure generated in saturated soils during undrained heating. A thermo-elastic analysis was calibrated using experimental data presented in the literature for normally consolidated soils having different mineralogical compositions. The magnitude of thermally induced excess pore water pressure for these soils was observed to depend on the initial void ratio, the initial effective stress, the thermal coefficient of cubical expansion of the soil particles, the change in temperature, the compressibility of the soil skeleton, and the physico-chemical coefficient of structural volume change. An empirical relationship between the physico-chemical coefficient of structural volume change and the plasticity index was proposed to predict the thermally induced excess pore water pressure for saturated, normally consolidated soils. To validate the model, an undrained heating test was performed independently on a specimen of normally consolidated Kaolinite clay, and the measured thermally induced excess pore water pressures were found to match well with the model predictions.

2.2. Introduction

As a measure for preconsolidation of soft clay layers, incorporation of thermal energy from embedded geothermal heat exchangers with vertical drains can be effective to prepare a site for subsequent foundation or embankment loading, and for mitigating seismic amplification potential of deep clays sites because consolidation of the layers can be induced by expansion of heated water without surcharge from the surface. Since pore water pressures will increase in the clay depending on the change in temperature induced by conductive heat flow away from the drain, the excess

pore water pressure will dissipate geometrically away from the drain, as well as toward the free drainage boundary of the drain itself. As the magnitude of permanent contraction by heating significantly affects the thermal changes of clay in strength and hydraulic conductivity, it is important for the engineers to preliminarily predict the magnitude of excess pore water pressure generated by temperature change.

This paper is focused on predicting the magnitude of excess water pressure generated in clays during undrained heating. This information is needed for the engineering design of thermal drain systems that are used to improve the response of soft clays (Abuel-Naga et al. 2006; Salager et al. 2012). Many researchers have evaluated the undrained heating response of different types of clays under different stress states such as Campanella and Mitchell (1968), Plum and Esrig (1969), Houston et al. (1985), Moritz (1995), Burghignoli et al. (2000), Abuel-Naga et al. (2007), and Uchaipichat and Khalili (2009). Although Campanella and Mitchell (1968) developed an approach to estimate the magnitude of change in excess pore water pressure for a given change in temperature using concepts of thermo-elasticity and linear elasticity, some of the parameters in their analysis are not straightforward to define. A relationship was proposed between the key unknown parameters governing thermal excess pore water generation and the geotechnical index properties of soils using data reported in the studies mentioned above. Undrained heating triaxial tests were performed to measure the thermally induced excess pore water pressure under undrained heating conditions of Kaolinite clay and validate the developed relation in this study with experimental test results. Images were taken by using high resolution camera to observe the specimen volume changes during the heating.

2.3. Theoretical Background

Campanella and Mitchell (1968) developed a theoretical approach to estimate the excess pore water pressure generation in a specimen of saturated soil during undrained heating using the concepts of thermo-elasticity and linear elasticity. Specifically, to ensure compatibility of strains during undrained heating, the sum of the changes in volume of the soil constituents due to changes in both temperature and pressure must equal the sum of the volume changes of the total soil mass during changes in temperature ΔT and pore water pressure Δu, as follows:

$$\alpha_w V_w \Delta T + \alpha_s V_w \Delta T - (\Delta V_{st})_{\Delta T} = - m_v V_m \Delta u - m_w V_w \Delta u \quad (2.1)$$

where α_w is the cubical coefficient of thermal expansion of the pore water, α_s is the cubical coefficient of thermal expansion of the mineral solids, V_w is the initial volume of pore water before heating, V_s is the volume of solids, V_m is the total volume of the soil mass equal to the sum of V_w and V_s, ΔT is the change in temperature of the soil, Δu is the change in pore water pressure, $(\Delta V_{st})_{\Delta T}$ is the volume change of the soil due to the reorientation and relative movement of the soil particles during heating, m_w is the coefficient of volume compressibility of water and m_v is the coefficient of volume compressibility of soil skeleton. The coefficient of volume compressibility is conventionally defined as the volumetric strain divided by the change in vertical effective stress. However, in this study it is defined as the volumetric strain divided by the change in mean stress, as isotropic conditions are assumed. The compressibility of the water is assumed to be negligible compared to the value of compressibility of the soil skeleton. As the porosity of a saturated soil is equal to $n = V_w/V_m$, Equation 2.1 can be rearranged to estimate the excess pore water pressure generated by a change in temperature during undrained conditions, as follows:

$$\Delta u = \frac{n \Delta T (\alpha_s - \alpha_w) + \frac{(\Delta V_{st})_{\Delta T}}{V_m}}{m_v + n \cdot m_w} = \frac{n \Delta T (\alpha_s - \alpha_w) + \alpha_{st} \Delta T}{m_v + n \cdot m_w} \quad (2.2)$$

For most soils, the value of m_v is much greater than $n \cdot m_w$ (Campanella and Mitchell 1968), so Equation 2.2 can be simplified as follows:

$$\Delta u = \frac{n\,\Delta T\,(\alpha_s - \alpha_w) + \alpha_{st}\Delta T}{m_v} \tag{2.3}$$

2.4. Estimation of Soil Properties for Pore Water Pressure Prediction

Evaluation of Equation 2.3 indicates that the factors affecting the change in pore water pressure change of saturated soil during undrained heating are the magnitude of the temperature change, the porosity, the difference between the coefficients of thermal expansion for soil grains and water, and the physico-chemical coefficient of the structural volume change. Of these different factors, most can be readily estimated for the soils reported in the literature except for the physico-chemical coefficient of the structural volume change. Specifically, the compressibility of the soil skeleton m_v can be estimated from the compression curve, the values of porosity can be calculated using the initial gravimetric water content and specific gravity, the value of α_s depends on the clay mineral, and α_w is a constant. The values of α_s and α_w used by most researchers such as Campanella and Mitchell (1968), Burghignoli et al. (2000) were equal to 0.000035/°C and 0.00017/°C, respectively. The value of α_s does not vary significantly for the tests on different clay minerals reported in the literature, so the value used by Campanella and Mitchell (1968) can be used to analyze the results from other clays. It is important to clarify that the value of α_w is an order of magnitude greater than α_s, which is one of the primary reasons for the pore water pressure change in saturated clays. However, because the difference between these two parameters is similar for most clays, there must be another parameter that affects the thermal volume change of clays.

Regarding the estimation of the value of m_v from the compression curve, Mitchell and Campanella (1968) and Uchaipichat and Khalili (2009) found that a saturated soil will expand

along the recompression line during undrained heating. On this basis, the value of m_v can be determined from the isotropic recompression curve $(m_v)_r$ at a given value of mean effective stress, as follows:

$$(m_v)_r = \frac{1}{1+e_o}\frac{\kappa}{p'} \tag{2.4}$$

where κ is the slope of the isotropic recompression line which is equal $\Delta v/\Delta \ln p'$, e_0 is the initial void ratio, and p' is the mean effective stress. As the slope of the isotropic compression line is more commonly reported than the isotropic recompression line in studies on the thermal volume change of normally consolidated soils, the value of κ can be assumed to be related to the slope of the isotropic compression line λ using the ratio $\Lambda = (1-\kappa/\lambda)$. The ratio Λ is typically ranges from 0.7 to 0.9 for low plasticity clays (Schofield and Wroth 1984), and a value of 0.9 was used when the actual value of κ was not reported. Equation 2.3 can be rewritten in the following form after incorporating the definition of mv, and the ratio Λ , as follows:

$$\Delta u\left(\frac{1}{1+e_o}\right)\frac{(1-\Lambda)\lambda}{p'} = n\,\Delta T(\alpha_s - \alpha_w) + \alpha_{st}\,\Delta T \tag{2.5}$$

This equation can be solved for the ratio of the pore water pressure to the initial mean effective stress p'_0 before the start of undrained heating, as follows:

$$\frac{\Delta u}{p'_0} = \frac{[n(\alpha_s - \alpha_w) + \alpha_{st}]\,(1+e_o)\Delta T}{(1-\Lambda)\,\lambda} \tag{2.6}$$

This equation confirms that the magnitude of thermally induced excess pore water pressure depends on the initial mean effective stress, a trend that is clear in the data presented in several studies like Uchaipichat and Khalili (2009). The remaining parameter that is not straightforward to estimate for a clay soil is the value of the physico-chemical coefficient α_{st}, which may depend on several parameters. For a normal consolidated clay, it is expected that this parameter depends

primarily on the soil mineralogy. Accordingly, the values of α_{st} can be estimated from the Δu data reported for a given ΔT by the different studies in the literature, as follows:

$$\alpha_{st} = \left[\frac{\Delta u}{p'_0} \cdot \frac{(1-\Lambda)\,\lambda}{1+e_o} \cdot \frac{1}{\Delta T}\right] - n(\alpha_s - \alpha_w) \quad (2.7)$$

2.5. Thermal Soil Response

Data from undrained heating tests on saturated soils collected from the literature are investigated in this study. Properties of the soil specimens are shown in Table 2.1. The Atterberg limits for these clays vary widely (liquid limit LL ranging from 21 to 186 and plasticity index PI ranging from 6 to 109), and the coefficient of compressibility indicates that the soils range from soft (high λ) to stiff (low λ). The liquidity index is greater than 1.0 for many of the soils listed below, indicating that they are wetter than the liquid limit and could have a sensitive response. A summary of the 13 normally-consolidated soil specimens under investigation from these different studies is shown in Table 2.2, along with the initial mean effective stress at the start of heating of each soil specimen. The soils were all heated by different magnitudes, with the greatest change in temperature being approximately 80 °C.

The results of the change in pore water pressure with change in temperature are shown in Figure 2.1 for the different soil specimens listed in Table 2.2. Due to the difference in the thermal expansion coefficient of water and soil particles, the change in pore water pressure increases with increasing change in temperature. The excess pore water pressure induced by the change in the temperature normalized by the initial effective stress is shown in Figure 2.2. The spread in the normalized pore water pressure changes is lower than the raw changes in pore water pressure shown in Figure 2.1. The initial mean effective stress plays an important role, as the stiffness of the soil skeleton is expected to increase with increasing mean effective stress which may affect the pore water pressure generation during heating. The results in Figure 2.2 imply that greater pore

water pressures will be expected deeper in a soil deposit. Further, evaluation of the results in Figure 2.2 indicates that, for most soils, the thermally induced pore water pressure is greater than half the mean effective stress during a change in temperature of 35 °C. The normalized pore water pressures were consistently less than 1.0, which confirms that thermal failure did not occur in the specimens evaluated in this study.

2.6. Data Synthesis

The values of α_{st} were calculated using Equation 2.7 for each of the data points in Figure 2.2. As there is some scatter in the increase in pore water pressure with temperature for the soil specimen (SPC2), the average value was obtained for this soil specimen. The trend between the average values of α_{st} and the plasticity index (PI) for the different soil specimens listed in Table 2.2 is shown in Figure 2.3. The only study that reported a value of α_{st} was Campanella and Mitchell (1968), who reported a value of 0.00005/°C for SPC1. This value is slightly different from the value of 0.0006/°C calculated for SPC1 using Equation 2.7 and the normalized changes in pore water pressure for this soil shown in Figure 2.2. However, they used the results from drained thermal consolidation tests to estimate the value of α_{st}, and observed a discrepancy when using their value of α_{st} to predict the change in pore water pressure observed during a separate undrained heating test. This may have been due to experimental differences between their drained and undrained heating tests. Further, as noted in, Table 2.1Campanella and Mitchell (1968) did not report Atterberg limits, so the average PI for a pure Illite reported by Mitchell (1993) was used in plotting Figure 2.3. The trend in Figure 2.3 shows the PI has significant effect on the α_{st}. Although there is some scatter, the value of α_{st} decreases nonlinearly with PI. This is especially clear for specimens SPC2 and SPC3 which have very different PI values but were tested under the same initial effective stress and the same testing conditions. Comparison of the values of the α_{st} for the

soils that were tested at different initial effective stresses (Houston et al. 1985; Uchaipichat and Khalili 2009; Abuel-Naga et al. 2007) indicates that the initial effective stress does not have a major effect on the value of α_{st}. The small differences for the same soils tested under different effective stresses are due to scatter in the reported experimental changes in pore water pressure with temperature.

The effect of the liquidity index LI on the physico-chemical coefficient was studied as well, as this parameter may permit assessment of the role of sensitivity on the thermal volume change. This was performed as several of the clays in the literature had relatively high water contents compared to the liquid limit. The relationship between the physico-chemical coefficient α_{st} and LI is shown in Figure 2.4. Although no clear trend was observed for the specimens evaluated, it is interesting to note that the specimens with liquidity index values greater than 1.0 had relatively high values of α_{st} As the trends with the plasticity index was found to be the most significant, a best-fit empirical relation between the plasticity index and the physico-chemical coefficient α_{st} was fit to the data as shown in Figure 2.5. The empirical relationship can be expressed as follows:

$$\alpha_{st} = 1.0\times10^{-4}\, e^{-0.014\ PI} \tag{2.8}$$

Despite the scatter in the data and the low R^2 value, the empirical expression provides a reasonable representation of the trend in the data. Equation 2.8 may be useful in providing preliminary estimates of the change in pore water pressure during undrained heating of soils.

2.7. Validation of the Model

2.7.1. Materials and Specimen Preparation

To validate the prediction of the value of α_{st} for a soil in the prediction of the thermally induced pore water pressure, an independent experiment was performed on a saturated, normally consolidated clay specimen. Commercial Kaolinite clay from M&M Clays Inc., McIntyre, Georgia

was used for the experiment. The geotechnical properties of the clay are summarized in Table 2.3 As the clay has a liquid limit and plastic index of 47 and 19, respectively, it is classified as CL according to the Unified Soil Classification Scheme (USCS) medium plasticity. The clay has a specific gravity of 2.6.

The Kaolinite clay layer was prepared by mixing the Kaolinite clay powder and deionized water in a vacuum mixer to form a slurry with a water content of 135%. The slurry was then slowly poured into a 242 mm-diameter acrylic cylinder with a porous stone and filter on the top and bottom of the specimen. The clay layer was consolidated using a compression frame at a constant rate of 0.04 mm/min for 48 hours. After this point, constant vertical stresses of 124, 248, and 352 kPa were applied to the clay layer in 24-hour increments. The preconsolidated clay layer was extruded from the cylinder and divided into four equal pieces. One of these pieces was then trimmed into a cylindrical specimen having a diameter of 72.4 mm and a height of 147.3 mm. The specimen was then placed into the thermal triaxial cell for testing. The water content and initial void ratio values after consolidation but before application of a change in the temperature are also summarized in Table 2.3

2.7.2. Equipment and Procedures

The test was performed by using a modified triaxial system originally developed by Alsherif and McCartney (2013, 2015). A schematic of the system is shown in Figure 2.6. The cell is comprised of a Pyrex pressure vessel that has the advantage of having low thermal creep behavior while remaining transparent after repeated heating and cooling cycles. The temperature within the cell is controlled by circulating heated water from a heated water bath through a stainless-steel pipe bent into a “U” shape over the specimen. A solar pump is used to circulate the cell water to ensure that it is uniformly mixed, and a thermocouple is used to monitor the cell

temperature changes. A pore water pressure transducer is used to monitor the pore water pressure during undrained heating. The cell fluid temperature was monitored using a thermocouple and temperature recorder having a precision of 0.5 °C. The cell pressure and backpressure were controlled using a pressure panel.

The testing procedure first involved back-pressure saturation of the specimen, which was performed by applying the cell pressure and backpressure in stages until reaching a value of Skempton's pore water pressure parameter B of 0.98 while maintaining a constant seating mean effective stress of 69 kPa. The specimen was then consolidated isotropically to a mean effective stress of 414 kPa, which corresponds to normally consolidated conditions. After this point, the specimen was heated in undrained conditions from 23 °C to 54 °C in 5 to 10 °C increments. Each increment was maintained until the pore water pressure stabilized. The heating rate to change from increment to other is approximately 1.3 °C/ hr. During the heating process, images of the specimen were taken using a high-resolution camera (model D610 from Nikon) to measure changes in volume of the specimen throughout the test.

2.7.3. Experimental Results and Analysis

The experimental results from the undrained heating test were illustrated in Figure 2.7. The thermally induced excess pore water pressure was observed to increase linearly with the change in temperature for the normally consolidated Kaolinite clay. The physico-chemical coefficient ($\alpha_{st} = 7.7\times10^{-5}$ 1/°C) was calculated using Equation 2.8, which was then used to predict the pore water pressure as a function of temperature using Equation 2.3. The predicted thermally induced pore water pressure is also shown in Figure 2.7. Good correspondence between the experimental and predicted pore water pressures for the normally consolidated Kaolinite clay are observed. Also, the physico-chemical coefficient was calculated by Equation 2.8 using the measured pore water

pressure (α_{st} = 9.1×10^{-5} 1/°C). This observation confirms that the proposed empirical equation can be used to predict generation of pore water pressure during heating, and the magnitude can be determined by basic properties of soils and knowledge of the current stress condition without having to perform complex experiments. Images were taken during the test to measure the effect of the temperature change on the specimen volume. The specific volume plotted against the mean effective stress (calculated as the initial effective stress minus the thermally induced pore water pressure) at temperatures of 24, 40.5, and 53 °C is shown in Figure 2.8. The specific volume increased with temperature along the elastic recompression curve (κ= -0.0136). The compression curve with an unloading cycle for the Kaolinite clay (measured from the isotropic consolidation test done on the same sample) is also shown in this figure, and the value of κ from the recompression curve is similar to that from the undrained heating test. This confirms the choice of κ in the definition of the physico-chemical coefficient of structural volume change in Equation 2.4.

2.7.4. Role of Stress History in Pore Water Pressure Prediction

Although the model for the physico-chemical coefficient in Equation 2.8 was developed using tests on soils under normally consolidated conditions, it may also be possible to apply use this parameter to predict the thermally induced pore water pressures in overconsolidated soils. When unloading a normally consolidated soil along the recompression curve, the void ratio will increase and the value of p' will decrease. These two variables play a key role in the predicting the thermally induced pore water pressure using Equation 2.6. Relatively few studies have investigated the thermally induced pore water pressure in overconsolidated clays. In addition to investigating the effects of temperature on the pore water pressure in normally consolidated Bangkok clay specimens, Abuel-Naga et al. (2007) also evaluated the behavior of overconsolidated specimens. Their experimental results were compared with the prediction from Equation 2.6 using the same

value of α_{st} as that defined for the normally consolidated specimens, but with different values of initial void ratio and initial effective stress. The comparison is shown in Figure 2.9. A good match was obtained for the specimens as the OCR increases, which confirms the flexibility of the model in considering different stress states.

2.8. Conclusions

A prediction model for the thermally induced pore water pressure was proposed and experimentally validated in this study. Normalized pore water pressures measured during changes in temperature during undrained heating tests on soil specimens reported in the literature were used to calculate the physico-chemical coefficient. Normalization of the pore water pressures helped remove the effects of the initial effective stress from the analysis, and specimens of the same soil tested under different initial mean effective stresses had similar physico-chemical coefficients of structural volume change. Relationships between the calculated values of the physico-chemical coefficient and the plasticity index and liquidity index were investigated. Although a nonlinear decreasing trend was observed with the plasticity index, no trend was observed with the liquidity index. A prediction model was proposed based on an empirical relationship between the physico-chemical coefficient of structural volume change and plasticity index. The pore water pressure values predicted by this model for Kaolinite clay were matched well with those measured in an independent undrained heating test. This confirms that this simple, empirical approach to define the physico-chemical coefficient in the thermo-elastic model is effective in making preliminary estimates of the thermally induced pore water pressures expected in saturated soils used in thermal soil improvement or in thermally active geotechnical engineering systems. The thermal expansion of the specimen calculated using image analysis was found to match well with the slope of the recompression curve, confirming the assumption of the magnitude of the coefficient of volume

compressibility used in the analysis. Although only limited data is available in the literature for overconsolidated clays, the validated model was found to also provide a good fit to the thermally induced pore water pressure in saturated, overconsolidated clays.

2.9. Acknowledgements

Chapter 2.2, in full, has been published as it appears in the following journal publication (The dissertation author was the primary investigator and author of this paper):

Ghaaowd, I., Takai, A., Katsumi, T. and McCartney, J.S. (2016). "Pore water pressure prediction for undrained heating of soils." Environmental Geotechnics. 1-9. 10.1680/jenge.15.00041.

Table 2.1. Properties of the soil specimens reported in the literature.

Reference	Soil Type	e_0	w (%)	LL	PI	λ	Main Minerals
Campanella and Mitchell (1968)	Remolded Illite Clay	0.90	34	94*	62*	0.39	Illite
Plum and Esrig (1969)	Newfield Clay	0.50	18	25	11	0.09	Chlorite, Mica
Houston et al. (1985)	Illite Clay	2.90	111	88	47	0.43	Quartz, Illite
Houston et al. (1985)	Pacific Smectite Clay	3.70	138	186	109	0.52	Smectite, Illite
Abuel-Naga et al. (2007a)	Bangkok Clay	2.50	93	103	60	0.46	Smectite, Kaolinite, and Mica
Uchaipichat and Khalili (2009)	Bourke Silt	0.70	26	21	6	0.09	Not reported
Burghignoli et al. (2000)	Todi Clay	0.89	40	52	30	0.1	Montmorillonite, Illite, Kaolinite, Calcite, Quartz
Burghignoli et al. (2000)	Fiumicino Clay	0.81	30	55	32	0.09	Not reported

*Note: Values not reported in the original study, the values shown here are for a typical pure Illite clay

Table 2.2. The numbers designations for the soil specimens evaluated in the study.

Specimen Number	Soil Type	p' (kPa)
SPC1	Remolded Illite Clay	196
SPC2	Pacific Smectite-Rich	98
SPC3	Illite Clay	98
SPC4	Illite Clay	29
SPC5	Bourke Silt	50
SPC6	Bourke Silt	100
SPC7	Bourke Silt	150
SPC8	Bangkok Clay	200
SPC9	Bangkok Clay	300
SPC10	Bangkok Clay	400
SPC11	Todi Clay	196
SPC12	Fiumicino Clay	147
SPC13	Newfield Clay	275

Table 2.3. Properties and initial conditions of the Kaolinite clay specimens evaluated in this study.

Liquid limit, LL	47
Plastic limit, PL	28
Plasticity index, PI	19
Initial gravimetric water content, w_0 (%)	31
Specific gravity, G_s	2.6
Initial void ratio, e_0	0.81
Initial porosity, n_0	0.45

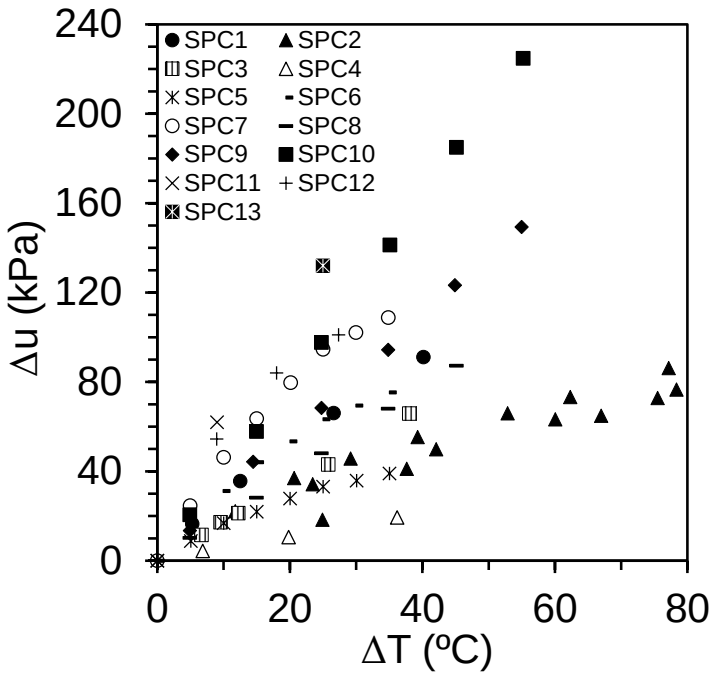

Figure 2.1. Effect of temperature change on the change in pore water pressure for all soils.

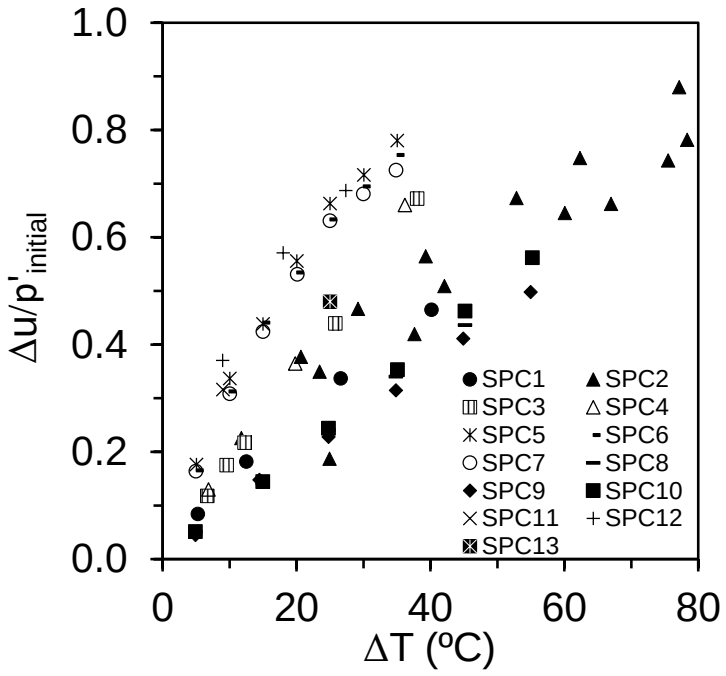

Figure 2.2. Effect of temperature change on the change in pore water pressure normalized by the initial effective stress for all soils specimens.

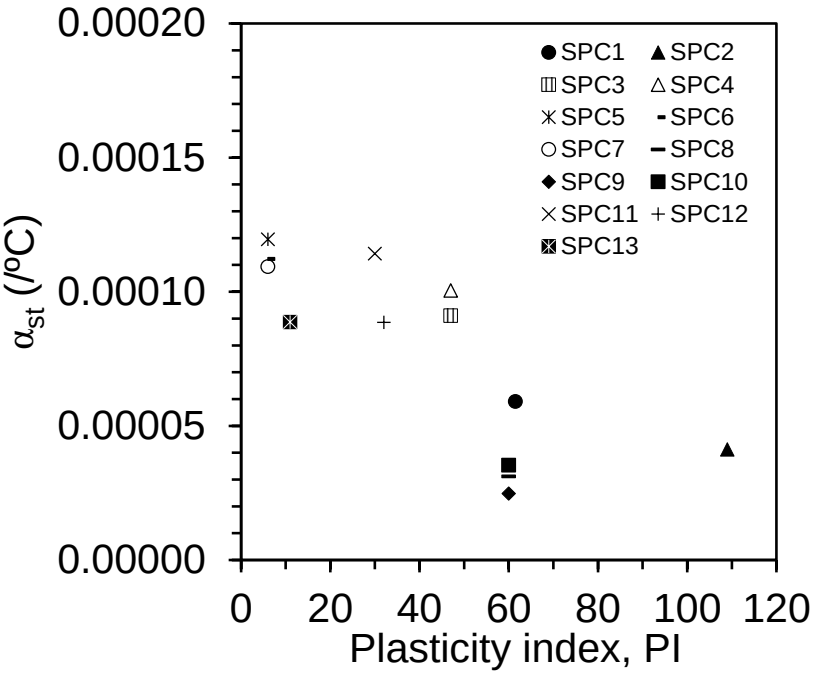

Figure 2.3. Physico-chemical coefficient values as a function of plasticity index for different normally consolidated clays.

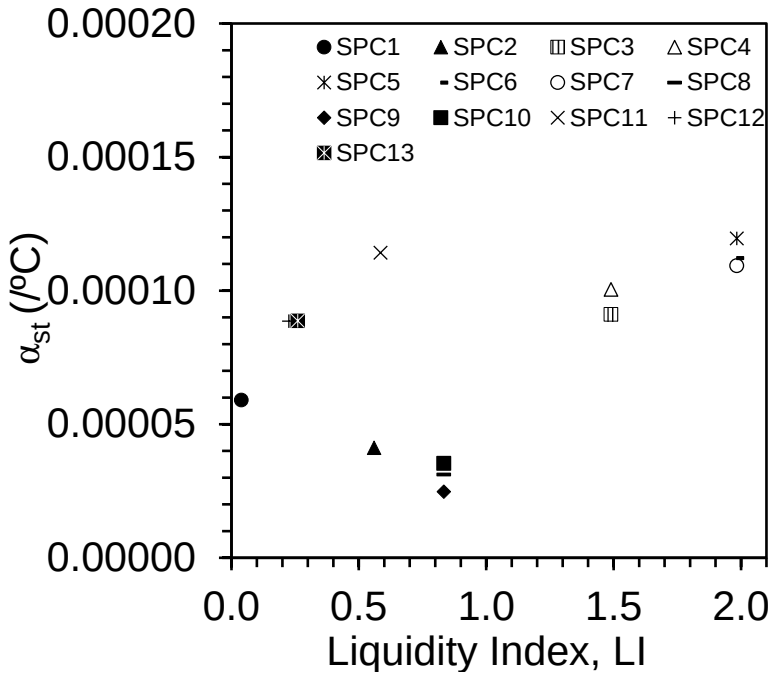

Figure 2.4. Physico-chemical coefficient as a function of liquidity index for different normally consolidated clays from the literature.

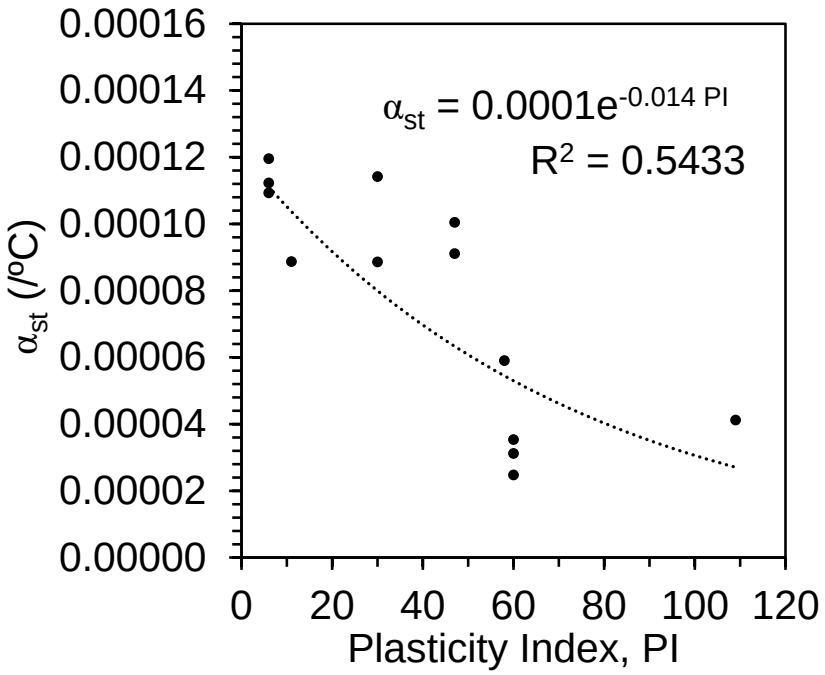

Figure 2.5. Physico-chemical coefficient as a function of plasticity index for different clays from the literature.

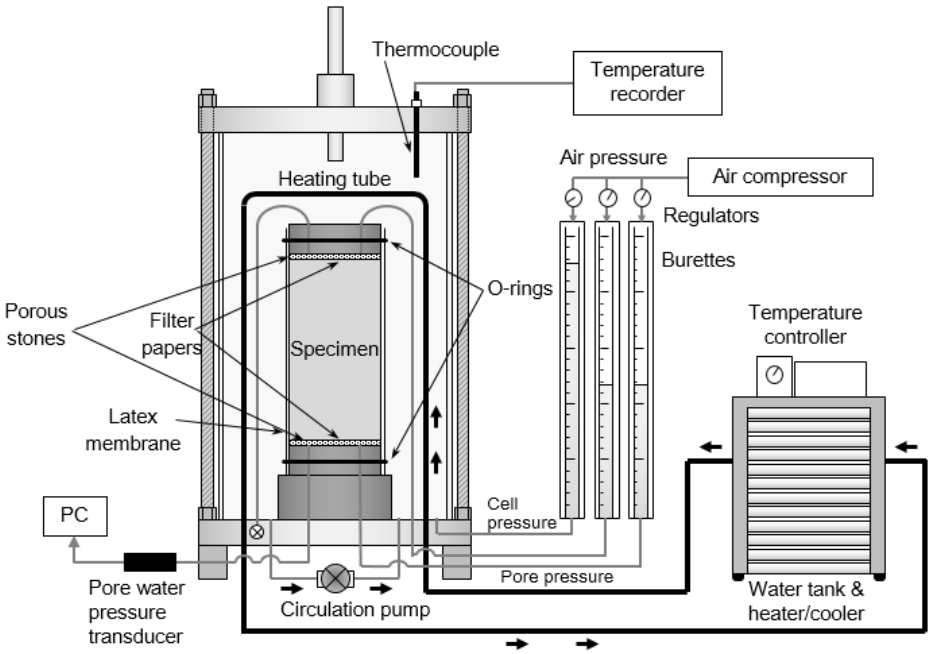

Figure 2.6. Thermal triaxial cell schematic.

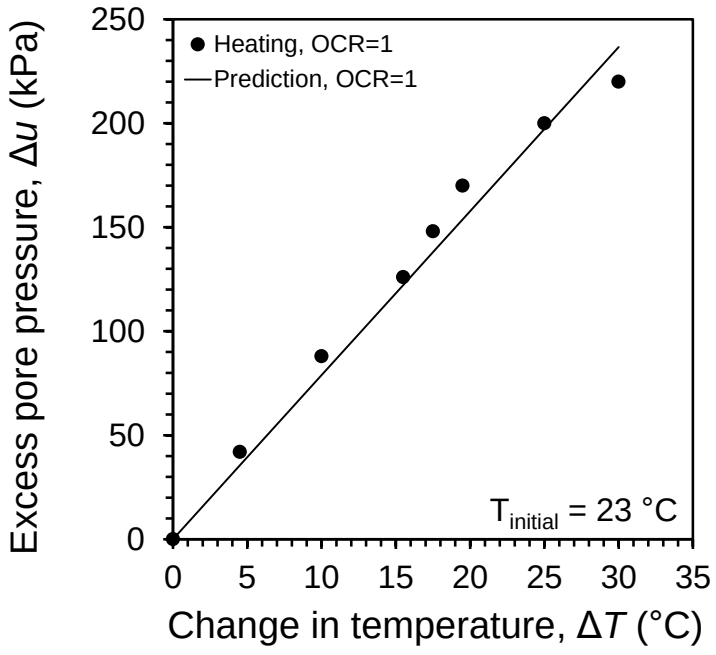

Figure 2.7. Effect of temperature change on the change in pore water pressure for Kaolinite clay along with the predicted trend using the estimated value of the physico-chemical coefficient of structural volume change.

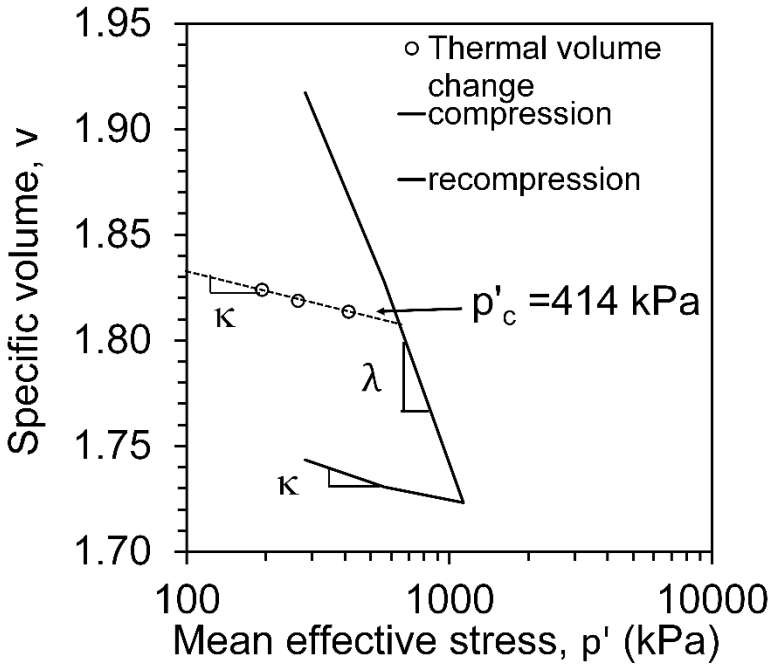

Figure 2.8. Specific volume against isotropic effective stress during heating

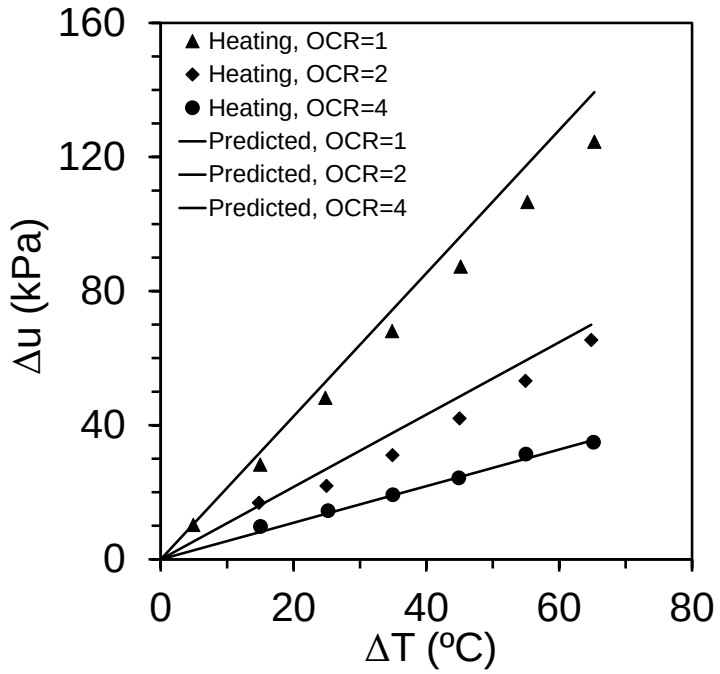

Figure 2.9. Impact of temperature change on the change in pore water pressure in Bangkok clay specimens having different OCRS along with predicted pore water pressure trends.

Chapter 3. Impact of Drainage Conditions on Thermal Volume Change of Soft Clay

3.1. Abstract

This study focuses on an evaluation of the thermal volume change of normally-consolidated Kaolinite clay under drained and undrained conditions. For both drained and undrained conditions, separate clay specimens were heated in a modified triaxial test setup from ambient temperature (23°C) to approximately 60 °C and subsequently cooled. In both tests, the thermal volume change of the clay specimen was inferred using image analysis. As expected, plastic contraction was observed during the test with drained conditions and elastic expansion was observed during the test with undrained conditions. The thermally induced excess pore water pressure during the test with undrained conditions were measured and compared with predicted values from a mechanistic model. The pore water pressures were then used to predict the thermal volume change of the drained specimen using a consolidation analysis.

3.2. Introduction

A clear understanding for the effect of temperature on the soil behavior is needed in many geotechnical engineering applications, such as design of deep repositories of radioactive waste (Gens et al. 2010), energy piles (Murphy and McCartney 2015), thermal ground improvement (Abuel-Naga et al. 2006) and thermally-active geotechnical systems (Coccia and McCartney 2013; Stewart et al. 2014). These applications have led to increasing considerations of the temperature effects on the engineering properties of soils and have made the thermo-mechanical behavior of soils as one of the major issues in latest geotechnical engineering.

The aim of this research is to study the thermo-mechanical behavior of normally-consolidated Kaolinite clay under temperatures up to approximately 60 °C. Laboratory test

program using modified triaxial test covered the effect of temperature on the thermally induced pore water pressure generation in undrained condition and thermally induced volume change in drained condition. The thermally induced volume change was compared with recompression curve obtained from isotropic consolidation in the triaxial cell.

3.3. Prediction of Excess Pore Water Pressure

Campanella and Mitchell (1968) developed a theoretical approach to estimate the excess pore water pressure generation in a specimen of saturated soil during undrained heating using the concepts of thermo-elasticity and linear elasticity. Specifically, to ensure compatibility of strains during undrained heating, the sum of the changes in volume of the soil constituents due to changes in both temperature and pressure must equal the sum of the volume changes of the total soil mass during changes in temperature ΔT and pore water pressure Δu. On this basis, the excess pore water pressure generated by a change in temperature during undrained conditions can be expressed as follows:

$$\Delta u = \frac{n\Delta T(\alpha_s - \alpha_w) + \alpha_{st}\Delta T}{m_v} \tag{3.1}$$

where n is the porosity of a saturated soil, α_w is the cubical coefficient of thermal expansion of the pore water, α_s is the cubical coefficient of thermal expansion of the mineral solids, ΔT is the change in temperature of the soil, Δu is the change in pore water pressure, α_{st} is the physico-chemical coefficient of structural volume change, and m_v is the coefficient of volume compressibility. The values of α_s and α_w used by Campanella and Mitchell (1968) were used in this study, and are equal to 0.000035/°C and 0.00017/°C, respectively. The value of α_s does not vary significantly for the tests on different clay minerals reported in the literature, so the value used by Campanella and Mitchell (1968) can be used to analyze the results from other clays. It is

important to clarify that the value of α_w is an order of magnitude greater than α_s, which is one of the primary reasons for the pore water pressure change in saturated clays.

Regarding estimation of the value of m_v, Campanella and Mitchell (1968) and Uchaipichat and Khalili (2009) observed that a saturated soil will expand along the recompression line during undrained heating. On this basis, the value of m_v can be determined from the isotropic recompression curve $(m_v)_r$ at a given value of mean effective stress, as follows:

$$\left(m_v\right)_r = \frac{1}{1+e_0}\frac{\kappa}{p'} \tag{3.2}$$

where κ is the slope of the isotropic recompression line, e_0 is the initial void ratio, and p' is the mean effective stress. The physico-chemical coefficient of soil structural volume change is a coefficient representing the volumetric strain of soil structure due to physico-chemical effects and depends primarily on the soil mineralogy for normally-consolidated clays. Despite the scatter in the data, Ghaaowd and McCartney (2015) proposed an empirical relationship between the physico-chemical coefficient of structural volume change, α_{st}, and the plasticity index, *PI*, as a summary of 13 normally-consolidated soil specimens from these different studies as follows:

$$\alpha_{st} = 1.0\times10^{-4}\cdot e^{-0.014PI} \tag{3.3}$$

3.4. Materials and Specimen Preparation

In this study, commercial Kaolinite clay from M&M Clays Inc., McIntyre, Georgia was used for the experiment. The geotechnical properties of the clay are summarized in Table 3.1. As the clay has a liquid limit of 47% and a plasticity index of 19, the clay is classified as CL according to the Unified Soil Classification Scheme (USCS). The clay has a specific gravity of 2.6. The isotropic compression curve is shown in Figure 3.1. The slopes of the normal compression line (λ) and the recompression line (κ) are equal to 0.1 and 0.016, respectively.

3.5. Experimental Methodologies

3.5.1. Equipment and Procedures

The test was performed by using a modified triaxial system originally developed by Alsherif and McCartney (2013, 2015). A schematic of the system is shown in Figure 3.2. The cell is comprised of a Pyrex pressure vessel that has the advantage of having low thermal creep behavior while remaining transparent after repeated heating and cooling cycles. The temperature within the cell is controlled by circulating heated water from a heated water bath through a stainless steel pipe bent into a "U" shape over the specimen. A solar pump is used to circulate the cell water to ensure that it is uniformly mixed, and a thermocouple is used to monitor the cell temperature changes. A pore water pressure transducer is used to monitor the pore water pressure during undrained heating. The cell fluid temperature was monitored using a thermocouple and temperature recorder having a precision of 0.5 °C. The cell pressure and backpressure were controlled using a pressure panel.

The testing procedure first involved back-pressure saturation of the specimen, which was performed by applying the cell pressure and backpressure in stages until reaching a value of Skempton's pore water pressure parameter B of 0.95 while maintaining a constant seating mean effective stress of 21 kPa, then the specimen was consolidated isotropically to a mean effective stress of 276 kPa. During the drained heating test, the drainage valves at the top and bottom of the specimen were kept open, while during the undrained heating test they were all maintained closed except the one leading to the pore water pressure transducer. In both the tests with undrained and drained conditions, the specimens were heated from 23 °C to approximately 60 °C in 5 to 10 °C increments, and each increment was maintained until the pore water pressure or volume change stabilized. Also, during the drained heating test the outflow drainage was also recorded. Images of

the specimens were taken using a high-resolution camera (model D610 from Nikon) during both the tests to measure changes in volume of the specimen.

3.6. Results and Discussion

3.6.1. Volume Change during Undrained Heating

The thermal volume change of the specimen during undrained heating is shown in Figure 3.3, along with the normal compression and recompression curves from Figure 3.1. During undrained heating, the specific volume was observed to increase with temperature, approximately along the elastic recompression curve ($\kappa = 0.02$). These results verify that the value of κ from the recompression curve is similar to that from the undrained heating test. This confirms the choice of κ in the definition of the physico-chemical coefficient of structural volume change in Equation 3.2.

3.6.2. Excess Pore Water Pressure Generation During Undrained Heating

The change in pore water pressure as a function of the change in temperature is shown in Figure 3.4(a). The same data normalized by the initial mean effective stress is shown in Figure 3.4(b). The thermally induced excess pore water pressure was observed to increase linearly with the change in temperature for the normally consolidated Kaolinite clay. The physico-chemical coefficient ($\alpha_{st} = 7.7\times10^{-5}$ 1/°C) was calculated using Equation 3.8, which was then used to predict the pore water pressure as a function of temperature using Equation 3.3. The predicted thermally induced pore water pressures are also shown in Figure 3.4. Good correspondence between the experimental and predicted pore water pressures for the normally consolidated Kaolinite clay are observed. This observation confirms that the proposed empirical equation can be used to predict generation of pore water pressure during heating, and the magnitude can be determined by basic properties of soils and knowledge of the current stress condition without having to perform complex experiments.

3.6.3. Volume Changes during Drained Heating

A volumetric strain of Kaolinite clay specimen was induced during heating as shown in Figure 3.5. The specimen was observed to contract nonlinearly during heating, which was partially recoverable during cooling. The results show that void ratio change induced due to the change of the temperature. The volume of the water drained is not corrected, the results will be more accurate, if the thermal volume change of the water inside the connection pipe and porous stones were measured. The volume of water drained from the specimen due to the temperature change $(\Delta V_{DR})_{\Delta T}$ can be predicted from the measured value of pore water pressure during the undrained test using the following equation from Campanella and Mitchell (1968):

$$(\Delta V_{DR})_{\Delta T} = m_v V_m \Delta u \tag{3.4}$$

where V_m is equal to 509.87 cm^3 and Δu is the measured value of thermally induced pore water pressure from the undrained test. This was rewritten into the form of the isotropic compression curve as follows:

$$\left(\Delta V_{DR}\right)_{\Delta T} = -\frac{1}{1+e_0}\frac{\lambda}{p'}V_m \Delta u \tag{3.5}$$

Also, the overall change in volume of the soil specimen $(\Delta V_m)_{\Delta T}$ due to a change in temperature could be determined using Equation 3.6 developed by Campanella and Mitchell (1968):

$$(\Delta V_m)_{\Delta T} = \alpha_w V_w \Delta T + \alpha_s V_s \Delta T - (\Delta V_{DR})_{\Delta T} \tag{3.6}$$

where V_w is the initial volume of pore water before heating (242 cm^3), and V_s is the volume of mineral solids (268 cm^3). A comparison between the measured specimen volume change and the prediction is shown in Figure 3.6. The difference in results may be because a similar thermally induced pore water pressure may not occur initially in the drained test due to partial drainage.

3.7. Conclusions

Drained and undrained heating triaxial tests were performed to evaluate the impact of the drainage on the volume change during the specimen temperature change. As the increase in temperature induced volume contraction during the drained heating test, part of the volume contraction is irreversible. However, the specimen expanded due to the undrained heating, and the pore water pressure was increased. The pore water pressure measured during the undrained test could be used to predict drained water due to the temperature increase during the drained test which could be used to predict the volume change of the sample.

3.8. Acknowledgments

Chapter 3, in full, has been published as it appears in the following conference publication (The dissertation author was the primary investigator and author of this paper):

Takai, A., Ghaaowd, I., Katsumi, T., and McCartney, J.S. (2016). "Impact of drainage conditions on the thermal volume change of soft clay." GeoChicago 2016: Sustainability, Energy and the Geoenvironment. Chicago. Aug. 14-18. pp. 32-41.

Table 3.1. Properties of the Kaolinite clay and initial conditions of the specimen used in this study.

Liquid limit	47%
Plastic limit	28%
Plasticity index	19
Specific gravity	2.6
Initial gravimetric water content	31%
Initial void ratio	0.90
Initial porosity	0.47

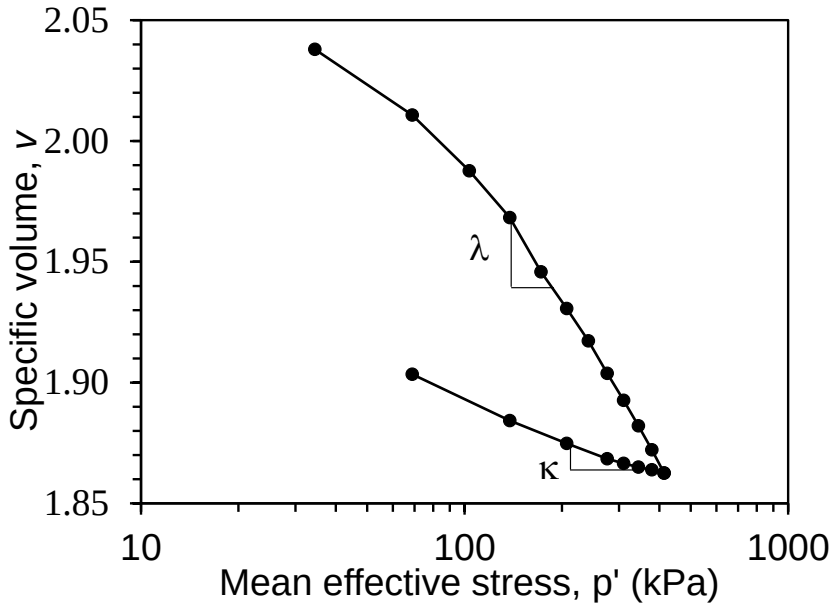

Figure 3.1. Isotropic compression curve for Kaolinite clay.

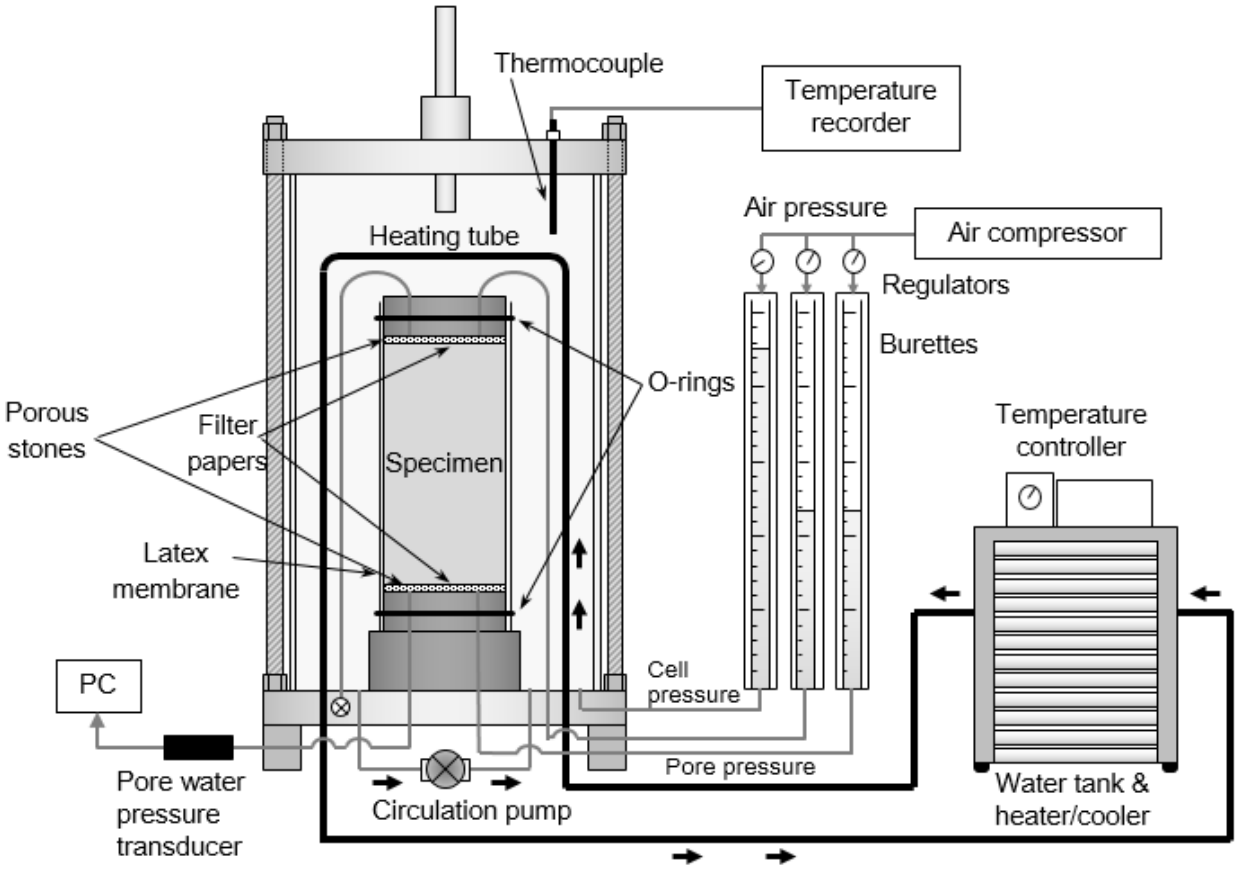

Figure 3.2. Schematic view of the thermal triaxial system.

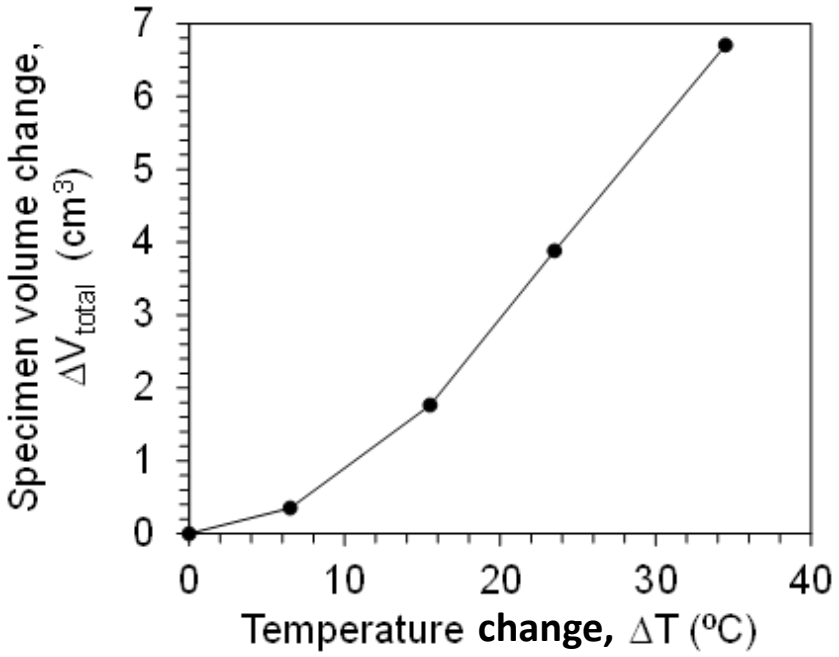

(a)

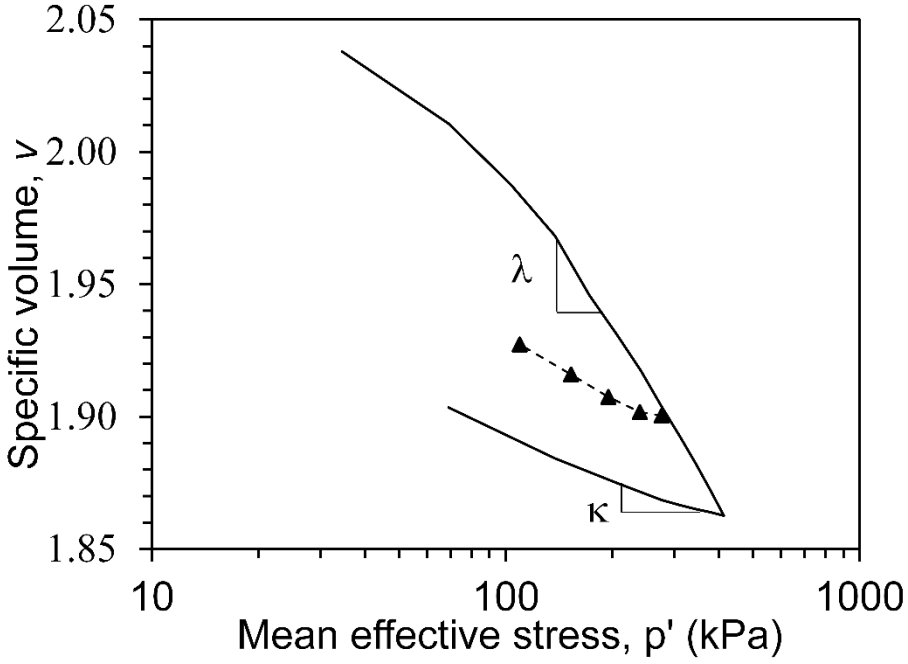

(b)

Figure 3.3: (a) Volume change versus temperature; (b) Specific volume vs. mean effective stress during undrained heating with comparison to the isotropic compression curve.

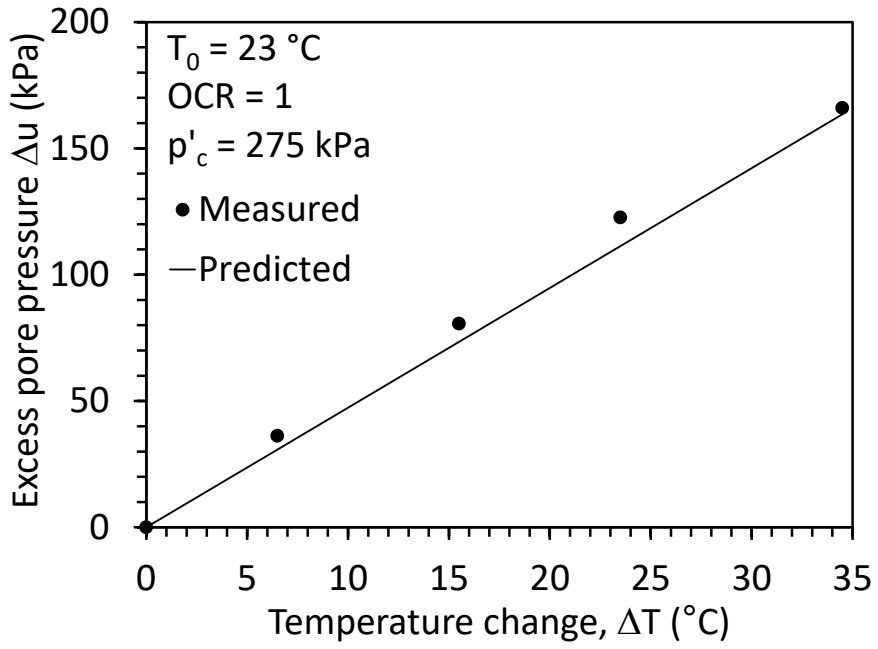

(a)

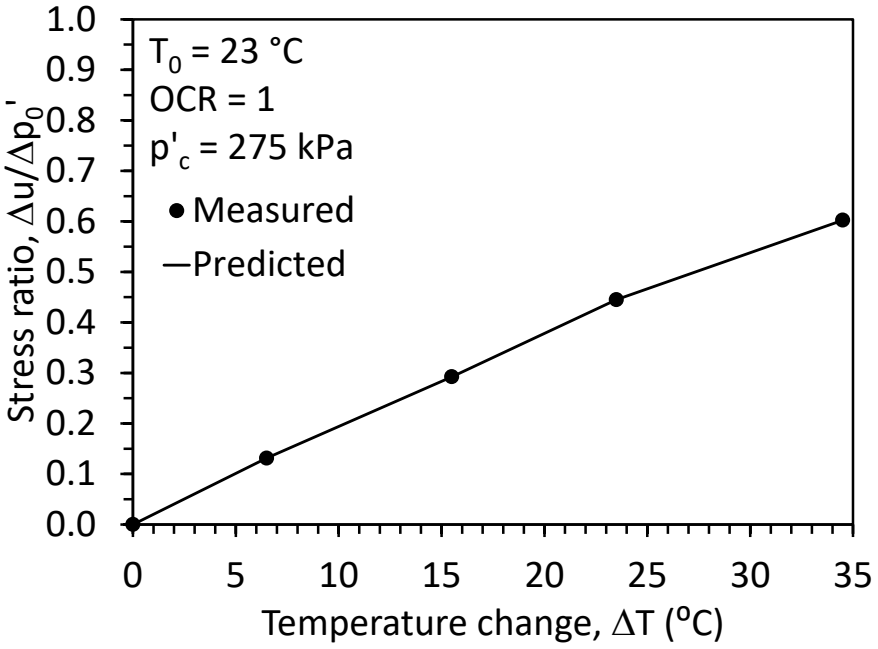

(b)

Figure 3.4. Effect of temperature change on the change in pore water pressure for Kaolinite clay along with the predicted trend: (a) Pore water pressure; (b) Pore water pressure normalized by the initial mean effective stress

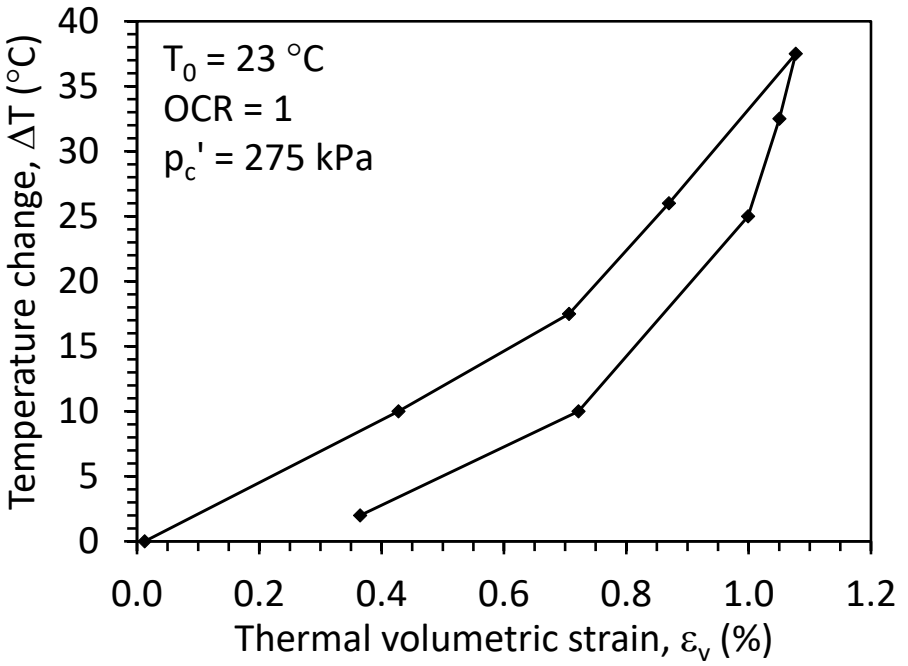

Figure 3.5. Volumetric strain under drained heating/cooling cycle of normally consolidated Kaolinite clay.

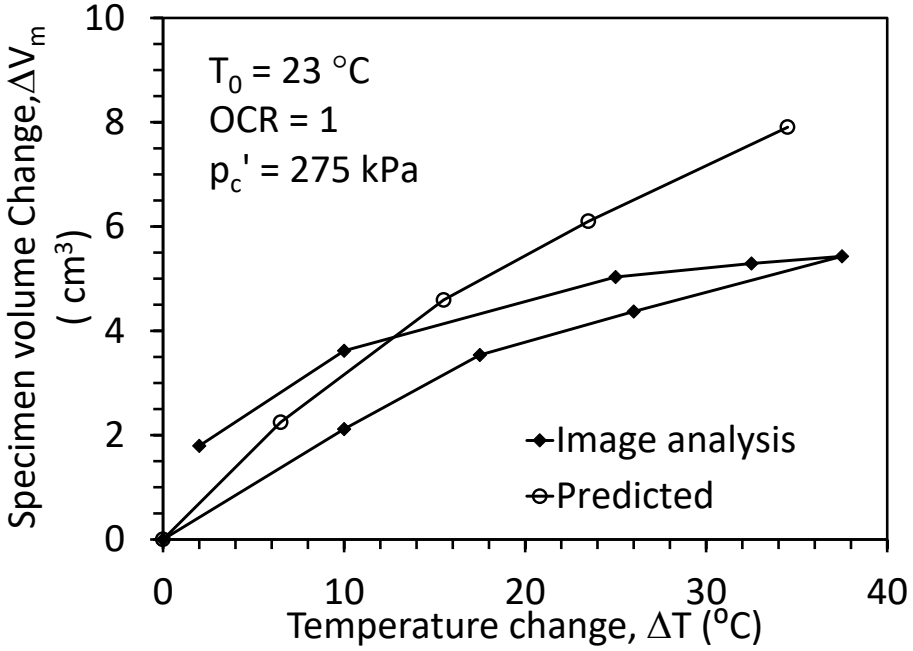

Figure 3.6. Specimen volume change during the drained heating test.

Chapter 4. Impact of Drained Heating and Cooling on Undrained Shear Strength of Normally Consolidated Clay

4.1. Abstract

This study focuses on the effects of a heating-cooling cycle on the undrained shear strength of normally consolidated clay specimens. A clear increase in undrained shear strength was observed for specimens sheared after drained heating to an elevated temperature, while a further increase in undrained shear strength was observed for specimens sheared after a drained heating-cooling cycle. This is attributed to the permanent decrease in volume during drained heating followed by the elastic decrease in volume during drained cooling. The initial mean effective stress was also observed to play an important role in the magnitude of the increase in undrained shear strength, with greater increases observed for normally consolidated specimens with lower mean effective stresses.

4.2. Introduction

The impact of temperature on the shear strength of clays has been widely studied since the 1960's and several constitutive relationships have been developed to consider the impacts of stress history and drainage conditions (Laloui et al. 2015). General observations from the literature include: (1) temperature changes are not expected to affect the friction angle of clays (defined at peak or critical state conditions), (2) the undrained shear strength is dependent on the pore water pressure during shearing, the initial effective stress, and the void ratio; and (3) the drainage conditions during heating will lead to different trends in the shear strength. Shearing after undrained heating typically leads to a decrease in undrained shear strength associated with the

increase in excess pore water pressures (and decrease in mean effective stress) during undrained heating, while shearing after drained heating leads to an increase in undrained shear strength for normally consolidated clays due to a reduction in void ratio during drained heating. One situation that has not been fully studied is shearing of normally consolidated clays after a drained heating-cooling cycle, such as that experienced by the soil surrounding a thermal drain system (Abuel-Naga et al. 2006). It is expected that plastic contraction will occur during drained heating, followed by elastic contraction during drained cooling. This implies that after cooling, specimens will have a slightly lower void ratio and should have a greater undrained shear strength than that observed during shearing after drained heating. However, it is not clear if the change in temperature will lead to a transition in the magnitude of excess pore water pressure during undrained shearing. This study focuses on results from triaxial compression tests on saturated normally consolidated clay following different temperature paths and drainage conditions.

4.3. Methods

4.3.1. Materials

Kaolinite clay obtained from M&M Clays Inc. of McIntyre, GA was used in this study. As the clay has a liquid limit of 47% and a plasticity index of 19, the clay is classified as CL according to the Unified Soil Classification Scheme. The clay has a specific gravity of 2.6, and the slopes of the normal compression line (λ) and recompression line (κ) are 0.100 and 0.016, respectively. The excess pore water pressure during undrained heating of this clay was characterized by Ghaaowd et al. (2015), while the volume change during drained heating was characterized by Takai et al. (2016).

4.3.2. Experimental Setup

The nonisothermal triaxial compression tests were performed using the thermal triaxial system developed by Alsherif and McCartney (2015) that was further adapted for testing saturated clays by Takai et al. (2016). A schematic of the system is shown in Figure 4.1. The cell is comprised of a Pyrex pressure vessel exhibiting low thermal creep while remaining transparent after repeated heating and cooling cycles. The temperature within the cell is controlled by circulating heated water from a temperature-controlled circulating bath through a stainless-steel pipe bent into a "U" shape over the specimen. A pump able to accommodate high fluid temperatures and pressures is used to circulate the cell water to ensure that it is uniformly mixed. The cell fluid temperature was monitored using a thermocouple and temperature recorder having a precision of 0.5 °C. The cell pressure and specimen backpressure were controlled using a pressure panel, and a temperature-corrected pore water pressure transducer was used to measure changes in pore water pressure during undrained heating and shearing. In addition to monitoring the drainage from the specimen during consolidation and drained heating and cooling, images of the specimens were taken using a high-resolution camera (model D610 from Nikon) during the tests to measure changes in volume using the approach of Uchaipichat et al. (2011).

4.4. Procedures

The clay specimens were prepared from sedimentation using an approach described by Ghaaowd et al. (2015), and trimmed specimens were backpressure-saturated in the thermal triaxial cell, which involved applying the cell pressure and backpressure in stages until reaching a value of Skempton's pore water pressure parameter B of at least 0.95. The specimens were then consolidated isotropically to a desired mean effective stress. Some specimens were sheared in undrained conditions at ambient temperature conditions to provide a baseline case for comparison.

For the specimens tested at different temperatures, the drainage valves at the top and bottom of the specimen were kept open during heating and cooling. Another set of specimens were heated from 23 °C to 66 °C at a relatively fast rate (0.2 °C/min) after which the elevated temperature was maintained until the volume change stabilized, after which the specimens were sheared in undrained conditions. The last set of specimens were heated from 23 °C to 66 °C in drained conditions, then cooled back to 23 °C before shearing in undrained conditions.

4.5. Results and Discussion

The principal stress difference versus axial strain results from three consolidated undrained triaxial compression tests conducted at a mean effective stress of 310 kPa following three different temperature paths are shown in Figure 4.2. The OCR of 1.0 refers to the initial state of the specimen where it was normally consolidated prior to the application of any mechanical or thermal loading. An increase in the maximum principal stress difference can be observed for the specimen sheared after drained heating to 66 °C, and a further increase in undrained shear strength is observed for the specimens sheared after drained heating to 66 °C followed by drained cooling back to 23 °C. The shapes of the stress-strain curves for the three tests were relatively similar despite different peak values. The corresponding reductions in the excess pore water pressure for each of the three tests are shown in Figure 4.2(b). Although the magnitude of excess pore water pressure was similar in all three tests, all three specimens showed positive strains during shearing as expected for normally consolidated specimens. The effective stress paths for the three tests are shown in Figure 4.3. An interesting observation is that the maximum principal stress values fall onto the same peak failure envelope

The results from tests performed at other initial mean effective stresses are shown in Figure 4.4. Like the observation drawn from the effective stress paths in Figure 4.3, the results in

Figure 4.4 indicate that the specimens following different temperature paths tested at different initial mean effective stresses all fall onto the same peak failure envelope. The slope shown in Figure 4.4 of 1.29 is not equal to the slope of the critical state line but corresponds to the slope of the peak failure envelope. Assuming that the maximum principal stress differences from each of the tests corresponds to the undrained shear strength of the soil, the trends in the undrained shear strength for specimens sheared under ambient temperature conditions, after heating, and after a heating-cooling cycle are shown in Figure 4.5(a). A clear increase in undrained shear strength after a heating-cooling cycle is observed. The percent increase in undrained shear strength following a heating-cooling cycle is appreciable, and ranges from 16 to 54%. The percent increase in undrained shear strength was observed to decrease as the initial mean effective stress increased, which is counterintuitive to the trends in the thermally induced excess pore water pressures during undrained heating observed by Ghaaowd et al. (2015). Specifically, it was observed that greater changes in excess pore water pressure are observed for specimens with higher initial mean effective stress. The final void ratio values of specimens sheared at ambient temperature, after heating and after a heating-cooling cycle are shown in Figure 4.5(b). It can be observed that the void ratio decreases when the specimen is subjected to drained heating and even further after a drained heating-cooling cycle, conforming to the corresponding increase in undrained shear strength.

In addition, to investigate more the effect of the void ratio change on the undrained shear strength, Figure 8.9 shows a correlation between the void ratio at failure and the undrained shear strength results from the triaxial tests. Based on the results, the undrained shear strength follows a log-linear trend with the void ratio at failure as follows:

$$c_u = c \times exp^{-d \times e_f} \tag{4.1}$$

where c and d are empirical fitting parameters and e_f is the void ratio at failure.

4.6. Conclusions

The results presented in this study indicate that the impact of a heating-cooling cycle such as that used in a thermal improvement application (i.e., thermal drains) will have a positive effect on the undrained shear strength of normally consolidated clays. This trend in undrained shear strength is attributed to the plastic decrease in volume during drained heating combined with the elastic decrease in volume during drained cooling. It was observed that this positive effect was greater for specimens tested at lower initial mean effective stresses. Despite the clear effects of temperature on the undrained shear strength, the changes in temperature were not observed to affect the slope of the peak failure envelope, which is consistent with previous studies on the effects of temperature on the shear strength of clays.

4.7. Acknowledgements

Chapter 4, in full, has been published as it appears in the following conference publication (The dissertation author was the primary investigator and author of this paper):

Samarakoon, R. Ghaaowd, I. and McCartney, J.S. (2018). "Impact of drained heating and cooling on undrained shear strength of normally consolidated clay." International symposium on Energy Geotechnics 2018. September 26-28. 8 pg.

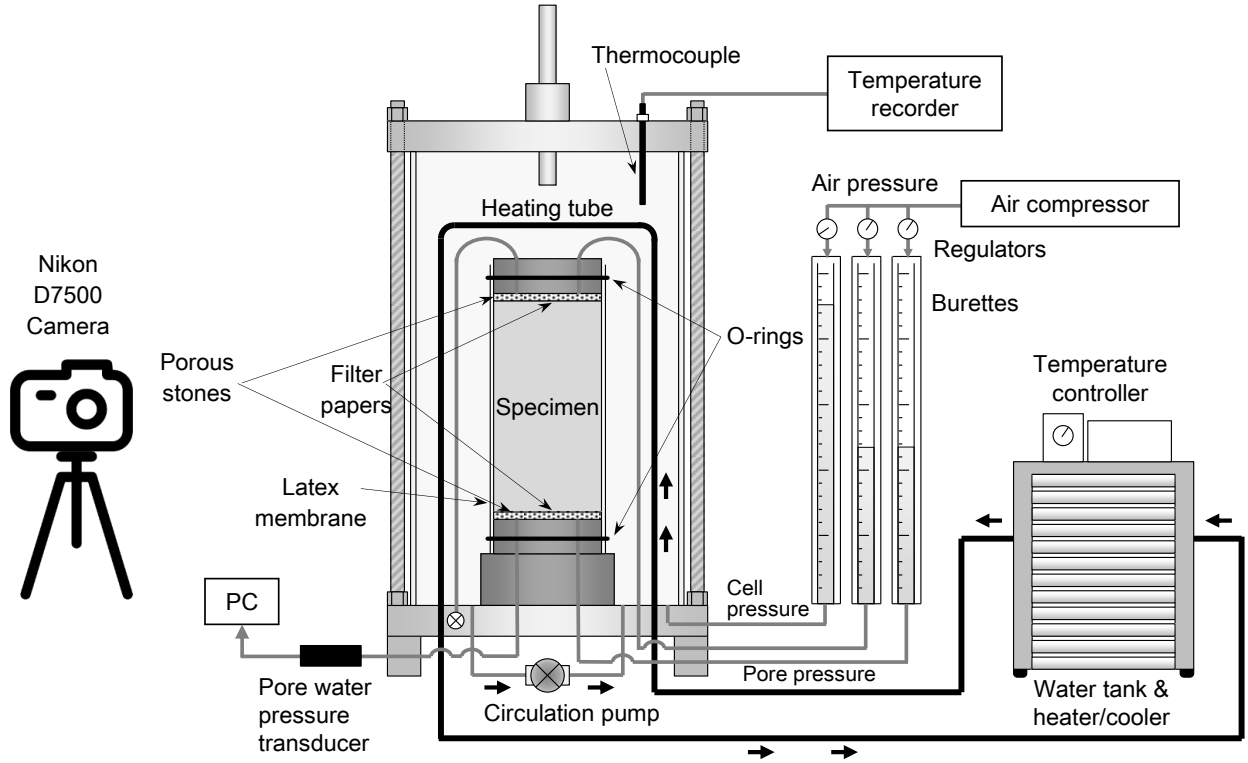

Figure 4.1. Thermal triaxial setup

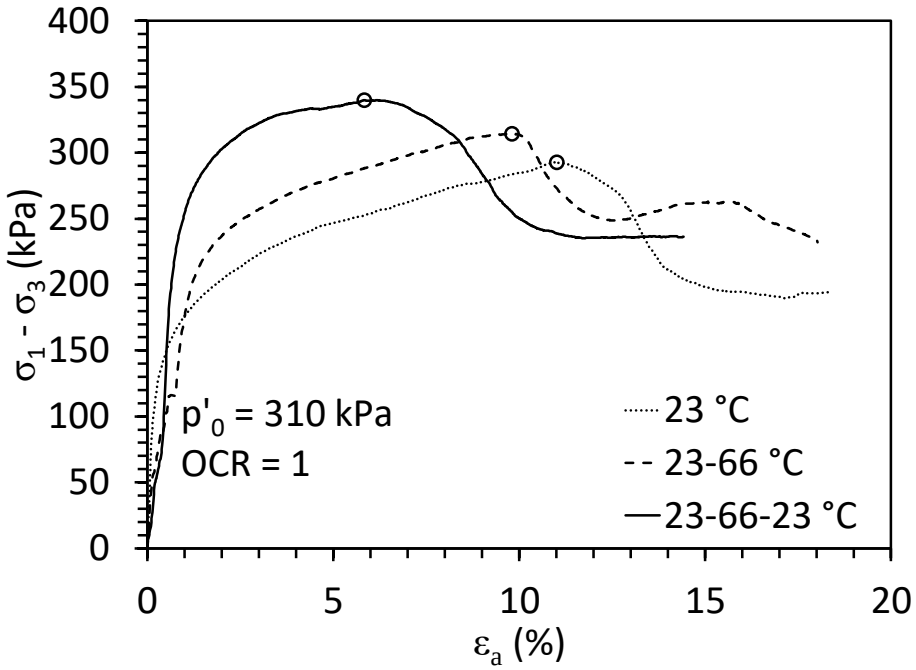

(a)

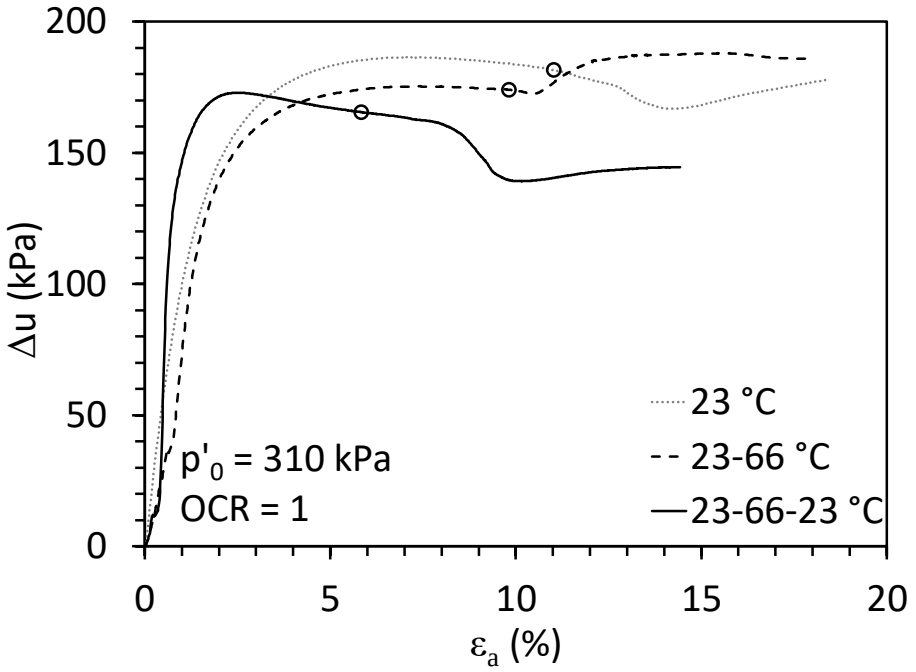

(b)

Figure 4.2. Examples of consolidated undrained triaxial compression test results for the saturated clay following different temperature paths (points denote the maximum principal stress): (a) maximum principal stress difference vs. axial strain (b) excess pore water pressure vs axial strain.

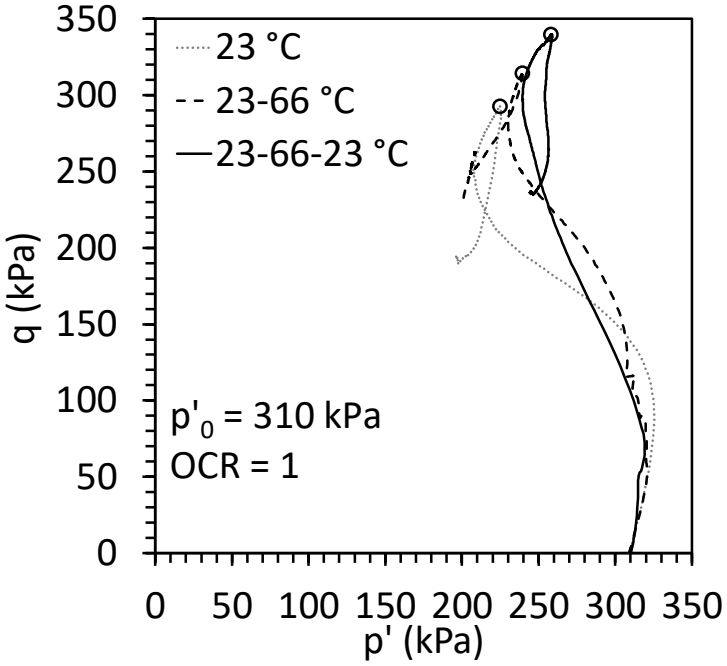

Figure 4.3. Examples of effective stress paths for the saturated clay following different temperature paths

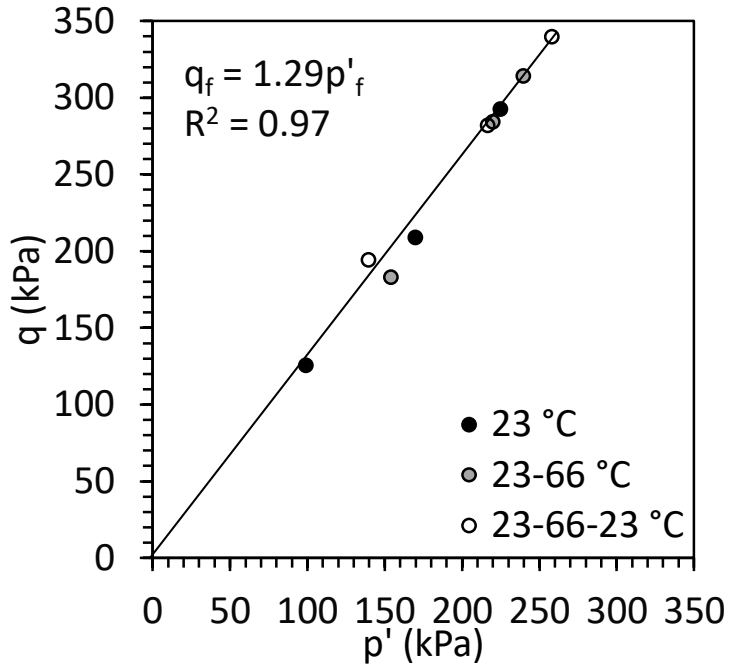

Figure 4.4. Maximum principal stress differences for specimens sheared at ambient temperature, after heating, and after a heating cooling cycle versus the mean effective stress at failure

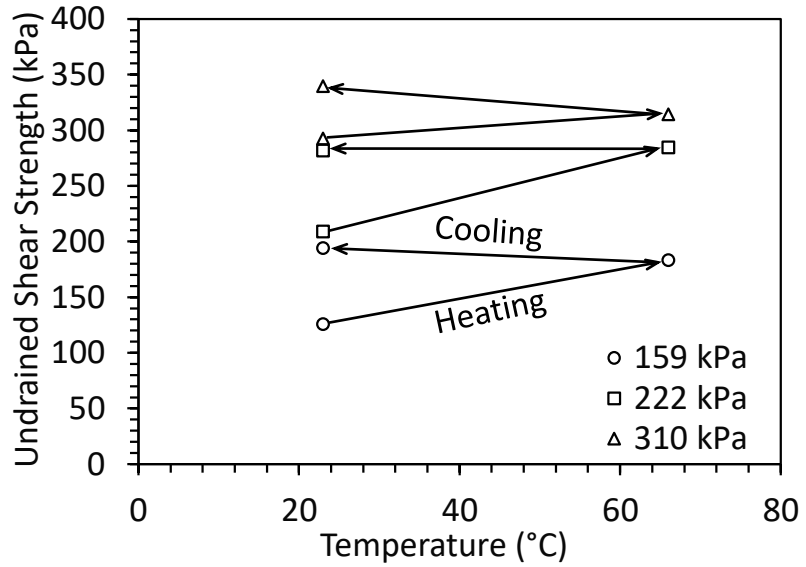

(a)

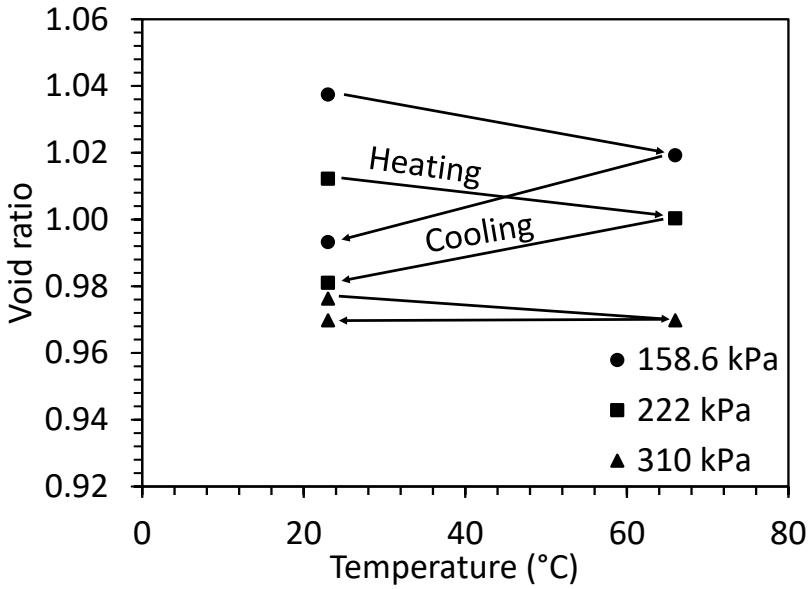

(b)

Figure 4.5. (a) Undrained shear strength at different mean effective stresses for specimens sheared at ambient temperature, after heating, and after a heating cooling cycle; (b) Final void ratio at different mean effective stresses for specimens sheared at ambient temperature, after heating and after a heating cooling cycle

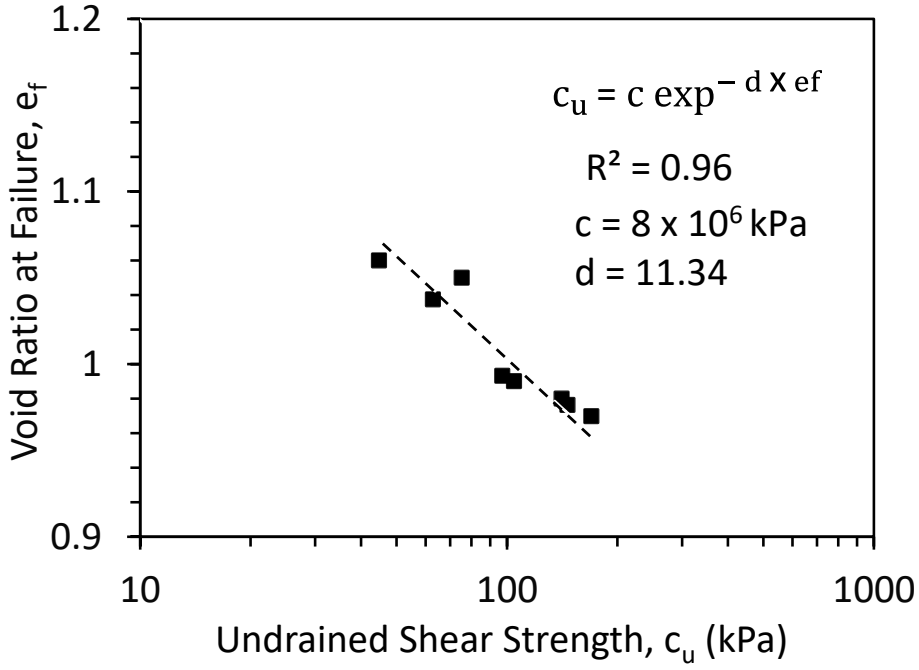

Figure 4.6. Relationship between undrained shear strength and the void ratio at failure for Kaolinite clay

Chapter 5. Centrifuge Modeling of Offshore Piles in Soft Clay: Materials

5.1. Kaolinite Clay

The soil used in the experiments was commercially-available Kaolinite clay from M&M Clays Inc. of McIntyre, Georgia whose geotechnical properties of the clay are summarized in Table 5.1. The clay classifies as CL according to the Unified Soil Classification Scheme (USCS). The liquid limit results are shown in Figure 5.1. The liquid limit of the Kaolinite clay is around 47%, and the plastic limit was 28%. An isotropic compression test indicates that the slopes of the normal compression line (λ) and the recompression line (κ) for the clay are 0.080 and 0.016, respectively. The compression and recompression curves are shown in Figure 5.2. The clay specimens were formed from a slurry to reach initially normally consolidated conditions. The permeability of Kaolinite clay was studies in the literature, the coefficient of permeability ranges from 2.8×10^{-9} to 8.2×10^{-9} m/s for a void ratio range from 1.05 to 1.45 respectively. Relationships between void ratio and coefficient of permeability for Georgia Kaolinite clay reported by McGinley et al. (1981) are shown in Figure 5.3.

Also, the thermal clay conductivity of the Kaolinite clay as a function of void ratio was measured in this study. For high void ratios ranging from 3.0 to 1.2, a thermal needle was incorporated into the centrifuge container to monitor the evolution in thermal conductivity during consolidation of the clay from a slurry, as shown in Figure 5.4. The thermal conductivity for lower void ratios ranging 1.2 to 0.8 was investigated in a triaxial setup developed by McCartney et al. (2013) shown in Figure 5.5. The void ratio versus the mean effective stress during the testing are shown in Figure 5.6 for both approaches. The measured thermal conductivity versus the void results are shown in Figure 5.7 have a clear trend, and the obtained linear relationship between

thermal conductivity and void ratio was used in the heat transfer analysis presented in Chapter 8. The thermal conductivity test in the large container was measured two times, using two different thermal probes (TR-1 and SH-1) connected to KD2 Pro Utility. The TR-1 sensor is expected to provide more reliable measurements of the thermal conductivity, but the SH-1 sensor can measure the thermal conductivity and the volumetric heat capacity.

5.2. Ottawa Sand

Ottawa F-65 sand is famous type of soil has been used in the liquefaction testing for long time. Because of its fine grained and high permeability coefficient compare to clay, Ottawa sand was used in this study as drainage layer beneath the clay layer. The sand grain size varies from 0.1 mm to 0.5 mm and hydraulic conductivity varies from 0.0022 to 0.00118 m/s for the loosest and densest states, respectively (Bastidas 2016).

5.3. Scale-Model Jacked-In Pile

The scale-model jacked-in pile is a 25 mm-diameter, 255 mm-long, split-shell aluminum cylinder having a wall thickness of 3.3 mm, as shown in Figure 5.8. At 50 g, the model pile corresponds to a prototype pile having a diameter of 1.25 m and a length of 12.75 m. The insides of the cylinder halves were instrumented thermocouples which measure the temperature at the pile wall. The halves are held together by screw-on top and bottom caps. An internal electrical resistance heater running the length of the energy pile (Figure 5.9) is connected to the top cap, and heat is conducted from the heater to the outside of the pile through a sand fill. To assure there was no temperature transfer to the soil surface, the top cap was fabricated from Delrin to provide an insulating effect. This approach was found to not lead to a heating of the water on top of the clay surface.

5.4. Scale-Model Torpedo Pile

The scale-model Torpedo pile is a 17 mm-diameter, 175 mm-long, fabricated from four parts as shown in Figure 5.10. The main part is a stainless-steel cylinder having a wall thickness of 3 mm. A tip part is connected to the cylinder by thread. The heat source is an electrical resistance heater that fits inside the cylinder. The heater has an embedded thermocouple which can be used to control the temperature of the Torpedo pile. The fourth part is the pile top cap that includes a pulling connection and has four fins welded to it to simulate the shape of a Torpedo pile. The thermocouple and voltage wires pass through the pile cap. The whole pile was connected to the steeper motor rod via a stainless-steel wire as shown in Figure 5.11. The pile was installed into the clay layer under its self-weight and was pulled out vertically using the stainless steel wire.

5.5. Acknowledgements

Chapter 5, in full, is currently being prepared for submission for publication of the material as it may appear in part of the following journal publication (The dissertation author was the primary investigator and author of this paper):

Ghaaowd, I. & McCartney, J.S. (In preparation). "Test setup for centrifuge modeling of energy piles in saturated soft clay." To be submitted to ASTM Geotechnical Testing Journal.

Table 5.1. Properties of the Kaolinite clay and initial conditions of the specimen used in this study.

Liquid limit	47%
Plastic limit	28%
Plasticity index	19
Specific gravity	2.6

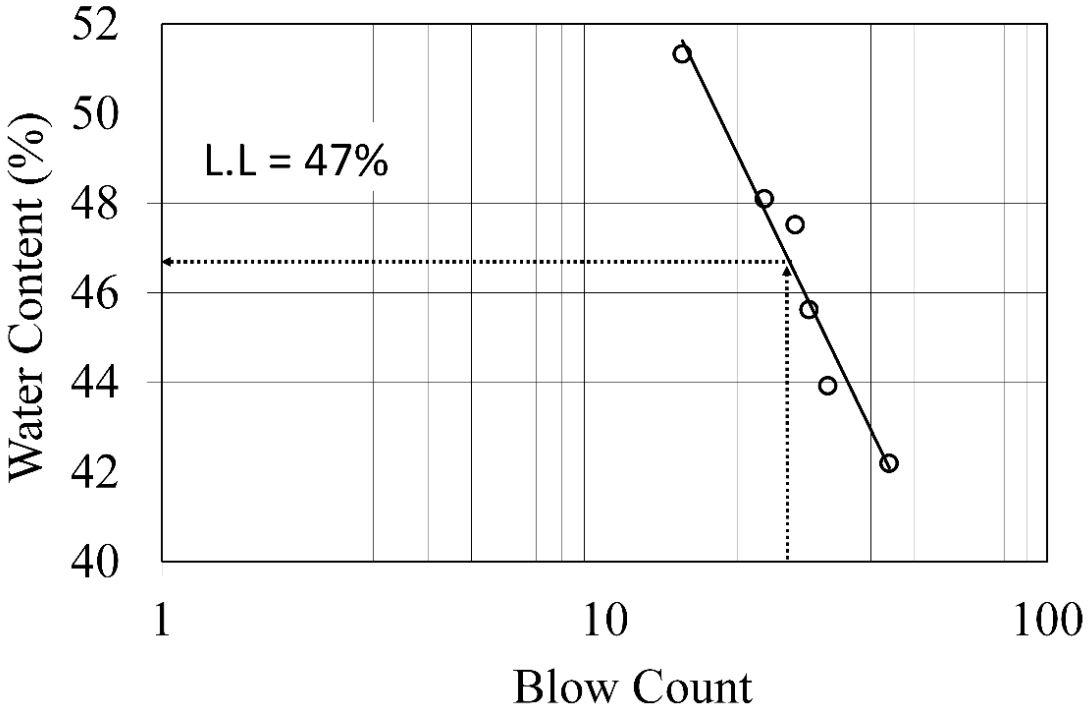

Figure 5.1. Results from the liquid limit test performed on Kaolinite clay.

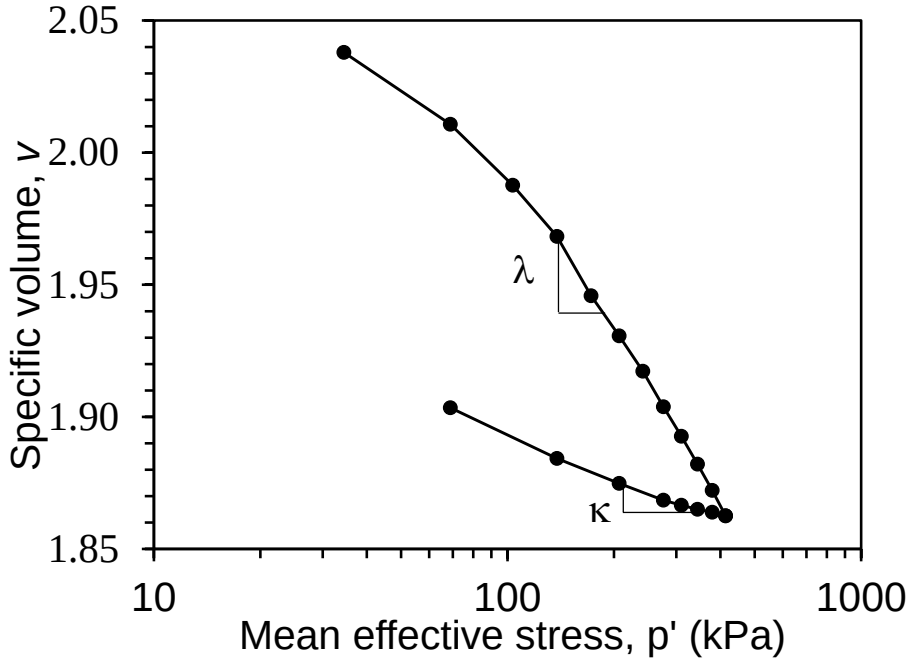

Figure 5.2. Isotropic compression curve for Kaolinite clay.

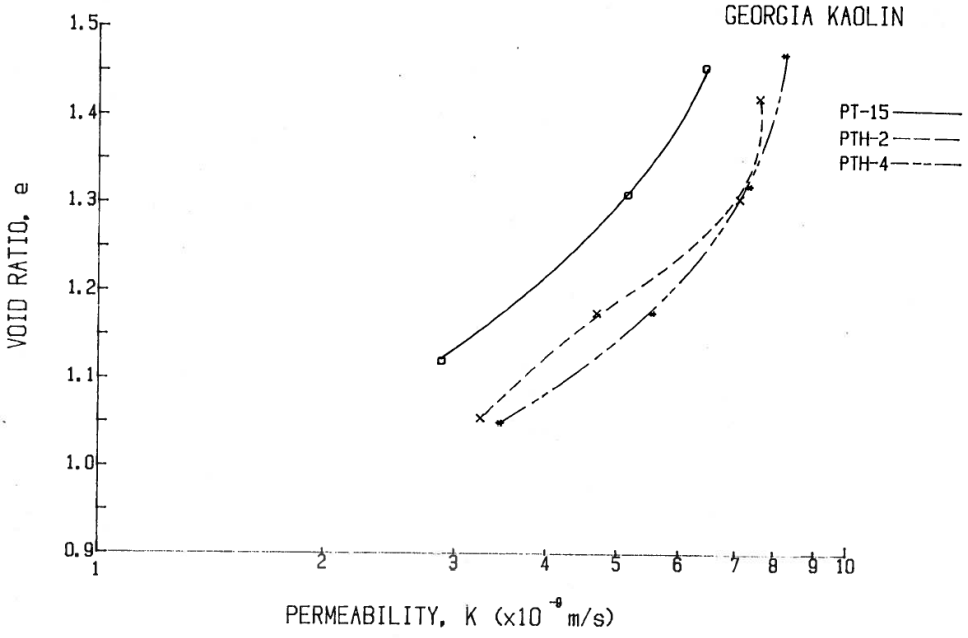

Figure 5.3. Void ratio versus the coefficient of permeability of Georgia (McGinley et al. 1981)

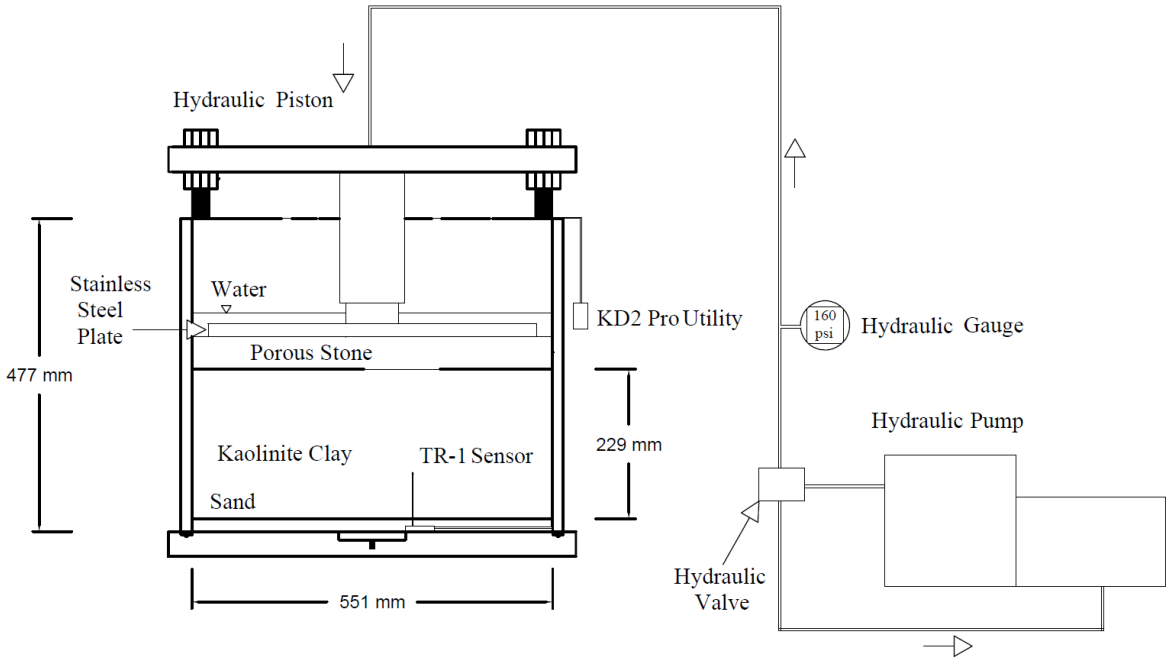

Figure 5.4. Thermal needle (TR-1 Sensor) configuration in the centrifuge container.

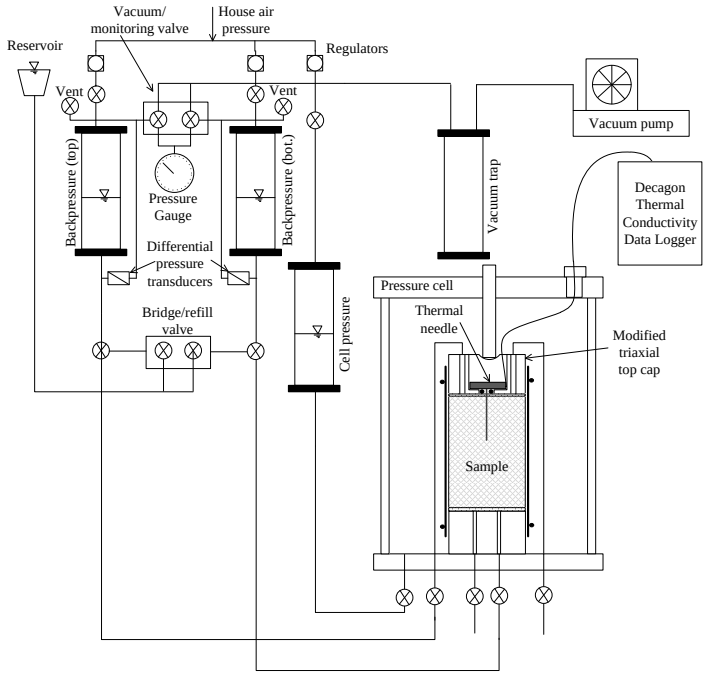

Figure 5.5. Thermal conductivity setup developed by McCartney et al. (2013) involving a thermal needle in a triaxial cell.

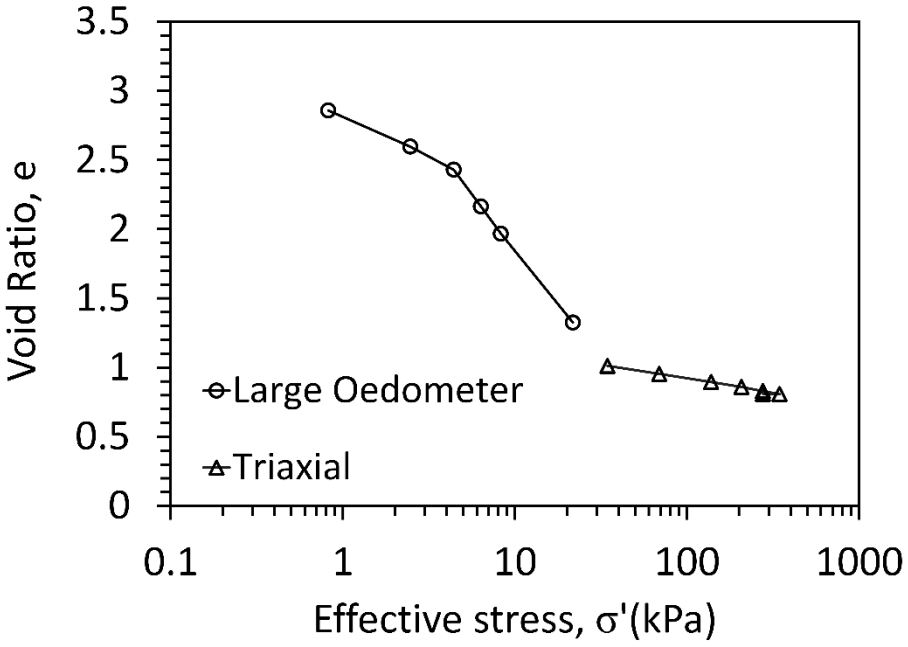

Figure 5.6. Void ratio versus effective stress for Kaolinite specimens consolidated from a slurry in a large-diameter oedometer and from isotropically compressed specimens in a triaxial cell

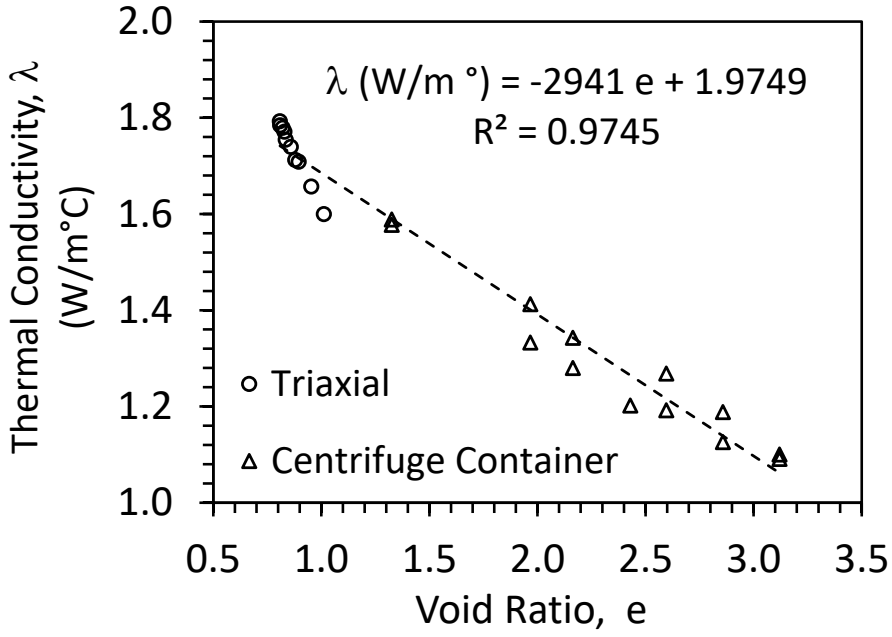

Figure 5.7. Relationship between the void ratio of Kaolinite versus the thermal conductivity

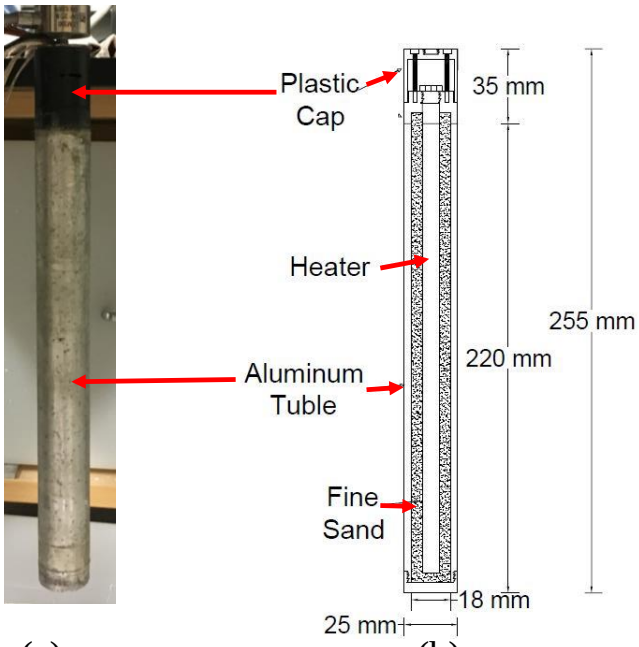

Figure 5.8: Details of the centrifuge-scale jacked-in pile with internal heating element: (a) Assembled jacked-in pile, (b) Pile cross section with model-scale dimensions.

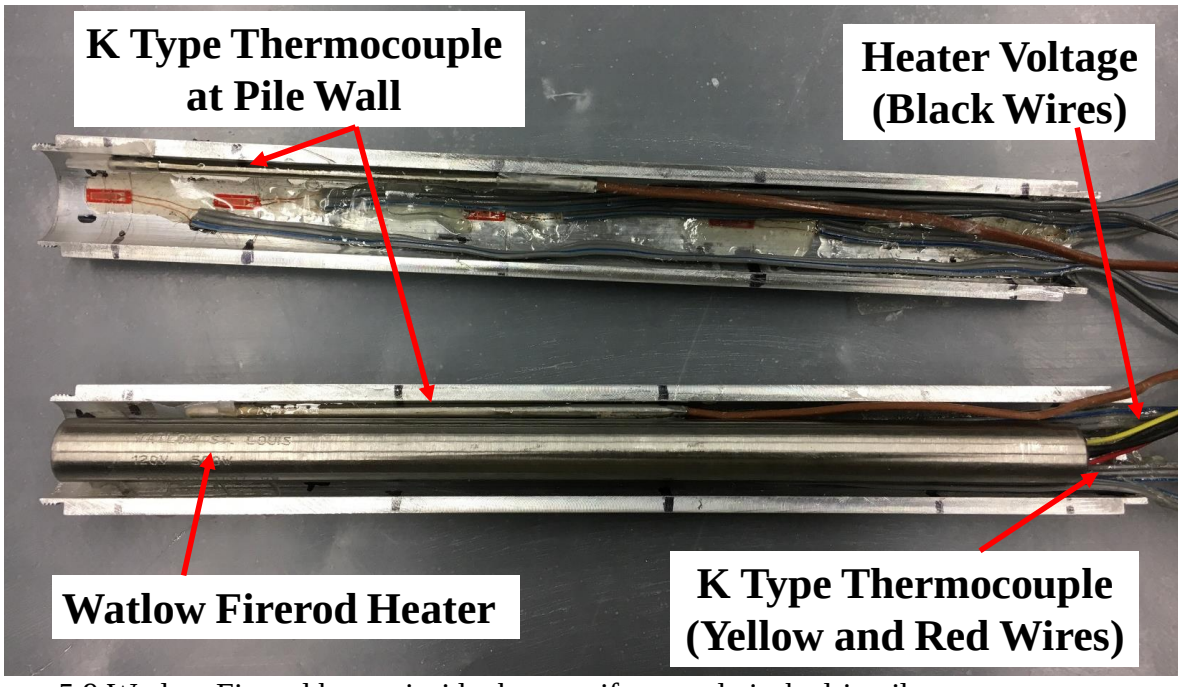

Figure 5.9 Watlow Firerod heater inside the centrifuge-scale jacked-in pile

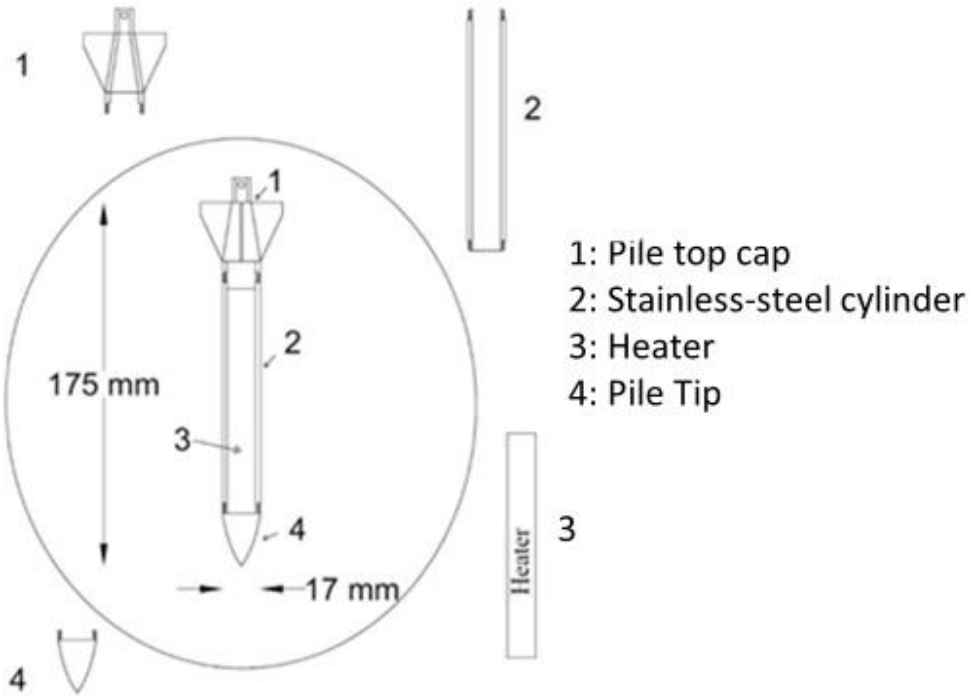

Figure 5.10. Schematic of the centrifuge-scale Torpedo pile: (1) Top cap; (2) Body; (3) Internal electric resistance heater; (4) tip

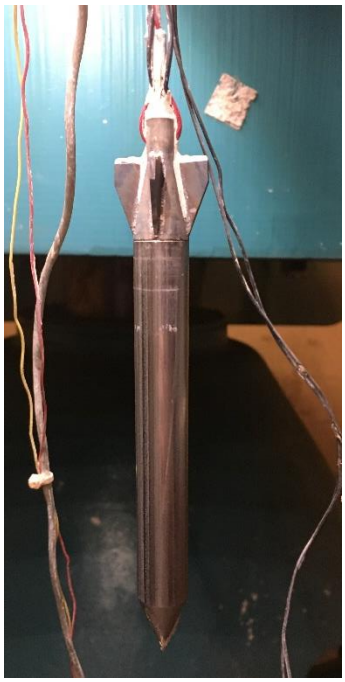

Figure 5.11. Pictures of the centrifuge-scale Torpedo pile

Chapter 6. Centrifuge Modeling of Offshore Piles in Soft Clay: Test Setup

6.1. Experimental Setup

The centrifuge was used for this study is C61-3 Geotechnical Centrifuge located at the Caltrans Seismic Response Modification Device (SRMD) Test Facility in the University of California San Diego as shown in Figure 6.1, this geotechnical centrifuge was designed to carry uniform loads with masses ranging from 0 to 500 kg at various centripetal accelerations corresponding to a 50 g-ton capacity. The specifications of the UCSD centrifuge are shown in Table 6.1. Centrifuge testing makes use of geometric similitude to properly scale the quantities obtained in the centrifuge model to quantities representative of a prototype system of interest (or vice versa). Table 6.2 provides a summary of scaling laws that are commonly used in geotechnical centrifuge practice, N refers to the gravitational acceleration imposed in the model during centrifuge testing, with the acceleration level during in-flight testing being equal to N times earth's gravity (g). In the case of the centrifuge testing program detailed in this study, all tests were performed at a centrifugal acceleration of 50g (i.e., N = 50). In this regard, model scale quantities are obtained by multiplying the factors presented at Table 6.2with the actual prototype scale quantities. Prototype quantities can be obtained by dividing the model scale quantities by the factors in Table 6.2. For example, the length of the pile foundation used in this study is 250 mm which is equivalent to (250 mm)×(50)/100 = 12.5 m pile foundation at the prototype scale.

Two identical aluminum cylindrical containers were used for this centrifuge testing program as provides a typical cross-section through the container as shown in Figure 6.2. The aluminum container consists of a base plate, a cylindrical tank, and an upper reaction plate. The base and reaction plates of the container have dimensions of 0.62 m×0.62 m×0.05 m. The

cylindrical tank has an inside diameter of 0.55 m, a wall thickness of 16 mm, and a height of 0.47 m, and was connected to the base plate via four threaded rods atop an "O"-ring seal as shown in Figure 6.3(a). The top reaction plate was connected to the top ends of the same threaded rods as shown in Figure 6.3(b). The reaction plate supports stepper motors for loading the energy pile and T-bar, as well as linearly variable differential transformers (LVDTs). As shown in Figure 6.3 and Figure 6.4, a porous stone was located at the base of the two containers. The porous stone was connected to a drainage line that extended through the base of the container reaching another drainage line that connected the bottom line to a 90-deg NPT elbow located in the top part of the containers. The purpose of the porous stone is to allow drainage of water during consolidation of the slurry and to provide a free-drainage bottom boundary during testing. The setup shown thus provided double drainage during the various consolidation stages.

Figure 6.5 and Figure 6.6 show the loading motors that were used for the pile and the T-bar and the drives that each motor controlled. The motors were controlled via NI-Compact-RIO data acquisition located on the arm of the centrifuge (Figure 6.6). The NI Compact-Rio recorded all pertinent data (load, pore-water pressure, displacement, time, and temperature) during testing and relayed the information to the host computer which controlled all centrifuge operations. All the recording and controlling was done by using Labview program. Displacement calibration was done for both motors to double check the displacement calibration factor (counts/mm) provided by the factory.

To control the pile temperature, heater was inserted inside the pile, it is in cylinder shape with 12 mm diameter, and 200 mm length. K-type thermocouples is embedded inside the heater as shown in Figure 6.7. The heater was connected to EZ Zone PM Controller to control the temperature during the spinning. The controller was controlled by using Labview program via a

computer located on the arm of the centrifuge as shown in Figure 6.8, the computer is remotely controlled from the host computer in the control room.

Instrumentation is included, linear variable displacement transducers, pore water pressure transducer, load cells. As shown in Figure 6.9, 10 inches linear variable deformation transformer (LVDT) was used to measure the vertical displacements of the pile, the T-bar, and the soil surface All LVDT's sensors were attached to the reaction top plate using clamps to fix them during spinning. In the case of the T-bar and pile, the LVDT tip was connected to stepper motor rod via light aluminum plate. The soil surface displacement was measured by attaching light thin aluminum plate with 4 inches diameter to the LVDT tip.

A tension and compression miniature/inline threaded load cell as shown in Figure 6.10 were used to record load during pile driving to the soil and during undrained shear strength measurements by using the T-bar. Two load cells were used with capacities of 1.11 kN. Two Druck PDCR81 pore pressure transducers (PPTs) as shown in Figure 6.11(a) were used to monitor the development of excess pore-water pressures throughout the consolidation and testing stages of the centrifuge testing program, both sensors have a range of 1500 kPa. To ease the sensor insertion from the side of container wall to the targeted location, the sensor wire was strengthened by a thin steel rod and constrained with heat shrink tubing. In addition, isolator connector was used at the outside of the container wall to prevent any leakage at location where the sensor wire.

Six thermocouples were used to measure the temperature at different radius from the pile. All thermocouples were connected to the NI compact-RIO data acquisition to record the temperature during the heating. K-thermocouples are located at different radii from the center as shown in Figure 6.11(b). In addition, two K-type thermocouples were added to the surface of the soil and the outside of the container to measure the temperature of the boundaries.

To characterize the undrained shear strength of clay, A 57.2 mm × 14.3 mm T-bar penetrometer as shown in Figure 6.12. was used to measure the measure the penetration and extraction force required to derive the T-bar, then the undrained of the clay was interpreted using correlations of Stewart and Randolph (1991). More information will be provided later regarding the correlation relationship between the T-bar measurements and the undrained shear strength of the clay.

6.2. Model Construction Procedure

Kaolinite clay in powder form was mixed with water by using vacuum mixer, and the water content was used is 135%. The total amount of powder clay used was 45 kg, mixed on two stages, and placed in the container as shown in Figure 6.13(a). Filter paper was placed at the top of the clay layer as shown in Figure 6.13(b). The the porous stone with same diameter of the container was placed for 24 hour on the top the slurry as shown in Figure 6.13(c). The porous stone was manufactured of course sand mixed with 6% epoxy and reinforced with stainless steel mesh at the middle. Then the dead loads were added in stages as shown in Figure 6.13(d). Each loading stage took 24 hours, then hydraulic pressure was applies on the top of the dead weights using self-reaction frame as shown in Figure 6.13(e), and the total surcharge load was kept at 21.7 kPa. The Schematic of the self-reaction frame is shown in Figure 6.14. Figure 6.15shown the clay specimen compression curve during the 1 g consolidation. Then the applied load was unloaded, and the porous stone and the filter paper was removed. Around 6 cm height of water was left above the consolidated clay layer to assure the specimen is saturated. By the end of the consolidation, the height of the clay layer was around 220 mm.

The pile and T-bar were connected to the stepper motor rods. The top reaction plate was then lowered into place on top of the container and fastened into place. Due the head limitation in

the centrifuge basket, half of the pile length initially penetrated into the clay, and the T-bar was already penetrated to a depth of 58 mm into the clay layer. The container was instrumented with thermocouples and pore water pressure sensors from the side at different radii from the center. All sensors and motors were checked, and all safety procedures followed before spinning the centrifuge.

6.3. Test Procedure

The testing stages are in-flight consolidation, pile installation, heating, cooling, and pullout tests as summarized in Table 6.3. All testing stages are similar for all tests. After the preconsolidation of clay layer at 1 g was complete, the container was placed inside the centrifuge basket for in-flight self-weight consolidation at 50 g. This procedure would produce a normally consolidated clay layer with an overconsolidated portion at its top. Due to the limitation of the heights at the centrifuge basket, the pile was inserted at 1 g to 108 mm under the clay surface which half of the total penetration depth as shown in Figure 6.16. During in-flight self-weight consolidation at 50 g, the excess pore-water pressures were monitored using pore pressure transducers (PPTs) for each test. An example of the excess pore water pressure measured by pore water pressure transducer (PPT4) done in one of the tests is plotted against the square root of time in Figure 6.17. This data permits definition of the value of t_{90} using the root time method (Taylor 1948). The measured pore water pressure at the end of the consolidation was compared with the theoretical hydrostatic pore water pressure profile in in Figure 6.18. These results confirm that primary consolidation was reached achieved throughout the clay layer. These values can be assumed to correspond to the initial conditions for the energy pile before pile installation stage.

Pile was installed to the bottom of the clay layer using loading motor controlled by LabVIEW program. Load was applied on the head pile to assure the pile tip reached the bottom

bearing sand layer. Then, the motor rod was moved 3 mm upward without moving the pile head, and the applied load was released to zero. The pile head force displacement curve during the installation are shown in Figure 6.19. To accomplish this process without moving the pile head during the load release, the joint between the pile head and the rod of the loading motor was designed to permit the motor rod moving up without moving the pile head within a limit of 10 mm upward movement. Figure 6.20 shows the pile after being installed fully into the clay layer.

After the pile was installed through the clay layer so that its tip was resting on the sand drainage layer, time was allowed until the no further pile head displacement was observed and the excess pore water pressure in the clay layer induced by pile installation dissipated. Then the pile was heated to the target temperature while the centrifuge spinning using a heat controller. The heat controller maintained the temperature of the pile measured by a thermocouple attached to the pile surface. The heat controller computer was connected to a computer mounted on the centrifuge, which was accessed using remote desktop. The heating period required in most of the experiments was approximately 30 hours. All heated tests were followed by cooling for a minimum of 6 hours, which was observed to be sufficient for the clay temperature and pore water pressures to stabilize. After this point the pile was pulled up at a speed of 0.1 mm/s, which is fast enough in prototype scale to ensure undrained pullout conditions.

To infer the profile of undrained shear strength in the clay layer, T-bar was inserted into clay layer at speed of 0.2 mm/s. Due to the stroke limitation of the T-bar motor and the space restriction within the centrifuge container, the initial position of the T-bar was not at the soil surface. Instead the T-bar was initially embedded in the clay layer at the beginning of the test, and penetration testing started from at depth of 58 mm from the clay surface. The T-bar was pushed at a constant rate into the clay layer until reaching a maximum depth of 220 mm, which was close to

the bottom of the clay layer. Then the T-bar was extracted at the same speed from the clay layer until returning to its initial position. At this point, the centrifuge was spun down to 1 g.

At the end of the test, the container was removed from the centrifuge. The final height of the clay layer was measured, and water content clay samples were taken at different radii from the pile surface and different depths from the clay surface. Also, the final locations of the sensors around the pile were measured. An example of the deconstruction of the clay layer to measure the final sensor positions is shown in Figure 6.21.

6.4. Typical Results

6.4.1. Temperature

The results from a typical jacked-in pile embedded into saturated Kaolinite clay during heating of the pile from a temperature of 23 °C to 65 °C is presented in this section. Time series of the pile and clay temperatures at different locations are shown in Figure 6.22(a). The pile temperature increased very quickly due to the rapid response of the electrical resistance heater, but the temperature of the clay increased gradually and stabilized after 10 hours in model scale (1041 days in prototype scale). Although the heater in the pile increased in temperature from 20.0 to 65 °C, the soil only reached a maximum temperature of 45 °C. The temperature decreased away from the energy pile with a negligible change at the container boundary of 276 mm. When the electrical resistance heater was turned off, the clay temperature rapidly decreased back to a temperature of 23 °C. In addition, the typical temperature change profiles at different heating times are shown in Figure 6.23. The temperature at the pore pressure transducer locations could be interpolated from the thermocouples sensors measurements as shown in Figure 6.24.

6.4.2. Pore Water Pressure

The pore water pressure was measured during in-flight self-weight consolidation at 50 g using two pore water pressure transducers (PPT4, PPT3) at different depths and heights as shown in Figure 6.22(b). The insertion of the pile was observed to generate excess pore water pressure in the clay, which dissipated over time. After stabilization of the excess pore water pressure induced by pile installation, the next stage of testing involving pile heating was started. As the temperature of the pile increased during this next stage, thermally induced excess pore water pressures were generated in the clay immediately after the increase in temperature, as shown in Figure 6.22(b). It is expected that the clay will be in partially undrained conditions due to the boundary conditions and the distribution in temperature in the soil layer. Specifically, the thermally induced excess pore water pressures were observed to immediately start dissipating after generation, with thermal consolidation finishing after approximately 21 hours in model scale. The maximum measured thermal excess pore water pressures measured in this test were 4.0 kPa and 4.5 kPa at the locations of PPT3 and PPT4, respectively, as shown in Figure 6.23(b), due to the combination of the depth of the sensor and the greater temperature change at this location. Although the effective stress at PPT4 smaller than PPT3, the thermal excess pore water pressure at PPT4 was larger. This inconsistent trend could be due the fact that PPT3 was closer to the sand drainage layer, or because the temperature at the location of PPT4 was higher. The thermally induced excess pore water pressure fully dissipated at the end of heating.

6.4.3. Pile Head Displacement

After the pile was installed and its tip reached the sand drainage layer, the pile head displacement was zeroed (i.e., at 23 hours of the testing time in model scale), as shown in Figure 6.22(c). During the heating stage, the pile head stabilized, and no obvious head movement

upward was observed, which means the pile tip likely penetrated more in the sand drainage layer during heating. During the cooling stage, the pile head moved downward by approximately 0.28 mm due to the pile thermal contraction. This downward movement corresponds to an axial strain of 1080 με during a decrease in temperature of 45 °C. This means the linear coefficient of thermal expansion for the pile is approximately 24 με/°C, which is consistent with the linear coefficient of thermal expansion of aluminum.

6.4.4. T-Bar Measurements and Interpretation

The T-bar measurements in the clay layers with heated and unheated energy piles provide further evidence as to the effects of heating and cooling on the temperature effects on the behavior of normally consolidated clay layers. The initial T-bar position is slightly below the clay surface to maximize the stroke of the T-bar test, so the undrained shear strength near the surface of the clay layer may not be well characterized. The interpretation of the undrained shear strength was done by using the correlations founded by Stewart and Randolph (1991)

$$c_u = \frac{F_v}{N_b\, D\, L} \tag{6.1}$$

where D is the T-bar diameter= 14 mm, L is the T-bar length = 57 mm, F_v is the T-bar pushing force, c_u is the undrained shear strength, and N_b is the T-bar bearing factor. The T-bar bearing factor was calculated using the equation proposed by Oliveira and Almeida (2010):

$$N_b = 0.0053\left(\frac{H}{D}\right)^6 - 0.1102\left(\frac{H}{D}\right)^5 + 0.9079\left(\frac{H}{D}\right)^4 - 3.7002\left(\frac{H}{D}\right)^3 + 7.2509\left(\frac{H}{D}\right)^2 - 3.9168\left(\frac{H}{D}\right) + 5.3519 \tag{6.2}$$

where H is the height of soil above the T-bar rod. In their model the value of the T-bar bearing factor N_b should be in the range of 5.14 to 10.50. The profile of undrained shear strength interpreted from the T-bar test is shown in Figure 6.25.

In addition, the undrained shear strength can be interpreted from the pile force displacement data presented in Figure 6.19 using the equations for skin friction bearing capacity and end bearing capacity of a pile in an undrained clay layer:

$$Q = Q_s + Q_p \tag{6.3}$$

$$Q_s = \alpha\, c_u\, A_s = c_u\, \pi\, D\, H_{penetration} \tag{6.4}$$

$$Q_p = 9\, c_u\, A_p = 2.25\, \pi\, D^2\, c_u \tag{6.5}$$

where c_u is the mean undrained shear strength of the clay layer, α is the side shear factor (equal to 1.0 for soft clays), A_s is the pile surface area, $H_{penetration}$ is the penetration depth of the pile, A_p is the point bearing area of the pile. The undrained shear strength can be estimated from the pile penetration as follows:

$$c_u = Q / (\pi\, D\, H_{penetration} + 2.25\, \pi\, D^2) \tag{6.6}$$

The interpreted undrained shear strength profile compared to the undrained shear strength profile interpreted from pile penetration is shown in Figure 6.25. A good match is observed between the two experimental approaches.

6.4.5. Pile Pullout Capacity

The pile was pulled out at speed of 0.1 mm/s in model scale, and the net pullout pile capacity for the energy piles in clay layers is shown in Figure 6.26. The maximum pullout capacity is -891 kN, corresponding to 0.16 m displacement at prototype scale. The average measured undrained shear strength by using the T-bar was around 10 kPa, equation 6.3 could be used to estimate the pullout capacity load which is around 431 kN, the main deference in the condition

between the pile location and the T-bar test location is the temperature increase. The change in the temperature at pile interface with soil is equal the pile temperature change 45 °C. This increase in temperature could cause large increase in the undrained shear strength.

6.4.6. Post Test Void Ratio Measurement

At the end of the test, water content clay samples were taken at different radii from the pile surface and different depths from the clay surface. Because the clay is saturated, the void ratio values were calculated directly from the gravimetric water content measurements. The distribution in void ratio at the end of the test is shown in Figure 6.27. Also, the final depths and radii of the sensors were measured during the disassembly of the clay layer.

6.5. Acknowledgements

Chapter 6, in full, is currently being prepared for submission for publication of the material as it may appear in part of the following journal publication (The dissertation author was the primary investigator and author of this paper):

Ghaaowd, I. & McCartney, J.S. (In preparation). "Test setup for centrifuge modeling of energy piles in saturated soft clay." To be submitted to ASTM Geotechnical Testing Journal.

Table 6.1. Details of the Actidyne C61-3 geotechnical centrifuge

Quantity	Value
Capacity (g-tons)	50
Radius (m)	2.0
Basket Width (m)	0.6
Basket Length (m)	1.0
Basket Depth (m)	0.60
Maximum Acceleration (g)	130
Maximum Load Under Maximum Acceleration (kg)	230
Maximum Load (kg)	500
Maximum Acceleration Under Maximum Load (g)	100

Table 6.2. Centrifuge scaling laws

Quantity	Units	Scale Factor
Length	L	1/N
Area	L^2	$1/N^2$
Volume	L^3	$1/N^3$
Acceleration, Gravity	L/T^2	N
Mass	m	$1/N^3$
Force	$m\ L/T^2$	$1/N^2$
Stress	m/LT^2	1
Strain	1	1
Mass Density	m/L^3	1
Young's modulus	m/LT^2	1
Strength	m/LT^2	1
Time (diffusion)	T	$1/N^2$
Time (dynamic)	T	1/N
Frequency	F	N
Bending stiffness (EI)	$m\ L^3/T^2$	1/N4
Axial stiffness (EA)	$m\ L/T^2$	$1/N^2$

Table 6.3. Summary of testing stages

Testing Stage	Stage Description
I	In-flight Consolidation
II	Pile Installation
III	Pile Heating
IV	Pile Cooling
V	Pile Pullout

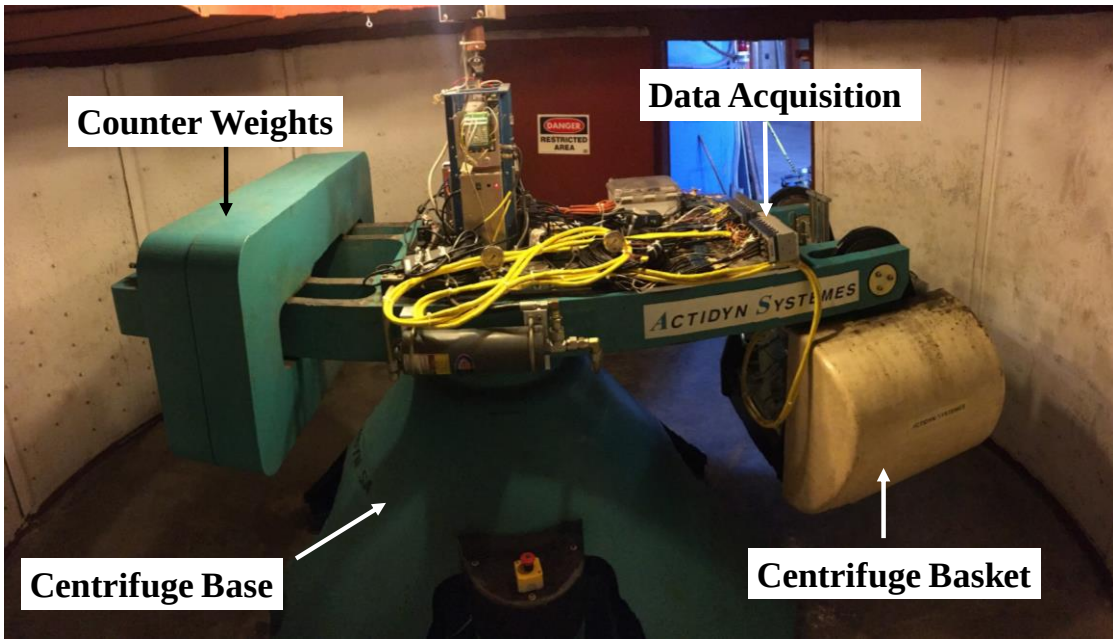

Figure 6.1. Actidyne C61-3 Centrifuge at the University of California San Diego

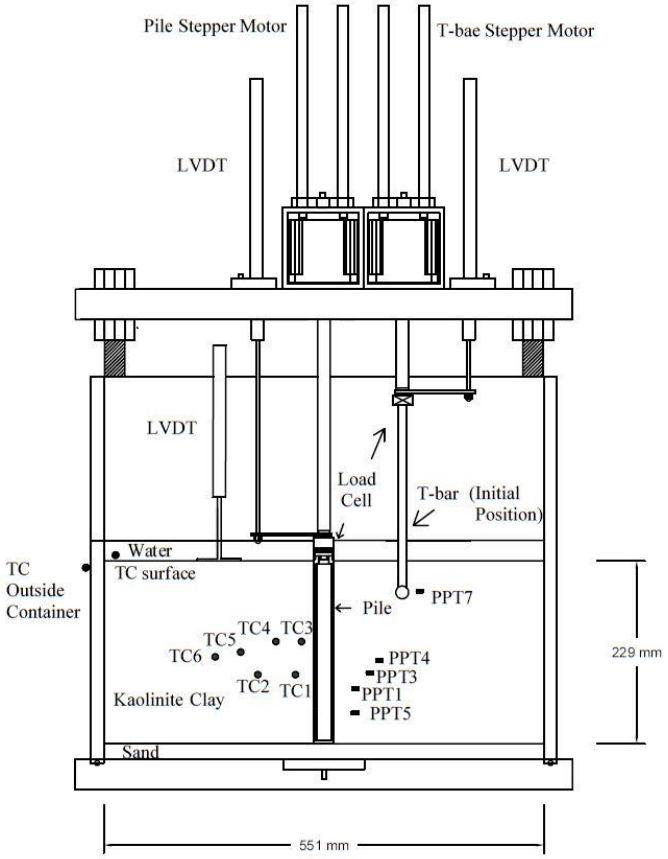

Figure 6.2. Cross-section of the setup using the experiments showing the energy pile, T-bar, thermocouples (TC), and pore water pressure transducers (PPT).

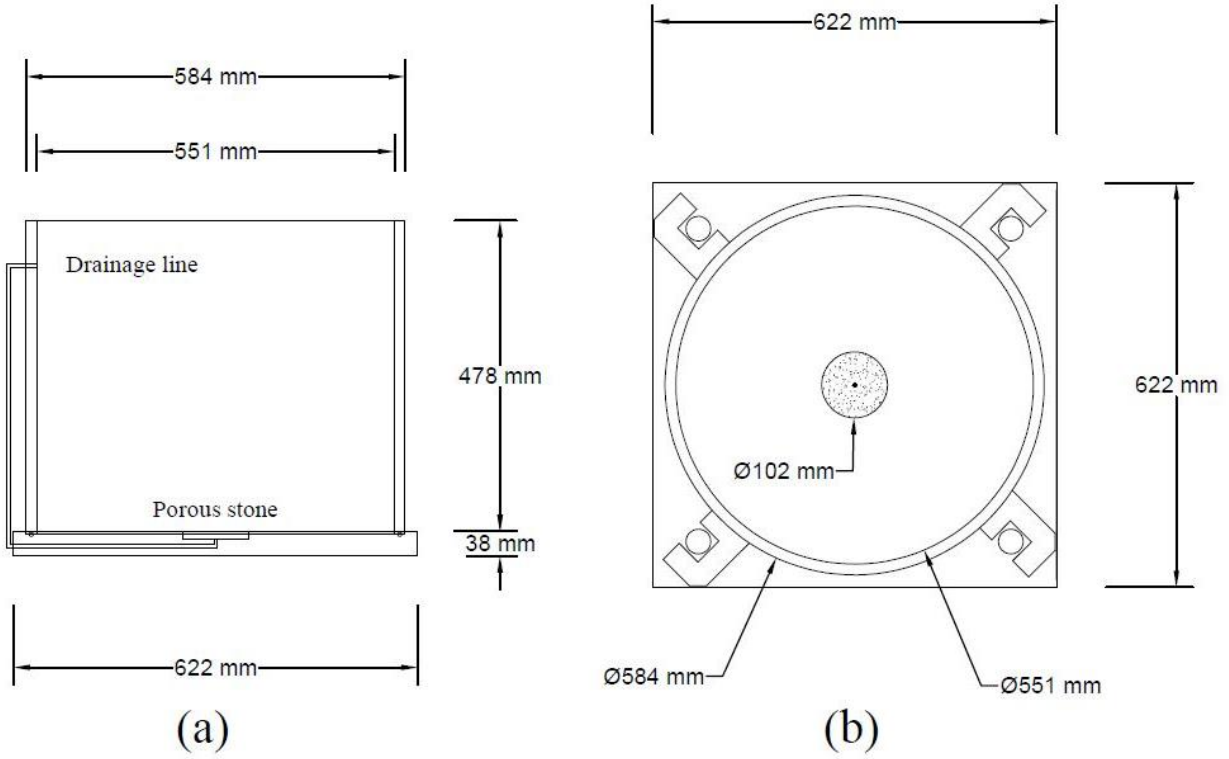

Figure 6.3. Cross-section views of the cylindrical containers

Figure 6.4. (a) The cylindrical container without reaction plate (b) The cylindrical container with reaction plate

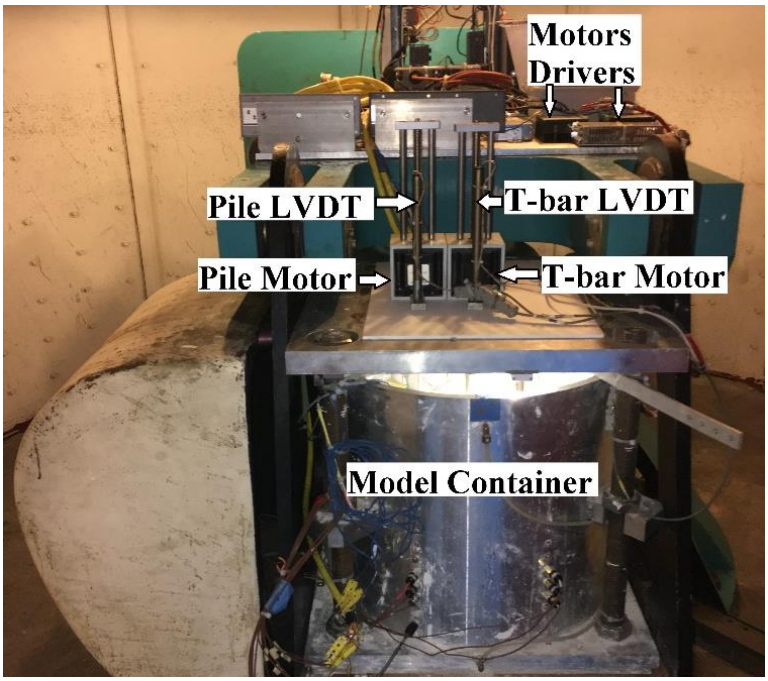

Figure 6.5. Stepper motors mounted to the reaction plate

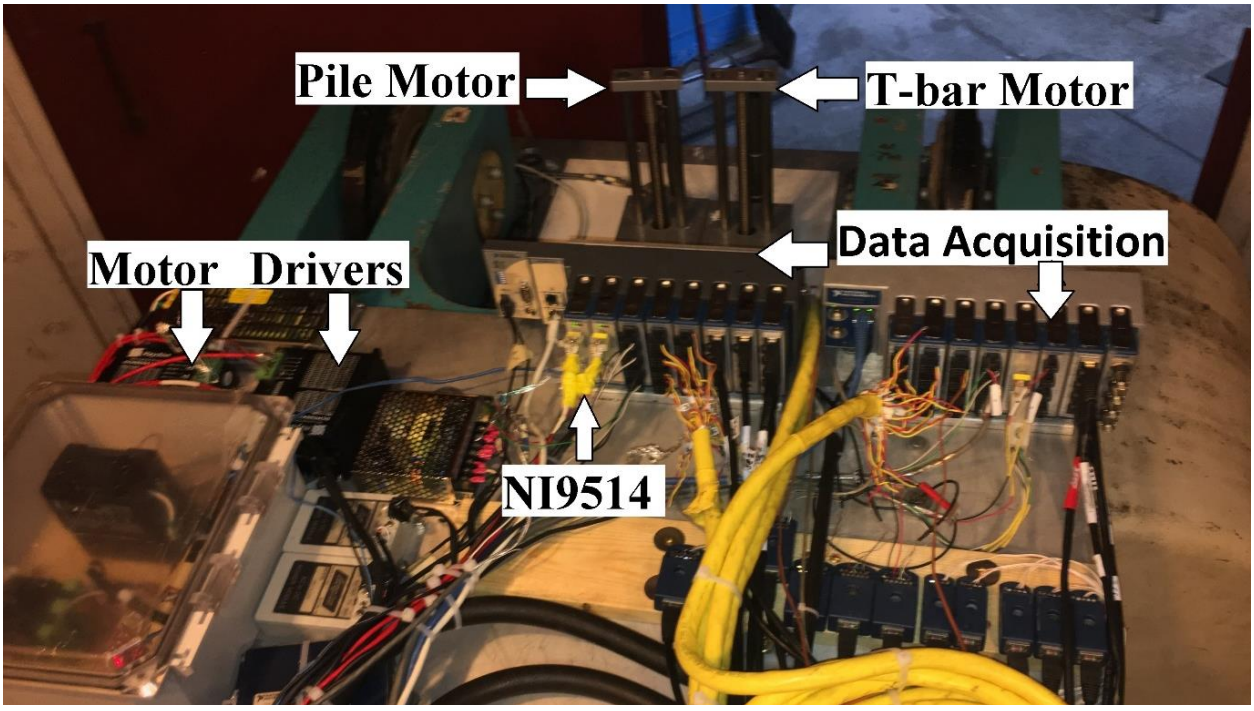

Figure 6.6. Data acquisition system components to control the motors

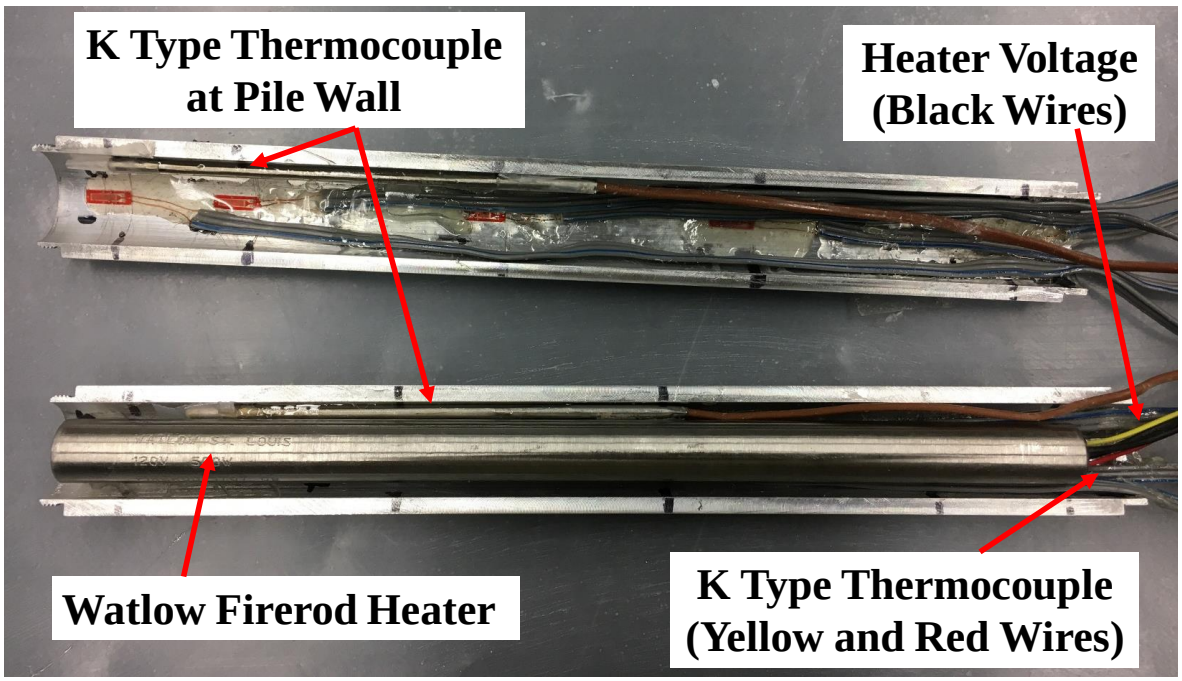

Figure 6.7. Watlow Firerod heater inside the pile

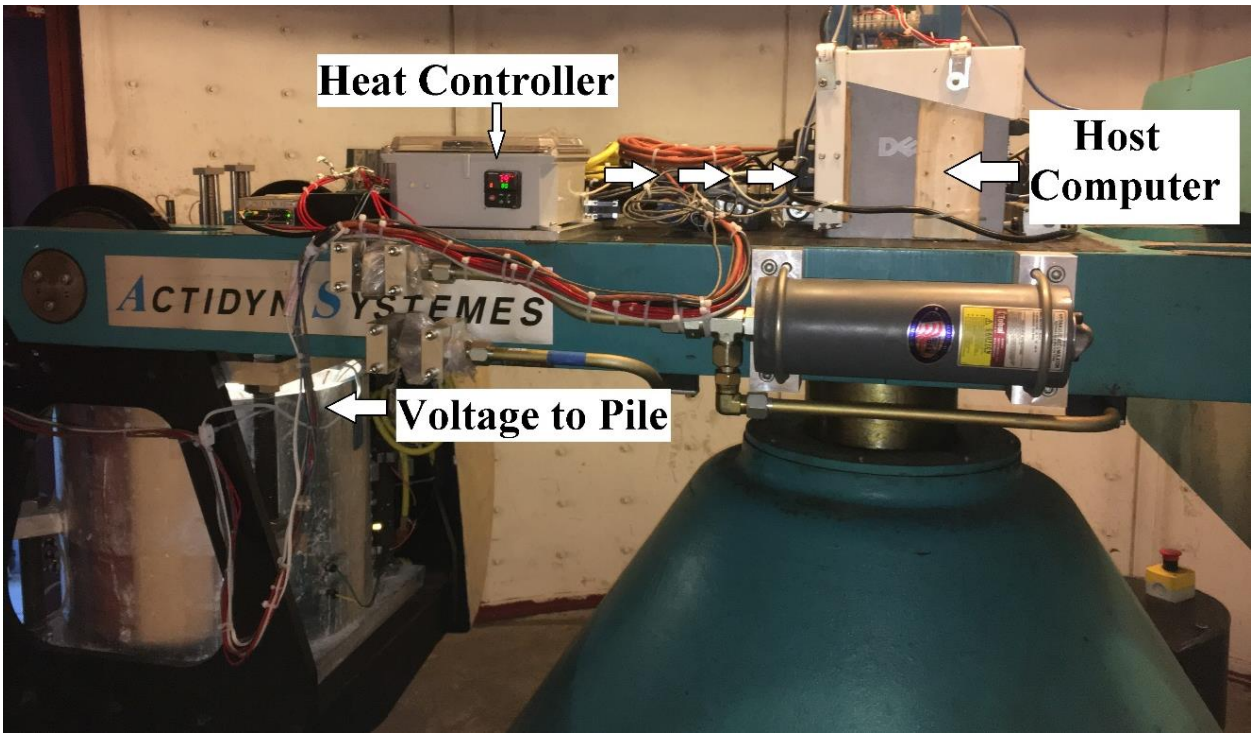

Figure 6.8. Heat controller setup

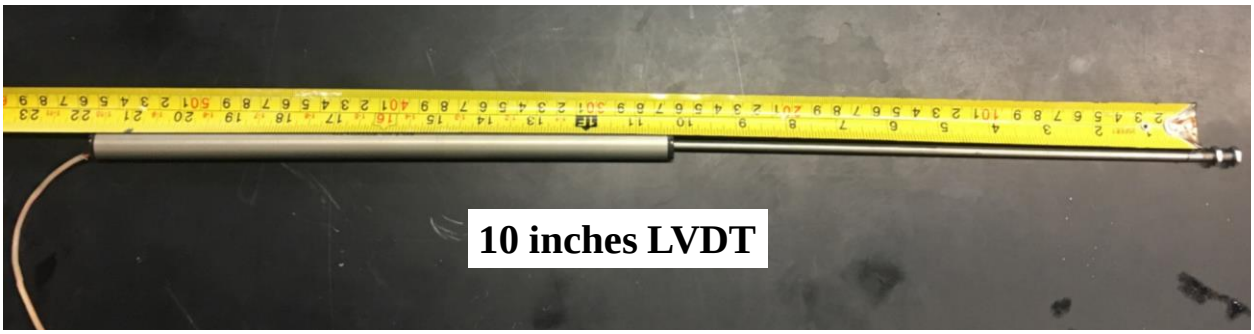

Figure 6.9. Linear variable deformation transformer (LVDT) used for monitoring of pile head movement

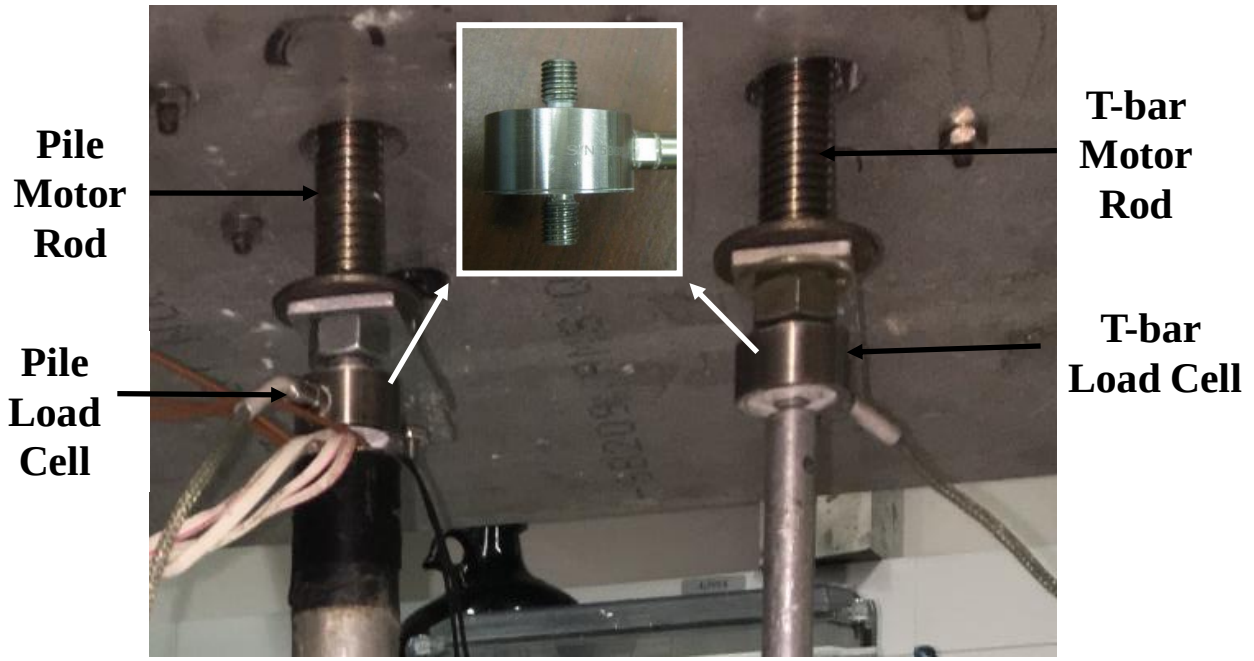

Figure 6.10. Miniature inline threaded load cell.

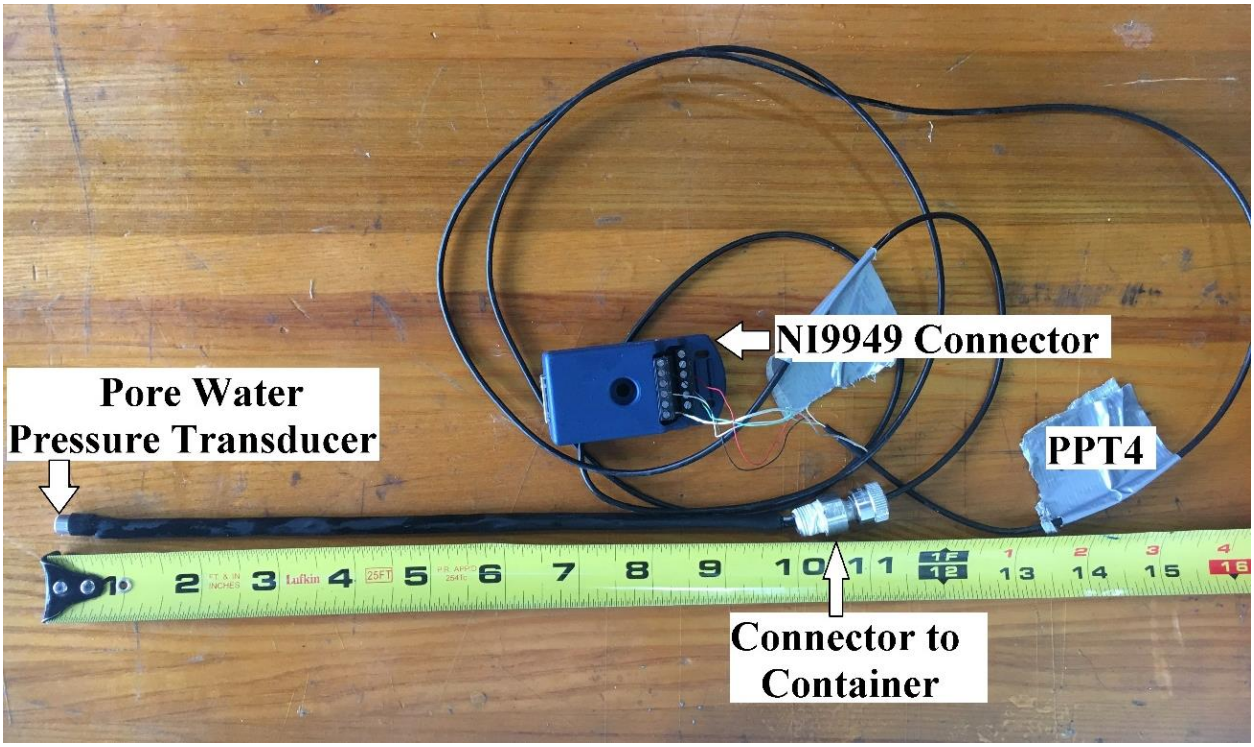

(a)

(b)

Figure 6.11: (a) Configuration of sensors inserted through the container wall into the soil layer: (a) Miniature Druck PDCR 81 pore water pressure transducers; (b) K-type thermocouples having different lengths

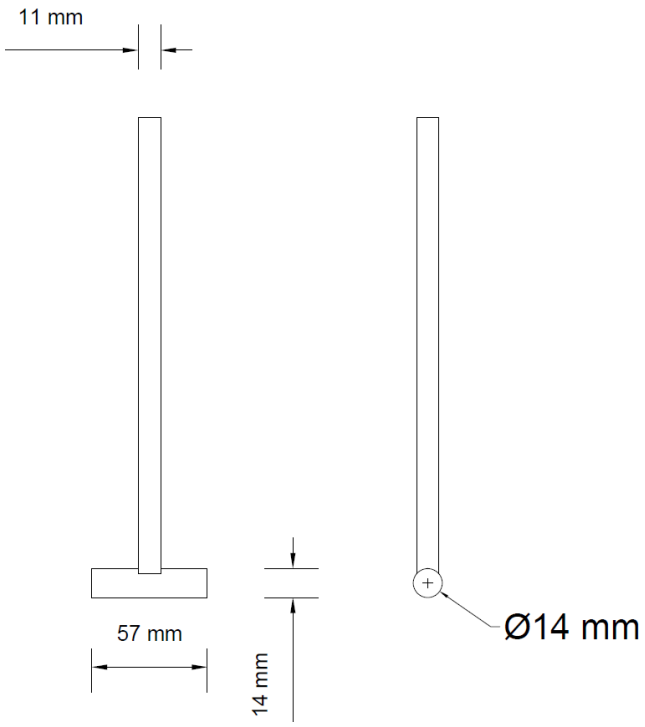

(a)

(b)

Figure 6.12: (a) T-bar dimensions, (b)T-bar photograph

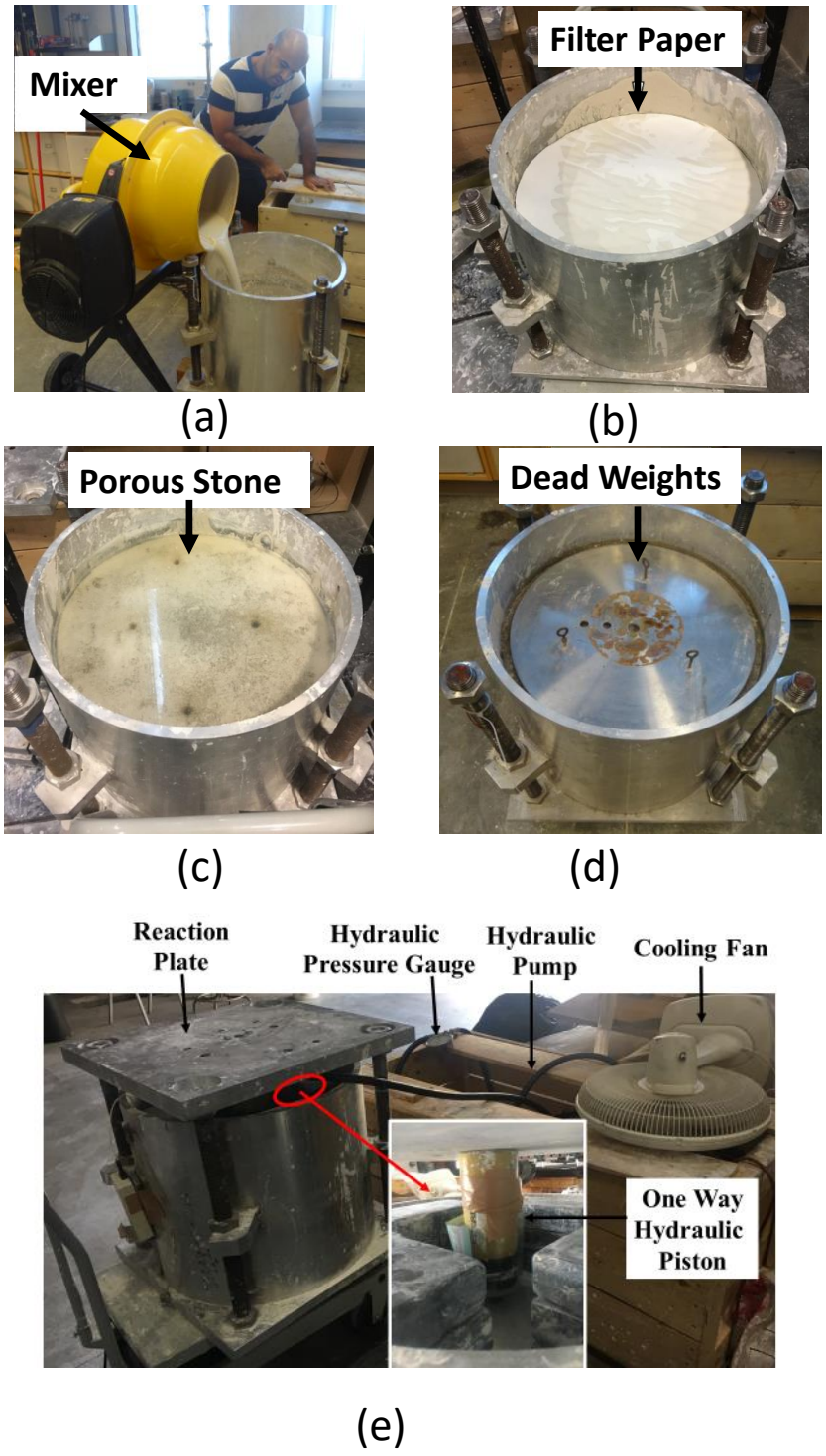

Figure 6.13: (a) Placing the mixed slurry in the container; (b) Filter paper placement; (b) Filter paper placement on the top of clay layer; (c) Porous stone on top of clay slurry mix; (d) Placement of loading plate on top of porous stone; (e) Slurry pre-consolidated under dead weights at 1-g.

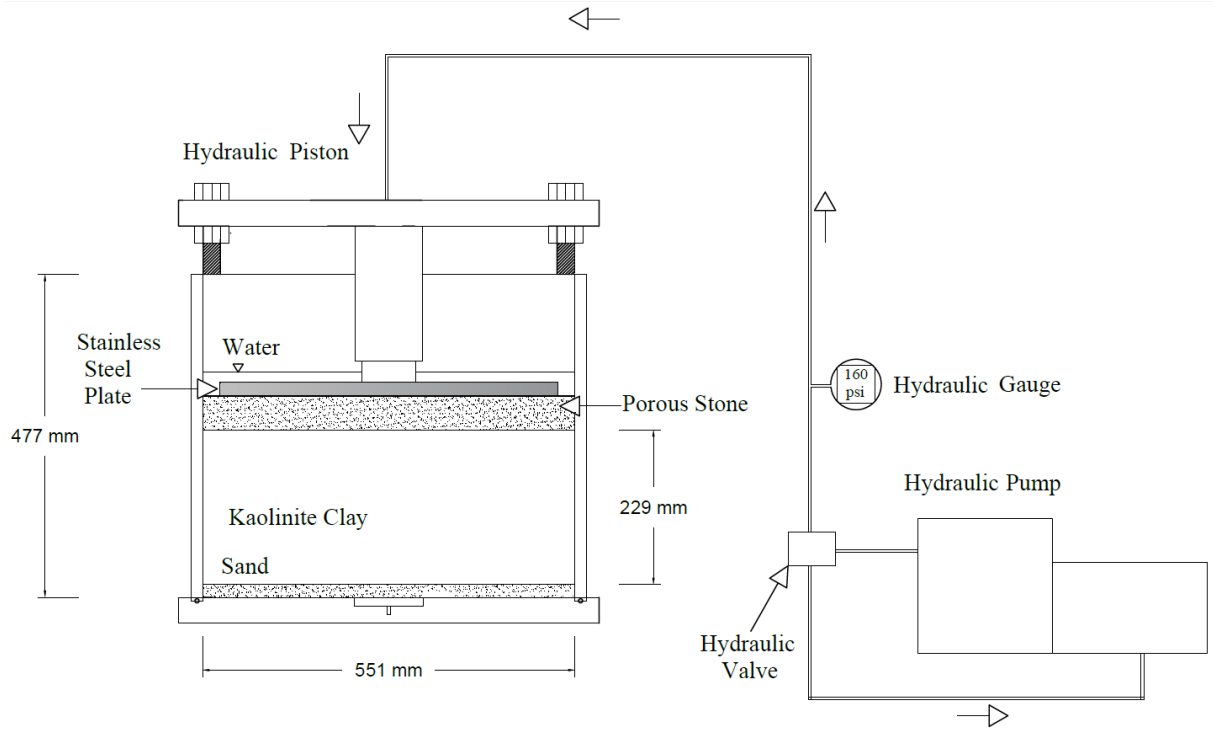

Figure 6.14. Schematic of the container along with the self-reaction consolidation setup

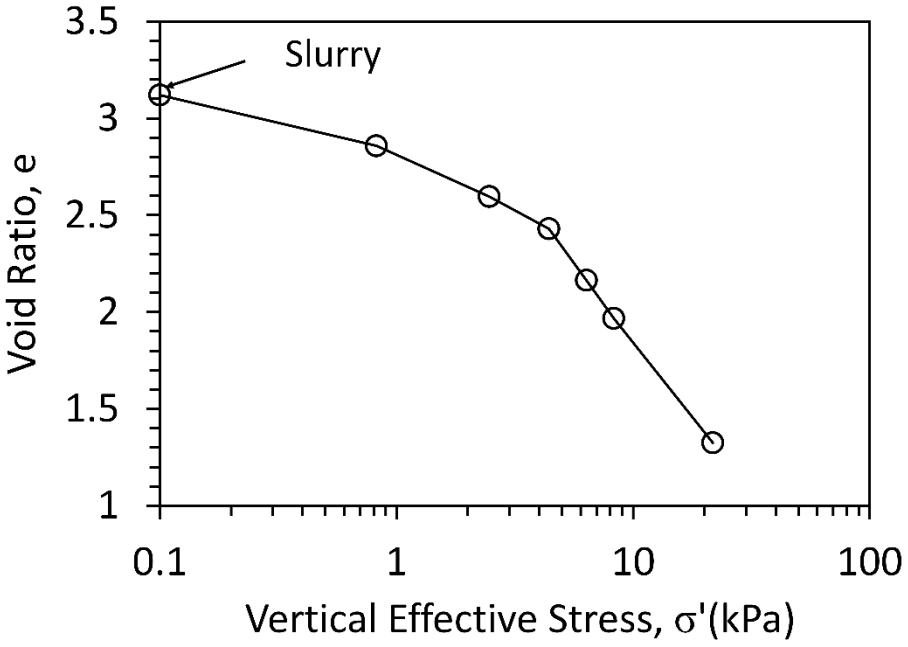

Figure 6.15. Typical compression curve for the Kaolinite clay during 1-g consolidation

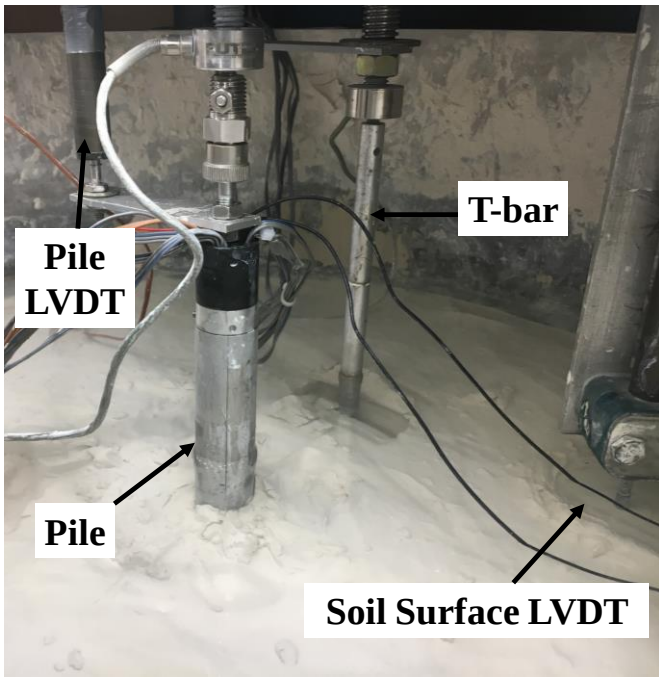

Figure 6.16. In-flight picture of the pile at initial position

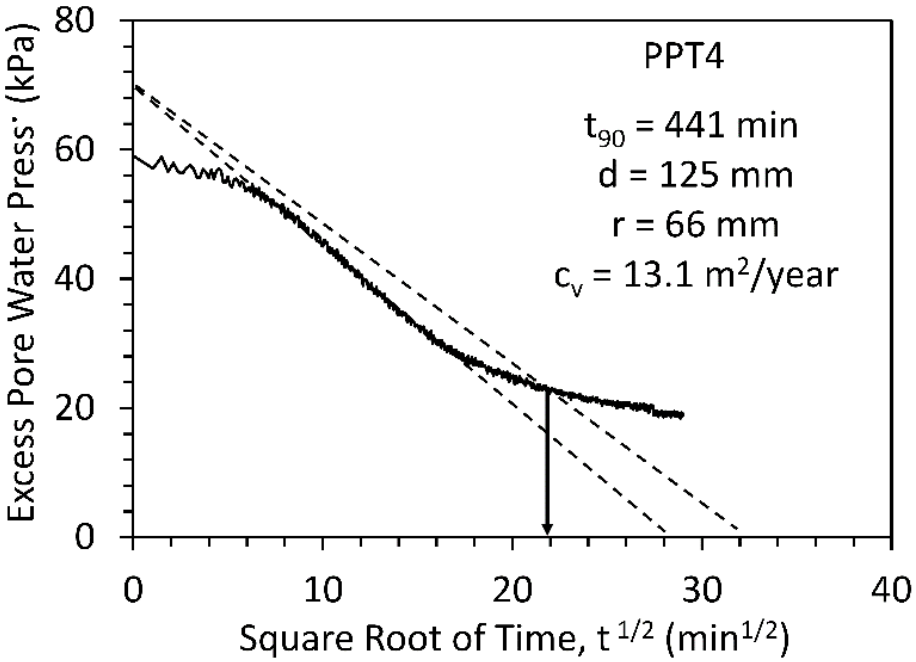

Figure 6.17. Typical trends in excess pore water pressure measured by PPT4 versus the square root of time

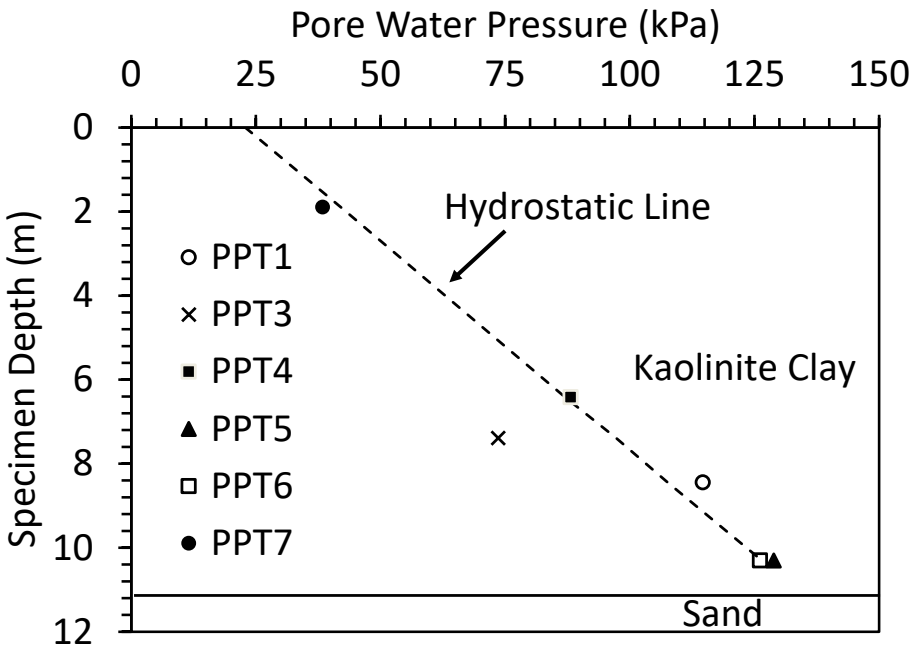

Figure 6.18. Typical pore water pressure profile after consolidation with depth in prototype-scale.

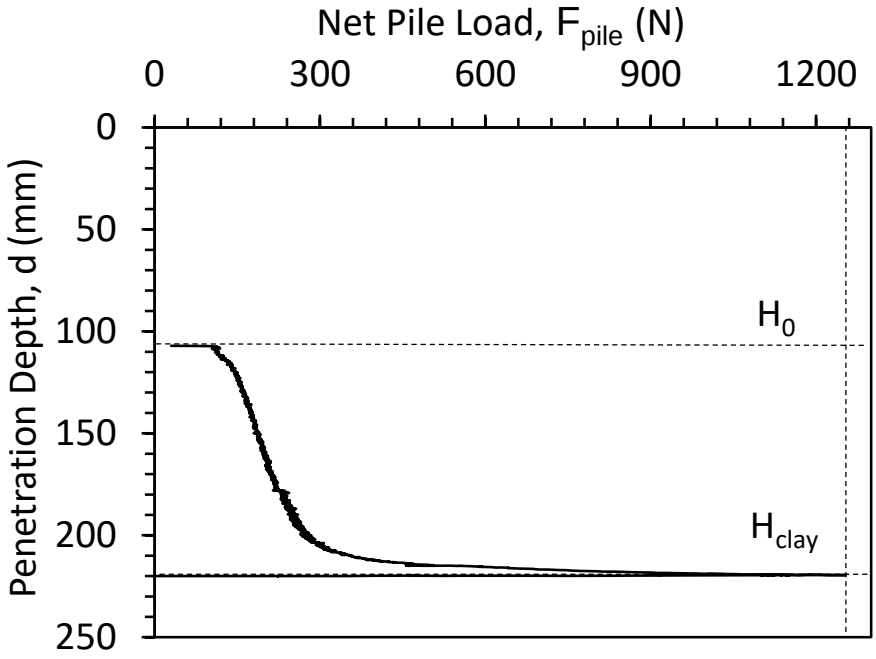

Figure 6.19. Typical trend in force applied to the pile head during pile insertion (note: Pile initially at a depth of 120 mm before insertion)

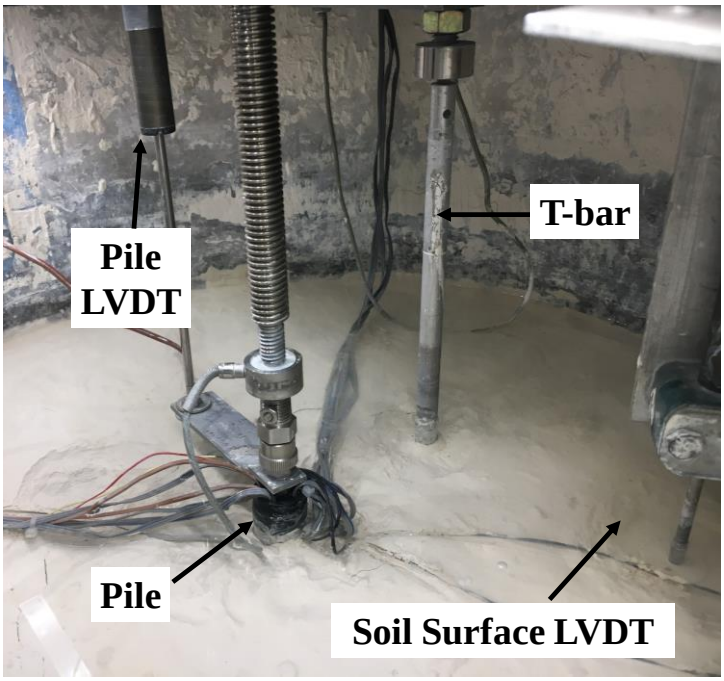

Figure 6.20. In-flight picture of the pile fully installed in the clay layer

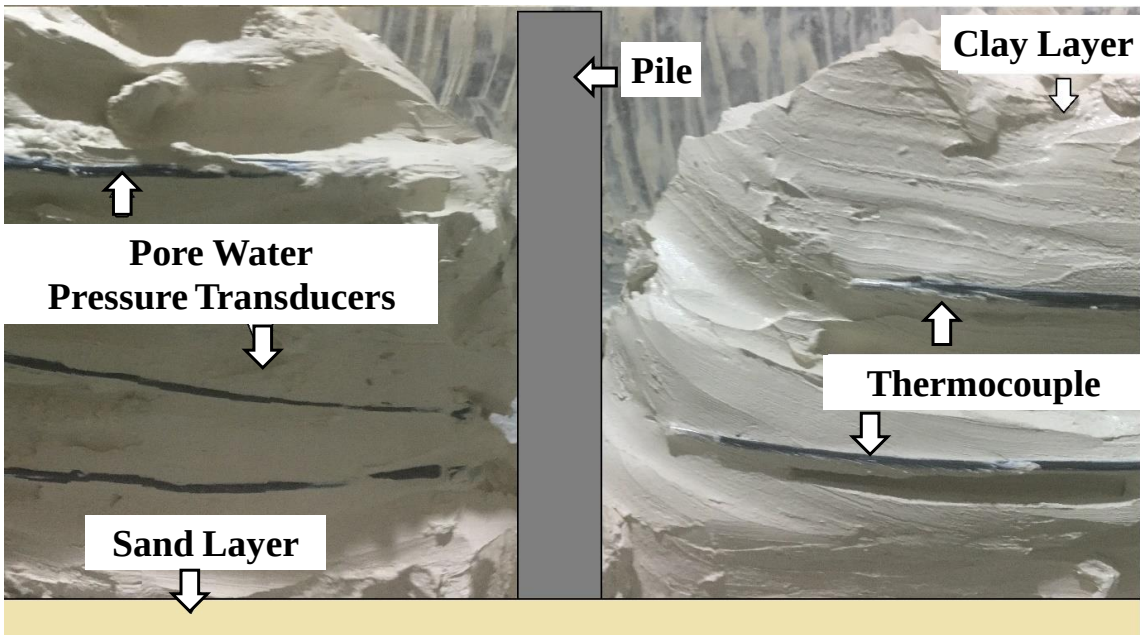

Figure 6.21. Picture showing the measurement of the post-test sensor locations

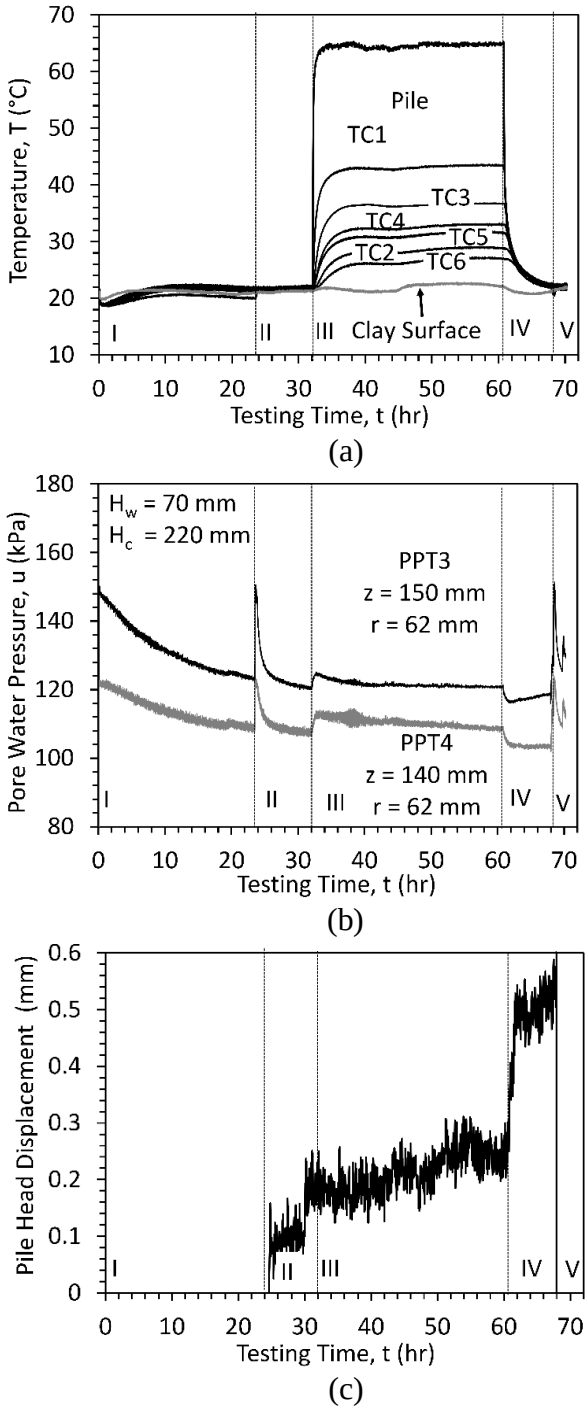

Figure 6.22. Typical time series of sensor results during the five testing stages described in Table 2: (a) Temperature versus testing time at different radii, (b) Pore water pressure versus testing time, (c) Pile head displacement versus testing time.

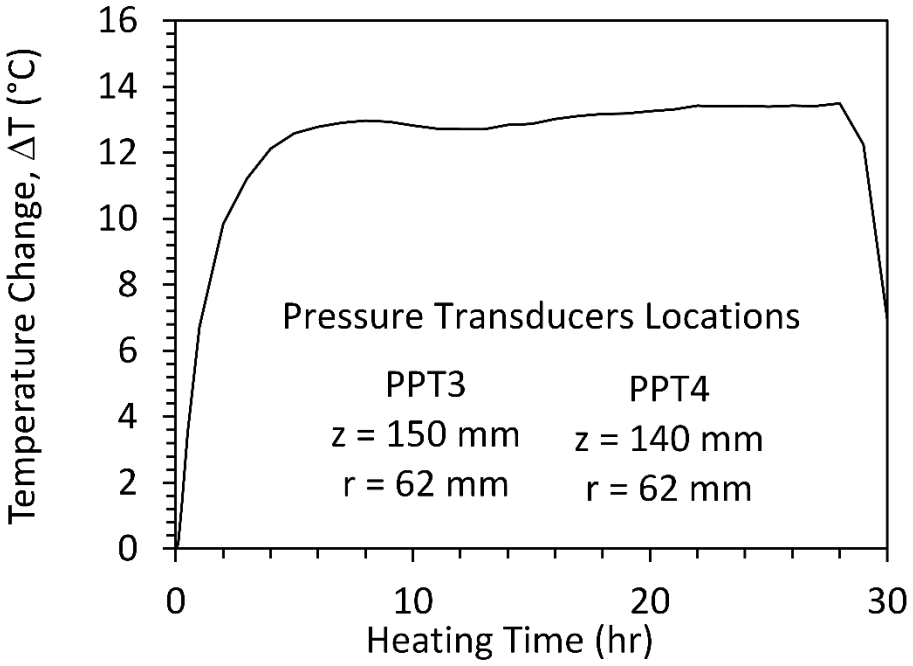

(a)

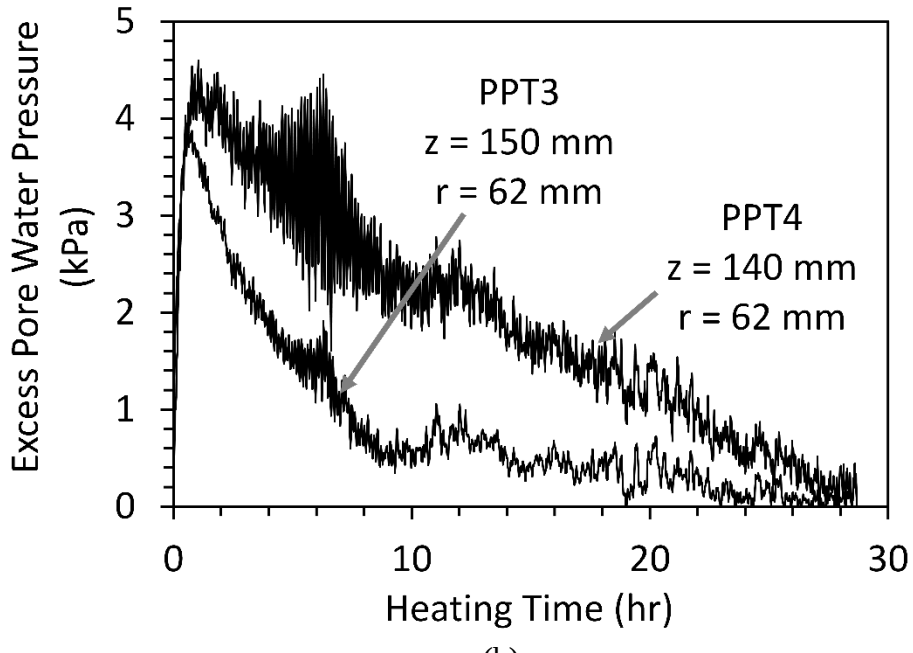

(b)

Figure 6.23: Typical time series of sensor results during the heating stage: (a) Temperature change versus heating testing time at pore water pressure transducers locations, (b) Thermal excess pore water pressure versus heating time

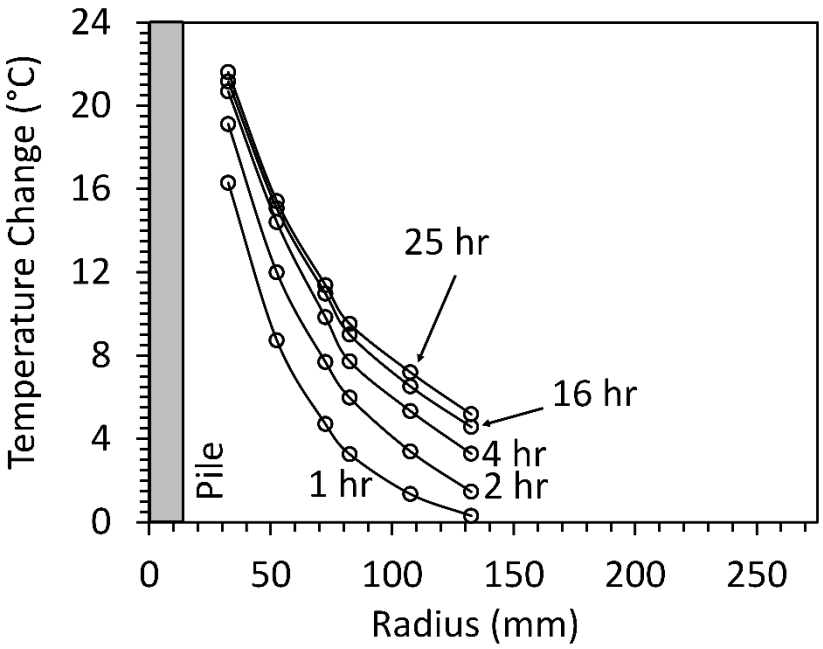

Figure 6.24. Typical temperature changes at different heating times.

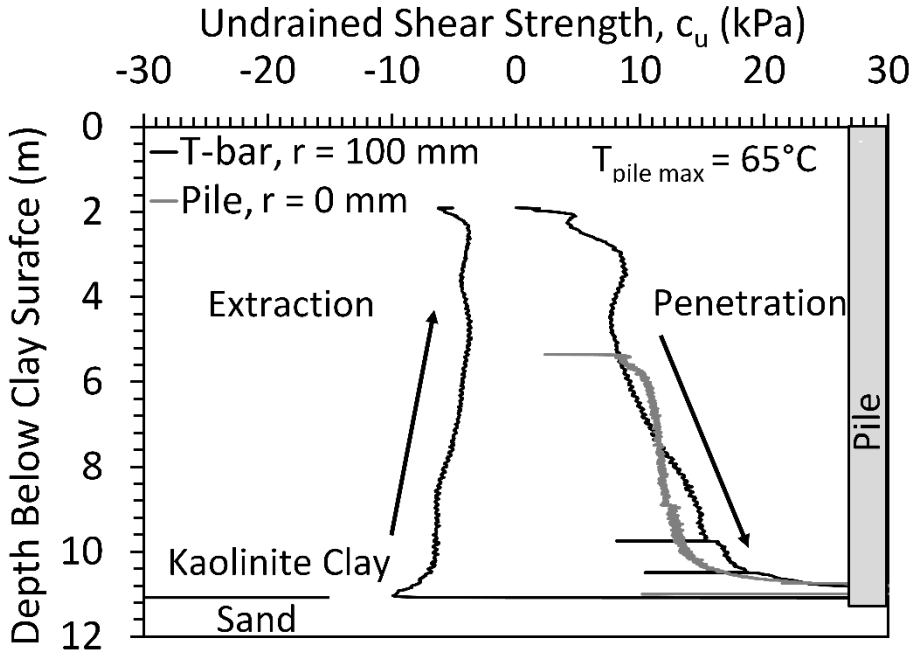

Figure 6.25: Comparison of the typical profiles of undrained shear strength measured from the T-bar test and those inferred from pile installation (positive values used to denote the undrained shear strength during insertion and negative values denote the undrained shear strength during extraction)

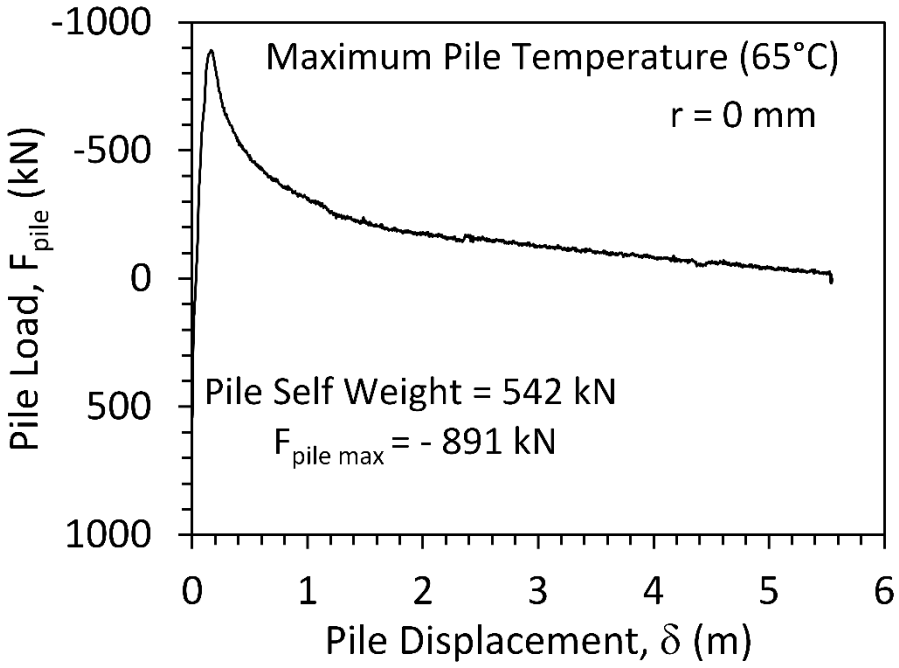

Figure 6.26. Typical pullout-displacement curve for a heated energy pile in prototype scale

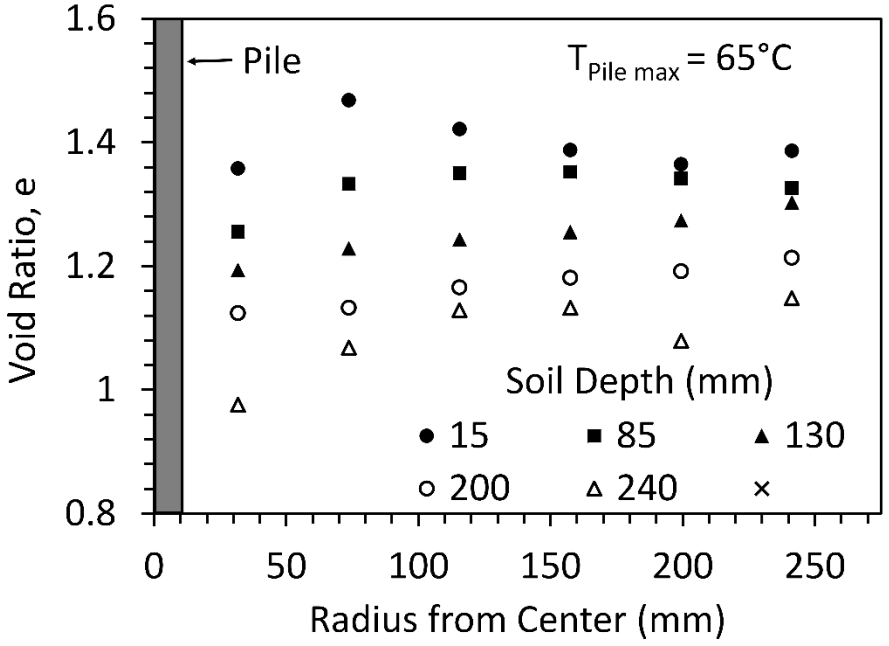

Figure 6.27. Typical post-test distribution in void ratio in the clay layer

Chapter 7. Centrifuge Modeling of Offshore Piles in Soft Clay: Results

7.1. Overview

The testing program and results for seven jacked-in piles without a seating load embedded into saturated soft clay were summarized in Table 7.1. In addition, three jacked-in piles with seating loads embedded into saturated soft clay were summarized in Table 7.1.The tests were performed to investigate the role of the temperature on the pullout pile load capacity and study the behavior of surrounded soil over pile temperature range of 23 °C to 80 °C. The initial void ratio of the clay at the end of the consolidation at 1g is approximately 1.2 at mid-height of the soil layer. A cross section of the pile model within the soil layer showing the radius and depth datum is also included in Figure 7.1.

7.2. Temperature Response

Time series of the pile and clay temperatures at different locations are shown for each test in Figure 7.6 (a), Figure 7.10(a), Figure 7.14(a), Figure 7.18(a), Figure 7.22(a), and Figure 7.26(a) for the heated piles. In the unheated pile, only soil surface temperature was measured and shown in Figure 7.3 (a). For all tests on piles heated to a given target temperature, the pile temperature increased very quickly due to the rapid response of the electrical resistance heater, but the temperature of the clay increased gradually and stabilized after approximately 10 hours in model scale (1041 days in prototype scale) in the different tests.

Table 7.3 includes a summary of the locations of the thermocouples sensors at the end of Test J2. Although the heater in the pile at Test J2 increased in temperature from 21 to 31 °C (□T = 10 °C) as shown in Figure 7.6(a), the soil only reached a maximum temperature change of 6 °C which was measured by TC1 at 36 mm from the container. The temperature decreased away from

the energy pile with a negligible change at the container boundary of r=276 mm and soil surface at z = 0 mm. When the electrical resistance heater was turned off, the clay temperature rapidly decreased to a temperature of 22 °C. Table 7.4 shows the thermocouples sensors location for Test J3, the pile temperature was increased from 21 to 39 °C (ΔT = 18 °C) as shown in Figure 7.11(a), the soil only reached a maximum temperature change of 9 °C measured by TC1 at 43 mm from the container center which. There wasn't temperature increase at the container boundaries. During the cooling, the clay temperature rapidly decreased to a temperature of 23 °C. This is greater than the initial temperature, perhaps because the heat pulse was still moving through the clay layer and because the temperature of the centrifuge chamber increased to nearly 24 °C in during the 80 hours of centrifuge testing.

The thermocouples at different radii for Test J4 are summarized in Table 7.5. The pile temperature was increased from 22 °C to 45 °C as shown in Figure 7.15(a). The maximum temperature at 36 mm from the container center was 31 °C was measured by TC3. The sensors at the boundaries didn't record during the test, but the temperature at the boundaries from the previous tests didn't shown obvious increase in the temperature. At Test J5, the pile temperature increased to maximum of 53 °C, then decreased, the average pile temperature was 49 °C as shown in Figure 7.19(a), and the maximum soil temperature measured by nearest thermocouple to the pile wall (TC1) is 33 °C.

Table 7.7 includes a summary of the locations of the thermocouple sensors at the end of Test J6. The pile temperature was increased to a maximum value of 65 °C in this test as shown in Figure 7.23(a). The pile temperature stabilized after 2 hours, but the soil temperature took 10 hours to stabilize. The maximum temperature recorded by the thermocouple nearest to the pile wall was 44 °C at radius of 36 mm from the pile center. The thermocouples at different radii for Test J7 are

summarized in Table 7.8. The pile temperature was increased from 22 ℃ to 80 ℃ as shown in Figure 7.26(a). The maximum temperature at 36 mm from the container center was 49 ℃ was measured by TC1.

7.3. Thermal Excess Pore Water Pressure

All heated tests experienced in thermal excess pore water pressures generation in the clay with immediately after the increase in temperature as shown in Figure 7.6 (b), Figure 7.10(b), Figure 7.14(b), Figure 7.18(b), Figure 7.22(b), and Figure 7.26(b). The thermal excess pore pressure value is function of the soil properties, temperature change at the location of the pore water pressure transducer, and the effective stress. This increase in pore water pressure occurs due to partially undrained conditions and the difference between the coefficients of thermal expansion of the clay solid skeleton and the water (e.g., Ghaaowd et al. 2015). Two pressure sensors where used to measure the pore water pressure. The pore water pressures after maximum 1 hour started to dissipate, with thermal consolidation finishing after approximately 10 hours. The maximum measured thermal excess pore water pressure during Test J7 where the highest temperature was applied were 10 kPa and 5 kPa at PPT3 and PPT4 respectively as shown in Figure 7.27(b). Due to the combination of the depth of the sensor and the greater temperature change at PPT3 location, the measurement at the PPT3 was greater.

7.4. Pile Head Displacement

After the pile installed and its tip reached the sand soil layer during the pile installing stage. The pile head displacement was zeroed. The pile head displacement was measured during the rest of the testing stages for all tests as shown in Figure 7.3(c), Figure 7.6(c), Figure 7.10(c), Figure 7.14(c), Figure 7.18(c), Figure 7.22(c), and Figure 7.26(c). During the heating for all heated tests, the pile head was stabilized and didn't move up as expected, pile show expansion according

the strain gauges was not included in this paper, the expansion movement could be caused movement in the pile tip and penetrate more the sand. During the cooling, the pile contracted, and the pile head moved down for all tests, and the calculated thermal coefficient from the measured displacement similar to the coefficient of linear thermal expansion of aluminum equal to 24 με/°C.

7.5. Undrained Shear Strength

The undrained shear strength could be interpreted using data from the pile installation as mentioned in Chapter 6. The undrained shear strength profile from 5.5 m under clay surface to the depth of 11 m in the prototype scale was interpreted and plotted in Figure 7.29. The undrained shear strength profiles have similar trends which is another evidence that the clay layer have initial condition for all tests. The average initial undrained shear strength was around 11 kPa for all tests.

Even though the T-bar test was done 100 mm fare from the center for each test after the pullout stage, but the T-bar measurements in the clay layers with heated and unheated energy piles provide further evidence as to the effects of heating and cooling on the temperature effects on the behavior of normally consolidated clay layers. The initial T-bar position is slightly below the clay surface to maximize the stroke of the T-bar test, so the undrained shear strength near the surface of the clay layer may not be well characterized. The interpretation of the undrained shear strength was done by using the correlations founded by Stewart Randolph (1991). More details about the calculation and T-bar dimensions are shown in Chapter 6. The undrained shear strength interpreted from T-bar tests for different for five tests are shown in Figure 7.30. Another three T-bar tests from Ghaaowd et al. (2018) are included in Figure 7.31, which show good agreement.

7.6. Pile Pullout Capacity

The pile was pulled out at speed of 0.1 mm/s in model scale, the net pullout pile capacity for the energy piles in clay layers are summarized in Table 7.1.The maximum pullout capacity

ranges from -462 at the unheated pile to -891 kN at heated to 80 °C corresponding to 0.16 m and 0.08 m displacement at prototype scale for both tests respectively. The pile pullout was improved dramatically by the increase of the temperature as shown in Figure 7.32. In addition, results from three pile pullout load tests with seating load done by Ghaaowd et al. (2018) were included in this study as shown in Figure 7.33, which show good agreement. The maximum pullout capacity ranges from -370 at the unheated pile to -723 kN at heated to 63°C, which follow the same trend of the other tests

7.7. Acknowledgements

Chapter 7, in full, is currently being prepared for submission publication of the material as it may appear in part of the following journal publication (The dissertation author was the primary investigator and author of this paper):

Ghaaowd, I. & McCartney (In preparation). "Centrifuge modeling of temperature effects on the pullout capacity of energy piles in saturated soft clay." To be submitted to Journal of Geotechnical and Geoenvironmental Engineering.

Table 7.1. Summary of tests on the jacked-in pile without a seating load

Test Number	Pile Wall Temperature	Temperature Change	Maximum Pullout Load	Pile Load Improvement
#	°C	°C	kN	%
J1	23.0	0.0	-462	0
J2	31.0	8.0	-539	17
J3	39.5	16.5	-563	22
J4	45.0	22.0	-597	29
J5	53.0	30.0	-789	71
J6	65.0	36.0	-891	93
J7	80.0	57.0	-963	109

Table 7.2. Summary of tests on the jacked-in pile with a seating load

Test Number	Pile Wall Temperature	Temperature Change	Maximum Pullout Load	Pile Load Improvement
#	°C	°C	kN	%
L1	23	0.0	-370	0
L2	44	21	-520	41
L3	63	40	-723	95

Table 7.3. Sensor locations in Test J2 determined after testing

Sensor	r	z
	mm	mm
TC1	36	180
TC2	86	180
TC3	46	140
TC4	68	160
TC5	86	160
TC6	146	200
PPT3	55	150
PPT4	75	140

Table 7.4. Sensor locations in Test J3 determined after testing

Sensor	r	z
	mm	mm
TC1	43	180
TC2	63	180
TC3	53	140
TC4	78	160
TC5	83	160
TC6	143	200
PPT3	55	120
PPT4	62	130

Table 7.5. Sensor locations in Test J4 determined after testing

Sensor	r	z
	mm	mm
TC1	51	225
TC2	76	160
TC3	36	190
TC4	91	145
TC5	101	165
TC6	146	180
PPT3	51	160
PPT4	56	155

Table 7.6. Sensor locations in Test J5 determined after testing

Sensor	r	z
	mm	mm
TC1	32	199
TC2	79	136
TC3	41	186
TC4	66	148
TC5	91	174
TC6	142	161
PPT3	148	46
PPT4	130	60

Table 7.7. Sensor locations in Test J6 determined after testing

Sensor	r	z
	mm	mm
TC1	36	142
TC2	94	162
TC3	46	102
TC4	81	112
TC5	101	122
TC6	146	122
PPT3	62	150
PPT4	62	140

Table 7.8. Sensor locations in Test J7 determined after testing

Sensor	r	z
	mm	mm
TC1	36	195
TC2	76	130
TC3	51	190
TC4	86	120
TC5	98	150
TC6	136	160
PPT3	50	150
PPT4	70	130

Table 7.9. Change in undrained shear strength after the heating cooling cycle with different maximum pile temperatures

Test No	Maximum Pile Temperature	Maximum Change in Pile Temperature	Temperature at T-bar Radial Location	Average Undrained Shear Strength after the Heating-Cooling Cycle	Percent Change in Undrained Shear Strength after the Heating-Cooling Cycle
#	℃	℃	℃	kPa	%
J1	23	0	0	8.1	0
J2	31	8	2	8.3	3
J3	39	16	5	8.7	8
J4	45	22	7	9.3	15
J5	53	30	6	8.8	8
J6	65	42	13	10.0	23
J7	80	57	17	11.0	37

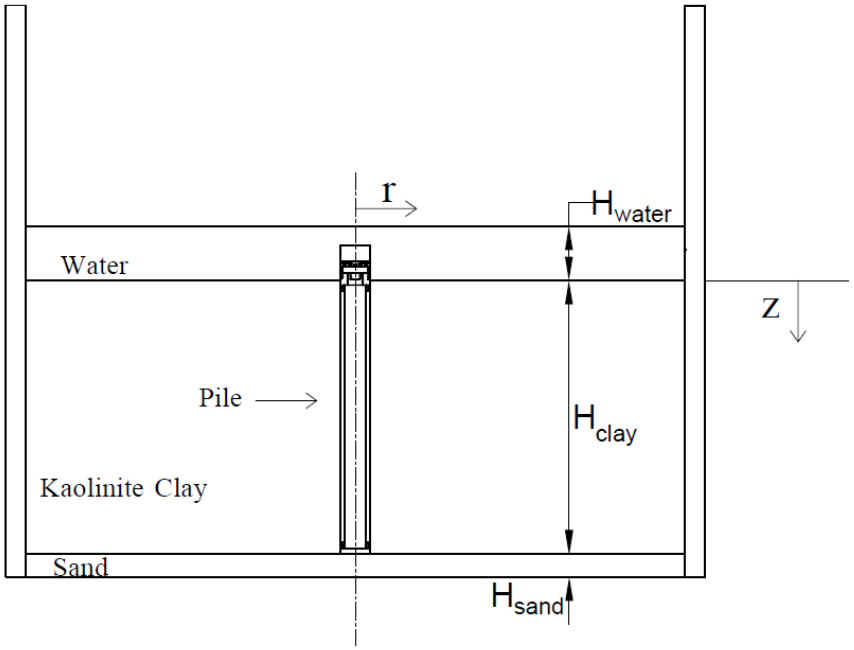

Figure 7.1 Typical cross section of the model jacked-in pile within the clay layer

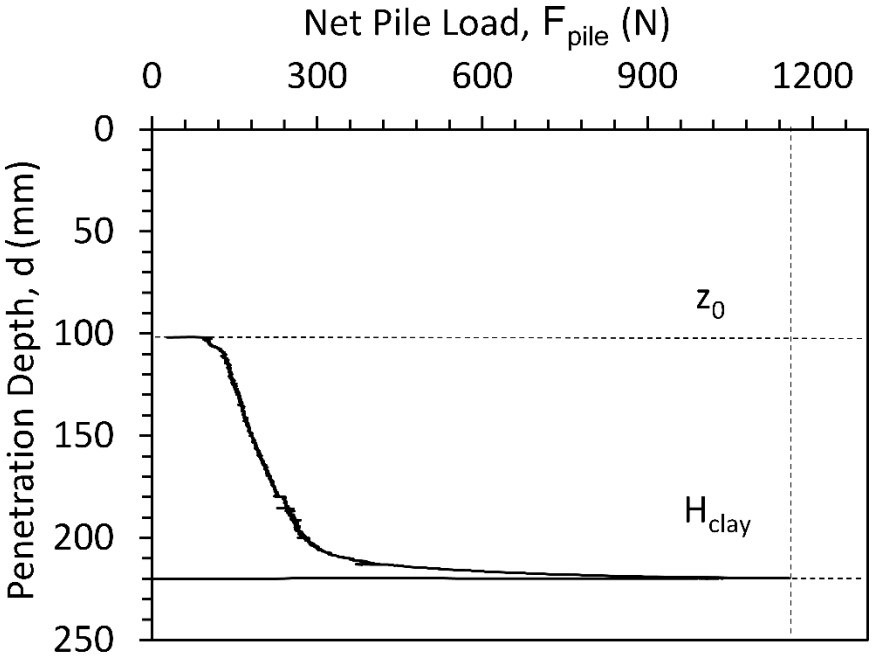

Figure 7.2. Installation of the pile in Test J1 from the initial position to the final position

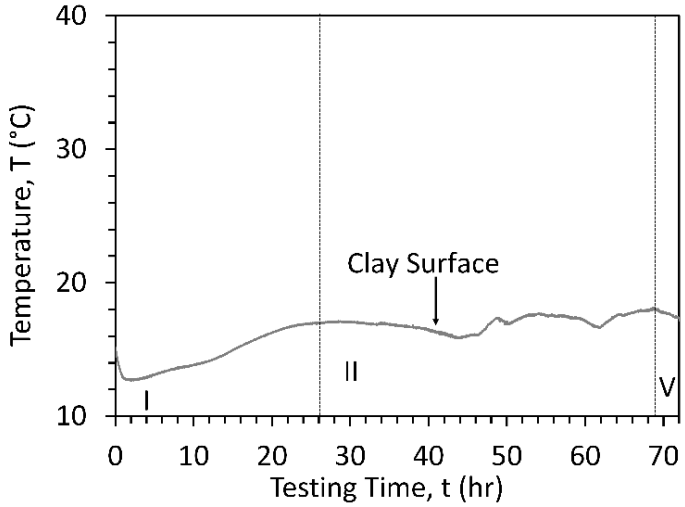

(a)

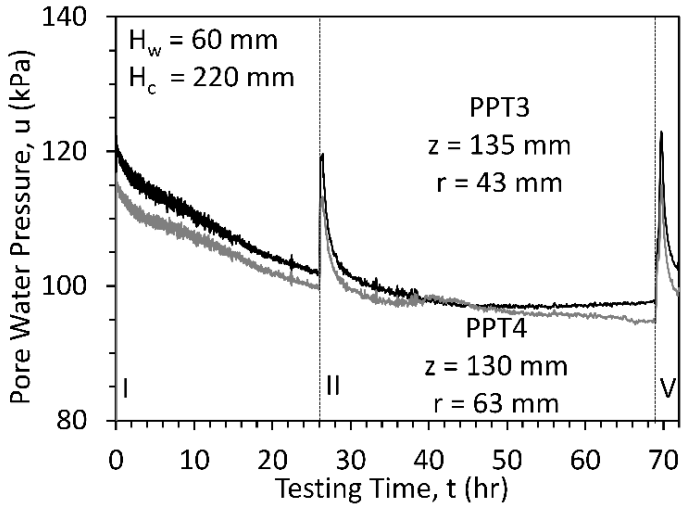

(b)

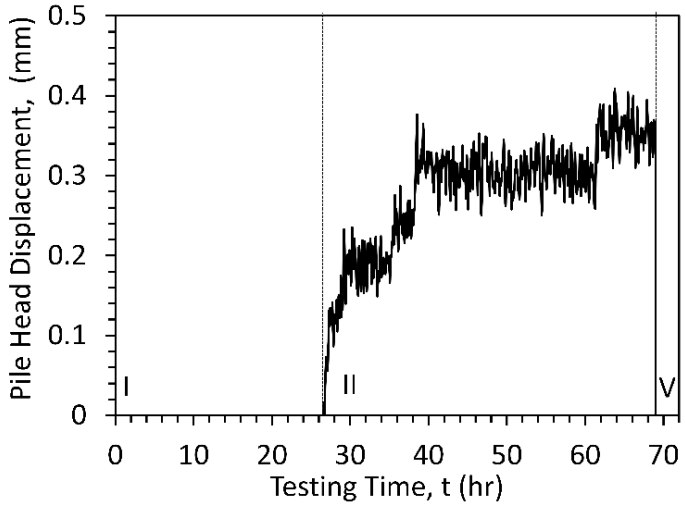

(c)

Figure 7.3: Time series results from Test J1: (a) Temperature versus testing time at different radii, (b) Pore water pressure versus testing time, (c) Pile head displacement versus testing time.

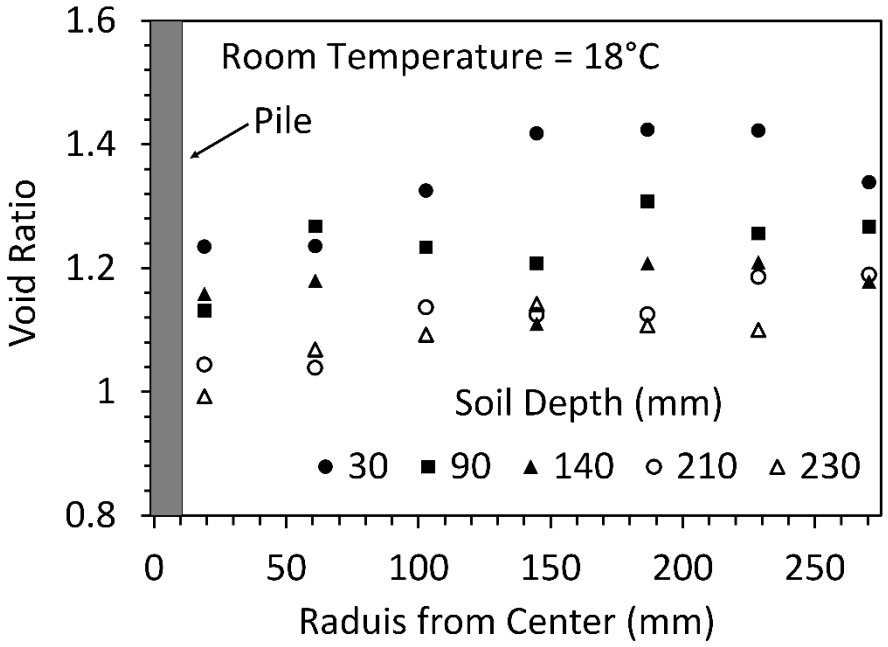

Figure 7.4. Void ratio profiles at the end of testing in Test J1 (model-scale dimensions)

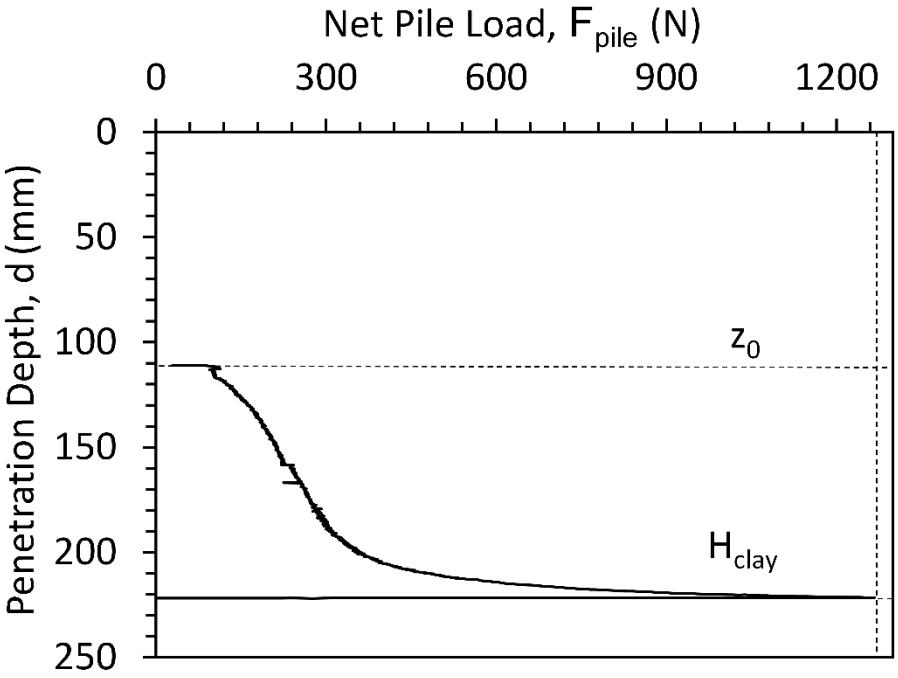

Figure 7.5. Installation of the pile in Test J2 from the initial position to the final position

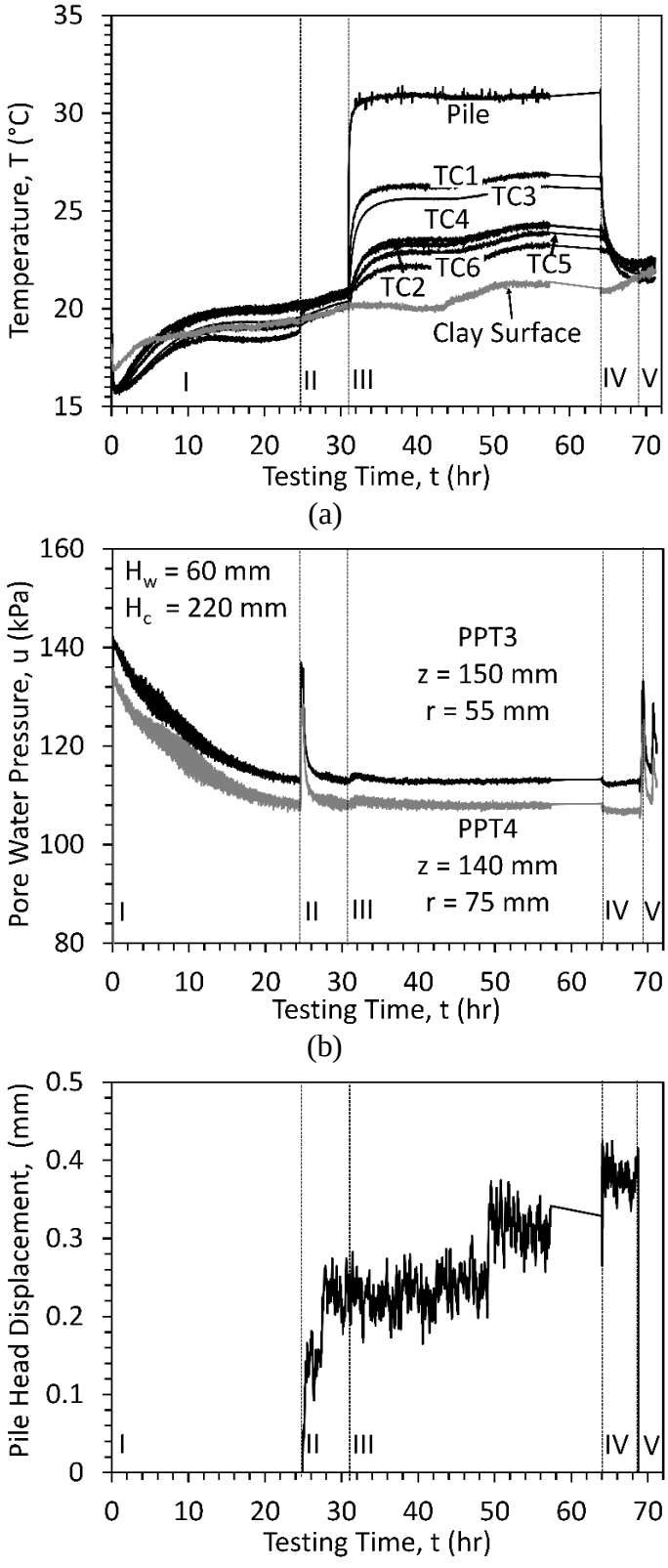

Figure 7.6: Time series results from Test J2: (a) Temperature versus testing time at different radii, (b) Pore water pressure versus testing time, (c) Pile head displacement versus testing time.

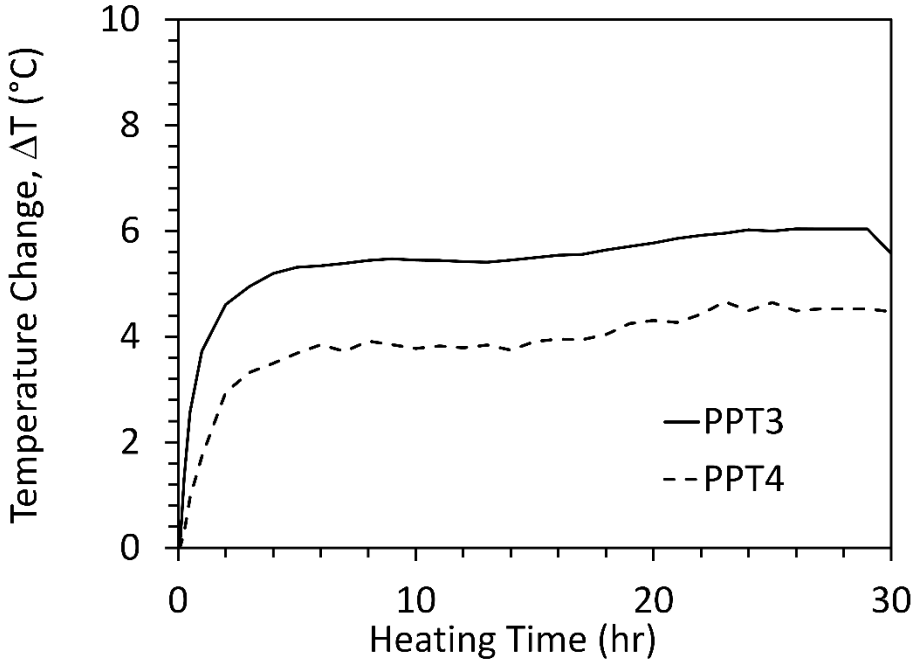

(a)

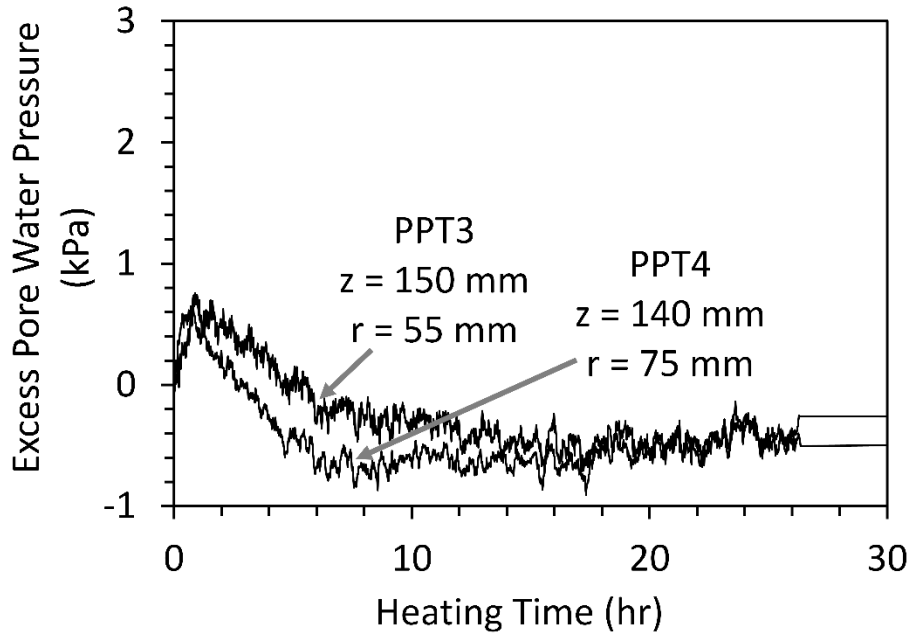

(b)

Figure 7.7: Test J2 time series of sensor results during the heating stage: (a) Temperature change versus heating testing time at pore water pressure transducers locations, (b) Thermal excess pore water pressure

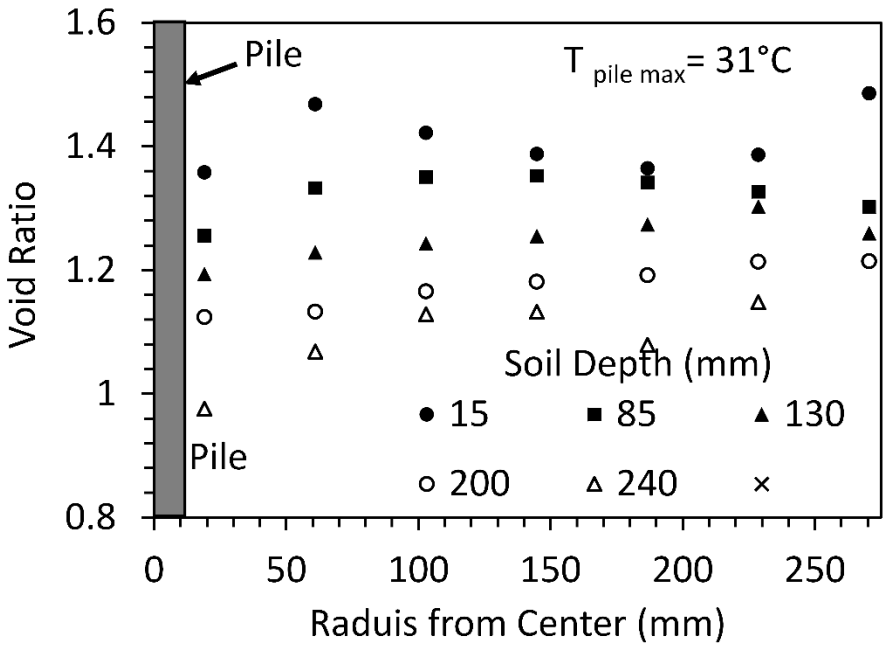

Figure 7.8. Void ratio profiles at the end of testing in Test J2 (model-scale dimensions)

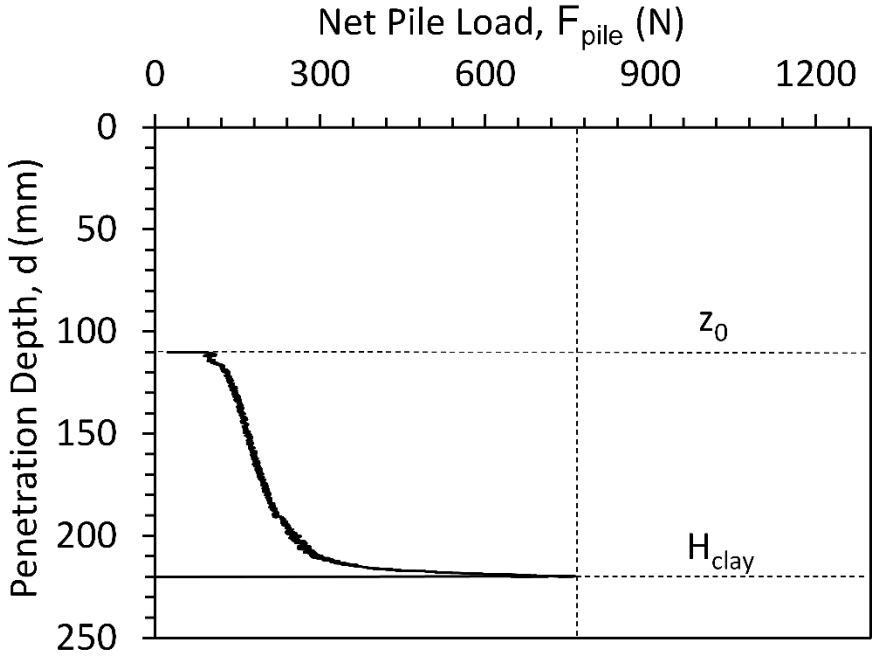

Figure 7.9. Installation of the pile in Test J3 from the initial position to the final position

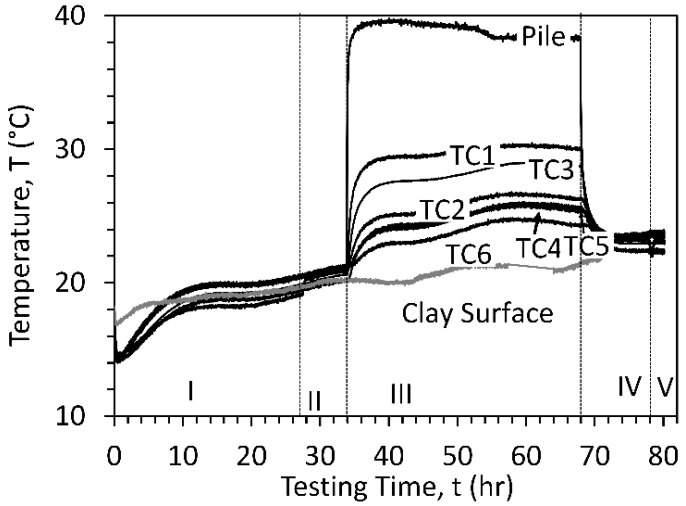

(a)

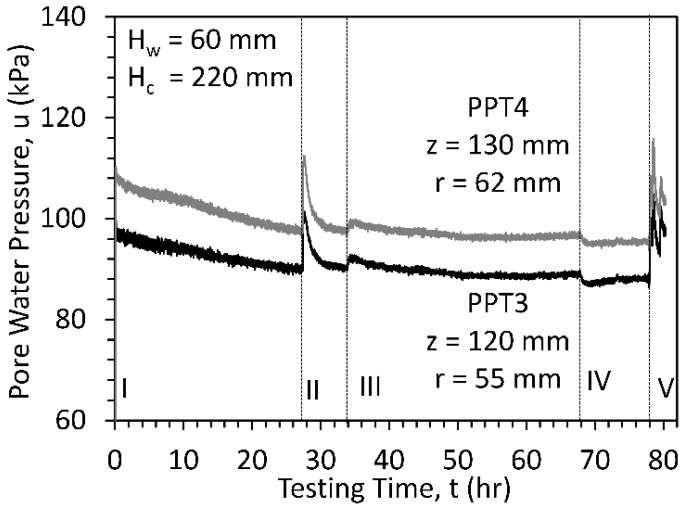

(b)

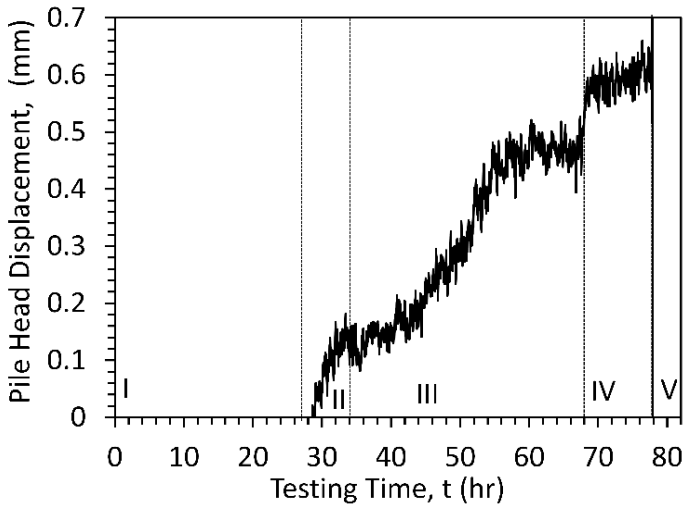

(c)

Figure 7.10: Time series results from Test J3: (a) Temperature versus testing time at different radii, (b) Pore water pressure versus testing time, (c) Pile head displacement versus testing time.

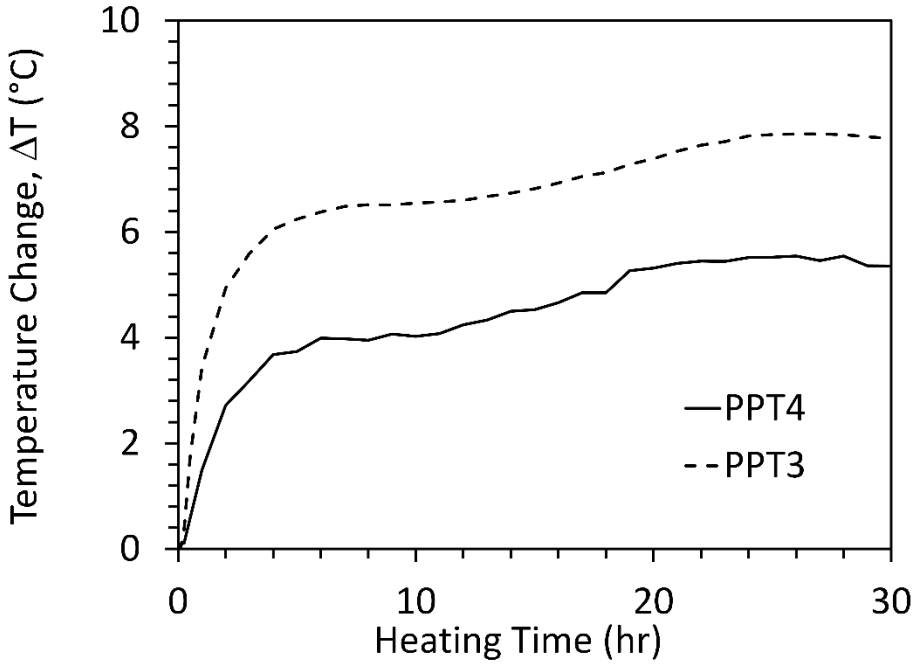

(a)

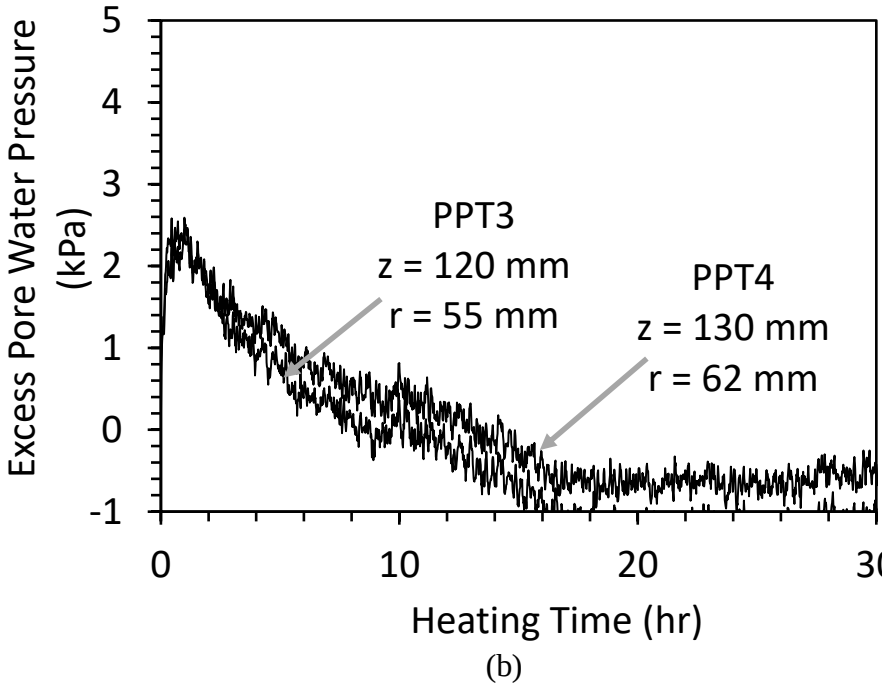

(b)

Figure 7.11: (a) Test J3 time series of sensor results during the heating stage: (a) Temperature change versus heating testing time at pore water pressure transducers locations, (b) Thermal excess pore water pressure

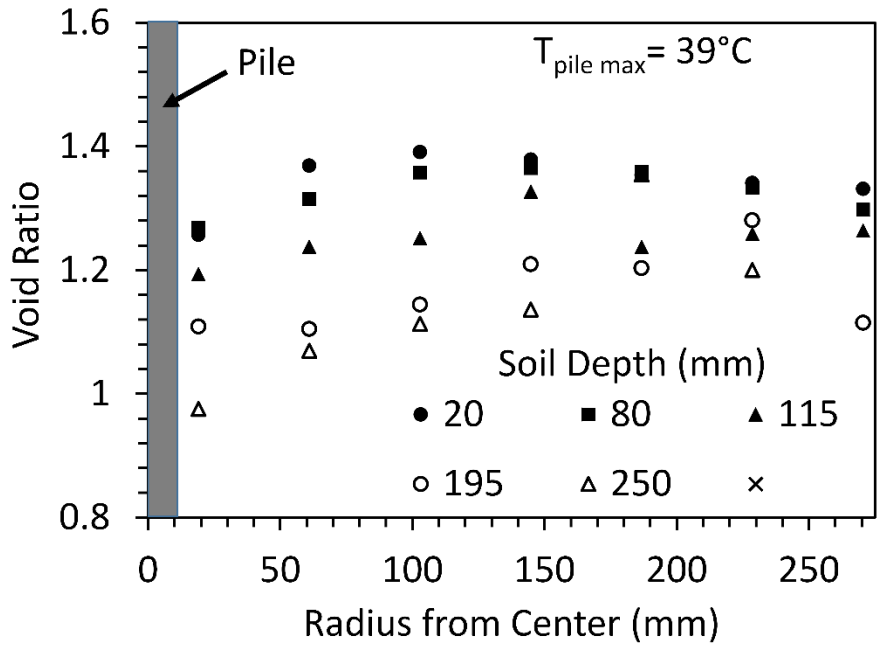

Figure 7.12. Void ratio profiles at the end of testing in Test J3 (model-scale dimensions)

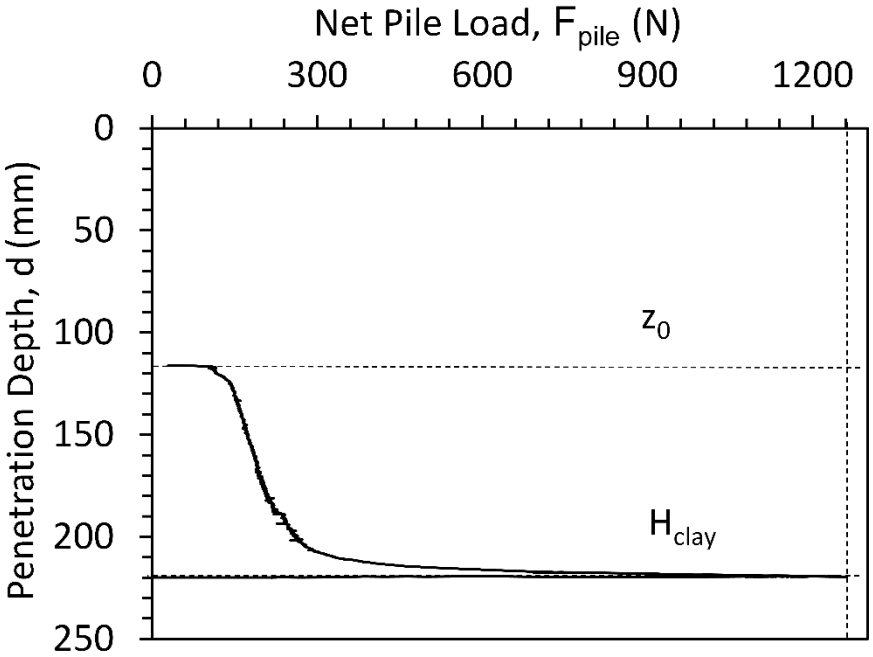

Figure 7.13. Installation of the pile in Test J4 from the initial position to the final position

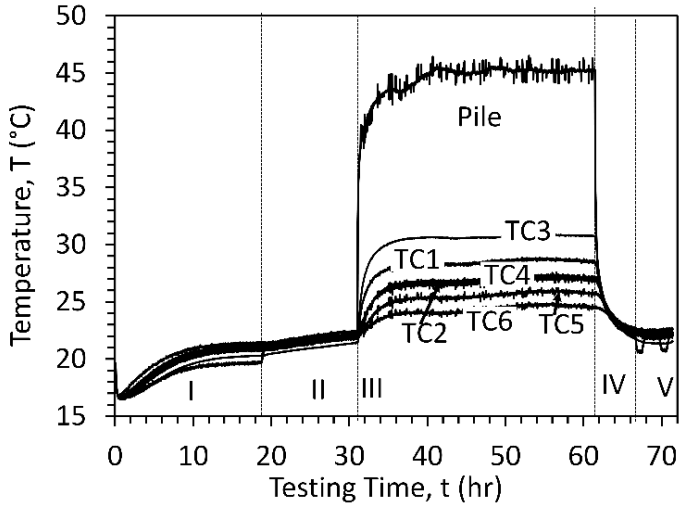

(a)

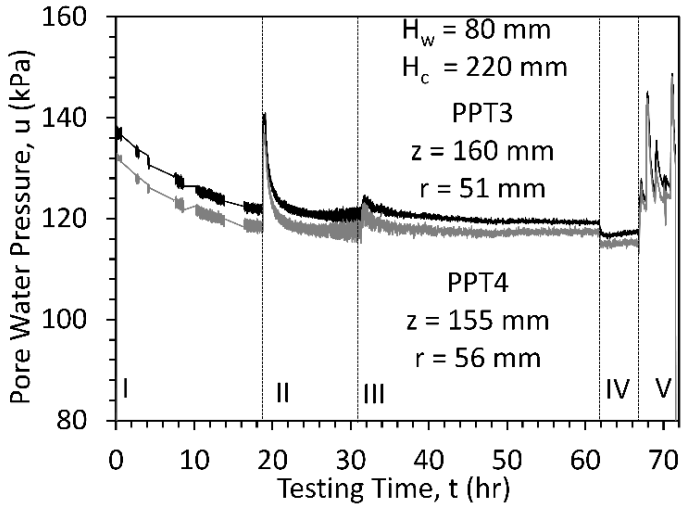

(b)

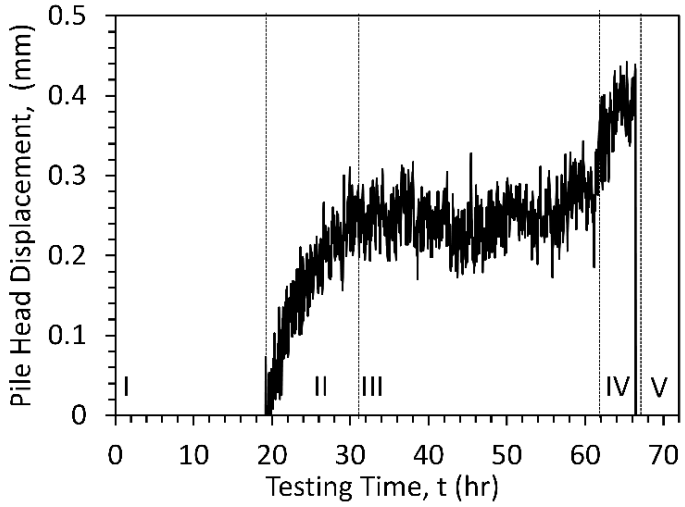

(c)

Figure 7.14: Time series results from Test J4: (a) Temperature versus testing time at different radii, (b) Pore water pressure versus testing time, (c) Pile head displacement versus testing time.

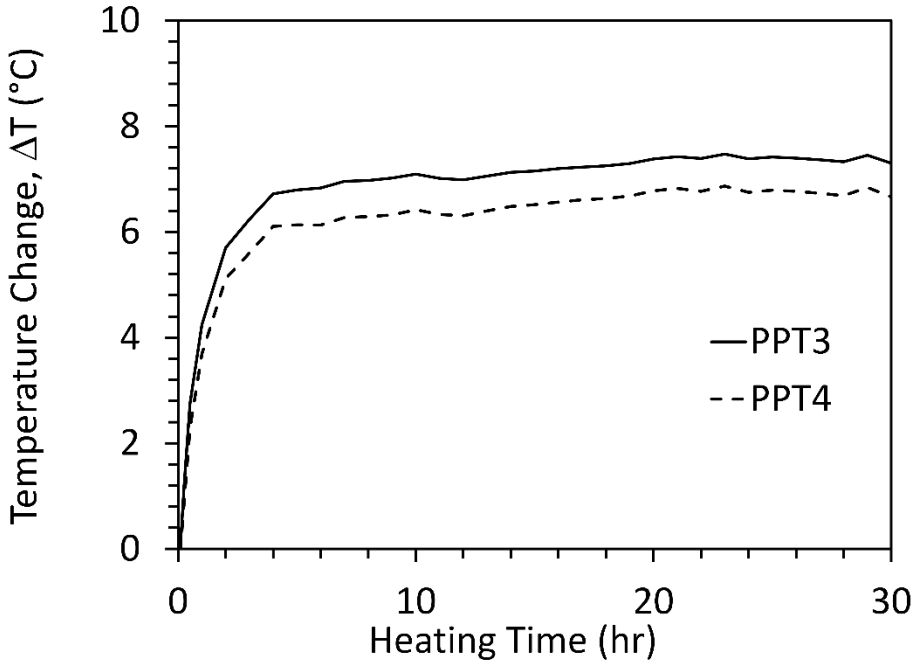

(a)

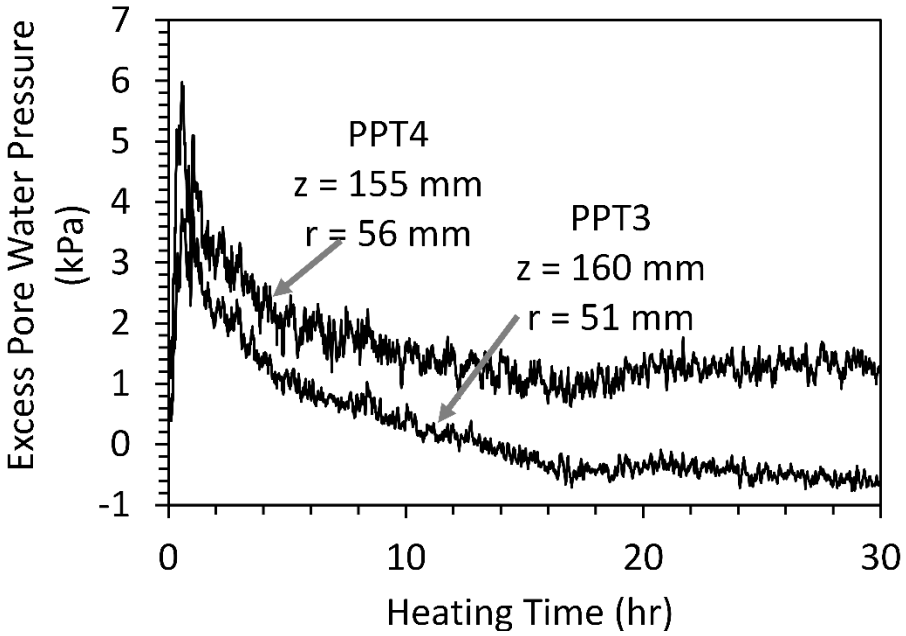

(b)

Figure 7.15: (a) Test J4 time series of sensor results during the heating stage: (a) Temperature change versus heating testing time at pore water pressure transducers locations, (b) Thermal excess pore water pressure

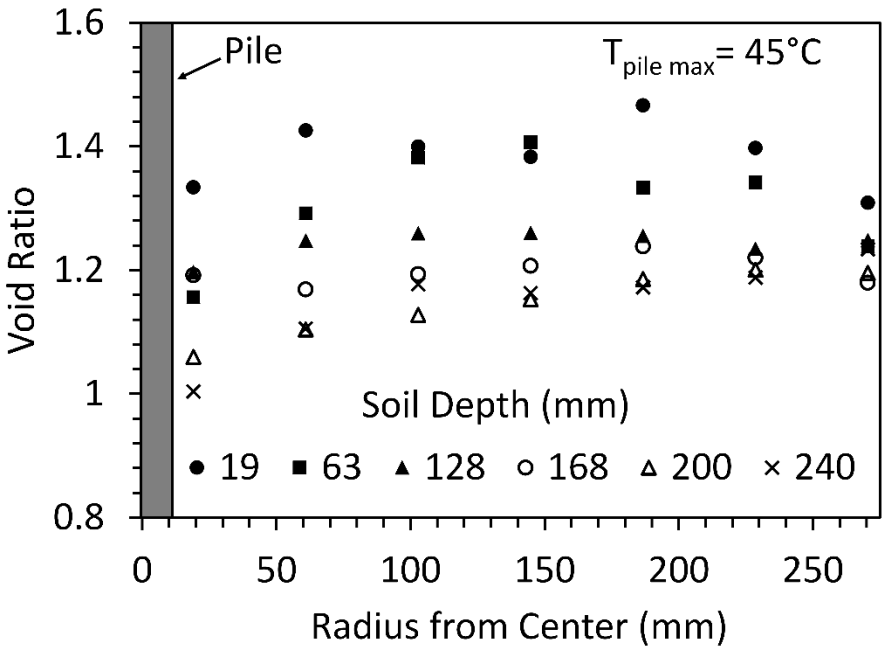

Figure 7.16. Void ratio profiles at the end of testing in Test J4 (model-scale dimensions)

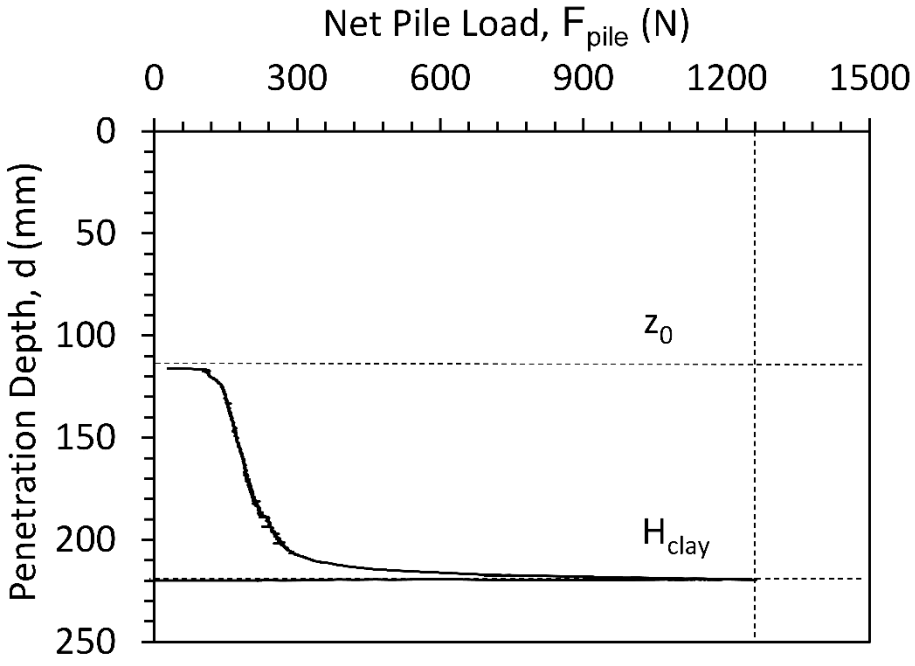

Figure 7.17. Installation of the pile in Test J5 from the initial position to the final position

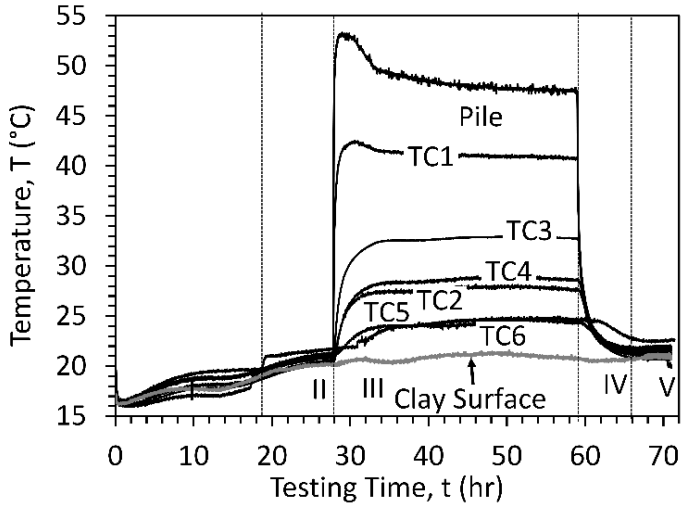

(a)

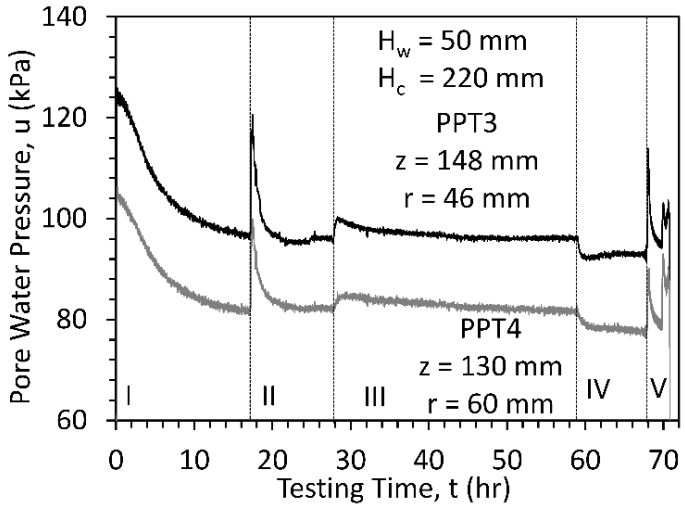

(b)

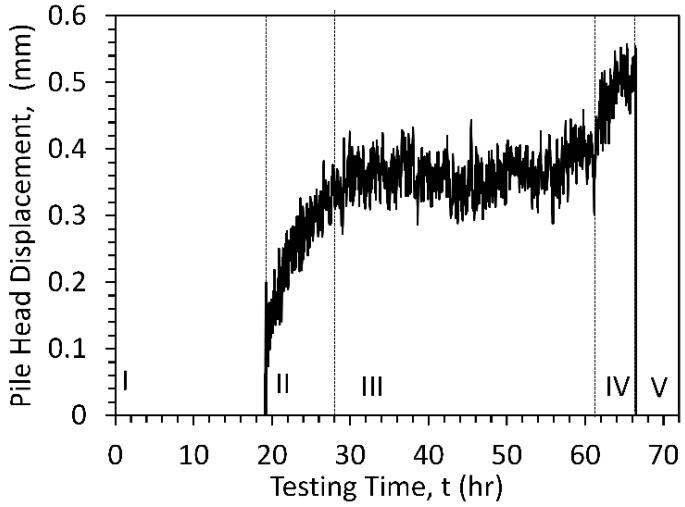

(c)

Figure 7.18: Time series results from Test J5: (a) Temperature versus testing time at different radii, (b) Pore water pressure versus testing time, (c) Pile head displacement versus testing time.

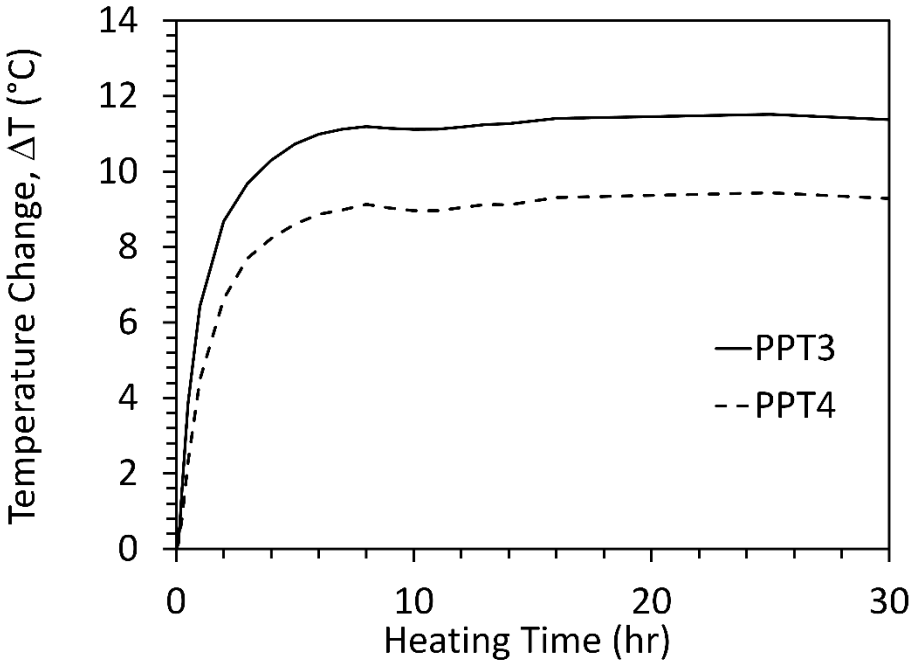

(a)

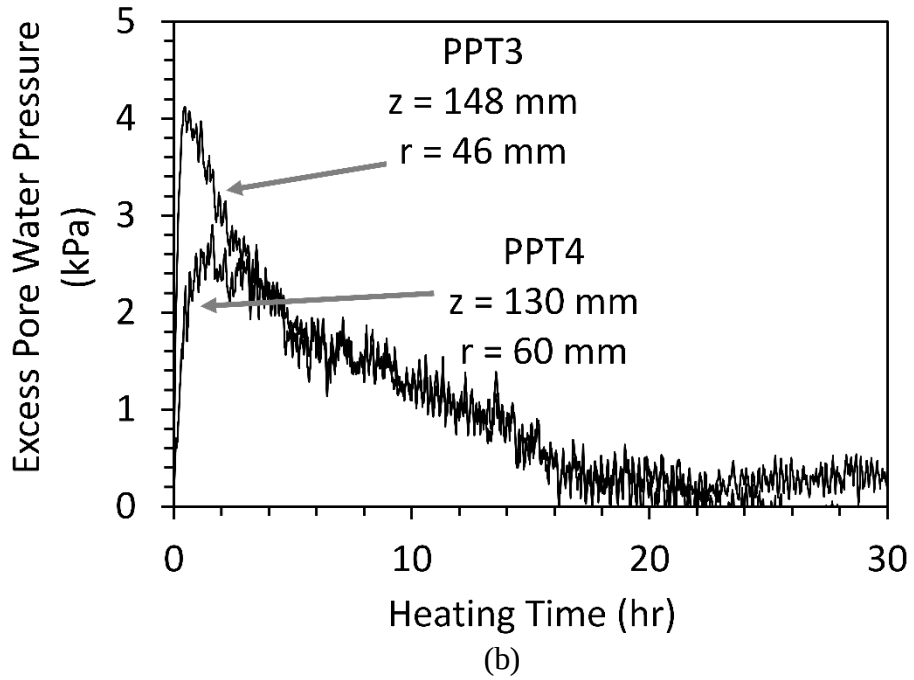

(b)

Figure 7.19: (a) Test J5 time series of sensor results during the heating stage: (a) Temperature change versus heating testing time at pore water pressure transducers locations, (b) Thermal excess pore water pressure

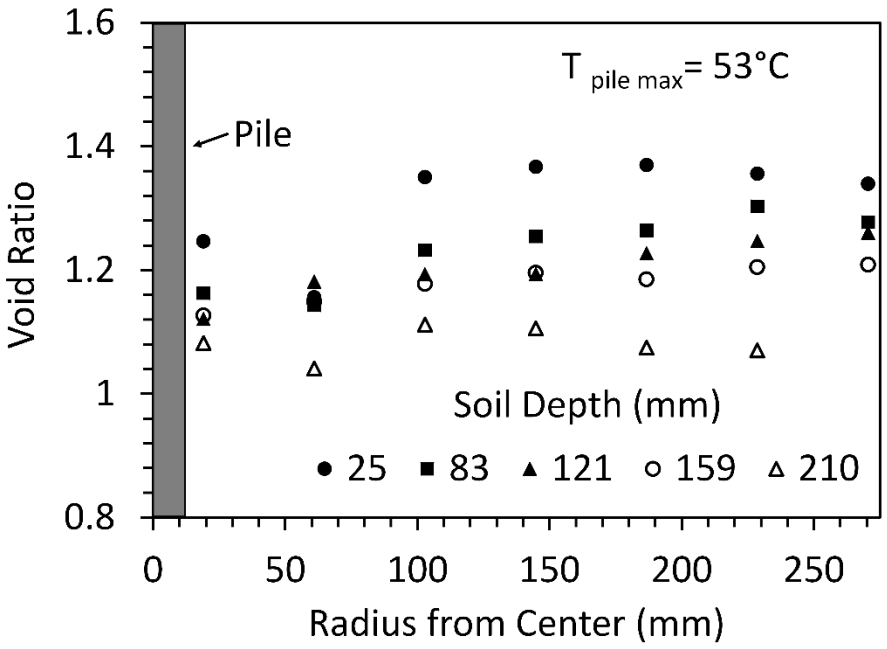

Figure 7.20. Void ratio profiles at the end of testing in Test J5 (model-scale dimensions)

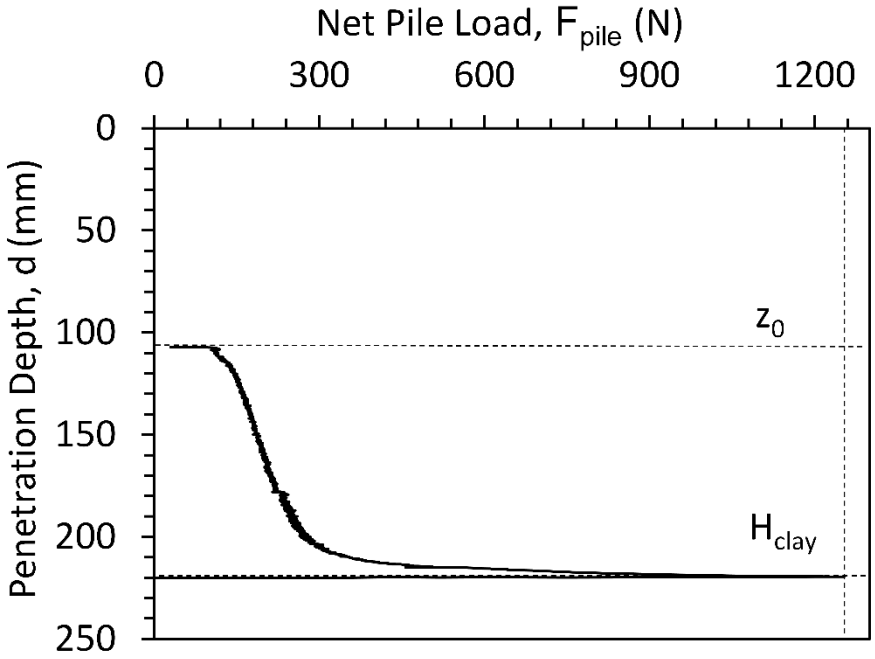

Figure 7.21. Installation of the pile in Test J6 from the initial position to the final position

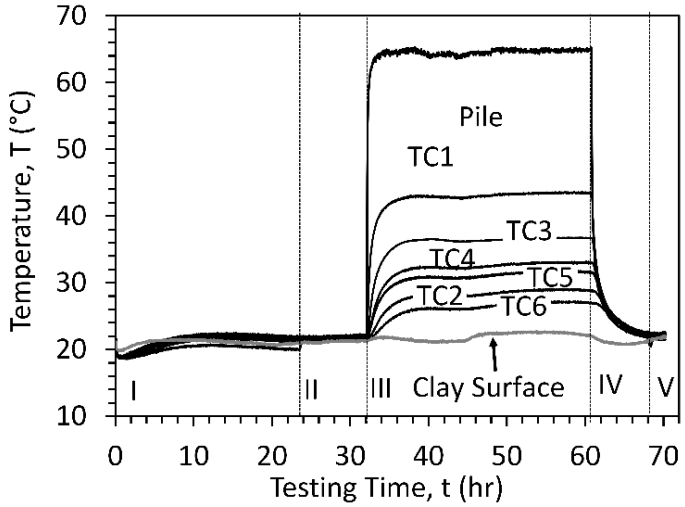

(a)

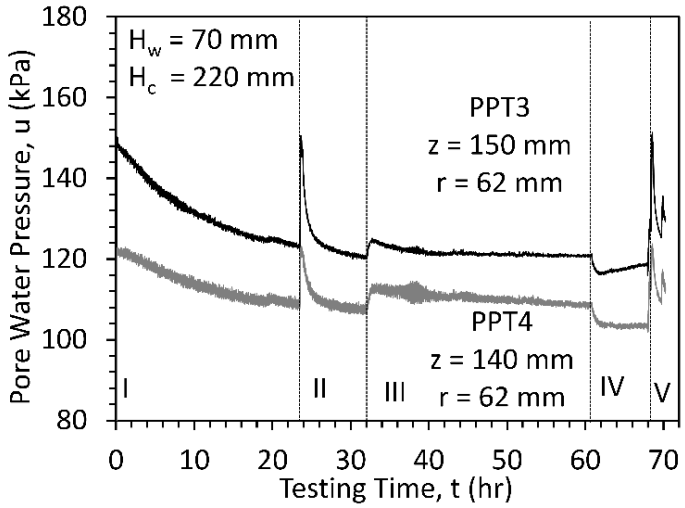

(b)

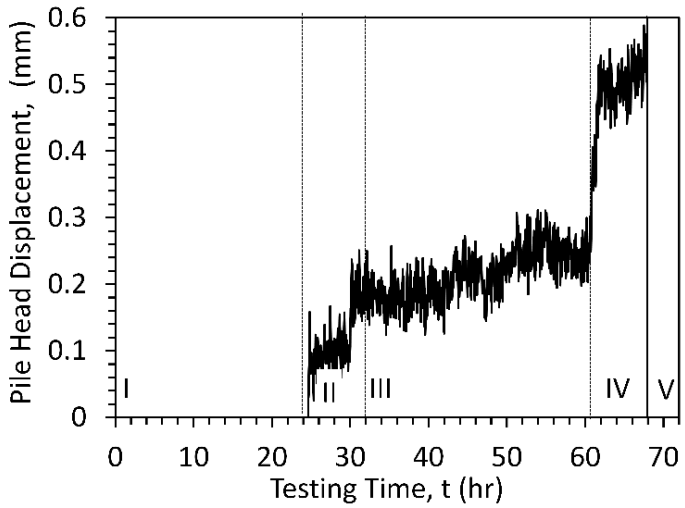

(c)

Figure 7.22: Time series results from Test J6: (a) Temperature versus testing time at different radii, (b) Pore water pressure versus testing time, (c) Pile head displacement versus testing time.

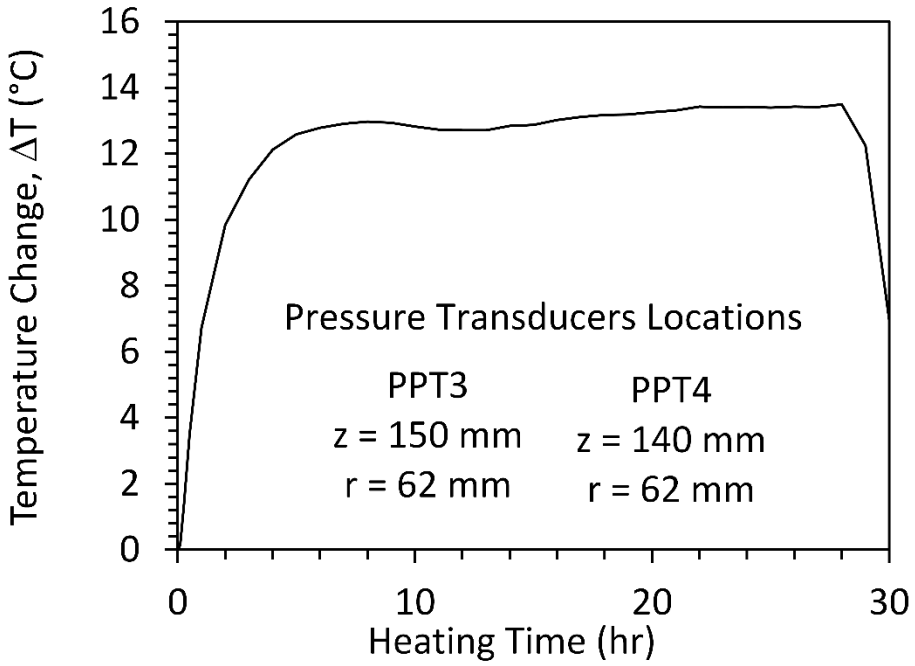

(a)

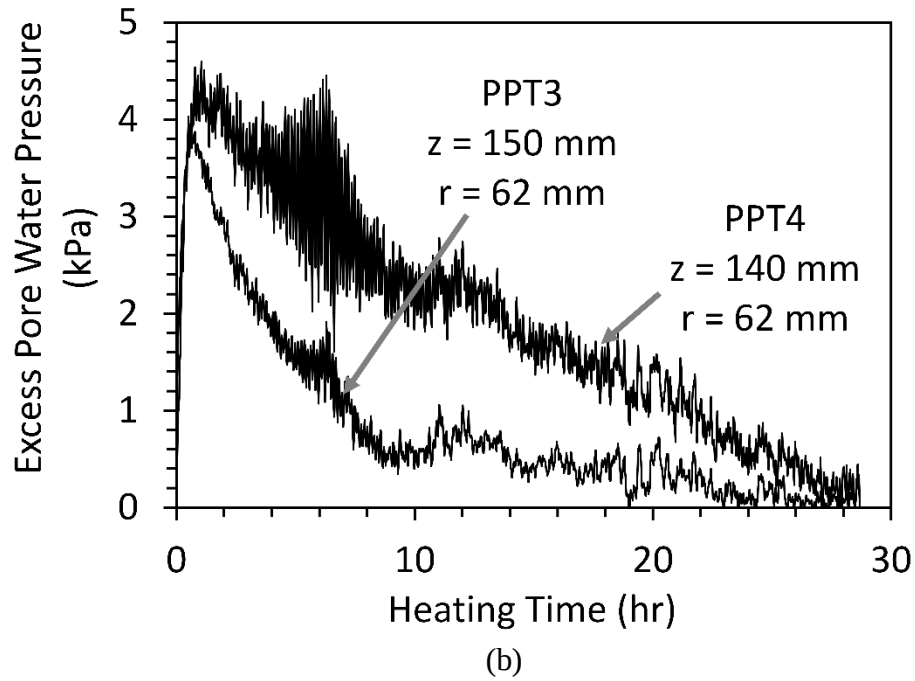

(b)

Figure 7.23: Test J6 time series of sensor results during the heating stage: (a) Temperature change versus heating testing time at pore water pressure transducers locations, (b) Thermal excess pore water pressure

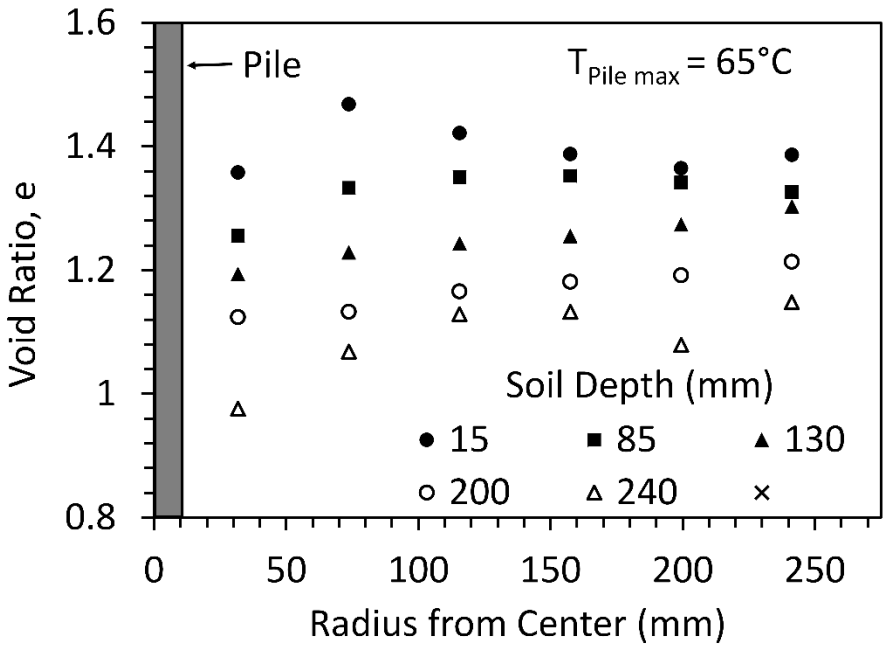

Figure 7.24. Void ratio profiles at the end of testing in Test J6 (model-scale dimensions)

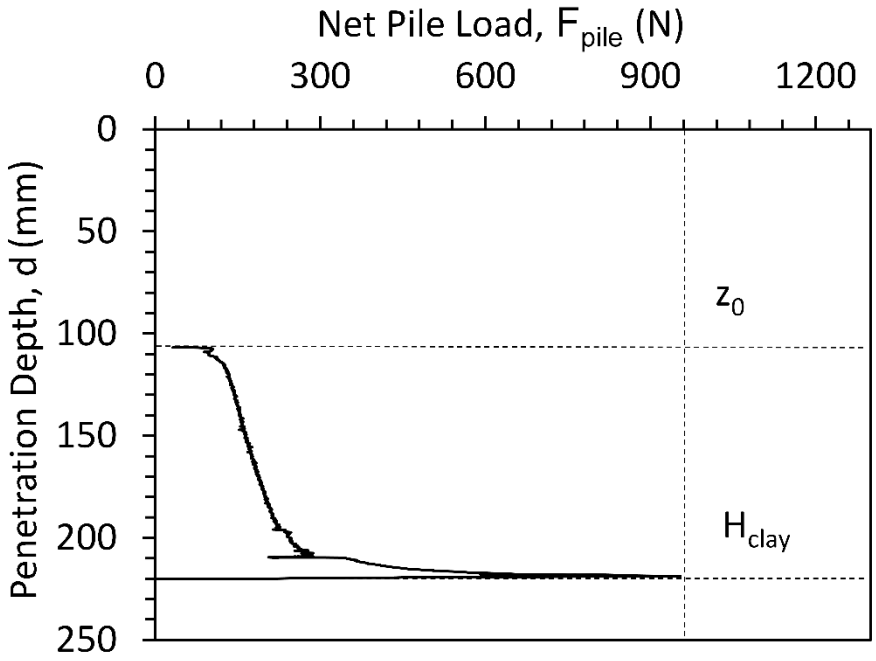

Figure 7.25. Installation of the pile in Test J7 from the initial position to the final position

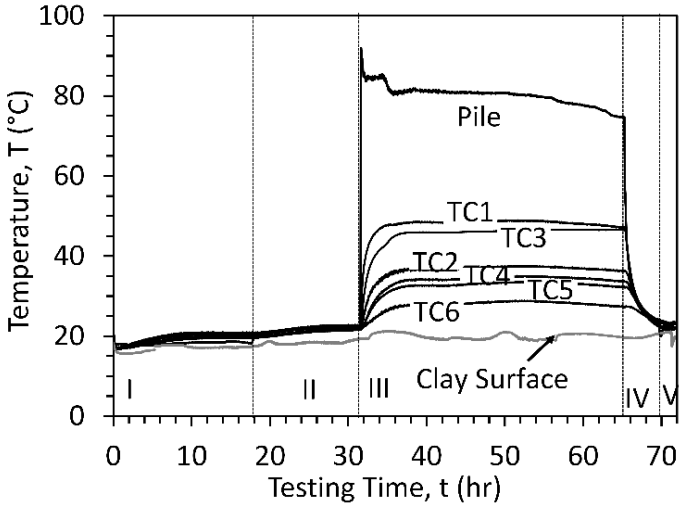

(a)

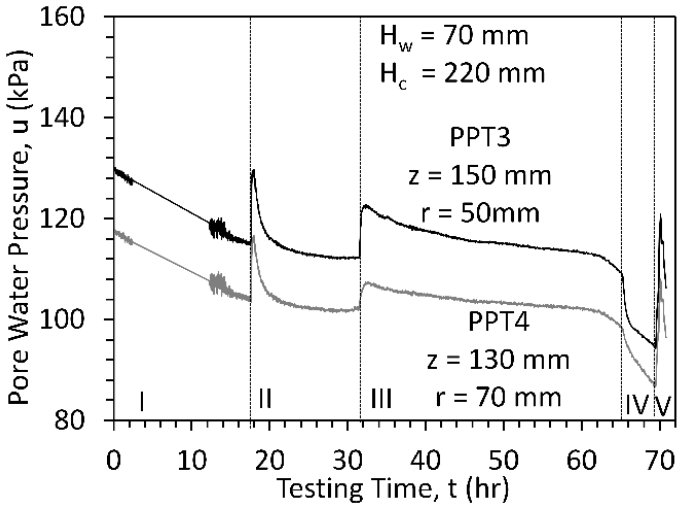

(b)

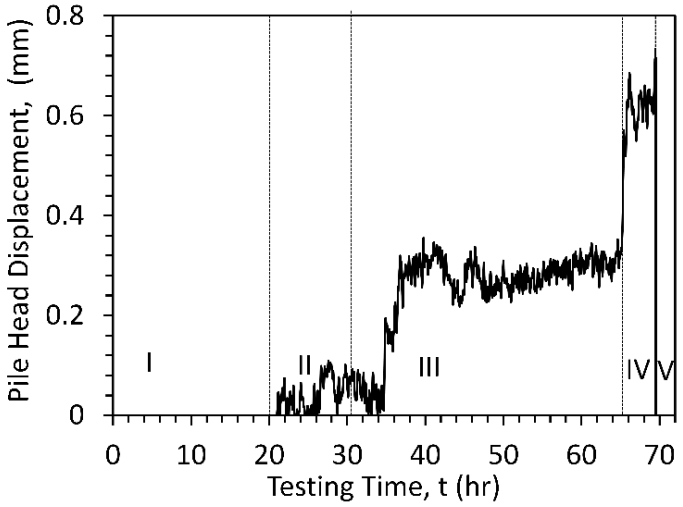

(c)

Figure 7.26: Time series results from Test J7: (a) Temperature versus testing time at different radii, (b) Pore water pressure versus testing time, (c) Pile head displacement versus testing time.

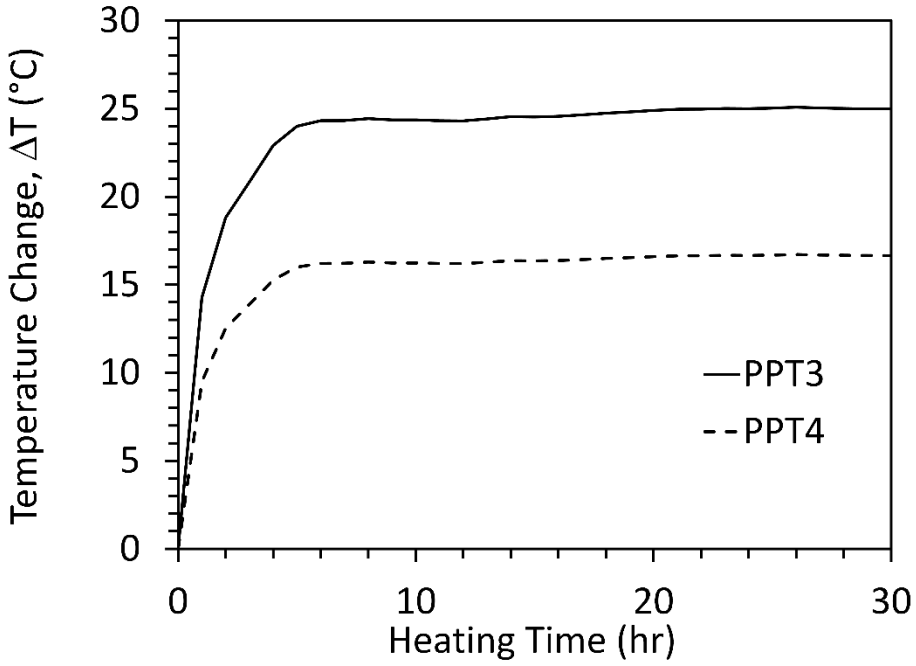

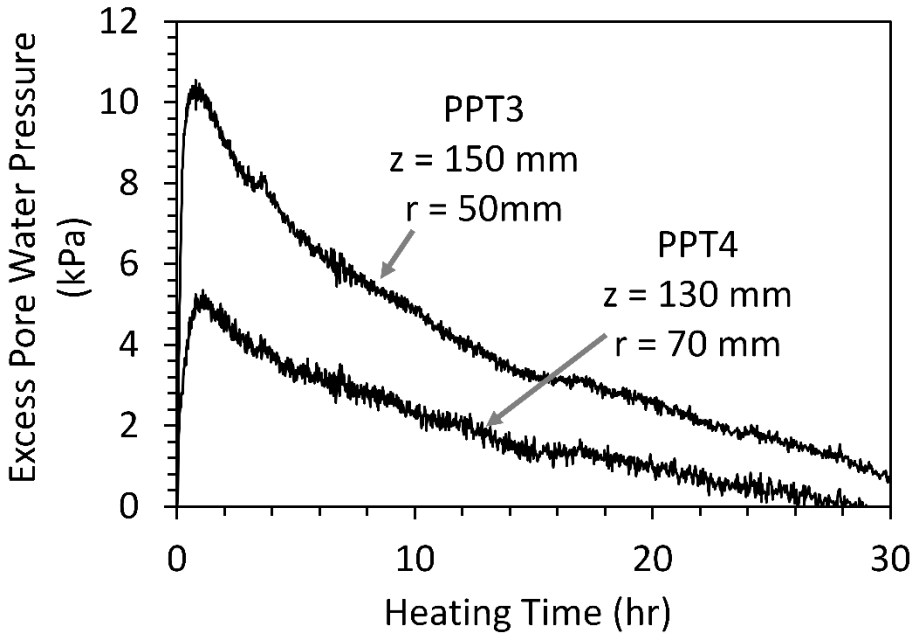

(b)

Figure 7.27: Test J7 time series of sensor results during the heating stage: (a) Temperature change versus heating testing time at pore water pressure transducers locations, (b) Thermal excess pore water pressure

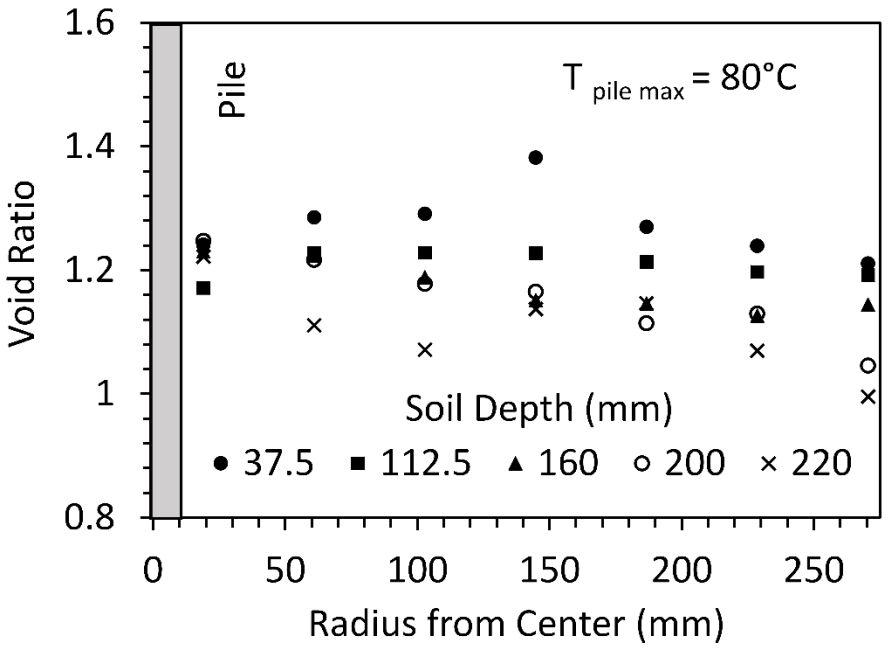

Figure 7.28. Void ratio profiles at the end of testing in Test J7 (model-scale dimensions)

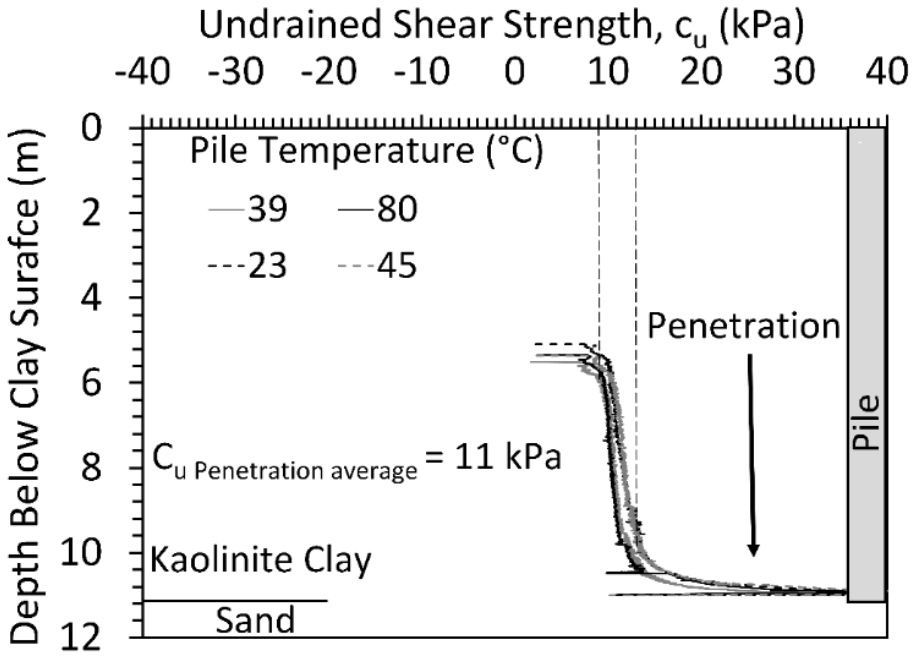

Figure 7.29. Undrained shear strength profiles measured during initial pile penetration in four of the jacked-in pile tests

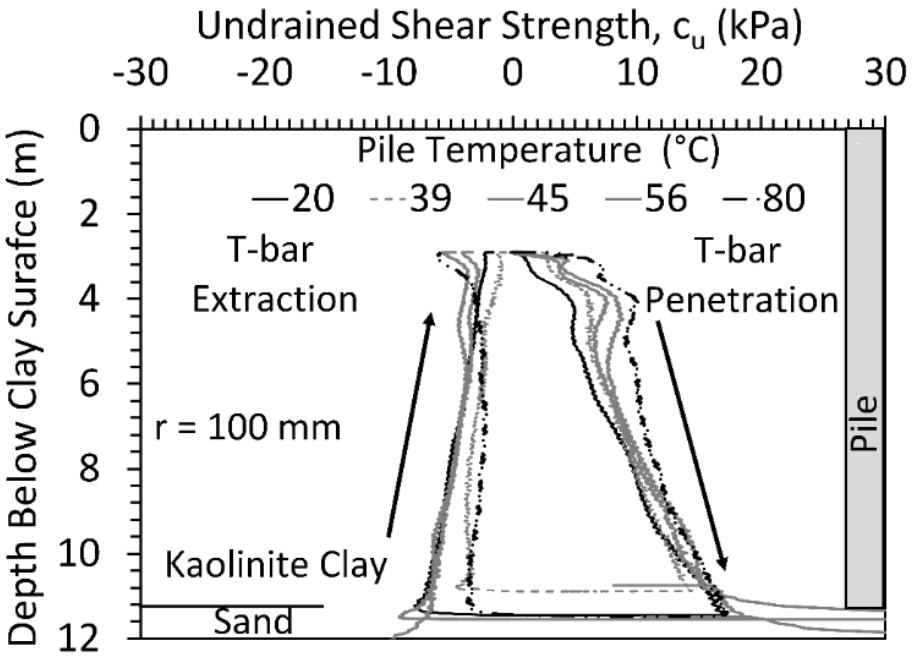

Figure 7.30. Undrained shear strength profiles measured by the T-bar in the five tests without seating loads on the pile head (positive values for insertion and negative values for extraction)

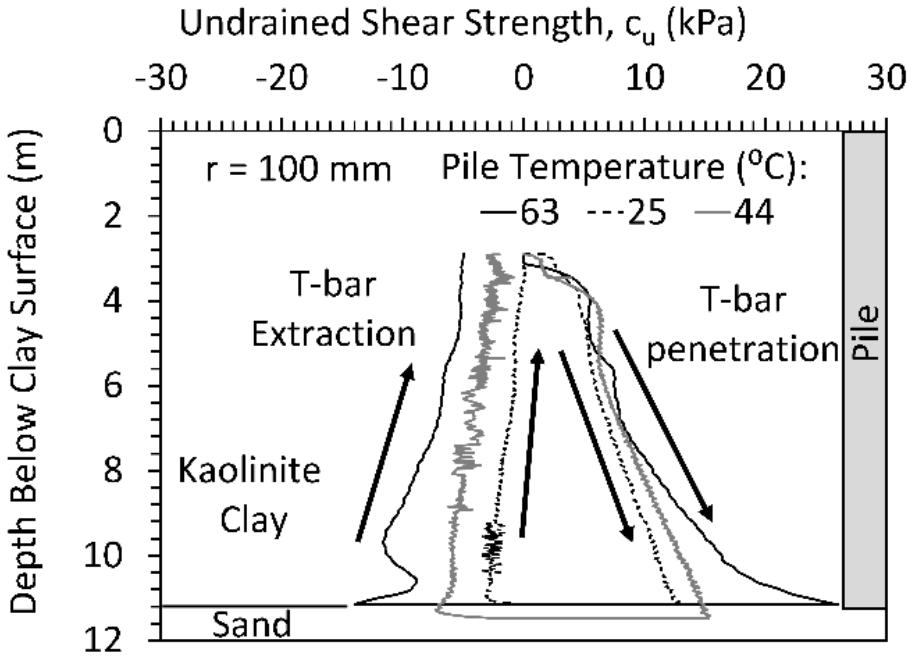

Figure 7.31. Undrained shear strength profiles measured by the T-bar in the three tests with seating load on the pile head (positive values for insertion and negative values for extraction) (Ghaaowd and McCartney 2018).

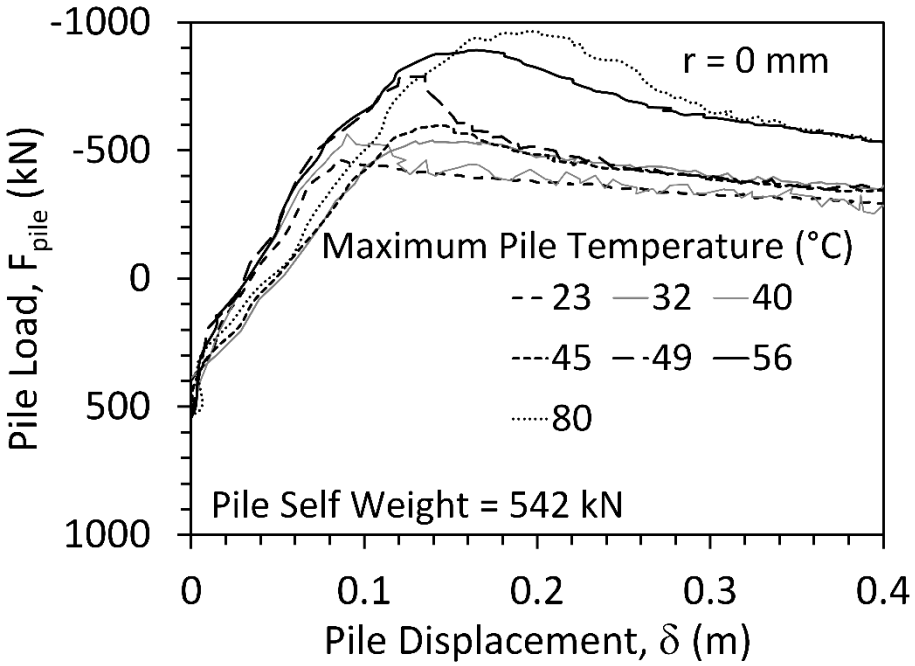

Figure 7.32. Pullout-displacement curves for energy piles without seating loads in prototype scale heated to different maximum temperatures before cooling to ambient temperature

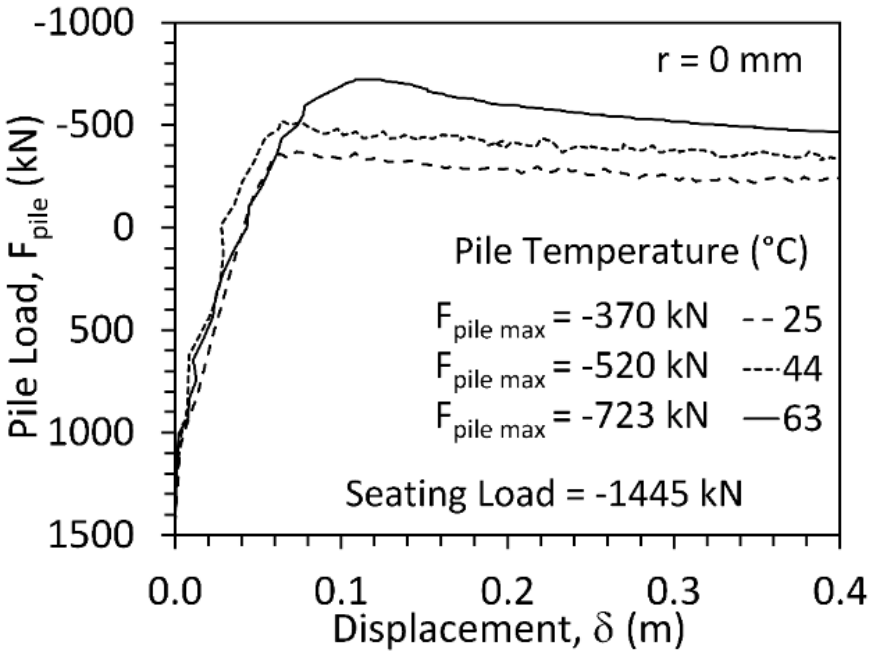

Figure 7.33. Pullout-displacement curves for energy piles with seating load on top in prototype scale at different temperatures (Ghaaowd and McCartney 2018)

Chapter 8. Centrifuge Modeling of Offshore Piles in Soft Clay: Analysis

8.1. Synthesis of Observed Changes in Soil Temperature

During the testing stage involving heating of the pile, it is assumed that conduction is the primary mechanism for heat transfer. After a target temperature of the pile is reached, it is expected that it will take some time for the temperature of the surrounding soil to stabilize. The temperature change ratio $(\Delta T_{pile})/(\Delta T_r)$ was defined as the ratio between the pile temperature change at $r = r_{pile}$ and the temperature change in the soil away from the pile by r. The ratios obtained from the sensors in the different tests on the jacked-in piles is plotted as a function of the radius ratio (r/r_{pile}) in Figure 8.1. Data from 8 heated tests at different temperatures shown in Table 7.1 and Table 7.2 was used in the temperature analysis. The container boundaries are far away from the affected zone ($r_{container}/r_{pile} = 22 >> r / r_{pile} = 12$) as shown in Figure 8, which confirms that there are minimal boundary effects in the tests.

8.2. Synthesis of Observed Thermally Induced Excess Pore Water Pressures

The change in pore water pressure at the effective stress and changes in temperature associated with the prototype locations of both PPT sensors during each of the tests were predicted using the model of Ghaaowd et al. (2015). A comparison between the predicted and measured maximum excess pore water pressure during the heating process is shown in Figure 8.4. The temperature change used in the prediction of the pore water pressure is at the same locations of the pore water pressure sensors, and the same time when the maximum pore water pressure was measured. In some measurements the predicted pore water pressures were above those measured by the sensors, and vice versa for other sensors. Differences in the predicted and measured values may be due to changes in vertical position of the PPTs due to consolidation, transient changes in

temperature at the different locations, and the different distances from the drainage boundaries that may result in partial drainage of the thermal excess pore water pressures.

8.3. Synthesis of Changes in Undrained Shear Strength after In-Situ Heating

The undrained shear strength profiles indicate that heating of the energy pile leads to an increase in undrained shear strength of the clay layer. Greater differences in undrained shear strength were observed shallower in the clay layer, which could be due to the lower effective strength, softer soil which contracted more during the thermal loading. The change in the undrained shear strength which normalized by the undrained shear strength of the unheated pile test profile are shown in Figure 8.5, the undrained shear strength changes with the change in the temperature. To exclude the effect of the boundary condition of the sand and the start of the test, the average of the undrained shear strength from depth of 4 m to 10 m. The undrained shear strength change $\Delta c_u / c_{u,23}$ is calculated as follows:

$$\Delta c_u / c_{u,23} = [\frac{c_{u,XX}}{c_{u,23}} - 1] \times 100 \quad (8.1)$$

where $c_{u,\,23}$ is the undrained shear strength of the clay at the interface of an unheated pile at an ambient temperature of 23 °C, and $c_{u,\,23}$ is the undrained shear strength of the clay at the interface of a pile heated to a temperature of XX °C

The average undrained shear strength and the percent change in undrained shear for each test are summarized in Table 7.9. The undrained shear strength results versus temperature change at the T-bar location are shown in Figure 8.6. The Undrained shear strength versus temperature followed same trend of the pile pullout force change versus temperature change.

To investigate the effect of the effective stress on the undrained shear strength change, triaxial tests were done on similar Kaolinite clay specimen at six different effective stresses. Two specimens for each effective stress were tested. All heated specimens was heated for 1 day under

66 °C and cooled to 23 °C for 1 day. All specimens showed improvement in the undrained shear strength due to the heating cooling cycle as shown in the Figure 8.7. The effective stress increase has inverse effect on the improvement of the undrained strength due to the heating cooling cycle. Higher effective stress applied on the clay, more restrain for the clay particle to reorient due to the thermal load.

The average percent change in undrained shear strength calculated from the T-bar results has similar trend of what was observed at the triaxial test result. The increase of the undrained shear strength is due to the irreversible contraction volume change after the heating and cooling cycle for the normally consolidated clay (Takai et al. 2016). The thermally induced volume change behavior can be related to the clay inter-particle forces and viscous shear resistance of adsorbed water that lead to fabric change. The thermal volumetric change induces part of the thermo-mechanical shear strength improvement, and the rest is induced by the fabric changes as was observed by Abuel-Naga et al. (2007).

8.4. Percent Improvement in Pile Pullout Capacity

The percent change in the pullout capacity of the heated piles with reference to the pullout capacity of the unheated pile can be calculated as follows:

$$\Delta Q/Q_{23} = \frac{(Q_{XX} - Q_{23})}{Q_{23}} \times 100 \qquad (8.2)$$

where Q_{23} is the maximum pullout capacity for an unheated pile at an ambient temperature of 23 °C, and Q_{XX} is the maximum pullout pile capacity for pile heated to a temperature of XX °C. The change in pullout capacity versus the pile temperature are shown in Figure 8.8. These increases in net pullout capacity confirms that the drained heating-cooling cycle in the clay layer leads to substantial improvements in the undrained shear strength of the clay surrounding the heated energy pile, resulting in an improvement in soil-pile interaction. The pile pullout improvement follows a

linear relation with the change in temperature as shown in Figure 8.8, for similar soil properties and same effective stress the pullout improvement could be predicted as function of the temperature change by the following equation:

$$\Delta Q/Q_{23} = 2.\Delta T \tag{8.3}$$

where ΔT is the pile temperature change in Celsius. The loading slope for all curves ranges from 990 kN/m to 13650 kN/m as shown in Chapter 7. It was expected that the increase in undrained shear strength of the clay layer with temperature would also correspond to an increase in stiffness. The similar slopes may have occurred because the heated aluminum energy piles experienced thermal axial strains in the direction opposite to the downward self-weight during heating that may have counteracted the positive effect of the thermal improvement of the soil layer. During pullout, the piles were likely following an elastic loading-unloading curve until shortly before failure.

8.5. Model to Predict Thermal Improvement of the Pile Pullout Capacity

The first step to predict the pullout capacity of the heated pile is to have an estimate of the change in temperature in the clay layer as a function of space and time. The infinite line source model developed by Carslaw and Jaeger (1959) was used to estimate the changes in temperature. The analytical solution to the heat diffusion equation in their model is given as follows:

$$v = \frac{V\, a^{\frac{1}{2}}}{r^{\frac{1}{2}}}\ erfc\ \frac{r-a}{2(kt)^{\frac{1}{2}}} + \frac{V\,(r-a)(kt)^{\frac{1}{2}}}{4\,a^{\frac{1}{2}} r^{\frac{3}{2}}}\ i \times erfc\ \frac{r-a}{2(kt)^{\frac{1}{2}}} + \\ + \frac{V(9a^2 - 2ar - 7r^2)(kt)}{32\,a^{\frac{3}{2}} r^{\frac{5}{2}}}\ i^2 \times erfc\ \frac{r-a}{2(kt)^{\frac{1}{2}}} + \ldots\ldots\ldots\ldots \tag{8.4}$$

where *v* is the change in temperature at the pile surface, a is the pile radius which equals 12.5 mm at model scale and 0.625 m at prototype scale, r is the radius where the temperature is measured, k is the thermal diffusivity of the Kaolinite clay equal to 4.6×10^{-7} m^2/s for the void ratio at mid-height of the clay layer, and t is the time when the temperature change is calculated. The calculated

temperature results using Equation 8.1 after 10 hours for the same tested model are shown in Figure 8.2. A good match is observed between the measured temperature of the clay from the different tests is observed. The same equation was also used calculate the temperature at the prototype scale of the same model as shown in Figure 8.3. In prototype scale, 1041 days would be needed for the temperature around the pile to fully stabilize. It should be noted that conductive heat transfer does not scale in the centrifuge, and by applying the scaling factors to the geometry and time, the changes in temperature after scaling affect a greater zone of soil around the pile than in reality. However, the soil at the pile interface is likely the most important to the change in pile capacity, so these scaling issues may not be relevant to the capacity determination.

At the end of the centrifuge consolidation stage, the vertical effective stress at the middle of the pile height reached a value of $\sigma' = 39$ kPa in all of the tests. Based on the compression curve for the clay, this effective stress corresponds to a void ratio of 1.2. The increase in pile temperature leads to an increase in the temperature of the surrounding soil, resulting in the generation of thermally induced pore water pressure as a function of physico-chemical coefficient and other properties of clay (α_w, α_s, κ, and σ') using the model of Ghaaowd et al. (2015). Due to the low permeability coefficient of the clay, the heating rate larger than the water drainage rate, the clay behaves as if is under undrained condition. The soil expands and follows the recompression line (Takai et al. 2016) without volume change. The effective stress deceases due to the thermal excess pore water pressure generation (Δu) from (σ') to (σ_0'-Δu). Once the pore water pressure starts dissipating, the effective stress increases back from (σ_0'-Δu) to the initial effective stress (σ_0'). The clay contracts again and follows the compression line. Takai et al. (2016) provided the thermal volumetric strain prediction model, this model was improved by adding the volumetric change due to physico-chemical phenomena introduced by Campanella and Mitchell (1968). Specifically, the

change in volume of water leaving the specimen due to drainage of thermally-induced excess pore water pressures from the model of Takai et al. (2016) is given as follows:

$$\left(\Delta V_{DR}\right)_{\Delta T} = -\frac{1}{1+e_0}\frac{\lambda}{p'}V_m \Delta u \tag{8.5}$$

This equation can then be incorporated into the equation of Campanella and Mitchell (1968) to estimate the change in total volume of a soil element during a change in temperature, given as follows:

$$(\Delta V_m)_{\Delta T} = \alpha_w V_w \Delta T + \alpha_s V_s \Delta T - (\Delta V_{DR})_{\Delta T} - \alpha_{st} V_m \Delta T \tag{8.6}$$

Equation 8.6 can be simplified by assuming $V_s = 1\ m^3$, $V_w = e$, and $V_m = 1+e_0$, resulting in the equation that can be used to estimate the change in void ratio of a clay after drainage of thermally induced excess pore water pressures Δu occurring during a given change in temperature ΔT of the clay:

$$(\Delta e)_{\Delta T} = e_0 \alpha_w \Delta T + \alpha_s \Delta T - [(\lambda \Delta u)/ p'] - \alpha_{st} \Delta T (1+e_0) \tag{8.7}$$

where e_0 is the initial clay void ratio before heating, α_w is c,ubical coefficient of thermal expansion of the pore water, ΔT is the change in temperature of the clay, α_s is the cubical coefficient of thermal expansion of the mineral solids, λ is the slope of the compression line, Δu is the thermal excess pore water pressure, p' is the mean effective stress, and α_{st} is the physico-chemical coefficient of structural volume change.

The change in the void ratio is expected to lead to a change in the undrained shear strength. If the change in void ratio is known, empirical correlations can be used to correlate the void ratio at failure with the undrained shear strength. For example, Figure 8.9 shows a correlation between the void ratio at failure and the undrained shear strength results from the triaxial tests from Chapter 4 along with undrained shear strength values from the T-bar measurements. The undrained

shear strength from both testing approaches follow the following relationship with the void ratio on the failure plane obtained in Chapter 4:

$$c_u = c \times exp^{-d \times e_f} \quad (8.8)$$

where c and d are empirical fitting parameters and e_f is the void ratio at failure. The values of c and d from the triaxial test data presented in Chapter 4 are 8×10^6 kPa and 11.34, respectively. As the T-bar data match well with the trend in the data from the triaxial tests, this provides additional validation of the relationship obtained from the triaxial tests.

During pullout, the pile is assumed to have negligible end bearing, so the pullout capacity depends only on the side shear resistance Q_s. Accordingly, the pullout capacity can be estimated using the α method, given as follows:

$$Q_{pile} = Q_s = \alpha \, c_u \, A_s = \alpha \, c_u \, \pi \, D_{pile} \, L_{pile} \quad (8.9)$$

where D_{pile} is the pile diameter, L_{pile} is the pile length, α is the pile interface parameter equal to 1.0 for soft clays, and c_u is the undrained shear strength of the clay at the pile wall interface. The value of cu calculated from Equation 8.8 for the void ratio after thermal contraction can then be used to estimate the impact of in-situ heating on the pullout capacity. The flow chart showing the integration of the different uncoupled models is shown in Figure 8.10.

8.6. Acknowledgements

Chapter 8, in full, is currently being prepared for submission for of publication of the material as it may appear in part of the following journal publication (The dissertation author was the primary investigator and author of this paper):

Ghaaowd, I. & McCartney (In preparation). "Centrifuge modeling of temperature effects on the pullout capacity of offshore energy piles in saturated soft clay." To be submitted to Journal of Geotechnical and Geoenvironmental Engineering.

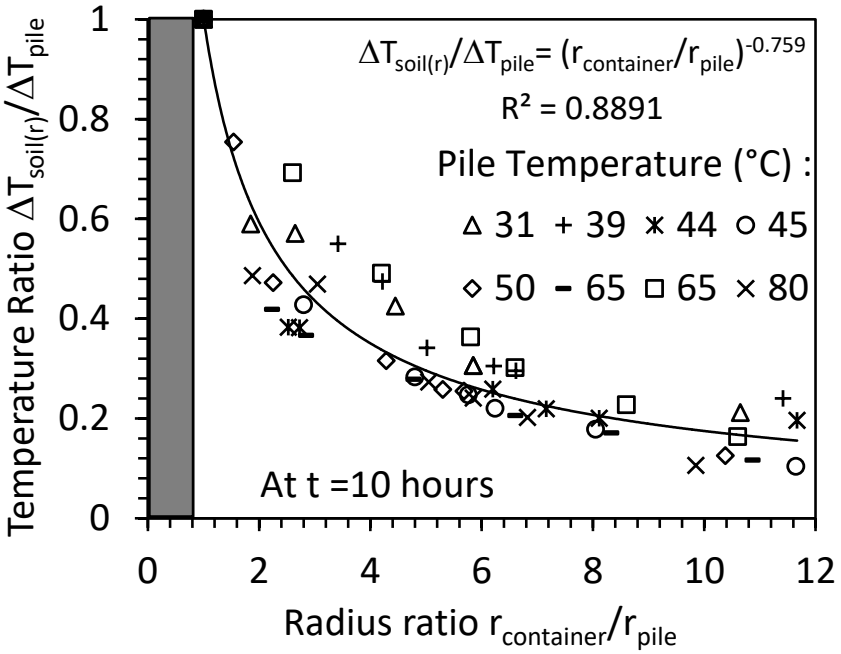

Figure 8.1. Temperature ratio ($\Delta T_{pile}/\Delta T_{soil}$) versus radius ratio for eight tests on jacked-in piles with no head load with a best fit empirical relationship

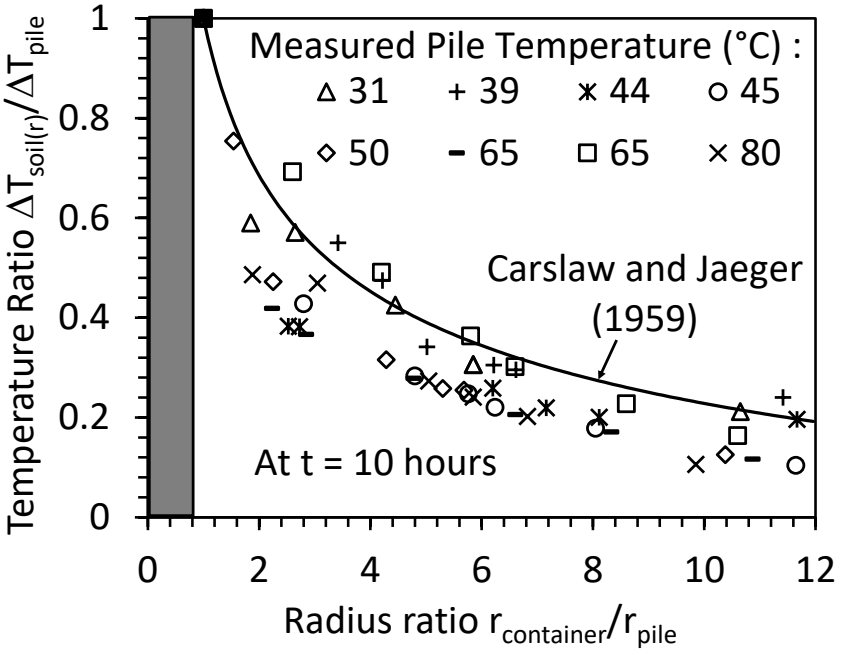

Figure 8.2. Measured and calculated distribution in temperature at model scale

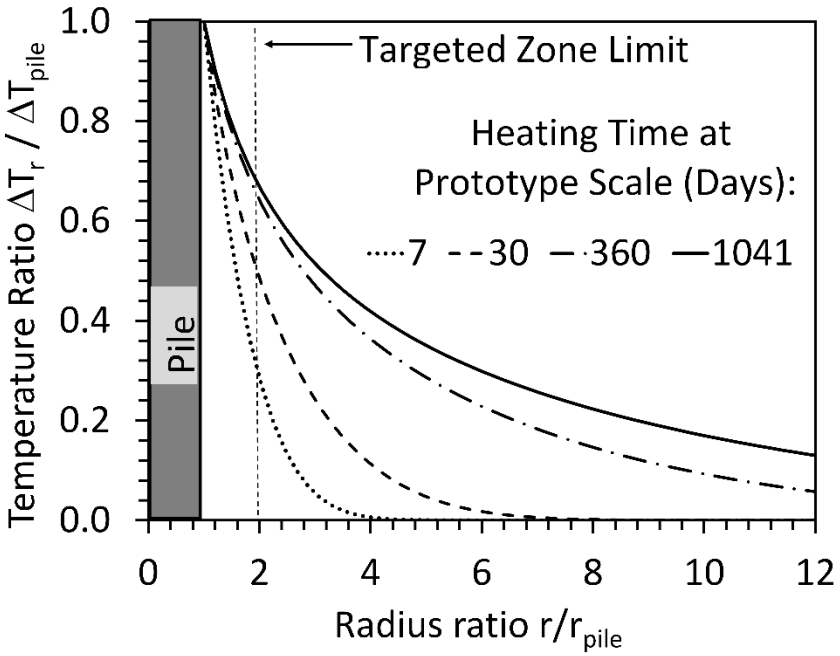

Figure 8.3. Calculated distribution in temperature at prototype scale

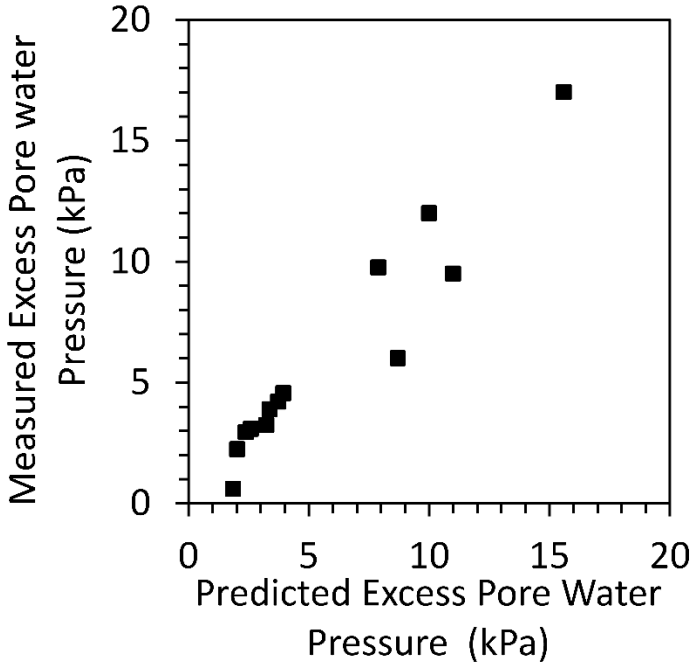

Figure 8.4. Measured excess pore water pressure at the locations of the two PPTs in the different tests versus predicted pore water pressure from the model of Ghaaowd et al. (2015).

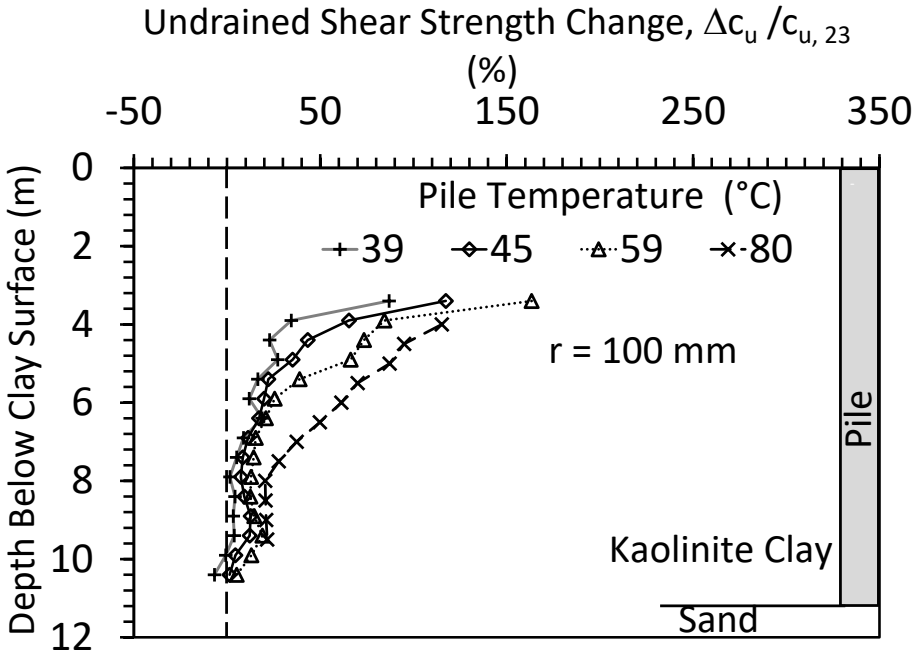

Figure 8.5. Profiles of percent change in undrained shear strength change in soil layers with different maximum pile temperatures after a heating-cooling cycle

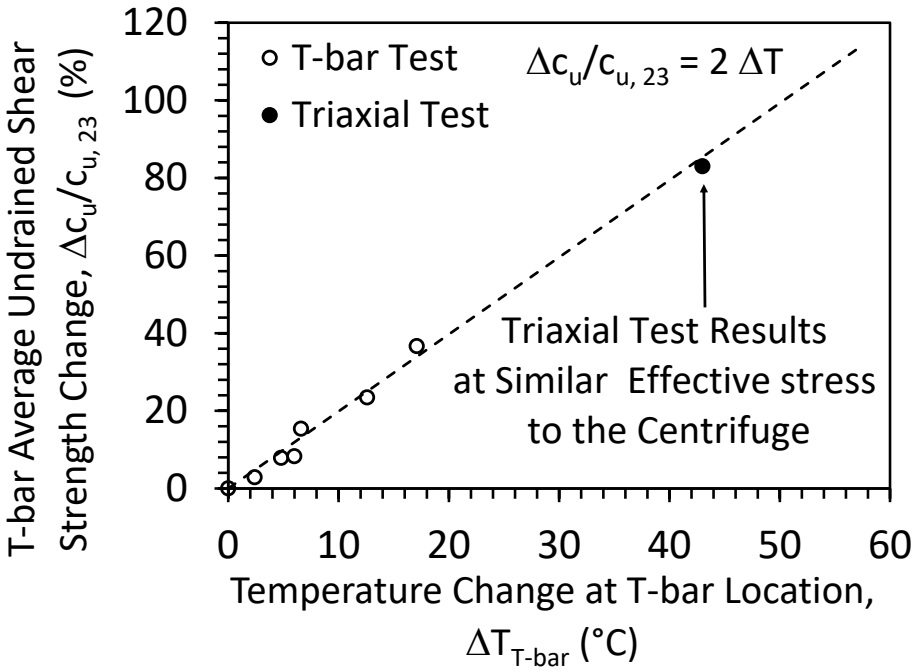

Figure 8.6. Percent change in undrained shear strength versus the change in temperature change from the T-bar tests in soil layers with different changes in temperature together with a best-fit relationship

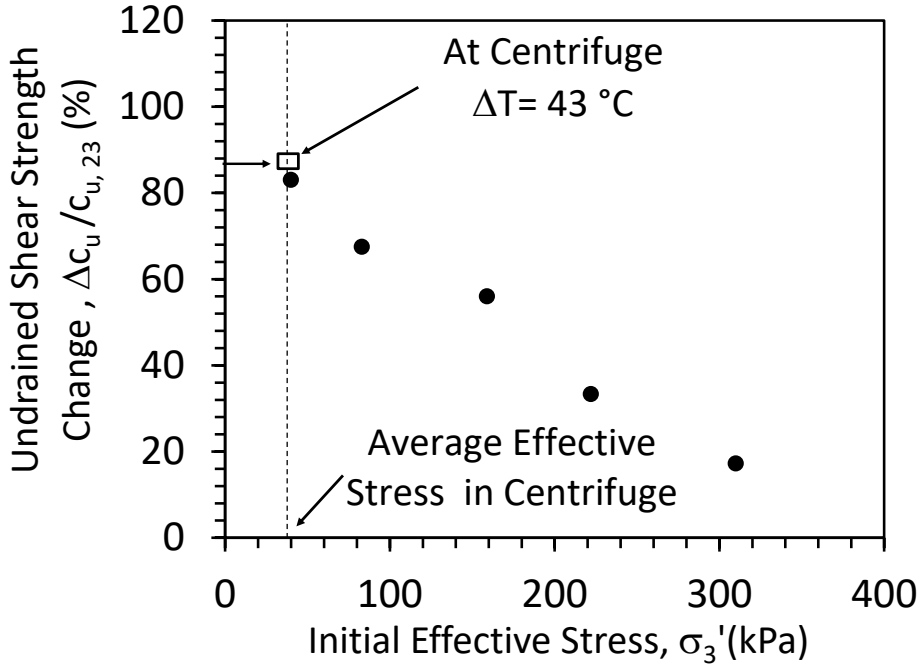

Figure 8.7. Triaxial undrained shear strength change percentage versus the initial effective stress after following a heating/cooling path of ((23– 66 – 23) °C

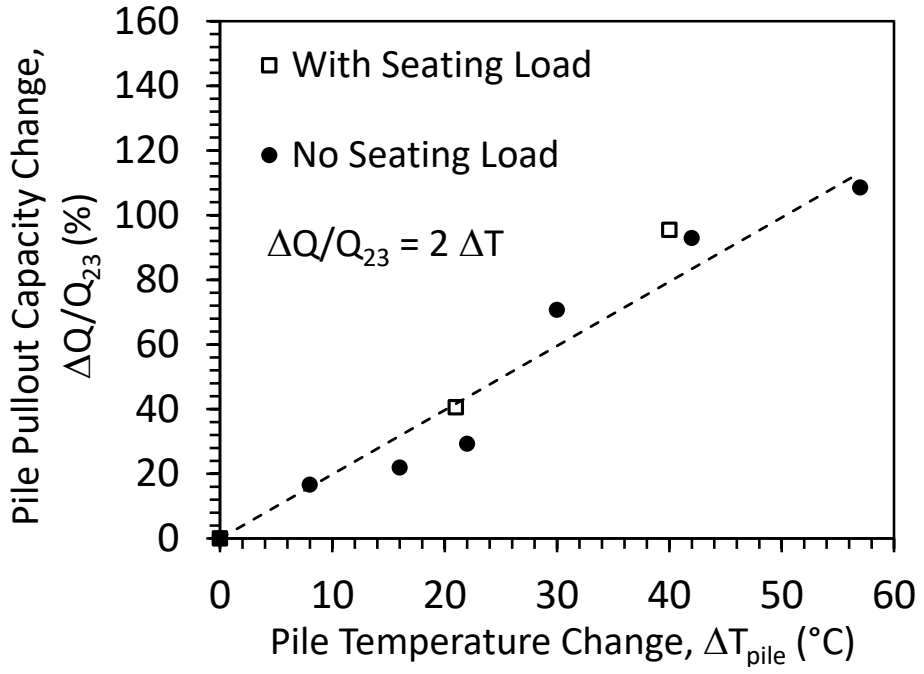

Figure 8.8. Pile load change versus maximum pile temperature change

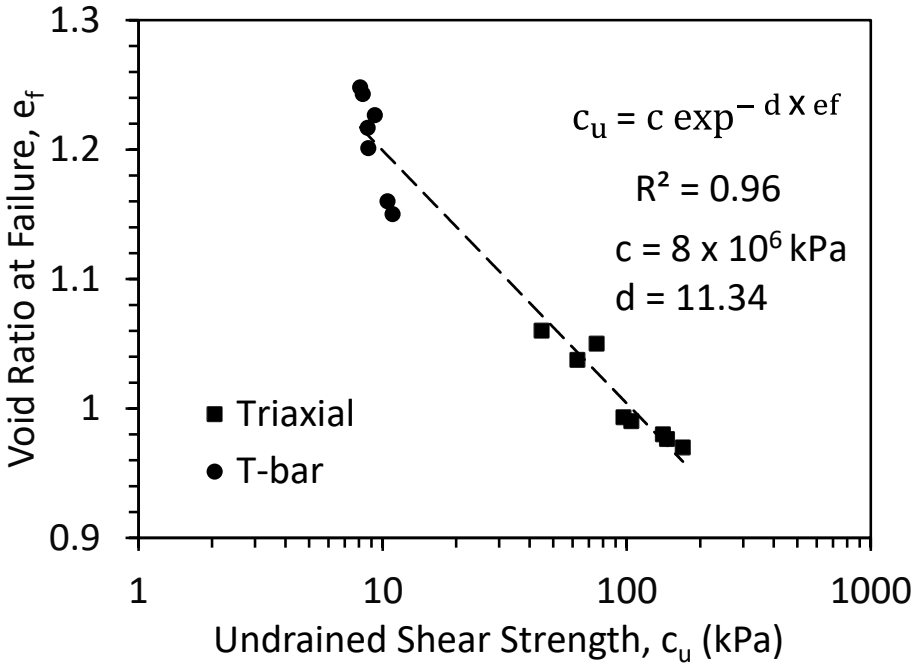

Figure 8.9. Undrained shear strength versus void ratio at failure

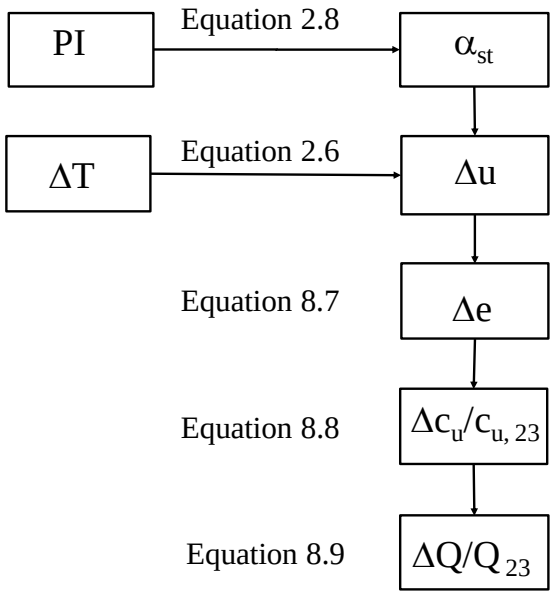

Figure 8.10. Pullout capacity improvement prediction flow chart model 1

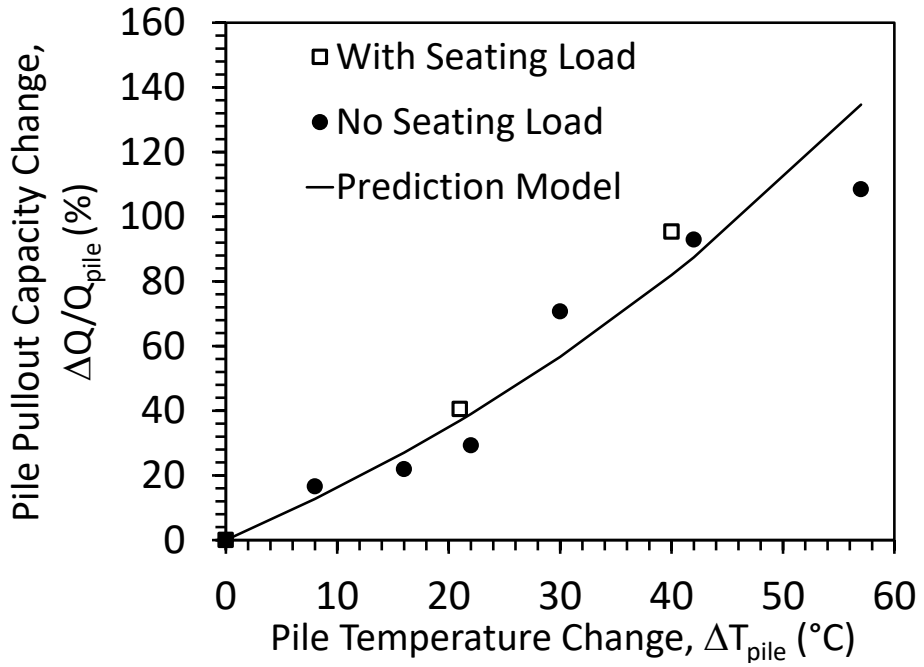

Figure 8.11. Predicted and measured percent increases in pile pullout capacity after a heating cooling cycle involving different temperature changes

Chapter 9. Centrifuge Modeling of Temperature Effects on the Pullout Capacity of Torpedo Pile in Soft Clay

9.1. Abstract

This study presents the results from centrifuge modeling experiments performed to understand the effects of temperature changes on the pullout capacity of scale-model Torpedo piles embedded in normally-consolidated clay layers. The Torpedo pile under investigation is a stainless steel cylinder with fins at the top, and its temperature is controlled using an internal electrical resistance heater. The torpedo pile was first heated until the temperature, pore water pressure, and volume change of the surrounding clay layer stabilized, after which the torpedo pile was cooled. Pullout tests were then performed on the torpedo piles heated to different temperatures to understand the effects of the preceding heating-cooling cycle on the pullout capacity. In addition, the clay undrained shear strength profiles were measured using push-pull T-bar penetration tests before and after heating.

9.2. Introduction

Torpedo piles are the most economical methods for anchoring oil company's facilities in the deep water using deep-water mooring system. Different sizes of torpedo were used in the past, varies from 0.75 to 1.1 m diameter, and 10 to 12 m long. The cost of the Torpedo pile installation is expensive, and any method to reducing the number of the piles used for a given site will lead to significant cost savings. If the pile is embedded into clay in deep water layers, all conventional soil improvement approaches (surcharge loading, vertical drains, electro-osmosis, etc.) are not expected to work. There are many researchers such as Abuel-Naga et al. (2007), and Samarakoon et al. (2018) who found that the saturated clay soil experienced permanent thermal contractile volumetric strain after a heating/cooling cycle. This permanent contraction also leads to an

increase in the undrained shear strength. The thermo-mechanical response of the soft clay to the temperature increase could be used as improvement method in soft clay.

This study uses a centrifuge modeling approach developed by Ghaaowd et al. (2018) to evaluate the effects of drained heating-cooling cycles on Torpedo pile embedded in soft clay layers. Centrifuge modeling was used in this study because the pore water pressure generation during undrained heating is sensitive to the initial mean effective stress in the clay layer, and the effective stresses in a centrifuge model clay layer are similar to those in a prototype clay layer. The Actidyne C61-3 centrifuge at the University of California San Diego was used to perform four tests on Torpedo piles in separate soil layers. The first four tests involved installation of torpedo pile into clay layers using jacked-in procedures (i.e., insertion at a constant displacement rate), heating to a target temperature (the first Torpedo pile was heated to 65°C, the second Torpedo pile was heated to 45°C, and the third was to 80°C), cooling back to ambient temperature, and finally pullout of the torpedo pile at a constant rate. The fourth test involved installation of a baseline torpedo pile using similar procedures to the other tests without heating followed by pullout at a constant rate after reaching equilibrium. In addition to presentation of the pullout versus displacement curves for the four tests, T-bar penetration results permit evaluation of the impact of heating and cooling on the undrained shear strength profiles in the four clay layers. Summary of tests on the Torpedo pile is shown in Materials

9.2.1. Kaolinite Clay

The soil used in the experiments was commercially-available Kaolinite clay from M&M Clays Inc. of McIntyre, Georgia whose geotechnical properties of the clay are summarized in Table 5.1. The clay classifies as CL according to the Unified Soil Classification Scheme. An isotropic compression test indicates that the slopes of the normal compression line (λ) and the

recompression line (κ) for the clay are 0.100 and 0.08, respectively. The clay specimens were formed from a slurry to reach initially normally consolidated conditions as will be described below.

9.2.2. Torpedo Pile

The scale-model Torpedo pile is a17 mm-diameter, 175 mm-long, fabricated from four parts as shown in Figure 9.1. The main part is stainless steel cylinder having a wall thickness of 3 mm, the tip part is connected to the cylinder by thread. The temperature source is the heater which pearly fits inside the cylinder. The heater has thermocouple embedded in it which connected together with the voltage wires to the heat controller. The fourth part is the pile cap, four vines were welded to its side, and both voltage wires and thermocouples wires were passed through opening at the top of the cap. In addition, the torpedo pile was holed by stainless steel wire connected to the torpedo pile cap from a side and connected to the load cell from the other side as shown in Figure 9.2 and Figure 9.3.

9.3. Centrifuge Container

A schematic of the container used in this study to evaluate temperature effects on the pullout capacity of Torpedo piles in clay is shown in Figure 9.3.The aluminum container consists of a base plate, a cylindrical tank, and an upper reaction plate. The base and reaction plates of the container have dimensions of 0.62 m×0.62 m×0.05 m. The cylindrical tank has an inside diameter of 0.55 m, a wall thickness of 16 mm, and a height of 0.47 m, and was connected to the base plate via four threaded rods atop an “O”-ring seal. The top reaction plate was connected to the top ends of the same threaded rods. The reaction plate supports stepper motors for loading the Torpedo pile and T-bar, as well as linearly variable differential transformers (LVDTs).

9.4. Experimental Procedures

Dry Kaolinite clay was mixed with water under vacuum to form a slurry having a gravimetric water content of 130%. The slurry was carefully poured into the container to avoid air inclusions. The clay layer was drained from the bottom via a sand layer having a thickness of 20 mm thickness and from the top via a filter paper and a 50 mm-thick porous stone placed on the top of the slurry. After 24 hours of self-weight consolidation, dead-weights applying vertical stresses of 2.4, 6.3, 10.2 kPa were added atop the porous stone in 24-hour increments. The surcharge was then increased to 23.6 kPa using a hydraulic piston and maintained for another 24 hours. The container was placed inside the centrifuge basket for in-flight self-weight consolidation at 50 g.

This procedure was found to produce a normally-consolidated clay layer with an overconsolidated portion near the surface. After the 1g consolidation of the clay layers was completed, six thermocouples and five miniature pore water pressure sensors were inserted through the container side wall into the clay layer at the locations shown in Figure 9.3 and Figure 9.4 During in-flight self-weight consolidation at 50 g, the excess pore-water pressures were monitored using the pore pressure transducers and the surface settlement was monitored. A typical time series of the pore water pressure during centrifugation was presented in Chapter 7 for Jack-in pile test that confirms that the clay layer reached more than 90% of the primary consolidation before moving to the next testing stage. The gravimetric water content of the clay layer with the unheated pile measured at the end of testing ranged from 38.5 to 52%, while the void ratio ranged from 1.0 to 1.35. These values can be assumed to correspond to the initial conditions for the Torpedo piles before application of the heating and cooling cycles. Because the positions of the sensors may change after consolidation in the centrifuge, the final positions of the sensors were verified at the end of the experiment by excavating the clay layer.

After the additional consolidation of the clay layer during centrifuge at 50 g, the Torpedo piles were installed in flight using a stepper motor into the sedimented clay layers having a thickness of 230 mm at a model-scale velocity of 0.1 mm/s until the pile tip reached the dense sand layer. The Torpedo pile was inserted so that the clay height above the torpedo pile is around 2 m. When the excess pore water pressure generated due to the pile insertion dissipated, the temperature of the heated Torpedo pile was increased using the Watlow heat controller until reaching the target temperature at the pile wall. Heating continued during centrifugation until the soil temperature and pore water pressure stabilized. After reaching equilibrium during heating, which required approximately 30 hours for the heat tests, the pile was cooled and was then pulled out at the same speed used for installation.

A T-bar with a diameter of 14 mm and length of 57 mm was used to measure the undrained shear strength profiles of the clay layers containing heated and unheated Torpedo piles. Insertion of the T-bar into the clay layer can be used to infer the undrained shear strength of the intact clay layer as a function of depth, while extraction of the T-bar can be used to infer the undrained shear strength of disturbed clay as a function of depth (Stewart and Randolph 1994). The T-bar was designed to permit model-scale penetrations up to 230 mm and was driven by a second stepper motor at a model-scale velocity of 0.2 mm/s to ensure undrained conditions during insertion and extraction. T-bar penetration tests were executed in each clay layer at a radius of 100 mm from the heated and unheated Torpedo piles, which is far enough away to be undisturbed from the pile insertion and extraction but close enough to be influenced by temperature.

9.5. T-Bar Measurements and Interpretation

The T-bar penetration results for the clay layers with unheated and heated Torpedo piles permit evaluation of the effects of cyclic heating-cooling to different temperatures on the behavior

of normally consolidated clay layers. The undrained shear strength profiles for the clay layer at a model-scale distance of 100 mm from the four Torpedo piles are shown in Figure 9.5. The correlations of Stewart & Randolph (1991) were used to interpret the undrained shear strength profiles from the T-bar penetration results. The pile temperatures are shown in Figure 9.4, but these do not correspond to the temperatures at the location of the T-bar penetration tests. When heating the Torpedo pile to 80 °C, the soil temperature at the location of the T-bar increased by 10 C, and when heating the Torpedo pile to 45 °C, the soil temperature increased by 8 °C. The initial T-bar position is slightly below the clay surface to maximize the stroke of the T-bar test, so the undrained shear strength near the surface of the clay layer was not characterized. The undrained shear strength profiles indicate that a drained heating-cooling cycle leads to an increase in undrained shear strength of the clay layer, and that heating the Torpedo pile to higher temperatures leads to a greater improvement. Greater differences in undrained shear strength were observed deeper in the clay layer, which may be because the thermally induced excess pore water pressures were greater at these depths (Ghaaowd et al. 2018). The T-bar at the unheated was started at soil level lower than the other (4.9m). The T-bar at test wasn't done at pile heated to 65 °C due to the problem in the stepper motor. The void ratios inferred from gravimetric water content samples at the end of the tests are shown in Figure 9.6. Lower void ratios are observed in the clay layers that experienced higher temperatures, which correspond well with the increases in the undrained shear strength with temperature inferred from the T-bar penetration tests.

9.6. Pullout Capacity Measurements and Interpretation

The pullout load versus displacement curves for the heated and unheated Torpedo piles in clay layers having similar initial conditions are shown in Figure 9.7(a). All four pullout curves start from a self-weight load of 122 kN. A clear increase in pullout capacity is observed with an

increase in the temperature that the Torpedo piles experienced during the heating stage. The net percent increase in pullout capacity versus the change in pile temperature is shown in Figure 7(b), indicating that the increase in pullout capacity may be approximately linear. The heated Torpedo pile at 65 °C had a net pullout capacity of -108 kN that is approximately 108% greater than that of the unheated Torpedo pile that had a net pullout capacity of -52 kN. The net pullout capacity for the Torpedo pile heated at 45 °C was -108 kN which is approximately 100% greater than that of the unheated Torpedo pile. The fourth torpedo pile was heated to 80°C, the net pullout capacity was -134 kN which corresponds to an approximate percent increase in pullout capacity of 123% with respect to the unheated pile.

These percent increases in net pullout capacity confirms that the drained heating-cooling cycle during in-situ heating of the clay layer leads to substantial improvements in the undrained shear strength of the clay surrounding the heated Torpedo pile, resulting in an improvement in soil-pile interaction. An unexpected observation in Figure 9.7(a) is that the slopes of the pullout curves are similar. It was expected that the increase in undrained shear strength of the clay layer with temperature would also correspond to an increase in stiffness. The similar slopes in Figure 9.7(a) may have occurred because the heated aluminum Torpedo piles experienced thermal axial strains in the direction opposite to the downward seating load during heating that may have counteracted the positive effect of the thermal improvement of the soil layer. During pullout, the piles were likely following an elastic loading-unloading curve until shortly before failure. Finally, the pullout capacity improvement matched the results shown in Chapter 7 for jacked-in pile as shown in Figure 9.8.

9.7. Conclusion

Heated and unheated scale-model stainless steel Torpedo piles were tested to evaluate the impacts of temperature on the normally consolidated clay layer and on the corresponding pullout capacity of the Torpedo pile. The following specific conclusions can be drawn:

- The undrained shear strength of the clay surrounding the heated-cooled Torpedo piles was greater than that of the clay surrounding the unheated Torpedo pile.
- The pullout capacities of the Torpedo piles that had experienced greater changes in temperature were greater than that of the unheated Torpedo pile. The slope of the pullout load versus displacement curves were similar, which may be due to the impact of upward displacements due to thermal expansion of the Torpedo pile prior to pullout, leading to an initially elastic pullout response for all the Torpedo piles.
- The amount of the torpedo pile pullout improvement increases with the temperature change has trend similar to the observations from Chapter 8.

9.8. Acknowledgements

Chapter 9, in full, is currently being prepared for submission for publication of the material as it may appear in the following conference publication (The dissertation author was the primary investigator and author of this paper):

Ghaaowd, I. & McCartney (In preparation). "Centrifuge modeling of temperature effects on the pullout capacity of torpedo piles in saturated soft clay." To be submitted to the 2019 Deep Foundation Institute Conference.

Table 9.1. Summary of tests on the Torpedo piles after a heating-cooling cycle involving different maximum pile temperature

Test Number	Pile Wall Temperature during Heating	Change in Pile Temperature	Maximum Pullout Load	Percent Improvement in Pile Pullout Capacity
#	°C	°C	kN	%
T1	23	0.0	-104	0
T2	45	22	-156	100
T3	65	42	-160	107
T4	80	57	-168	123

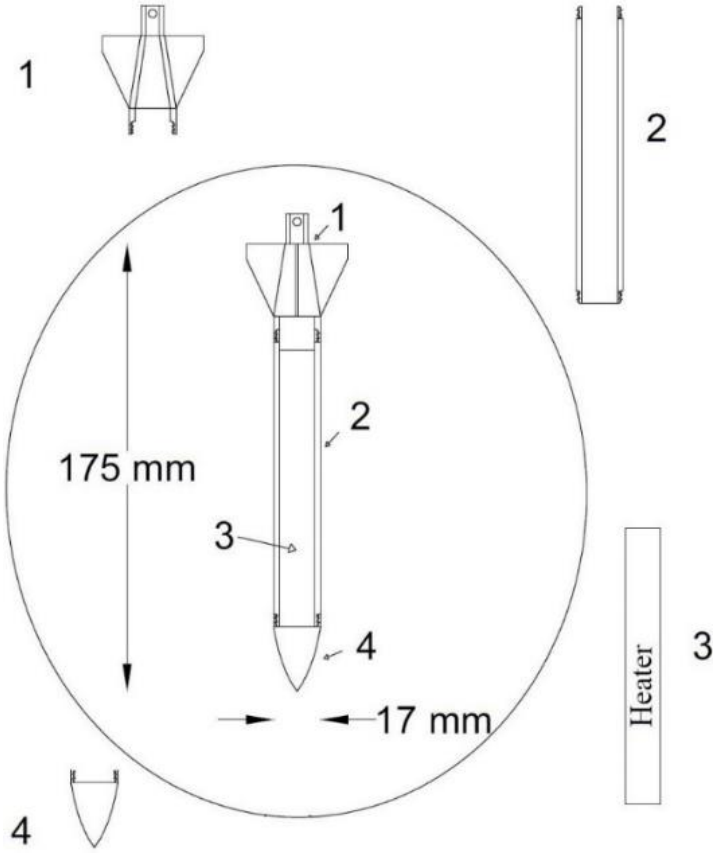

Figure 9.1. Schematic of the centrifuge-scale Torpedo pile: (1) Top cap; (2) Body; (3) Internal electric resistance heater; (4) tip

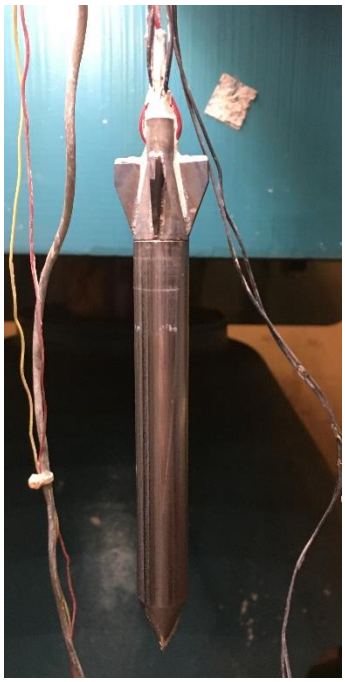

Figure 9.2. Picture of the centrifuge-scale Torpedo pile

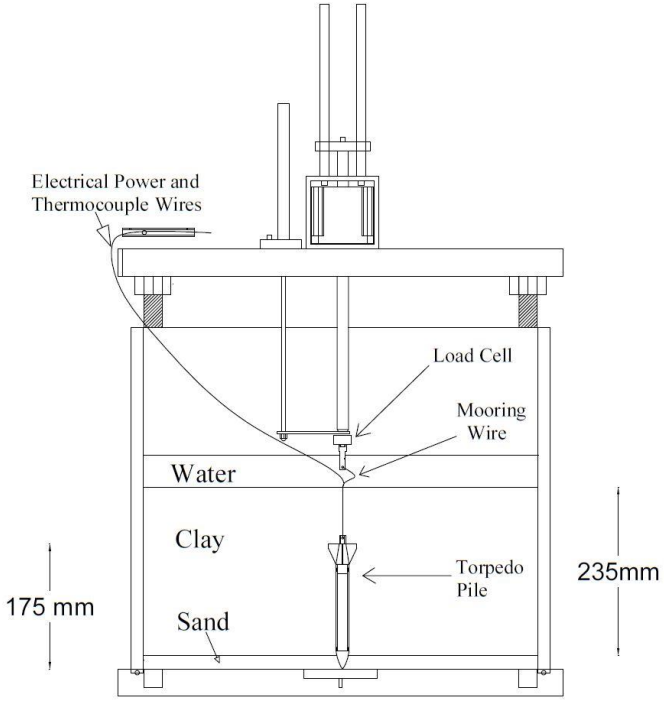

Figure 9.3. Cross-section of the setup using the four experiments showing the Torpedo pile

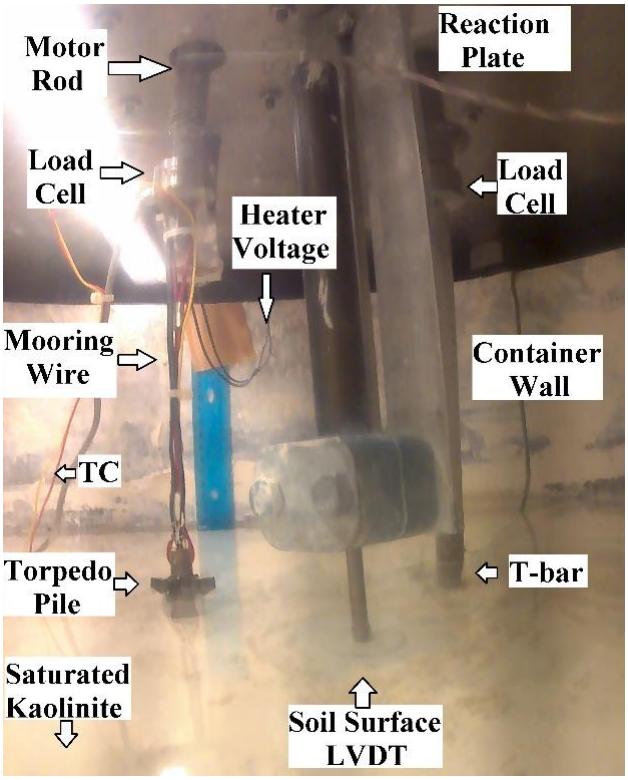

Figure 9.4. Picture of the setup during installation of the Torpedo pile while spinning at 50 g

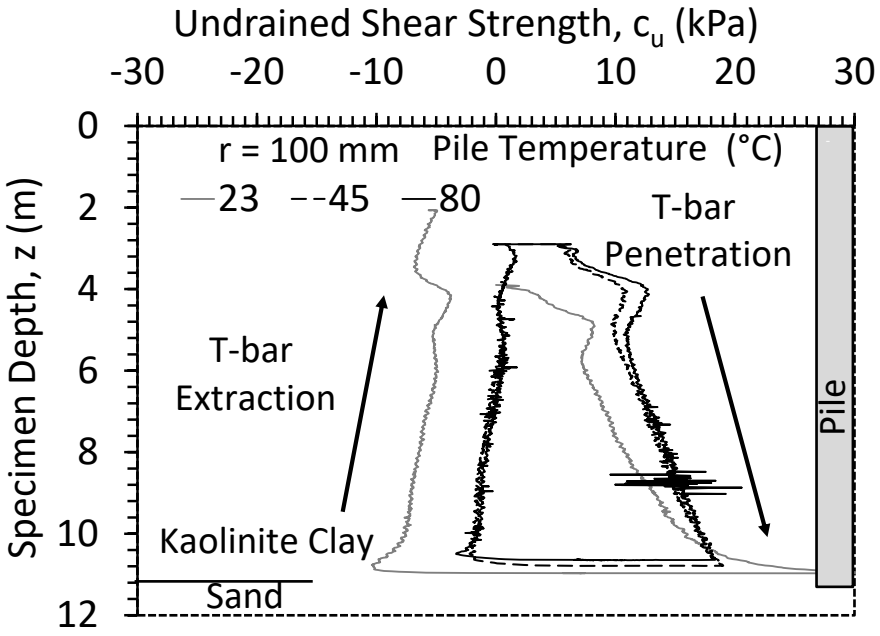

Figure 9.5. Profiles of undrained shear strength measured by the T-bar in three of the four tests on Torpedo piles heated to different temperatures (positive values for insertion and negative values for extraction)

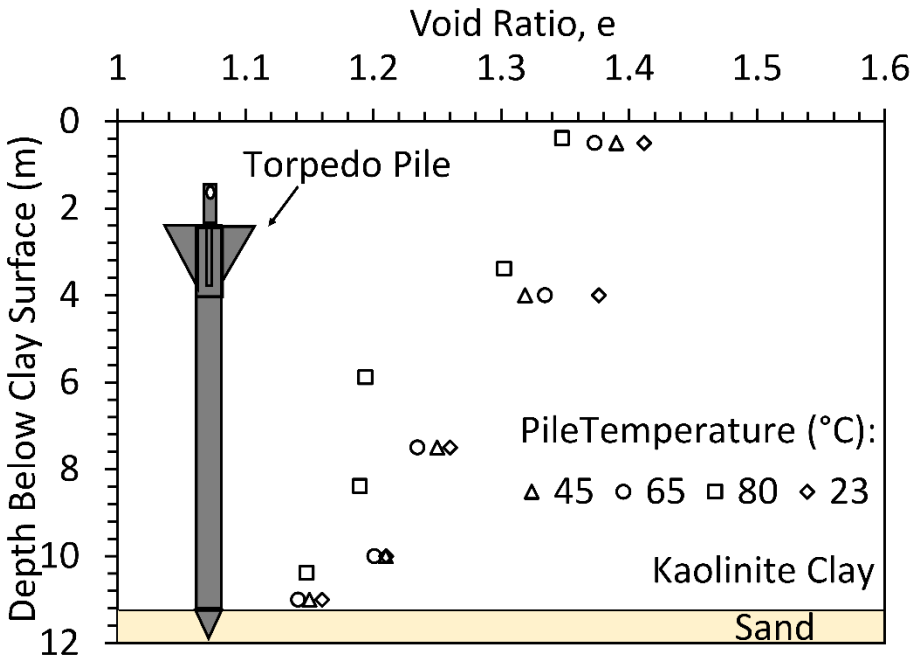

Figure 9.6. Prototype-scale profiles of void ratio at a model-scale distance of 100 mm from the Torpedo piles at the end of testing

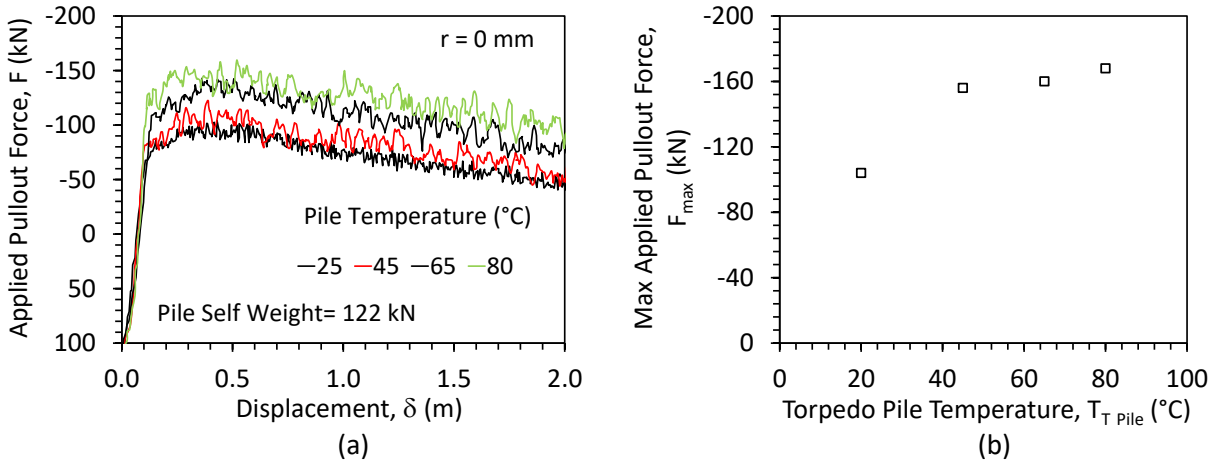

Figure 9.7: Results from pullout tests on Torpedo piles after a heating-cooling cycle involving different maximum pile temperatures: (a) Applied pullout force versus displacement curves (prototype scale), (b) Pullout capacity as a function of the maximum pile temperature experienced during a heating-cooling cycle

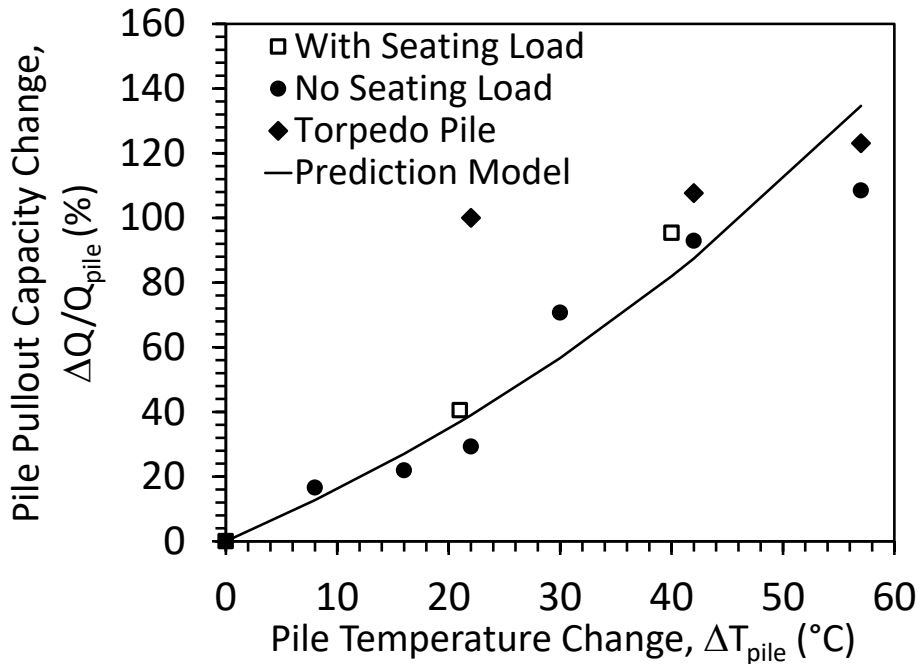

Figure 9.8. Percent increase in pullout capacity of the Torpedo piles after in-situ heating to different changes in pile temperature with a compar pullout Capacity improvement versus temperature change

Chapter 10. Conclusions

The main outcomes from this study are summarized according to the different topics studied in this thesis.

Heat Transfer in Saturated Soft Clay

Analysis was performed to estimate the change in temperature in the saturated clay layer around the circular pile using an analytical solution to the heat conduction equation for an infinite line source developed by Carslaw and Jaeger (1959). The calculated temperature results after 10 hours for the same tested model matched well with the measured temperature results from different tests. This confirms the assumption that natural convection due to the temperature effects on the density of pore water did not have a major effect on the heat transfer.

Prediction of Thermally Induced Pore Water Pressures during Undrained Heating

A prediction model for the thermally induced pore water pressure was proposed and experimentally validated in this study. Normalized pore water pressures measured during changes in temperature during undrained heating tests on soil specimens reported in the literature were used to calculate the physico-chemical coefficient. Normalization of the pore water pressures helped remove the effects of the initial effective stress from the analysis, and specimens of the same soil tested under different initial mean effective stresses had similar physico-chemical coefficients of structural volume change. Relationships between the calculated values of the physico-chemical coefficient and the plasticity index and liquidity index were investigated. Although a nonlinear decreasing trend was observed with the plasticity index, no trend was observed with the liquidity index. A prediction model was proposed based on an empirical relationship between the physico-chemical coefficient of structural volume change and plasticity index. The pore water pressure

values predicted by this model for Kaolinite clay were matched well with those measured in an independent undrained heating test. This confirms that this simple, empirical approach to define the physico-chemical coefficient in the thermo-elastic model is effective in making preliminary estimates of the thermally induced pore water pressures expected in saturated soils used in thermal soil improvement or in thermally active geotechnical engineering systems. The thermal expansion of the specimen calculated using image analysis was found to match well with the slope of the recompression curve, confirming the assumption of the magnitude of the coefficient of volume compressibility used in the analysis. Although only limited data is available in the literature for overconsolidated clays, the validated model was found to also provide a good fit to the thermally induced pore water pressure in saturated, overconsolidated clays.

Prediction of Volume Change after Drainage

Drained and undrained heating triaxial tests were performed to evaluate the impact of the drainage on the volume change during the specimen temperature change. The temperature increase induced volume expansion during the drained heating test, part of the volume contraction is irreversible. But, the specimen was expanded due to the undrained heating, and the pore water pressure was increased. The pore water pressure measured during the undrained test could be used to predict drained water due to the temperature increase during the drained test which could be used to predict the volume change of the clay.

Impact of Drained a Heating/Cooling Cycle on Undrained Shear Strength

The results presented in this study indicate that the impact of a heating-cooling cycle such as that used in a thermal improvement application (i.e., thermal drains) will have a positive effect on the undrained shear strength of normally consolidated clays. This trend in undrained shear strength is attributed to the plastic decrease in volume during drained heating combined with the

elastic decrease in volume during drained cooling. It was observed that this positive effect was greater for specimens tested at lower initial mean effective stresses. Despite the clear effects of temperature on the undrained shear strength, the changes in temperature were not observed to affect the slope of the peak failure envelope, which is consistent with previous studies on the effects of temperature on the shear strength of clays

Thermal Improvement of the Pullout Capacity of Jacked-in Offshore Pile Foundations

This study investigated the effect of the temperature on the pullout capacity of the offshore jacked-in pile foundation embedded into saturated soft clay using centrifuge modeling setup. Ten tests were performed involving five testing stages in the centrifuge: in-flight consolidation, pile installation, heating, cooling, and pullout stages. The temperature range was from 23 °C to 80 °C, and pile temperature to the soil temperature ratio at r from the center are similar for all tests. Thermal excess pore pressure generated during heating to these temperatures ranged from 1 kPa to 10 kPa. The magnitude of the thermal excess pore water pressure at a given location was found to be a function of the change in temperature of the soil at that location and the initial effective stress. The predicted thermal excess pore water pressure similar to the measured by the sensors. The pile driving force during the penetration versus depth can be used to estimate the undrained shear strength at the center during the penetration which have similar results. The undrained shear strength at the center was around 11 kPa which is similar to the average undrained shear strength calculated from the pullout capacity of the pile at 23 °C, the undrained shear strength calculated from the pullout ranges from 10.7 kPa to 22.3 kPa for pile temperatures of 23 °C and 80 °C. Even though the T-bar tests were done 100 mm from the center, great improvement in the undrained shear strength profile was observed at the higher temperature. The triaxial tests results show an

increase in the undrained shear strength similar to that observed during the centrifuge tests. The pile pullout increased dramatically by the temperature increase.

Thermal Improvement of the Pullout Capacity of Torpedo Pile Foundations

Heated and unheated scale-model stainless steel Torpedo piles were tested in a geotechnical centrifuge to evaluate the impacts of temperature on the normally consolidated clay layer and on the corresponding pullout capacity in the vertical direction. The undrained shear strength of the clay surrounding the heated-cooled Torpedo piles was found to be greater than that of the clay surrounding the unheated Torpedo pile. As expected, the pullout capacities of the Torpedo piles that had experienced a heating-cooling cycle with larger changes in temperature were greater than that of the unheated Torpedo pile. The slope of the pullout load versus displacement curves were similar for each of the piles indicating that the temperature did not affect the stiffness of the pile. This may have been due to the impact of upward displacements due to thermal expansion of the Torpedo pile prior to pullout, which may have mobilized a fraction of the side shear capacity. The amount of the torpedo pile pullout improvement increases with the temperature change were similar to those observed for the jacked-in piles after in-situ heating.

Prediction Model for Thermal Improvement in Pile Pullout Capacity

The prediction model presented in this study is an uncoupled prediction that includes conductive heat transfer, prediction of thermally-induced excess pore water pressures during undrained heating, prediction of changes in void ratio after drainage of these excess pore water pressures, and corresponding changes in undrained shear strength that can be integrated to predict the pullout capacity of the pile. The predicted improvements in the pullout capacity of the jacked-in piles after in-situ heating using both models matched well with the measured improvement in the pullout capacity of the jacked-in piles in the centrifuge physical modeling experiments.

Chapter 11. References

Abuel-Naga, H.M., Bergado, D.T., and Chaiprakaikeow, S. (2006). "Innovative thermal technique for enhancing the performance of prefabricated vertical drain during the preloading process." Geotextiles and Geomembranes, 24, 359–370.

Abuel-Naga, H.M., Bergado, D.T., Bouazza, A. (2007a). "Thermally induced volume change and excess pore water pressure of soft Bangkok clay." Engineering Geology. 89, 144-154.

Abuel-Naga, H. M., Bergado, D. T., Bouazza, A. and Ramana, G. V. (2007b). "Volume change behavior of saturated clays under drained heating conditions: experimental results and constitutive modeling." Canadian Geotechnical Journal. 44(8), 942-956.

Abuel-Naga, H. M., Bergado, D. T. & Lim, B. F. (2007c). "Effect of temperature on shear strength and yielding behavior of soft Bangkok clay." Soils and Foundations. 47(3), 423-436.

Abuel-Naga, H.M., Bergado, D.T., Bouazza, A., and Pender, M. (2009) "Thermomechanical model for saturated clays." Géotechnique. 59(3), 273-278.

Ahmed, I. (1993). Laboratory Study on Properties of Rubber Soils. Report No. FHWA/IN/JHRP-93/4, Purdue University, West Lafayette, Indiana.

Alsherif, N.A., McCartney, J.S. (2013). "Triaxial cell for nonisothermal shear strength of compacted silt under high suction magnitudes." Proceedings of the 1st Pan-American Conference on Unsaturated Soils. Feb. 20-22. Cartagena de Indias. Taylor and Francis Group, London. 147-152.

Alsherif, N.A., and McCartney, J.S. (2015). "Nonisothermal behavior of compacted silt at low degrees of saturation." Géotechnique. 65(9), 703-716.

Aversa, S., Evangelista, A. (1993). "Thermal expansion of Neapolitan yellow tuff." Rock Mechanics and Rock Engineering. 26(4), 281-306.

Baldi, G., Hueckel, T., Pellegrini, R. (1988). "Thermal volume changes of the mineral-water system in low-porosity clay soils." Canadian Geotechnical Journal. 25(4), 807-825.

Baldi, G., Hueckel, T., Peano, A., and Pellegrini, R. (1991). "Developments in modelling of thermo-hydro-geomechanical behavior of boom clay and clay-based buffer materials." Commission of the European Communities, Nuclear Science and Technology, EUR 13365/1 and EUR 13365/2.

Bastidas, A.M. (2016).). "Ottawa F-65 Sand Characterization." Ph. D. Dissertation, University of Califronia, Davis.

Brandl, H. (2006). "Energy foundations and other thermo-active ground structures." Géotechnique. 56(2), 81-122.

Booker, J.R. and Savvidou, C. (1985). "Consolidation around a point heat source." International Journal for Numerical and Analytical Methods in Geomechanics, (9): 173-184.

Burghignoli, A., Desideri, A., and Miliziano, S. (2000). "A laboratory study on the thermomechanical behavior of clayey soils." Canadian Geotechnical Journal. 37(4), 764-780.

Campanella, R.G., and Mitchell, J.K. (1968). "Influence of temperature variations on soil behavior." Journal of the Soil Mechanics and Foundation Division, 94(SM3), 709-734.

Cecinato, F., Zervos, A., and Veveakis, E. (2011). "A thermo-mechanical model for the catastrophic collapse of large landslides." Int. J. Numer. Anal. Meth. Geomech., 35(14), 1507-1535, doi:10.1002/nag.963.

Cinicioglu, O., Znidarčić, D. and Ko, H.-Y. (2006). "A new centrifugal testing method: Descending gravity test." Geotechnical Testing Journal. 29(5): 1-10.

Coccia, C.J.R., and McCartney, J.S. (2013). "Impact of heat exchange on the thermo-hydro-mechanical response of reinforced embankments." Proc. GeoCongress 2013. ASCE. pp. 343-352.

Cui, Y. J., Sultan, N., and Delage, P. (2000). "A thermomechanical model for clays." Canadian Geotechnical Journal. 37(3): 607–620.

Dennis, N.D. and Olson, R.E. (1983). "Axial capacity of steel pipe piles in clay." Proc., Conf. on Geotech. Pract. In Offshore Eng., S. G. Wright, ed., ASCE, New York: 370–388.

Graham, J., Tanaka, N., Crilly, T. and Alfaro, M. (2001). "Modified Cam-Clay modeling of temperature effects in clays." Can. Geotech. J. 38, No. 3, 608–621.

Gens, A., Garcia-Molina, A.J., and Olivella, S. (1998). "Analysis of a full scale in situ test simulating repository conditions." International Journal of Numerical and Analytical Methods in Geomechanics. 22: 515-548.

Gens, A., Guimaraes, L. do N., Olivella, S., and Sanchez, M. (2010). "Modelling thermo-hydro-mechano-chemical interactions for nuclear waste disposal." Journal of Rock Mechanics and Geotechnical Engineering, 2(2), 97–102.

Ghaaowd, I., and McCartney, J.S. (2015). "Prediction of thermally-induced pore water pressure in clays." 15th Pan-American Conf. on Soil Mechanics and Geotechnical Engineering (XV PCSMGE). Buenos Aires. Nov. 16-18. pp. 1-8.

Ghaaowd, I., Takai, A., Katsumi, T. and McCartney, J.S. (2016). "Pore water pressure prediction for undrained heating of soils." Environmental Geotechnics. 4(2): 70-78.

Ghaaowd, I., McCartney, J.S., Huang, X., Saboya, F., and Tibana, S. (2018). "Issues with centrifuge modeling of energy piles in soft clays." 9th International Conference on Physical Modelling in Geotechnics. London. Jul. 17-20. 1-6.

Ghaaowd, I. and McCartney, J.S. (2018). "Centrifuge modeling of temperature effects on the pullout capacity of energy piles in clay." Deep Foundation Institute, 43rd Annual Conference.

Ghaaowd, I., Takai, A., Katsumi, T., McCartney, J.S. (2017). "Pore water pressure prediction for undrained heating of soils." Environmental Geotechnics. 4(2): 70-78.

Houston, S.L., Houston, W.N., and Williams, N.D. (1985). "Thermo-mechanical behavior of seafloor sediments." Journal of Geotechnical Engineering. 111(12), 1249-1263.

Hueckel, T., and Baldi, M. (1990). "Thermoplasticity of saturated clays: experimental constitutive study." Journal of Geotechnical Engineering, 116(12), 1778–1796.

Hueckel, T., and Borsetto, M. (1990). "Thermoplasticity of saturated soils and shales: constitutive equations." Journal of Geotechnical Engineering, 116(12), 1765–1777.

Hueckel, T., François, B. and Laloui, L. (2009). "Explaining thermal failure in saturated clays." Géotechnique. 59(3), 197–212.

Kanno, T., Fujita, T. and Ishikawa, H. (1999). "Coupled thermo-hydro-mechanical modelling of bentonite buffer material." International Journal of Numerical and Analytical Methods in Geomechanics. 23: 1281–1307.

Hueckel, T., Pellegrini, R. and Del Omo, C. (1998). "A constitutive study of thermo-elastoplasticity of deep carbonatic clays," International Journal of Numerical and Analytical Methods in Geomechanics, Vol. 22, No. 7, pp.549-574.

Laloui, L., Nuth, M., and Vulliet, L. (2006). "Experimental and numerical investigations of the behaviour of a heat exchanger pile." International Journal of Numerical and Analytical Methods in Geomechanics. 30, 763-781.

Laloui, L. and Cekerevac, C. (2003). "Thermo-plasticity of clays: an isotropic yield mechanism." Computers and Geotechnics. 30(8), 649–660.

Laloui, L. and Cekerevac, C. (2008). "Non-isothermal plasticity model for cyclic behaviour of soils." International Journal of Numerical and Analytical Methods in Geomechanics. 32, 437-

Laloui, L., Nuth, M., and Vulliet, L. (2006). "Experimental and numerical investigations of the behavior of a heat exchanger pile." International Journal of Numerical and Analytical Methods in Geomechanics. 30, 763-781.

Laloui, L., Olgun, C.G., Sutman, M., McCartney, J.S., Coccia, C.J.R., Abuel-Naga, H.M., and Bowers, G.A. (2014). "Issues involved with thermo-active geotechnical systems: Characterization of thermo-mechanical soil behavior and soil-structure interface behavior." The Journal of the Deep Foundations Institute. 8(2): 107-119.

Lee S.H. and Ghassemi, A. (2011). "Three-dimensional thermo-poro-mechanical modeling of reservoir stimulation and induced microseismicity in geothermal reservoir," Proc. 36th E-6

Workshop on Geothermal Reservoir Engineering, Stanford University, Stanford, California, January 31 - February 3, 2011.

Leroueil, S. Tavenas, F., Brucy, F., Rochelle, P. and Roy, M. (1979). "Behavior of destructred natural clays." J. Geotech Engrg., ASCE, 105(6). 759-778.

Maddocks, D.V. and Savvidou, C. (1984). "The effect of the heat transfer from a hot penetrator installed in the ocean bed." Proc. Symp. On the Application of Centrifuge Modeling to Geotechnical Design. W.H. Craig. Manchester U.K

McCartney, J.S. and Murphy, K.D. (2017). "Investigation of potential dragdown/uplift effects on energy piles." Geomechanics for Energy and the Environment. 10(June): 21-28.

McKinstry, H.A. (1965). "Thermal expansion of clay minerals." The American Mineralogist, 50: 212–222.

Mitchell, J.K. (1993). Fundamentals of Soil Behavior. 2nd Edition. Wiley, New York.

Moritz, L. (1995). Geotechnical Properties of Clay at Elevated Temperatures. Report 47, Swedish Geotechnical Institute, Linköping, Sweden.

Murphy, K.D. and McCartney, J.S. (2015). "Seasonal response of energy foundations during building operation." Geotechnical and Geological Engineering. 33(2), 343-356.

Ng, C.W.W., Gunawan, A. & Laloui, L. (2014). "Centrifuge modelling of energy piles subjected to heating and cooling cycles in clay." Géotechnique Letters, 4(4): 310-316.

Olivella, S., Carrera, J., Gens, A. and Alonso, E.E. (1996a). "Porosity variations in saline media caused by temperature gradients coupled to multiphase flow and dissolution/precipitation." Transp. Porous Media 25, No. 1, 1–25.

Olivella, S., Gens, A., Carrera, J. and Alonso, E.E. (1996b). "Numerical formulation for a simulator (CODE_BRIGHT) for the coupled analysis of saline media," Engng Comput. 13, No. 7, 87–112.

Bourne-Webb, P.J., Amatya, B., Soga, K., Amis, T., Davidson, C. and Payne, P. (2009). "Energy pile test at Lambeth College, London: Geotechnical and thermodynamic aspects of pile response." Géotechnique. 59(3), 237–248.

Paaswell, R.E. (1967). "Temperature effects on clay soil consolidation." Journal of the SoilMechanics and Foundation Engineering Division, 93(SM3), 9–22

Plum, R.L., Esrig, M.I. (1969). "Some temperature effects on soil compressibility and pore water pressure." Highway Research Board, Washington, DC. Report 103. 231–242.

Push, R. and Guven, N. (1990). "Electronic microscopic examination of hydrothermally treated Bentonite clay." Engrg. Geol, (28): 303-31.

Rice, J.R. (2006). “Heating and weakening of faults during earthquake slip.” J. Geophys. Res., 111, B05311, doi: 10.1029/2005JB004006.

Salager, S., Laloui, L., Nuth, M. “Efficiency of thermal vertical drains for the consolidation of soils.” Proceedings of 2nd Int. Conf. on Transportation Geotechnics, Hokkaido, Japan. (2012). 1-10.

Samarakoon, R. Gaaowd, I. & McCartney, J.S. (2018). “Impact of drained heating and cooling on undrained shear strength of normally consolidated clay.” International Symposium on Energy Geotechnical SEG-2018, Switzerland. 243-250.

Savvidou, C. (1988). “Centrifuge modelling of heat transfer in soil.” Proc. Centrifuge 88. Balkema: 583–591.

Savvidou, C. and Booker, J.R. (1988). “Consolidation around a spherical heat source with decaying power output.” Computers and Geotechnics. 5, pp. 227-244

Schiffman, R.L. (1971). “A thermoelastic theory of consolidation.” Env. and Geophysical HeatTransfer. pp. 78–84.

Schofield, A., Wroth, P. Critical State Soil Mechanics. Cambridge University. (1973).

Sivakumar, V., Dorgan, I.G, and Graham, J. (2002). “Particle orientation snd itd influence on the mechanical behavior of isotropically consolidated reconstituted clay.” Engrg. Geol: (66) 243-250.

Stewart, D. and Randolph, M. (1994). “T-Bar penetration testing in soft clay.” Journal of the Geotechnical Engineering Division. ASCE. 120(12): 2230-2235.

Stewart, M.A. and McCartney, J.S. (2013). “Centrifuge modeling of soil-structure interaction in energy foundations.” Journal of Geotechnical and Geoenvironmental Eng. 04013044.

Stewart, M.A., Coccia, C.J.R., and McCartney, J.S. (2014). “Issues in the implementation of sustainable heat exchange technologies in reinforced, unsaturated soil structures.” Proc. GeoCongress 2014. ASCE. pp. 4066-4075.

Sulem, J., Lazar, P., and Vardoulakis, I. (2007). “Thermo-poro-mechanical properties of clayey gouge and application to rapid fault shearing.” Int. J. Numer. Anal. Methods Geomech., 31(3), 523-540.

Sultan, N., Delage, P., and Cui, Y.J. (2002). “Temperature effects on the volume change behavior of boom clay.” Engineering Geology. 64, 135-145.

Takai. A,, Ghaaowd, I., Katsumi, T., McCartney, J.S. (2016). “Impact of drainage conditions on the thermal volume change of soft clay.” GeoChicago 2016: Sustainability, Energy and the Geoenvironment. Chicago. Aug. 14-18. pp. 32-41.

Towhata, I., Kuntiwattanakul, P., Seko, I., and Ohishi, K. (1993). “Volume change of clays induced by heating as ob-served in consolidation tests.” Soils and Foundations. 33(4), 170–183.

Taylor, D.W. 1948. Fundamentals of Soil Mechanics. John Wiley and Sons, New York.

Uchaipichat, A., Khalili, N., Zargarbashi, S. (2011). “A temperature controlled triaxial apparatus for testing unsaturated soils.” Geotechnical Testing Journal. 34(5): 1-9.

Uchaipichat, A. Khalili, N. “Experimental investigation of thermo-hydro-mechanical behaviour of an unsaturated silt.” Géotechnique. 59(4), (2009), 339–353.

Vardoulakis, I. (2002). “Dynamic thermo-poro-mechanical analysis of catastrophic landslides.” Geotechnique, 52, 157-171.

Vega, A., Coccia, C.J.R., El Tawati, A. and McCartney, J.S. (2012). “Impact of the rate of heating on the thermal consolidation of saturated silt.” Proceedings of GeoCongress 2012 (GSP 225). R.D. Hryciw, A. Athanasopoulos-Zekkos, and N. Yesiller, eds. ASCE. pp. 4476-4485.

Vega, A. and McCartney, J.S. (2015). “Cyclic heating effects on thermal volume change of silt.” Environmental Geotechnics. 2(5): 257-268.

Veveakis, E., Stefanou, I., and Sulem, J. (2013). “Failure in shear bands for granular materials: Thermo-hydro-chemo-mechanical effects. Geotech. Lett. 3(2), 31-36.

Wibberley, C. and Shimamoto, T. (2005). “Earthquake slip weakening and asperities explained by thermal pressurization.” Nature, 426(4), 689-692.